Engineering of biomolecular systems for anti-tumoral immunotherapy

Biagio Todaro

THÈSE

Pour obtenir le grade de

DOCTEUR DE L'UNIVERSITÉ GRENOBLE ALPES

Spécialité : Chimie Biologie

Arrêté ministériel : 25 mai 2016

Présentée par

Biagio TODARO

Thèse dirigée par **OLIVIER RENAUDET**

préparée au sein du **Laboratoire Département de Chimie Moléculaire**
dans **l'École Doctorale Chimie et Sciences du Vivant**

Ingénierie de systèmes biomoléculaires pour l'immunothérapie anti-tumorale

Engineering of biomolecular systems for anti-tumoral immunotherapy

Thèse soutenue publiquement le **9 décembre 2020**,
devant le jury composé de :

Monsieur OLIVIER RENAUDET
PROFESSEUR DES UNIVERSITES, UNIVERSITE GRENOBLE ALPES, Directeur de thèse
Monsieur FRANCK FIESCHI
PROFESSEUR DES UNIVERSITES, UNIVERSITE GRENOBLE ALPES, Président
Monsieur VINCENT FERRIERES
PROFESSEUR DES UNIVERSITES, UNIVERSITE RENNES 1, Rapporteur
Monsieur MICHELE FIORE
MAITRE DE CONFERENCES HDR, UNIVERSITE LYON 1, Rapporteur
Madame CRISTINA NATIVI
PROFESSEUR, UNIVERSITE DE FLORENCE - ITALIE, Examinatrice

TABLE OF CONTENTS

Abbreviations

ABMs: Antibody binding modules

Abs: Antibodies

Ac_3ManNAz: 1,3,4-O-acetyl-*N*-azidoacetylmannosamine

ACT: Adoptive T cell therapy

ADCC: Antibody dependent cellular cytotoxicity

ADCP: Antibody dependent cellular phagocytosis

ADP-ribose: Adenosine diphosphate-ribose

AF-488: AlexaFluor™ 488

Alk: Alkyne

APC: Antigen-Presenting Cells

ARMs: Antibody recruiting molecules

ARM-H: Antibody recruiting molecule targeting HIV

ARM-Ps: Antibody recruiting molecules targeting prostate cancer cells

ARM-U: Antibody recruiting molecules targeting urokinase receptor

ATP: Adenosine triphosphate

BCECF: fluorescent 2',7'-bis-(2-carboxyethyl)-5(6)-carboxyfluorescein

BCECF_AM: 2',7'-bis-(2-carboxyethyl)-5(6)-carboxyfluorescein acetoxymethyl ester

BCM: Biotinylated C-glycoside of mannose

BG: background

Bn: Benzil

Boc: Butyloxycarbonyl

BPC: Biphenyl-carbonyl

BsAb: Bispecific antibody

BTTAA: 2-(4-((Bis((1-(tert-butyl)-1H-1,2,3-triazol-4-yl)methyl)amino)methyl)-1H-1,2,3-triazol-1-yl)acetic acid

BTTES: 3-(4-((Bis((1-(tert-butyl)-1H-1,2,3-triazol-4-yl)methyl)amino)methyl)-1H-1,2,3-triazol-1-yl)propane-1-sulfonic acid

C1q: Complement component 1q

Cbz: Carboxybenzyl

CCR5: Chemokine receptors type 5

CDC: Complement dependent cytotoxicity

cHx: Cyclohexyl

cRGD: cyclic Arg-Gly-Asp-(D-Phe)-Lys pentapeptide

CTLA-4: Cytotoxic T lymphocyte associated protein 4

CuAAC: Copper(I)-catalyzed alkyne-azide cycloaddition

DART: D-amino acid Antibody Recruitment Therapy

DBCO: Dibenzocyclooctyne

DCC: N,N'-dicyclohexylcarbodiimide

DCM: Dichloromethane

DCs: Dendritic cells

Dde: N-(1-(4,4-dimethyl-2,6-dioxocyclohexylidene)ethyl

DFT: Density functional theory

DIC: N,N'-diisopropylcarbodiimide

DIPEA: N,N-diisopropylethylamine

DMEM: Dulbecco's Modified Eagle Medium

DMF: N,N-dimethylformamide

DNA: Deoxyribo Nucleic Acid

DNP: 2,4-Dinitrophenyl

DOX: Doxorubicin (DOX)

EGFR: Epidermal growth factor receptor

ELISA: Enzyme-linked immunosorbent assay

Env: Envelope

ESI: Electrospray ionization

ET_A/ET_B: Endothelin receptor A/B

FA: Folic acid

Fab : Fragment antigen binding

FACS: Fluorescence-activated cell sorting

Fc : Fragment crystallizable

FDA: U.S. Food and Drug Administration

FITC: Fluorescein isothiocyanate

Fmoc: 9-Fluorenylmethoxycarbonyl

FR: Folate receptor

FSC: Forward scatter

Gal: Galactose

Glc : Glucose

GLUT-1: Glucose transporter 1

^{1}H-NMR: Proton nuclear magnetic resonance

HBSS: Hank's Balanced Salt Solution

HBSS*: Hank's Balanced Salt Solution with divalent cations

HBTU: hexafluorophosphate benzotriazole tetramethyl uronium

HBV: Hepatitis B virus

HCV: Hepatitis C virus

HCMV: Human Cytomegalovirus

HDAC: Histone deacetylases

HDIL-2: High-dose interleukin-2

HeLa: Henrietta Lacks

HER2: Human Epidermal growth factor Receptor 2

HIHS: Heat-inactivated human serum

HIV: Human immunodeficiency virus

HPV: Human papilloma virus

HRMS: High resolution mass spectrometry

HS: Human serum

HSV: Herpes simplex virus

HVH: Arg-Lys-Asp-His-His-Val-His-Leu-Pro-Asn-Asn-Gly dodecapeptide

Ig: Immunoglobulin

IFN: Interferon

IGTAV: integrin subunit alpha v

IL: interleukin

KLH: Keyhole limpet hemocyanin

LacNAc: N-Acetyl-D-Lactosamine

LHRH: Luteinizing hormone releasing hormone

LT : Leu-Ala-Arg-Leu-Leu-Thr hexapeptide

mAb: Monoclonal antibody

MAC: Membrane attack complex

MALDI-ToF: Matrix Assisted Laser Desorption Ionization - Time of Flight

MCF_7: Michigan Cancer Foundation-7

MDR: Multidrug-resistant

mTor: Mammalian target of rapamycin

MTT: mitochondrial dehydrogenase activity

Mw: Molecular weight

NaAsc: Sodium ascorbate

Nbs: Nanobodies

Neu5Gc: N-Glycolylneuraminic acid

NK: Natural killer

PARP: Poly (ADP-ribose) polymerase

PBMCs: Peripheral blood mononuclear cells

PBS: Phosphate buffer saline

PD-1: Programmed cell death protein 1

PE: Phycoerythrin

PEG: Polyethylene glycol

Pen: Penicillin

PFA: Paraformaldehyde

PMT: Photo multiplying tube

PSMA: Prostate-specific membrane antigen

PyBOP: (Benzotriazol-1-yloxy) tris (dimethylamino) phosphonium hexafluorophosphate

RAFT: Regioselectively Addressable Functionalized Template

Rha: Rhamnose

RNA: RiboNucleic Acid

RP-HPLC: Reversed Phase - High Performance Liquid Chromatography

RSV: Respiratory syncytial virus

Rt: Retention time

SAR: structure–activity relationship

Sia: Sialic acid

Sieglec: Sialic acid-binding immunoglobulin like lectins

SPAAC: Strain-Promoted-Azide-Alkyne Click Chemistry

SPPS: Solid phase peptide synthesis

SPR: Surface Plasmon Resonance

SrtA: Sortase A

SSC-A: side scatter – area

Strep: Streptomycin

SVF: Fetal bovine serum,

TAAs: Tumor-associated antigens

TBMs: Tumor Binding Molecules

tBu: tert-butyl

TFA: Trifluoroacetic acid

THPTA: tris(hydroxypropyltriazolylmethyl)amine

TIS: Triisopropyl silane

TLC: Thin Layer Chromatography

TLR: Toll like receptor

TNBS: Trinitrobenzene sulfonic acid

Trt: Trityl

uPAR: urokinase-type plasminogen activator receptor

UPLC-MS: Ultra performance liquid chromatography - mass spectrometer

VEGF: Vascular endothelial growth factor

VZV: Varicella zoster virus

Chapter I.

Introduction

I.1. Preface

Cancer remains one of the major causes of mortality worldwide. Despite the variety of anticancer treatments, the development of new approach remains of paramount importance to achieve higher efficiency with minimal side effects. Immunotherapy was recently revealed as a highly promising approach to fight cancer. In this context, our group started a project in 2015 whose objective is the development of Antibody Recruiting Molecules (ARMs) for cancer immunotherapy. These molecules are composed by two part: an Antibody Binding Molecule (ABM), able to recruiting endogenous antibody, and a Tumor Binding Molecule (TBM), able to selectively target tumor cells. ABMs and TBMs have been developed previously by two PhD students, Dr. Eugenie Laigre and Benjamin Liet. At this stage of the project, the objective of my thesis was to synthesize ARMs combining different previously identified ABMs and TBMs and evaluate their ability to mediate immune clearance of tumor. In this manuscript, we first provided an overview of cancers and ongoing treatments. Then we described ARMs developed to treat cancer, as well as other pathogens, such as bacteria and virus.

I.2. Overview of cancer

Cancer is a group of more than 100 diseases that involve the uncontrolled growth of cells. Although cancer can progress in any of the body's tissues, and each type of cancer has its unique features, the basic processes that produce cancer are quite similar in all forms of the disease. A proliferation of a single cell may lead to many abnormal cells. This tumor mass may remain within the tissue in which it originated (a condition called in situ cancer), or it may start to invade surrounding tissue (a condition called invasive cancer). An invasive tumor is said to be malignant, and these cells may spread into the blood or lymph to establish new tumors (metastases) to distant sites throughout the body. The cell alteration may be started by hereditary genetic factors and/or external agents: physical carcinogens, such as ultraviolet and ionizing radiation; chemical carcinogens, such as vinyl or benzyl chloride, naphthalene, formaldehyde, components of tobacco smoke, aflatoxin (a food contaminant), arsenic (a drinking-water contaminant); and biological carcinogens, such as infections from certain viruses, bacteria or parasites.

There were an estimated 3.91 million new cases of cancer (excluding non-melanoma skin cancer) and 1.93 million deaths from cancer in Europe in 2018. 53% (2.05 million) occurring in men and 47% (1.85 million) in women. The most common cancer sites in Europe were cancers of the female breast (523,000 cases), colorectal (500,000), lung (470,000) and prostate cancer (450,000). Lung cancer continued to be the most common cause of death from cancer in men (267,000, 24.8%) followed by colorectal (almost 130,000 deaths, 12.0%) and prostate (107,000, 10.0%) cancer. Breast cancer was the leading cause of death in women (138,000, 16.2%), followed by lung (121,000 deaths, 14.2%) and colorectal (113,000, 13.2%) cancers (Figure 1).[1]

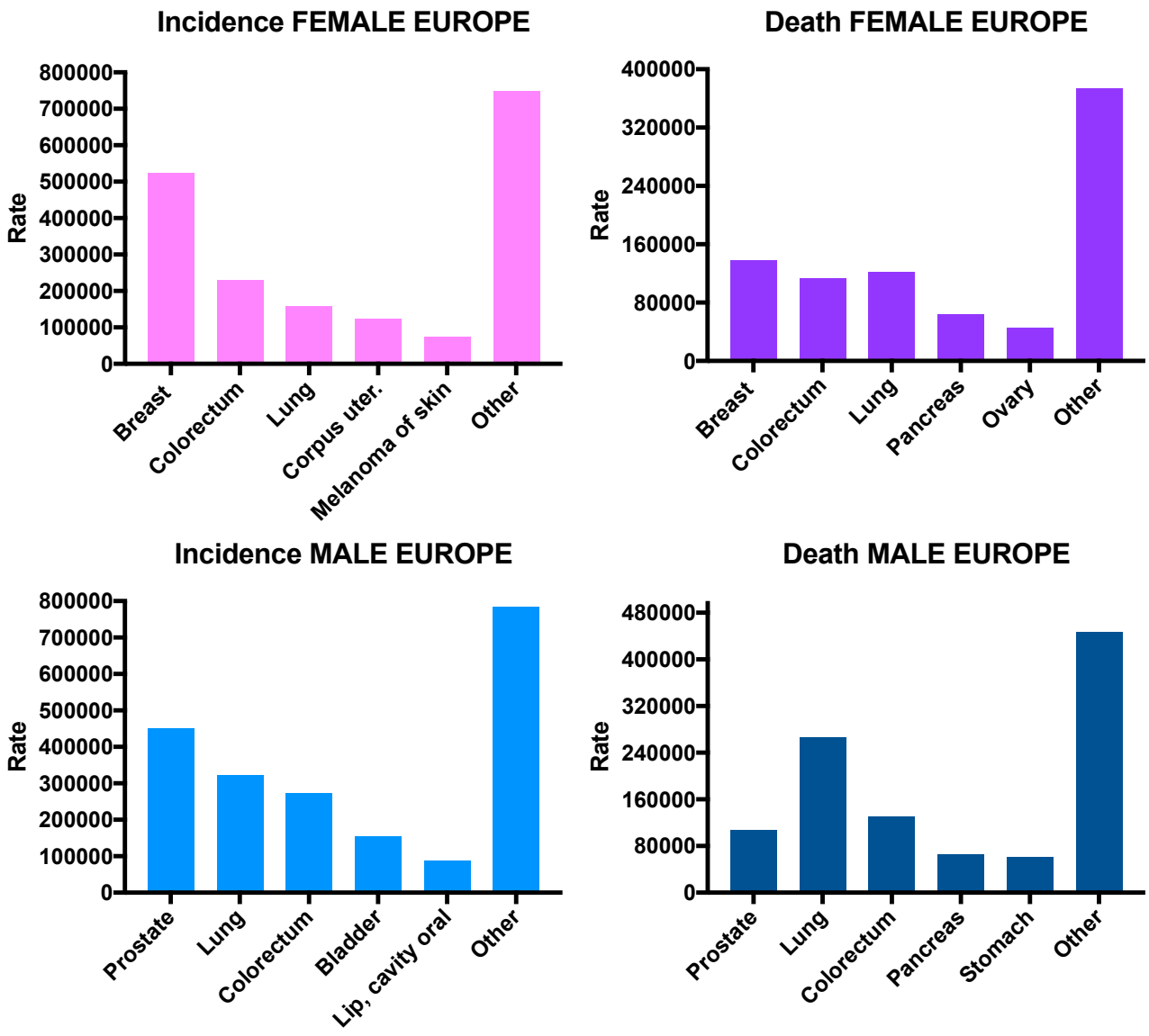

Figure 1 *Rate of cases and deaths for the 5 most common cancers in Europe 2018 for females and males (adapted from Ferlay and co-workers, Eur J Cancer, 2018).*[1]

I.3.Cancer treatments

Many cancers can be prevented by avoiding exposure to common risk factors, such as tobacco smoke. In addition, a significant proportion of cancers can be cured by several ways, especially if they are detected early. The main current cancer treatments are surgery, radiotherapy, chemotherapy, stem cells transplant and immunotherapy (Figure 2).

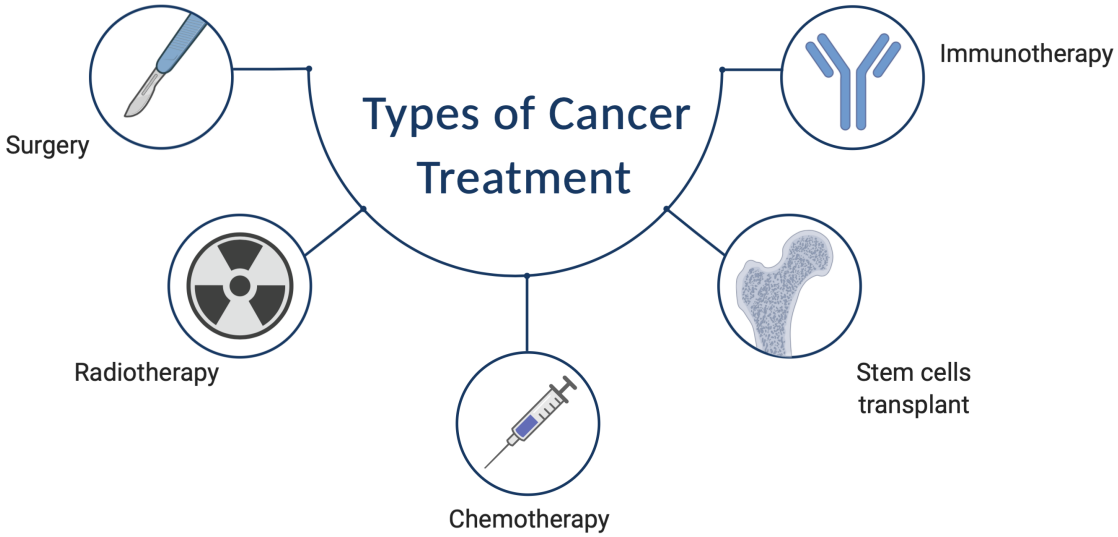

Figure 2 *Main current cancer treatments.*

Surgery is a procedure in which a surgeon removes cancer from the body. The 4 classical ways of performing surgery are cryosurgery, lasers, hyperthermia and photodynamic therapy. Surgery is a local treatment, meaning that it's more suitable for solid tumors that are contained in one area. Its commons problems are pain, infection but especially an increased formation of new metastatic foci (manipulation of tumor can result in at least a 10-fold increase in circulating tumor cells[7]) and an increased risk for accelerated growth of micrometastatic cells.[2] To successfully metastasize to a distant organ, cancer cells must reach the circulation, survive the host defensive mechanisms, mostly macrophages and natural killer (NK) cells, get entrapped at a regional or distant site, and finally invade the new site. Here they may form clinically undetectable micrometastases that can wait in a dormant equilibrium. This retarded growth of metastatic foci is known as concomitant tumor resistance. Upon removal of the primary tumor, the local and systemic inflammatory events associated with surgical trauma, such as reduced NK cytotoxicity and loss of macrophage function, could increase the levels of growth factors and of proangiogenic compounds and might be able to awaken and quickly grow the undetectable micrometastases.[3-5]

Often associated with surgery, **radiotherapy** relies on the use of high doses of radiation to treat pain caused by the tumor and to kill cancer cells by damaging their DNA, directly or by producing free radicals, in 2-3 weeks of treatment. There are two main types of radiation therapy, depending on many factors like the type, the size and the localization of cancer in the body: external beam therapy or brachytherapy. Both are expensive local treatments treating only a specific part of the body, with a machine sending radiation for the external beam therapy or with capsules that contain a radiation source placed near the tumor for the brachytherapy. Side effects

of radiation are related to close healthy cells damage even if cancer cells are less efficient in repairing their DNA damage, resulting in differential killing.[6,7]

Chemotherapy uses chemicals or drugs in order to slow the tumor mass growth, which grows and divides quickly, to ease cancer symptoms (palliative chemotherapy), to improve other treatments, for example to make a tumor smaller before surgery, or to kill cancer cells. There are several different classes of anticancer drugs based on their mechanisms of action, and they include the following: a) alkylating agents which damage DNA;[8] b) anti-metabolites that replace the normal building blocks of RNA and DNA;[9] c) antibiotics that interfere with the enzymes involved in DNA replication;[10] d) topoisomerase inhibitors that inhibit either topoisomerase I or II, which are the enzymes involved in unwinding DNA during replication and transcription;[11] e) mitotic inhibitors that inhibit mitosis and cell division;[12] f) inhibitors of protein kinase, a class of enzyme that promote phosphorylation;[13] g) aromatase inhibitors, one of the principal therapeutic approaches for estrogen receptor-positive breast cancer in postmenopausal women;[14] h) HDAC inhibitors, that inhibit Histone deacetylase enzyme induces DNA damage;[15] i) PARP inhibitors that inhibit Poly (ADP-ribose) polymerase enzyme that play a role in DNA repair pathways;[16] j) mTor inhibitors that inhibit the mammalian target of rapamycin involved in cellular regulation processes;[17] k) anthracycline that promotes creation of free radicals which destroy nucleic acids and other;[18] l) retinoids that elicit physiologic changes inducing cell differentiation, anti-proliferation, pro-apoptotic, and anti-oxidant effect;[19] m) vinca alkaloids that prevent cancer cells from successfully dividing by occupying microtubulin's building block structure;[20] n) corticosteroids.[21] Since single-agent chemotherapy is often not enough to treat tumors and given the development of drug resistance, the utilization of different combination of molecules is the standard clinical practice.[22] Side effects can mainly occur with chemotherapy because of the lack of selectivity between normal and cancer cells which is susceptible to damage both cell populations.

Stem cell transplants are very expensive, complicated and long procedures, that don't usually work against cancer directly. Instead, they help to restore blood-forming stem cells in people who had theirs destroyed by the very high doses of chemotherapy and/or radiation therapy. Stem cell transplants are most often used to help people with leukemia, lymphoma, neuroblastoma or multiple myeloma. [23]

I.4. Cancer Immunotherapy

I.4.A. Overview of immunotherapy

Immunotherapy, harnessing the immune system and the power of its antibodies, is the most important targeted cancer treatment. The antibodies (Abs) are glycoproteins belonging to the

family of immunoglobulins (Ig), produced by B lymphocytes (Figure 3 A). They are composed by two Fab fragments (Fab = Fragment, Antigen Binding) and by one Fc fragment (Fc = Fragment, crystallizable). The variable regions (contained in Fab) are responsible for antigen recognition, while the constant parts (contained in Fc), identical for all individuals of the same species, is responsible for the interactions with the immune system cells.[24] There are 5 isotypes of immunoglobulin (Ig) that differ from their Fc, their specific functions and their number of monomers (Figure 3 B). Among these, IgG and IgM are the key antibodies involved during an immune response. IgG are the most abundant Ig of the human serum (almost 80%). These antibodies, secreted as monomers, are located in the blood, tissue and placenta where they have a lot of functions, such as opsonization, complement activation and cytotoxicity. IgM are the main and the first produced Ig during the first week of infection. These antibodies, secreted as pentamers, are located only in the blood (due to large size) with agglutinative and complement activation activities.[25]

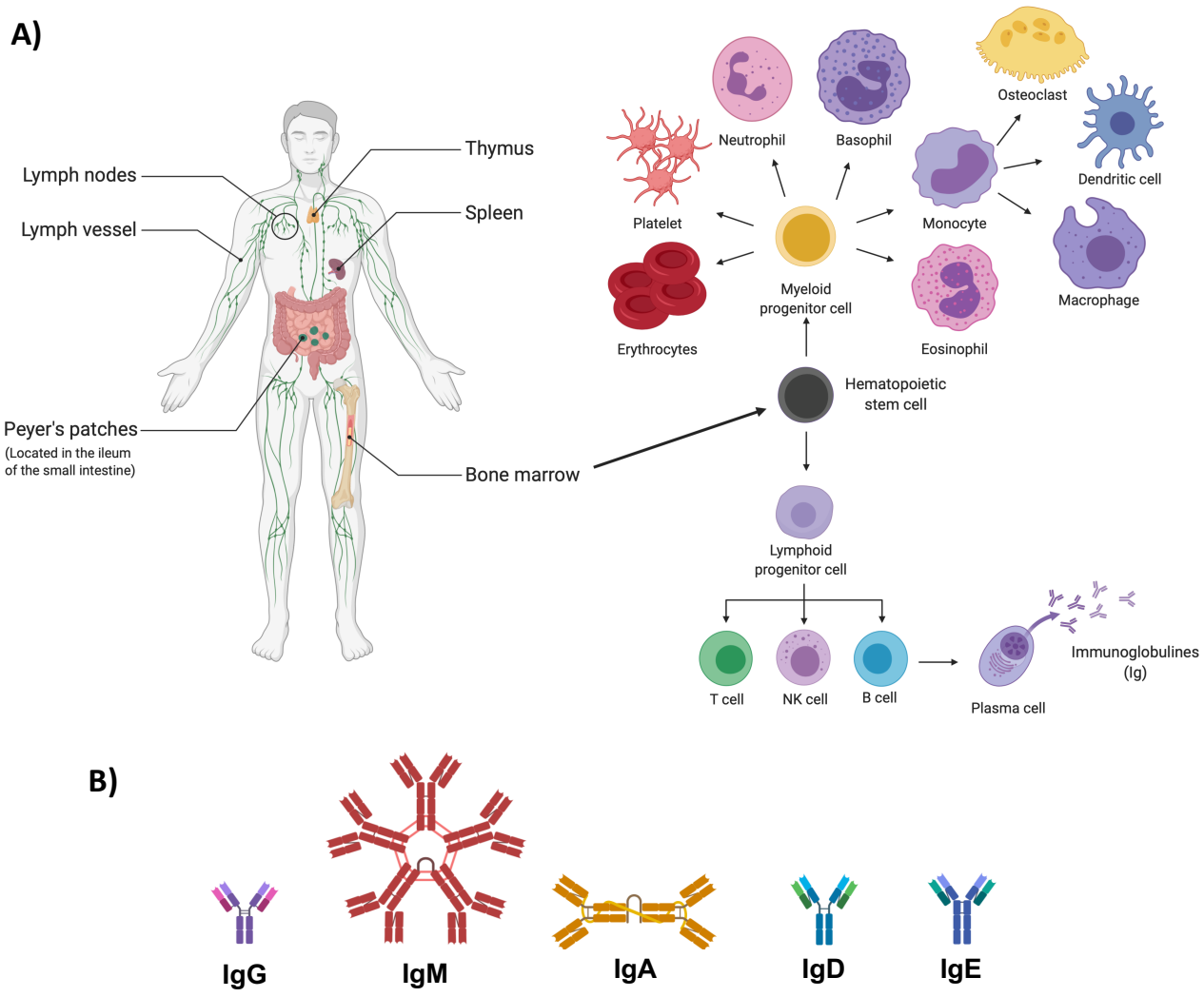

Figure 3 A) *Overview of immune organs and cells in the human body.* ***B)*** *The 5 isotypes of immunoglobulin (Ig) present on the human blood.*

Among the many immune responses, the most common effector mechanisms are antibody-dependent cellular cytotoxicity (ADCC), antibody-dependent cellular phagocytosis (ADCP) and complement-dependent cytotoxicity (CDC). ADCC is a cellular response where effector cells of the immune system (typically natural killer cells, but also monocytes, macrophages and mast cells), once bounded the Fc region through a specific receptor, release substances such as perforins, causing the lysis of the cell (Figure 4 A). ADCP is a cellular response involving the action of macrophage effector cells recognizing the Fc part of the antibodies. When they recognize the antibody, a signaling pathway is activated which causes phagocytosis of the target cell by internalization in a phagosome. Here mature lysosomes will degrade the cell (Figure 4 B). CDC is a humoral response involving a complement system, plasma proteins produced by the liver, normally present in inactive form. When an antibody/antigen complex is formed, the C1q complement protein bounds the Fc region on the antibody. This activation triggers a cascade of events involving several other complementary proteins such as the Membrane Attack Complex (MAC) that will induce the release of proteolytic agents generating pores on the cell membrane. The cell is thus destroyed by osmotic shock (Figure 4 C). It's worth noting that the activation of the immune system is possible only if the Fab region has recognized the antigen. [26]

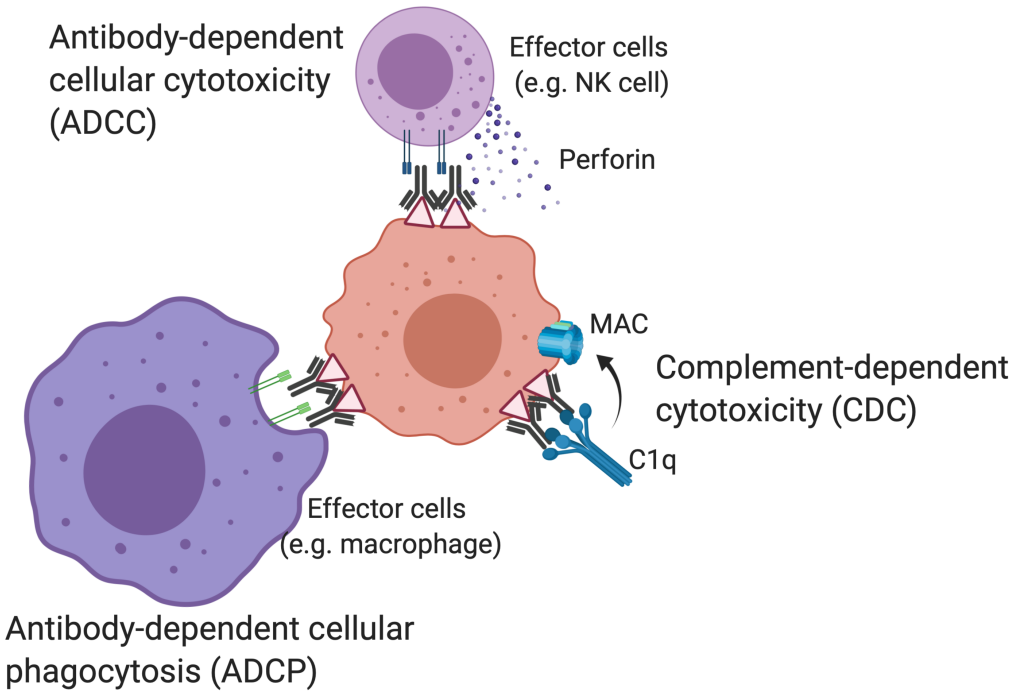

Figure 4 *Possible effector functions of immune system. ADCC: antibody-dependent cellular cytotoxicity. NK: natural killer cell ADCP: antibody-dependent cell-mediated phagocytosis,* ***C)*** *CDC: complement-dependent cytotoxicity. MAC: Membrane Attack Complex.*

As opposed to surgery, chemotherapy, or radiation therapies that are non-specific treatments, immunotherapy is a specific approach that can reach tumor areas where the others cannot and thus many side effects can be avoided. Tumor-associated antigens (TAAs) were identified in the 1990s and represent interesting moieties for targeted therapy.[27] They can be classified into two major groups: 1) Antigens which are present on healthy tissue but are over-expressed in cancer, often because they provide a growth advantage to the cell; 2) Neo-antigens from somatic mutations in cancer.[28]

The origins of immunotherapy date back as far as 1774, when a Parisian physician injected pus into the leg of a patient with advanced breast cancer and subsequently observed tumor regression as the infection worsened.[29] Administration of interleukin-2 (IL-2), a cytokine known for stimulating T-cell proliferation, is another earliest approach tested for cancer treatment and IL-2 is one of the oldest immune based drug approved for the treatment of cancer.[30] However, the first generation of immunotherapies were limited by low response rates and high incidence of serious adverse events. Today, several types of immunotherapy are used to treat cancer, such as immune checkpoint inhibitors, T-cell transfer therapy, cytokines, vaccines, and immune system modulators.

I.4.B. Immune checkpoint

Immune checkpoint are proteins expressed on the surface of T cells that, interacting with Antigen-Presenting Cells (APC), are crucial for maintaining physiological immune responses in order to minimize collateral tissue damage. Tumors hijack certain immune checkpoint pathways as a major mechanism of immune resistance. Strategies to activate T cells against tumors may include targeting of both inhibitory and activating receptors, resulting in a robust and durable antitumor immune response. Among the checkpoints, cytotoxic T-lymphocyte associated protein 4 (CTLA-4) and programmed cell death protein 1 (PD-1) are the most reliable targets for advanced cancers, both found on surface of T cell. Therefore, blocking CTLA-4 or PD-1 binding can increase antitumor immunity.[31] The impact of CTLA-4 and PD-1 blockers on cancer research and their success in cancer treatment is acknowledged by researchers as well as clinicians worldwide. The Nobel Prize in Physiology or Medicine for 2018 was indeed awarded to Professor James Allison, MD Anderson Cancer Center, USA and Professor Tasuku Honjo, Kyoto University, Japan for their research on CTLA-4 and PD-1 respectively.[32] However, while checkpoint blockade is universally effective against a broad spectrum of cancer types, only a minority of patients achieve a complete response and sometimes with autoimmune toxicities, due to the release of autoimmune T cell responses against healthy host tissue.[33]

I.4.C. Adoptive T cell therapy (ACT)

Another methodology within cancer immunotherapy is the adoptive T cell therapy (ACT). Using this approach, tumor - specific cytotoxic T cells are collected from a patient's blood or tumor,

then isolated, stimulated and expanded *in vitro*. After sufficient *in vitro* expansion, these cells are reinfused into the patient, with the goal of recognizing, targeting, and destroying tumor cells. Since all the process is very expensive and the anti-tumor response cannot be used broadly due to the specificity of T cells, ACT represents a powerful approach to expand the benefits of cancer immunotherapy when other therapies fail.[34]

I.4.D. Cytokines

Cytokines are key proteins for the activity of immune and blood cells.[35] Although many different types are dominant factors in cancer immunotherapy, only few cytokines have been approved for the treatment of malignancies because of sometimes severe toxicities. Interferon alpha (IFN α) is approved for adjuvant treatment of completely resected high-risk melanoma patients and several refractory malignancies. High-dose interleukin-2 (HDIL-2) is approved for treatment of metastatic renal cell cancer and melanoma.[36] Granulocyte-macrophage colony-stimulating factor (GM-CSF), IFN gamma (IFN γ), IL-7, IL-12, and IL-21 are part of certain investigational trials. To circumvent toxicity and to increase cellular responses and anticancer efficacy, engineered cytokine mutants (superkines)[37] and chimeric antibody-cytokine fusion proteins (immunokines)[38] were clinically investigated and proposed as a predictive tool for cancer progression.

I.4.E. Therapeutic vaccines

Therapeutic vaccines represent a possible option for active immunotherapy of cancers that aim to treat the disease in complement of surgery for example or to generate prophylaxis and long-lasting protective antitumor immunity. The goal of therapeutic cancer vaccines is to induce tumor-specific immunoreactivity *in vivo* by using a patient's own immune system. To this aim, preselected antigens are presented encoded in viral vectors, on antibody delivery vehicles, or administered as peptides or proteins in a suitable adjuvant and carrier. Adjuvants are usually co-injected with the antigen to regulate the quality and quantity of adaptive immune responses at the injection site, improving the total antibody amount, reducing the antigen dose and increasing the speed and duration of the protective response. To date, there are numerous adjuvants divided into exogenous compounds as inorganic chemicals, mineral oil, bacterial products, non-bacterial organics, plant saponins, Freund's complete or incomplete adjuvants and endogenous adjuvants such as cytokines, chemokines, alarmins and toll like receptor (TLR) ligands.[39,40] Although therapeutic cancer vaccines have been evaluated for over two decades, the FDA has approved only one therapeutic DC-based cancer vaccine, Sipuleucel-T (Provenge™), for the treatment of metastatic resistant prostate cancer.[41] However, if this vaccine was shown to stimulate high titers of IgG and IgM, no satisfactory antitumoral response could be observed.

I.4.F. Monoclonal antibody-based immunotherapeutic

Another immunotherapy strategy to treat cancer is based on immunomodulators, chemicals or biologicals, that boost or re-active to the immune system which was silenced by the tumor cells by several mechanisms such as production of genetic mutations and expression of surface proteins.[42] Monoclonal antibody-based immunotherapeutic relies on the utilization of specific antibody to target pathogen. A specific monoclonal antibody is produced by a specific B cell fused with transformed cells (myeloma cells) to acquire the ability to live for a longer time. Many of the resulting hybrid cells (or hybridomas) are grown *in vitro*, and are able to produce large amounts of the monoclonal antibody (mAb).[43] The selection of tumor antigens suitable for antibody targeting and therapy requires a comprehensive analysis of normal and tumoral tissue expression, as well as an understanding of the biologic role of the antigen in tumor growth. If the desired mechanism of action is engagement with cell surface receptors (to either activate or inhibit signaling), or to activate ADCC, CDC or ADCP, then it is desirable that the antigen-mAb complex is not rapidly internalized. This allows the maximization of the availability of the Fab region to appropriately engage with surface receptors, and of the Fc region to immune effector cells and complement proteins. In contrast, internalization is desirable for antibodies or proteins delivering toxins into the cancer cell and for antibodies whose action is primarily based on downregulation of cell surface receptors.[44]

There are three classes of immunotherapeutic mAbs depending on whether or not they carry drugs or radioactive substances. The first class is self-acting, non-conjugated, naked mAbs directly targeting antigens on cancer cells while the second class is mAbs conjugated with chemotherapeutic drugs or radioactive particles. In addition, there are bispecific antibodies (bsAb) that contain two different mAbs and can bind two different antigens at the same time, allowing to better affinity and the selectivity versus targets.[45] Although this different mechanisms of action, mAbs are often used in combination with chemotherapy and/or radiotherapy, and to date, the main types of cancer targeted by mAbs are breast, colon, lymphomas and others.[46] Nevertheless, mAbs-based therapeutics treatment suffer from multiple side effects such as fatigue, headache and muscle pain, nausea/vomiting to heavier as difficulty breathing, systemic inflammatory response syndrome, IgE-mediated acute anaphylactic reactions, serum sickness, cytokine release syndrome. Other limitation of mAb include their high molecular weights and a lack of oral bioavailability, difficulties in characterization and standardization, because individual can express different allelic variants of Fc receptors, and high costs.[47,48] In addition, antibody−toxin conjugates are associated with other drawbacks such as premature drug release arising from antibody−drug linker instability, which can lead to toxic effects in normal tissues, and identification of drug conjugation optimal levels; low loadings may render treatment ineffective, whereas high loadings may lead to excess toxicity or a loss of antigen specificity.[49]

I.5. General overview of Antibody Recruiting Molecules (ARMs)

To overcome monoclonal antibody-based immunotherapeutic issues, researchers started producing low molecular weight species including Antibody Recruiting Molecules (ARMs). An ARM is a molecule able to form a ternary complex with the target cell and with antibodies. Once formed, the immune cells or proteins can start an immune response destroying that target cell (Figure 5). In addition, ARMs are generally easier to produce, optimizable for oral bioavailability and less or not toxic. Historically, several ARMs were created to target cancer and pathogens.[50,51] Although traditional small-molecule-based antibacterial and antiviral therapeutics have also shown high efficacy, their utility has been hampered by resistance, i.e. bacteria against antibiotics. Therefore ARMs represent attractive therapeutic alternatives using the immune system. In the following sections we provide an overview of ARMs to treat cancer (I.5.A.) and pathogens (I.5.B.), such as bacteria, virus and fungi.

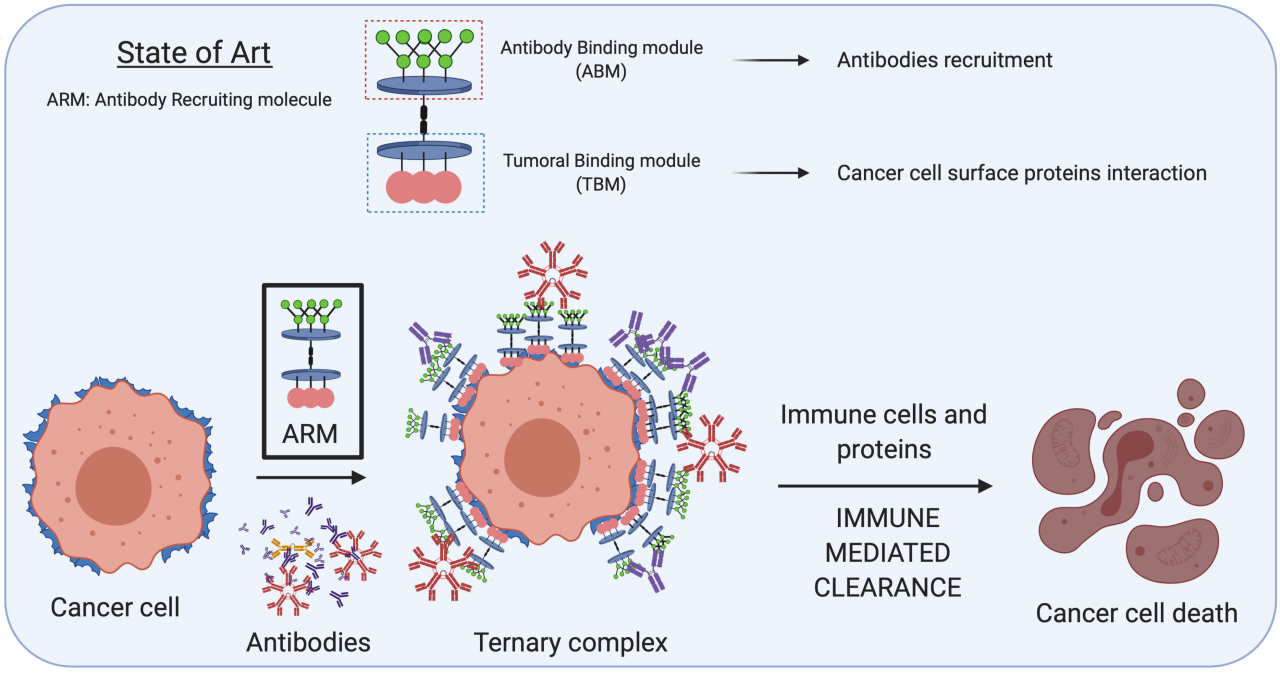

Figure 5 *ARMs are bifunctional small molecules leading to immune-mediated destruction of disease-causing species by forming ternary complexes with targets and antibodies.*

I.5.A. Antibody Recruiting Molecules (ARMs) to treat cancer

Since the 2000s, researchers regularly promoted ARMs development to treat cancer. Two categories of molecules were elaborated within this framework: “small” synthetic molecules and “large” semi-synthetic conjugates (TBM conjugated with antibodies). Unlike the first approach whose strategy is to link ABMs and TBMs basically composed of small organic molecules, the second approach effectively combines the function of definite small molecules (e.g. TBM) and peptides with the long serum half-life of an antibody into one unique therapeutic.

I.5.A.I. “Small” synthetic molecules

Paulson and colleagues were among the first investigators to demonstrate the power of small molecules targeting CD22, an important “taggable” protein in immunotherapy, that is a specific sialic-acid-binding immunoglobulin-like lectin (Siglec) found on B cells, with signal and cell adhesion regulatory functions, that are modulated by interaction with glycan ligands bearing the sequence NeuAcα(2–6)Galβ.[52] Since this CD22 is overexpressed in malignant B cells, blocking this protein or its interactions could be important to treat B cell lymphomas, autoimmune diseases and other hematopoietic malignancies. Since all carbohydrate binding proteins including CD22 have low intrinsic affinity that for its native ligands ($K_d \approx 0.2$ mM), only highly multivalent synthetic ligands could compete with natural ligands and bind native B cells. Reports from the Paulson and Bundle groups have divulged a class of ARM containing the natural CD22 glycan ligand as TBM, NeuAcα(2–6)Galβ(1–4)GlcNAc, modified at C-9 position of neuraminic acid with biphenyl-carbonyl amido (BPC) substituent, which is known to increase affinity for CD22 by 100 fold. On the other side, the small molecule hapten dinitrophenyl (DNP) moiety was used as ABM to bind endogenous anti-nitrophenol (anti-NP) antibodies.[53] DNP is one of the first small and easily manipulating hapten for immunological investigations. This nitroarene motif (not naturally present in human) binds endogenous anti-nitrophenol antibodies ($K_D = 1$ µM), resulting by an exposure to products as wood preservative and pesticide.[54] However, the presence of nitroreductases in the bloodstrem limit its use. At the end, this bifunctional molecule was able to efficiently drive assembly of antibody-CD22 complexes on the surface of native B cells; not only high valency decavalent IgM (n=10), but also anti-NP antibodies of lower valency, such as IgA (n =4) and IgG (n =2), were found to drive complex formation (Figure 6 A). Furthermore, bi-functional ligands with linkers of different length and/or with a heterocyclic triazole ring were synthesized and investigated (Figure 6 B).

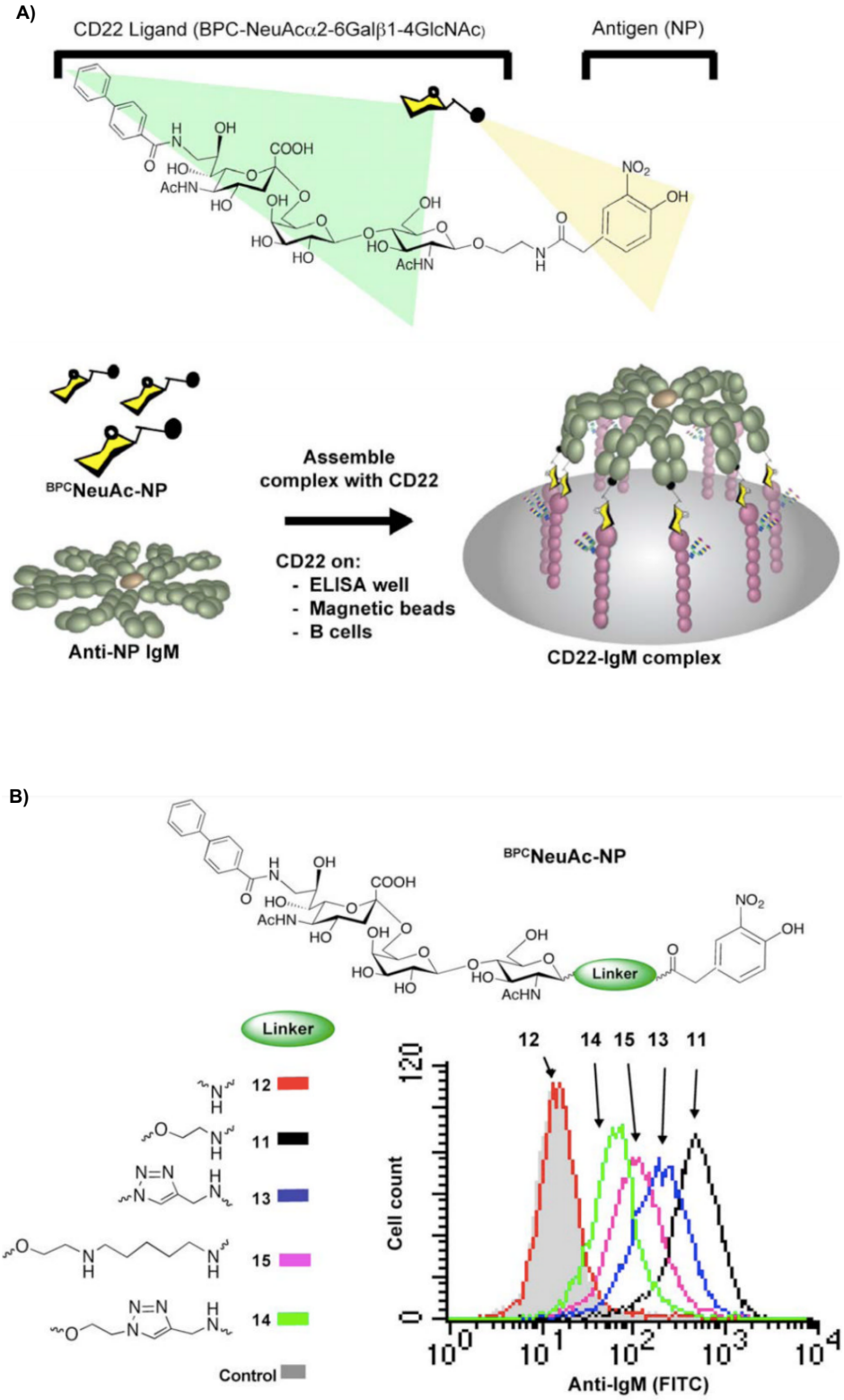

Figure 6 A) *Structure of the bi-functional ligand, BPCNeuAc-NP and representation of the ligand-driven complex formation between the decavalent scaffold, anti-NP IgM, and the B cell surface lectin CD22 on either B cells or on solid magnetic beads decorated with the extracellular domain of CD22.* ***B)*** *Influence of linker structure in bi-functional ligand driven assembly of IgM-CD22 complexes on B cells. Binding of anti-NP IgM was analyzed by flow cytometry following staining with anti-IgM (FITC) (adapted from Paulson and co-workers,. J Am Chem Soc. 2008).*[52]

The flow cytometry analysis revealed higher capacity of the ligands bearing smaller and short triazole linkers to form complexes on native B cells, with the exception of the shortest linker, which may impose steric constraints between IgM and CD22. The longer linker between the ligand and antigen (NP) reduces the ability of the bi-valent ligand to mediate formation of a ternary complex between these two multivalent proteins due to the loss of conformational entropy. Subsequent studies demonstrated that increases in TBT valency, through polyvalent heterobifunctional ligand conjugation to a polymer support, allow to 100-fold higher levels of anti-NP IgM recruitment to target B-cells versus negative controls lacking the terminal neuraminic acid moiety.[55]

Between 2002 and 2007, the Low group demonstrated the efficacy of ARM *in vivo* and the importance of T cells in tumor eradication.[56-59] They have developed ARMs targeting the folate receptor (FR), a cell-surface protein upregulated in many cancers, as ovary, cervix, endometrium, kidney, breast, brain, lung, myelocytic cells, and mesothelium.[60-62] ARMs were composed by folic acid (FA) at the TBT and either fluorescein (FITC) or DNP at the ABT (Figure 7).

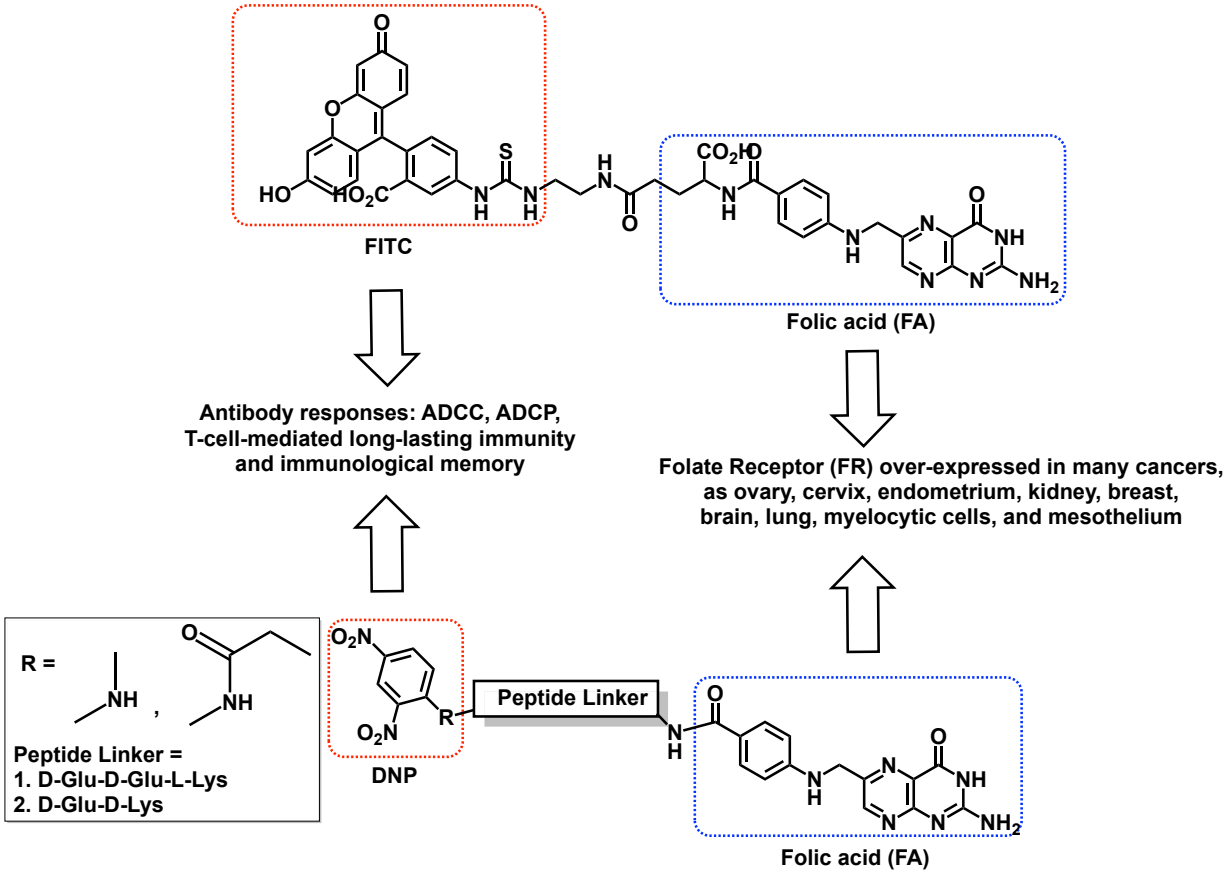

Figure 7 *FA–FITC or FA-DNP ARMs structure. FA: Folic acid. DNP: 2,4-Dinitrophenol. FITC: Fluorescein isothiocyanate.*

The cytotoxic tests were performed in M109 (syngeneic lung cancer model) tumor bearing wild-type female BALB/c mice. To generate anti-FITC antibodies, mice were preimmunized with BSA–FITC in TiterMax Gold, a non-ionic block co-polymer surfactant known to stimulate a strong and prolonged antigen specific IgG response in experiments with animals. Flow cytometry tests indicate that anti-FITC IgG antibodies are capable of recognizing the hapten on folate–FITC molecules already bound to FR on cancer cell surfaces, inducing their opsonization. In addition, this therapy didn't show any type of toxicity since toxicology studies reveal no damage to healthy tissues. Treatment with fluorescein-folate construct generated a modest improvement in median survival compared to control. Notably, this ARM co-administered with IL-2 enhanced median survival by 250% and co-administration of with both IL-2 and IFN-γ enhanced survival by at least 300%. In addition, it was demonstrated that these antitumor effects resulted from ADCP and ADCC mechanisms, and substitution of the fluorescein group with DNP have similar efficacy in these mice models. It's worth noting that the therapeutic efficacy is described by a bimodal concentration dependence (Figure 8 A): little efficacy was observed at low FA-FITC concentrations (due to an insufficient number of folate-FITC bridges) and at high FA-FITC (due to saturation of both ligands for the bridge, i.e., IgG and FR) (Figure 8 B), while high therapeutic activity occurred at intermediate FA-FITC concentrations.

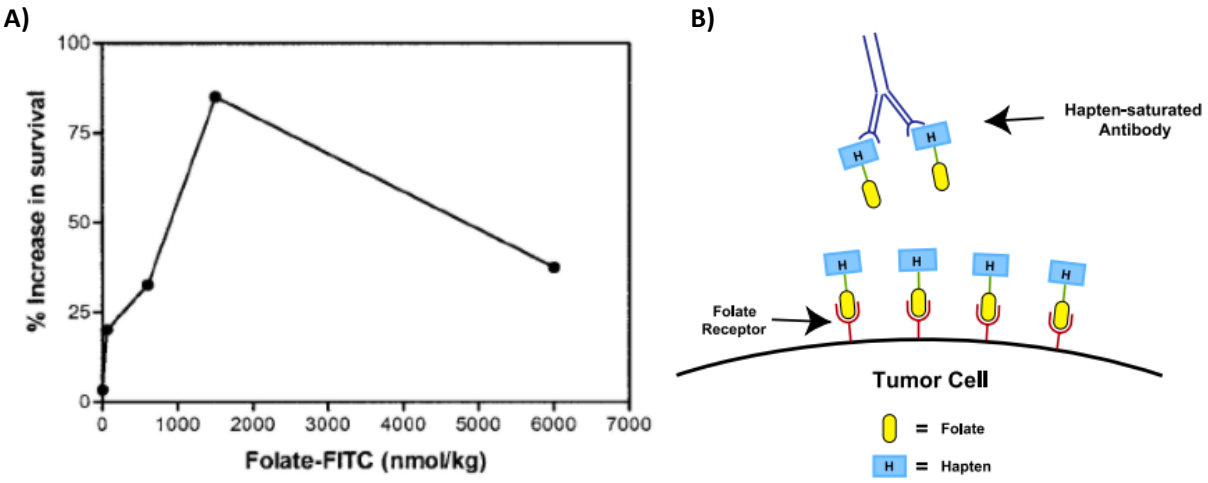

Figure 8 A) *Bimodal folate-hapten-targeted concentration dependence. KLH-FITC/TiterMax Gold-immunized mice (4 per group) were implanted intraperitoneally M109 tumor cells. Folate-FITC (0–6,000 nmol/kg) was administered with IL-2 (5,000units/day) and IFN-a (25,000 units/day). The percent increase in survival is calculated relative to that of a PBS-treated control. (adapted from Low and co-workers, Int J Cancer, 2005)*[58] ***B)*** *Folate – hapten saturation of both tumor-associated FRs and anti-hapten IgG at 6000 nmol/Kg ARM. Administration of folate – hapten at very high doses may simultaneously saturate both circulating anti-hapten antibodies and tumor surface FRs. Unbound material competes with the ternary complex, driving the system toward formation of binary complexes and preventing the ''bridging'' of anti-hapten antibody to FR positive tumor (i.e. opsonization would not occur). This self-antagonistic behavior in*

ARM-mediated cytotoxicity experiments is the confirmation that cell killing proceeds via reversible formation of a ternary complex. Additionally, from a clinical perspective, ARM are auto-inhibitory, and could serve clinically as the antidote for their own overdose (adapted from Low and co-workers, Adv Drug Deliv Rev. 2004).[57]

In 2007, Kiessling and co-workers were the first group to synthesize an ARM harnessing the ability of α-Gal carbohydrate antigen to recruit natural circulating anti α-Gal antibodies.[63,64] α-Gal carbohydrate antigen is present in most mammalian and bacterial cell surfaces, but not in human cells because they lack the functional glycosyltransferase that catalyzes the assembly of this structure. Consequently, constant exposure to α-Gal found on red meat or on bacteria within the normal intestinal flora elicits high level of anti-Gal antibody in humans (2% of the total IgG and 3–8% of the total IgM circulating in the bloodstream).[65-69] Like many carbohydrate-binding proteins, anti α-Gal antibodies interact weakly with a single α-Gal epitope (K_d ~ 1 μM) but this interaction become stronger once multiple copies of these epitopes are presented (multivalent effect, K_d ~ 10^{-5} μM).[70] Since the trisaccharide Galα(1–3)Galβ(1–4)Glc was indicated as the simplest α-Gal carbohydrate antigen able to recruit endogenous anti-αGal antibodies, Kiessling group synthesized an ARM composed by this trisaccharide as ABM, and by an RGD (Arg-Gly-Asp) peptidomimetic moiety, known to be an excellent $\alpha_v\beta_3$ integrin ligand (K_d ~ 10^{-3} μM).[71,73] Additional surface-bound studies have shown that the linker between this ABM and TBM should to be approximately 20 Å (at its full extension) to provide adequate separation between the two partners and to have an efficient interaction with target cells and antibodies (Figure 9).[74]

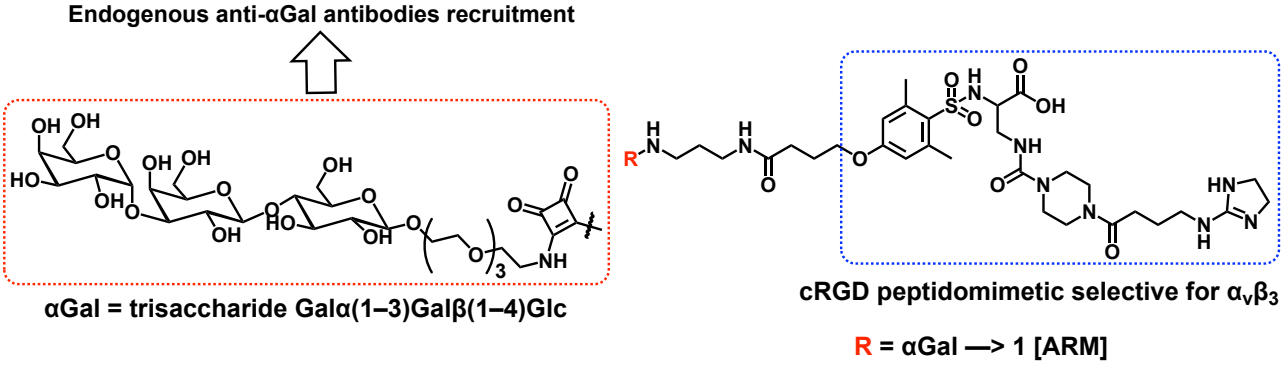

Figure 9 *cRGD peptidomimetic was functionalized with α-Gal carbohydrate epitope to get ARM.*

Several biological tests were carried out. Firstly, using saturating concentration of a fluorescent integrin ligand (Figure 10, R=FITC), it was determined the expression level of $\alpha_v\beta_3$ integrins on surface of M21 and WM115 which displayed more than 100,000 receptors per cell.

Then, ARM was incubated in presence of MCF7 human breast carcinoma cells (presenting low levels of $\alpha_v\beta_3$ and high levels of $\alpha_v\beta_5$ integrins) in order to demonstrate its $\alpha_v\beta_3$ selectivity. The selectivity was demonstrated since any replacement of vitronectin, natural ligand for this receptor, was revealed. Next, to evaluate the potency and affinity for $\alpha_v\beta_3$, inhibition ability of the selected ARM was confirmed against WM115 cells, an $\alpha_v\beta_3$-positive human melanoma cell line. At this point, in order to measure the anti-α-Gal antibodies recruitment titer, ARM was incubated against $\alpha_v\beta_3$-positive WM115 and M21 cells line and MCF7 human breast carcinoma cells line, with human serum as unique source of anti-Gal IgG. After treatment with a fluorescein-labeled anti-IgG secondary antibody, flow cytometry analysis has indicated that no anti-α-Gal antibodies binding could be detected in the absent of ARM or in MCF7 cells, while a significant increase in the anti-α-Gal antibodies IgG and IgM binding occurred with WM115 and M21. Subsequent cytotoxic study was finally performed between this selected ARM and another ARM which its α-Gal trisaccharide part was replaced by doxorubicin (DOX), a drug able to induce apoptosis in the tumor vasculature (Figure 10, R=DOX).[75,76]

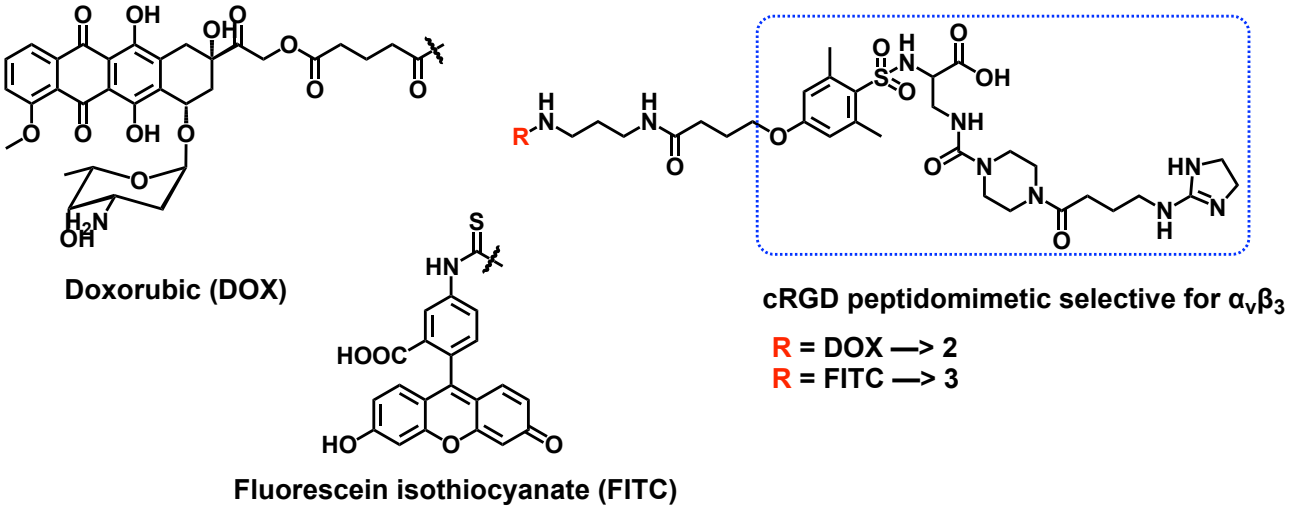

Figure 10 *cRGD peptidomimetic was functionalized with a cancer chemotherapeutic (DOX) or a fluorophore (FITC).*

Treatment with the DOX conjugate resulted in about 50% cell death, irrespective of the levels of $\alpha_v\beta_3$ integrin. Conversely, ARM, since relies on multivalent interactions, was about 60% cytotoxic only to cells presenting high $\alpha_v\beta_3$ levels (no complement-mediated destruction was not observed with others low $\alpha_v\beta_3$ levels cell types) (Figure 11 A). Additional control treatments such as 1) ARM lacking α-Gal epitope and human serum, 2) ARM with heat-inactivated HS (HIHS), and 3) ARM with human serum but in the presence of an anti-CD55 function-blocking antibody (CD55 is the most involved receptor in complement activation in relation to anti-α-Gal [77,78]) showed no activity in cell killing. These data suggest that this ARM exhibits excellent cell-targeting selectivity

and provides effective complement-dependent cytotoxicity using human serum. In addition, α-Gal ARM, opposed to DOX ARM, shows clear concentration dependence (Figure 11 B).

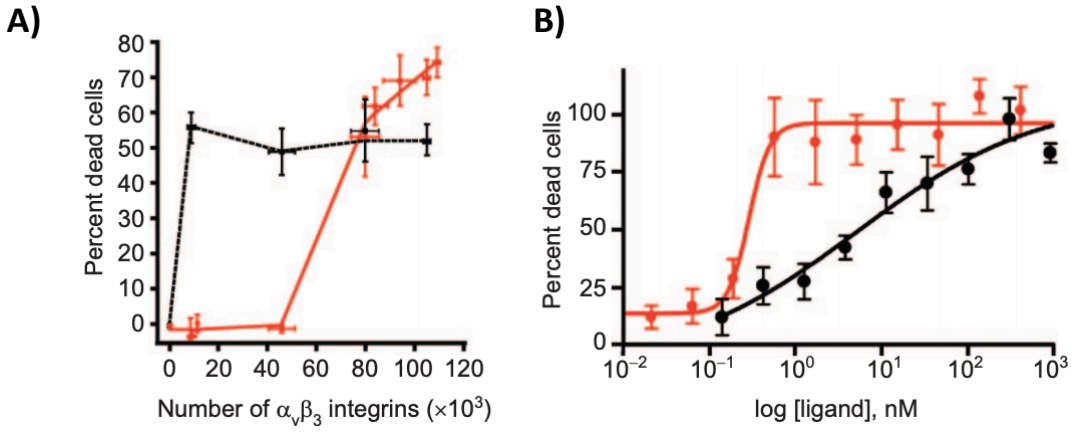

Figure 11 A) *The red curve described α-Gal ARM behavior results in selective lysis of cell lines with high levels of the target receptor. Inversely, the dashed black curve described the DOX ARM behavior results in not selective lysis* ***B)*** *Dose response curves for α-Gal ARM (red) and DOX ARM (black) (adapted from Kiessling and co-workers, ACS Chem Biol. 2007).*[63]

In 2009, Spiegel laboratory developed the first class of antibody-recruiting molecules targeting prostate cancer cells, called ARM-Ps.[79,80] This is achieved by binding simultaneously anti-dinitrophenyl (anti-DNP) antibodies and prostate-specific membrane antigen (PSMA), a membrane-bound glycoprotein overexpressed in most subtypes of prostate cancer cells,[81] as well as in the neovasculature of many solid tumors (e.g., glioblastoma multiforme, bladder cancer, gastric and colorectal cancer).[82-84] ARM-Ps contain glutamate urea moiety capable of inhibiting PSMA. ARM-P4, ARM-P6, ARM-P8 and ARM-P12 (containing 4, 6, 8 or 12 oxyethylene units in the linker) derivatives were synthesized and biologically assessed by flow cytometry assays with Alexafluor-488 conjugated anti-DNP antibodies (Figure 12).

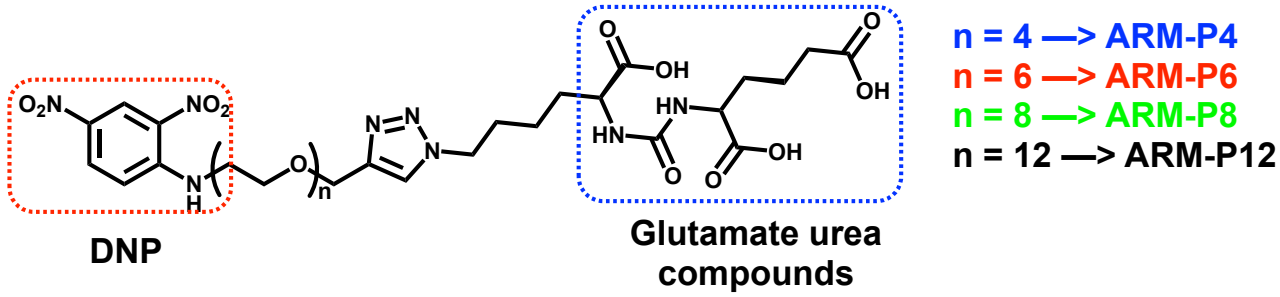

Figure 12 *Bifunctional ARM-Ps developed by Spiegel group.*

FACS results highlighted that ARM-P4 and ARM-P6 create unfavorable steric interactions between antibody and PSMA, even if ARM-P4 have demonstrated the highest affinity in PSMA binding assays. Conversely, ARM-P8 allowed the higher recruitment of antibodies (green curve - Figure 13 A). Once established that ARM-P8 represented optimal compromise between affinity to PSMA and ability to form ternary complex, its ability to induce cell-mediated cytotoxicity against androgen-sensitive human prostate adenocarcinoma cells (LNCaP) or DU145 cells (negative control) was assessed after preimmunization with the immunogen keyhole limpet hemocyanin (KLH)[85]. An important cytotoxic value was found only when ARM-P8 was incubated with LNCaP cell and only in presence of peripheral blood mononuclear cells (PBMCs) and anti-DNP antibodies, with an ADCC mechanism. Any cytotoxicity was observed against DU145 cell lines or in the absence of PBMCs (Figure 13 B). Remarkably, as already observed in various situations with ARMs, the bell-shaped curve observed in ADCC measurements with ARM-P8 results from the simultaneous saturation of both circulating anti-DNP antibodies and tumor surface receptors PSMA. This self-antagonistic behavior of ARM-P8 is characteristic of a reversible formation of a ternary complex.

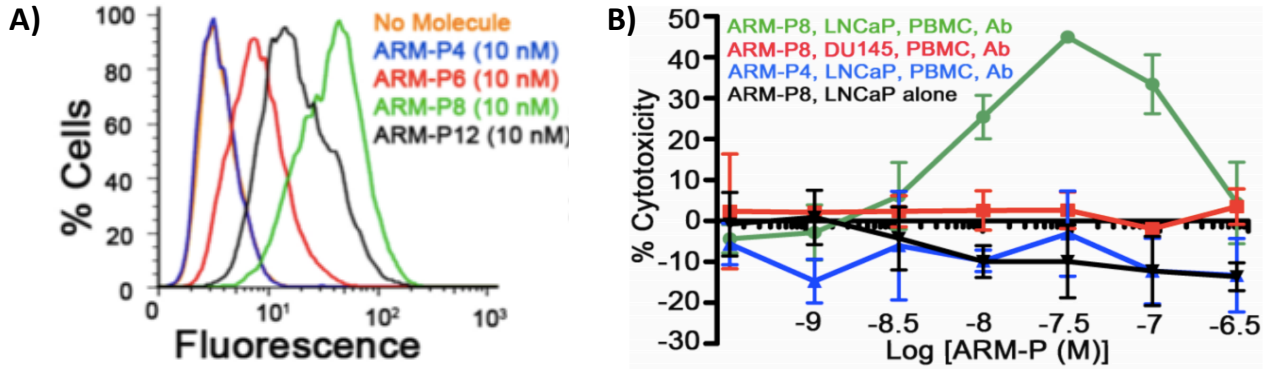

Figure 13 A) *Flow cytometry signals show that ARM-P8 is the best to form ternary complex between PSMA and anti-DNP antibodies, resulting in recruitment of secondary fluorescent antibody.* ***B)*** *Antibody-Dependent Cellular Cytotoxicity (ADCC) Assays. LNCaP cells: androgen-sensitive human prostate adenocarcinoma cells (positive in PSMA); DU145 cells: control cells negative in PSMA; PBMC: peripheral blood mononuclear cells (source of antibodies) (adapted from Spiegel and co-workers, J Am Chem Soc. 2009).*[79]

Several reports show that high levels of urokinase-type plasminogen activator receptor (uPAR) and its ligand urokinase-type plasminogen activator (uPA) are found in malignant cancer, such as breast, colon, stomach, and bladder, and may be used as diagnostic markers for metastatic cells. Specifically, uPA binds uPAR on the extracellular surface of cancer cells, begins the invasive process breaking down extracellular matrix proteins and actives the migration-inducing signal transduction cascades.[86,87] In this contest, researchers in the Spiegel laboratory

synthesized an ARM, called “ARM-U”, which can bind uPA by means of a chloromethyl ketone moiety, forming a 1:1 covalent complex and turning uPAR into inactive (Figure 14). FACS studies demonstrated that the ARM-uPA complex, triggered through the active site of uPAR-expressing A172 human glioblastoma cells, leaded to an high recruitment of anti-DNP antibodies from human serum, without pre-immunization.[88] Through computational, docking and SAR studies, it was discovered that ARM modification on uPA’s active site didn’t perturb its binding ability. Thus, in 2016, Spiegel and coworkers developed the second generation, low-molecular weight ARM-U derivative, termed ARM-U2 (Figure 14).[89,90] It is composed of an DNP moiety as ABM and an analogue of IPR-803 as TBM, an uPAR inhibitor,[91] and functionalized with PEG linker to drive solvent exposure of the ABM. The advantage is that ARM-U2 targets directly uPAR (on the uPA binding site), as opposed to ARM-U, that target uPA and the resulting complex subsequently target uPAR.

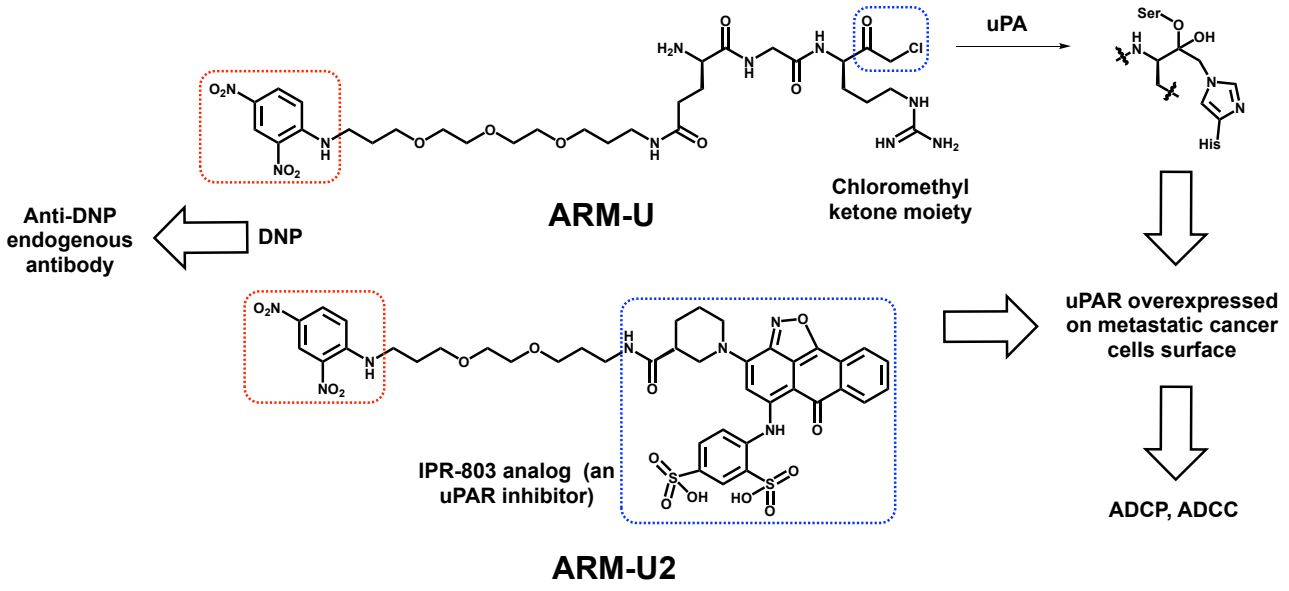

Figure 14 *ARM-U and the second generation ARM-U2 developed by Spiegel and co-workers.*

Tested on uPAR-expressing A172 glioblastoma cells, ADCP increases as a function of ARM-U concentration until to 40% value (100 nM ARM-U), while ADCC cytotoxicity levels get to 55% already at 50nM. Once again, the ARM-U2 behavior was described from a bell-shaped, autoinhibitory dose-response curve, typical of ARM and of formation of complex involving three partners (Figure 15).[92] Finally, B16-uPAR mouse model, previously immunized to produce anti-DNP IgG antibodies, were treated with ARM-U2. The significant inhibition of tumor growth was observed (approximately 90 % in 16 days compared to control), comparable with doxorubicin. Remarkably, ARM-U2 possesses a safer profile compared to doxorubicin, since it not causes weight loss of mice.

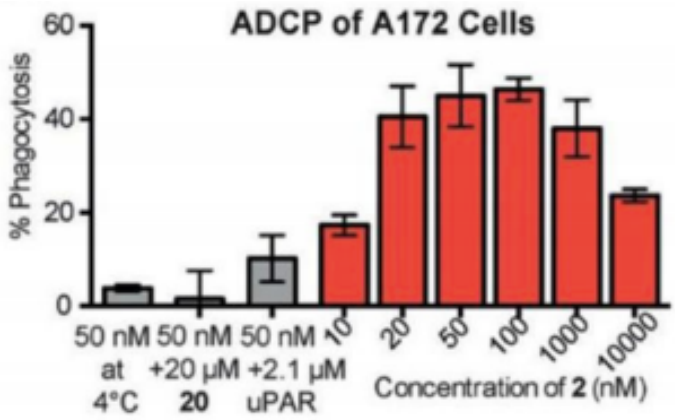

Figure 15 *ADCP of ARM-U2 (2) at various concentration (red) and negative control (20 = 2 without DNP; grey) on immunized A172 glioblastoma cells (adapted from Spiegel and co-workers, Angew Chem Int Ed Engl. 2016).*[89]

The first carbohydrate antigen arrays to profile human serum was developed for the first time in 2009. It was established the presence of about 1% of serum IgG in humans against the Galα(1–3)Galβ(1–4)Glc carbohydrate epitope (or α-Gal epitope). Additionally, high titers of antibodies against α-L-Rhamnose (α-L-Rha) and GalNAc-α(1,3)-GalNAc (Forssman disaccharide) carbohydrate epitopes have been discovered, suggesting that these may be useful alternatives to the α-Gal epitope. Despite a biological variability among individuals, the antibody levels against these antigens were relatively stable over a period of months (Figure 16). [93-95]

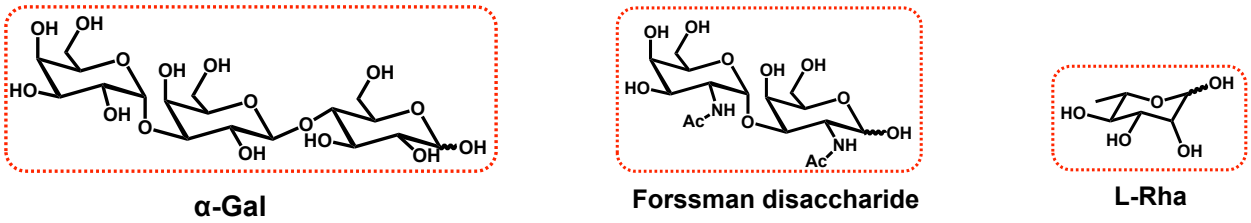

Figure 16 *Carbohydrate haptens able to interact with endogenous antibodies.*

L-Rha is a non-natural sugar found in microbes, plants and mammals, except human that represent the simplest alternative to α-Gal due to its structure and because of its commercial availability, overcoming α-Gal synthetic problems. The biggest problem of L-Rha is that wildtype mice do not produce anti-rhamnose antibodies. Thus, in order to have an animal model for preclinical evaluations, Wang et coworkers reported a well-established method for synthesize Rha-

conjugated immunogens and successfully induced high titers of anti-Rha antibodies in wildtype mice.[96] DNP, α-Gal, L-Rha candidate epitopes have been compared by L. Kiessling group (Figure 17 A).[97] The effectiveness of recruitment strategy was established according to three parameters: 1) the abundance of antibodies and their relative amount recognizing the correspondent antigen, 2) the antibody isotype distribution in order to ensuring engagement of both humoral and cellular immunity and 3) the antibody-antigen complex stability in human serum to have an optimal immune response. The first objective was determined through a biosensor assay to analyze serum antibodies. It was found that anti L-Rha antibodies are generally more prevalent than those recognizing αGal and DNP (Figure 17 B). The second objective was to search IgG and IgM-type antibodies on human serum of different donor. Both IgG- and IgM-type antibodies were detected with all the three epitopes (Figure 17 C). More recently, it was discriminated the different antibody subtype against Rha present in human serum.[98] Through a rhamnose specific ELISA test, they founded that most of the anti-Rha antibodies were IgM, and the others almost all IgG1 and IgG3. Concerning the third objective, it was determined through Surface Plasmon Resonance (SPR) studies showing the different the "interaction kinetic curve" the most stable antibody-antigen complex (Figure 17 D). From this Figure, it can be highlighted that the curve representing the "Rha complex" decrease much slower than DNP or α-Gal curves, meaning its higher stability.

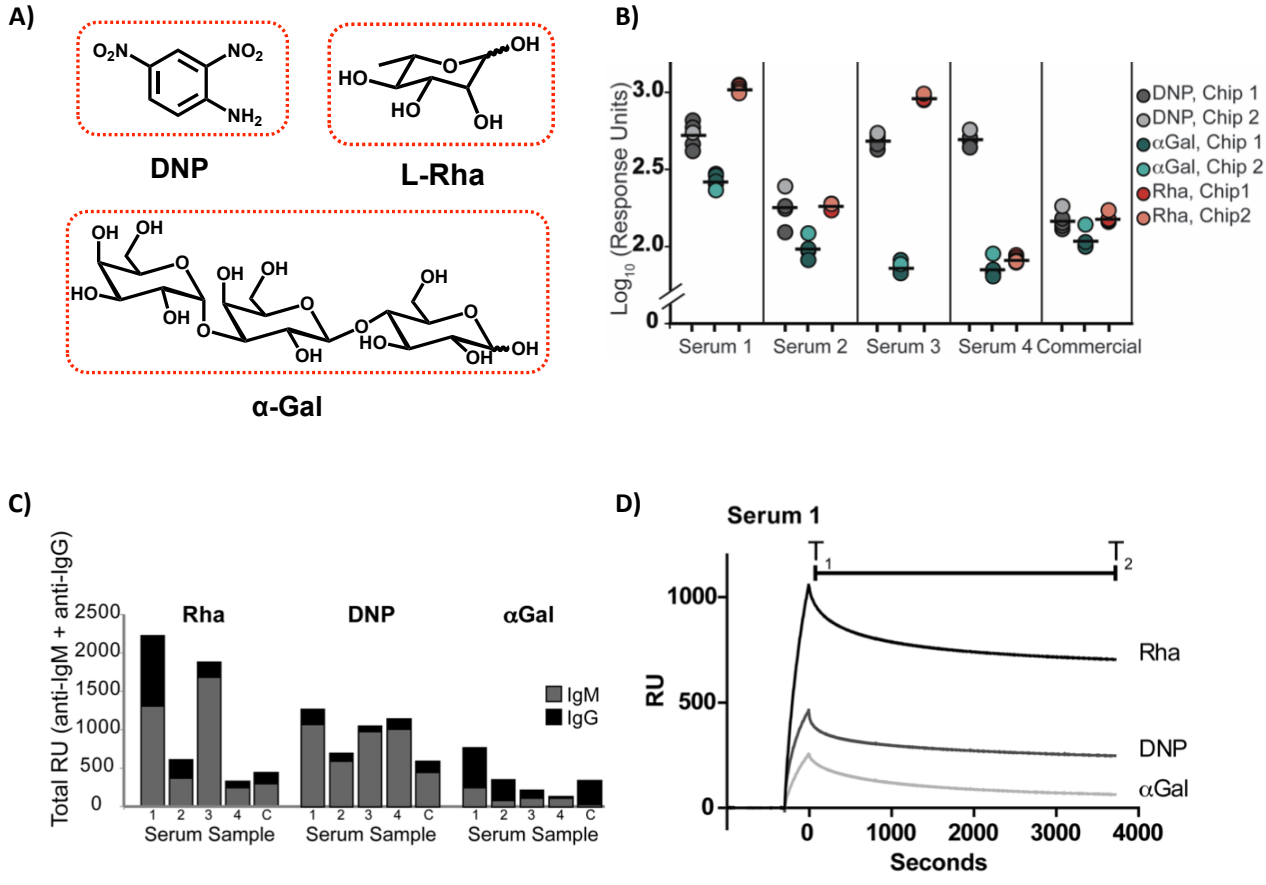

Figure 17 A) *DNP, αGal and L-Rha epitopes able to recruit endogenous antibodies* ***B)*** *Log plot of antibodies levels response against DNP, αGal and L-Rha epitopes* ***C)*** *Isotype distribution of antibodies* ***D)***

Analysis of the stability of the antigen-antibody complexes done by SPR (adapted from Kiessling and co-workers, ChemBioChem. 2014).[97]

More recent strategies rely on the marked propensity of tumors to take up labelled-metabolites on the tumor cells surface. For example, In 2016, Han group founded that sialic acid derivatives with selected substitutions at C-9 were installed into the cell surface glycocalyx by an endogenous sialylation pathway.[98] It was reported covalent incorporation of a non-self-immunogen DNP-conjugated Sia (^{DNP}Sia) into tumor glycocalyx of B16F10 cells in order to elicit immunity clearance (Figure 18). Importantly, the levels of glycocalyx-anchored ^{DNP}Sia remained high after 1 day of incubation.

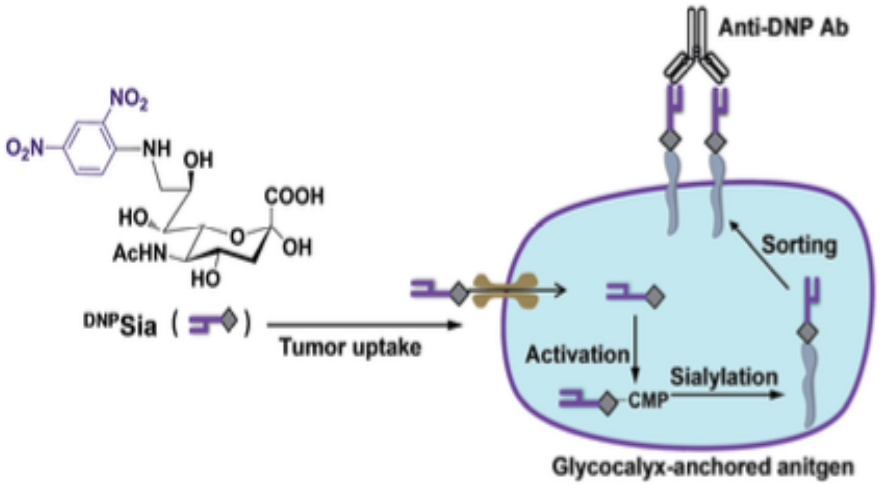

Figure 18 *Incorporation of the ^{DNP}Sia non-self-antigen, able to trigger immunity clearance, into glycocalyx (adapted from Han and co-workers, Chem Sci. 2016).*[98]

To assess its anti-tumor effects *in vivo*, the C57BL/6 type mice was firstly immunized with DNP-conjugated KLH and then incubated with ^{DNP}Sia. As a result, the level of anti-DNP antibodies in the serum of ^{DNP}KLH immunized C57BL/6 mice was 5-fold higher than in the untreated mice. Thus, ^{DNP}Sia-displaying B16F10 cells (^{DNP}Sia+) and cells lacking of ^{DNP}Sia (^{DNP}Sia-) were respectively subcutaneously inoculated into the ^{DNP}KLH-treated mice and into the unimmunized mice in order to observe a selectivity volume reduction in tumor cells. 7 days after inoculation, in unimmunized mice, the tumor volume from ^{DNP}Sia+ cells was about 50% smaller relative to that from the ^{DNP}Sia- cells, while in immunized mice, the tumor from the ^{DNP}Sia+ cells exhibited even higher volume reduction (about 75% volume reduction compared to that from the ^{DNP}Sia- tumor) (Figure 19). Following cytotoxic study indicated very low systemic toxicity of ^{DNP}Sia up to 14 days, even if injected into healthy mice at a dose of 300 mg/kg, which is 10-fold higher than the dose used for the systemic tumor suppression.

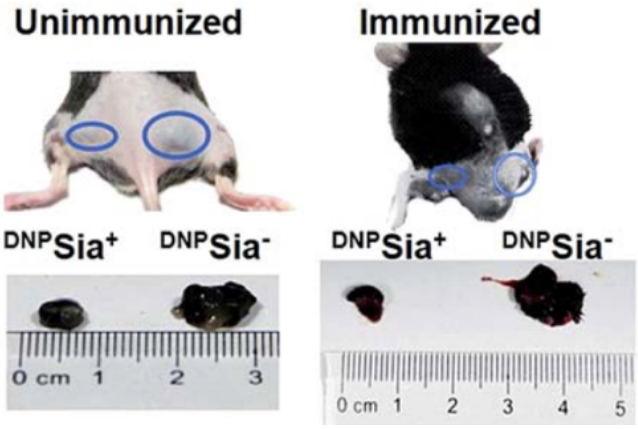

Figure 19 *^{DNP}Sia mediated anti-tumor responses in unimmunized or ^{DNP}KLH immunized C57BL/6 mice. ^{DNP}Sia+ or – are tumoral B16F10 cells with or without ^{DNP}Sia incorporated into glycocalyx, respectively (adapted from Han and co-workers, Chem Sci. 2016).*[98]

Similar strategy was harnessed by Wang group two years ago.[99] The 1,3,4-O-acetyl-*N*-azidoacetylmannosamine (Ac_3ManNAz or Mz) antigen was firstly conjugated with folate-PEG (FA-linker) for selectively folate receptor-mediated uptake by overexpressing cancer cells. Then, this complex was delivered to the target cells, internalized through receptor-mediated endocytosis and then metabolized into the cell. In this position, the N_3 azido moiety of the Mz was able to react with the alkyne moiety on the hapten, composed by two Rha moieties conjugated to an aza-dibenzocyclooctyne molecule (DBCO-Rha), recruiting thus anti Rha antibodies (Figure 20).

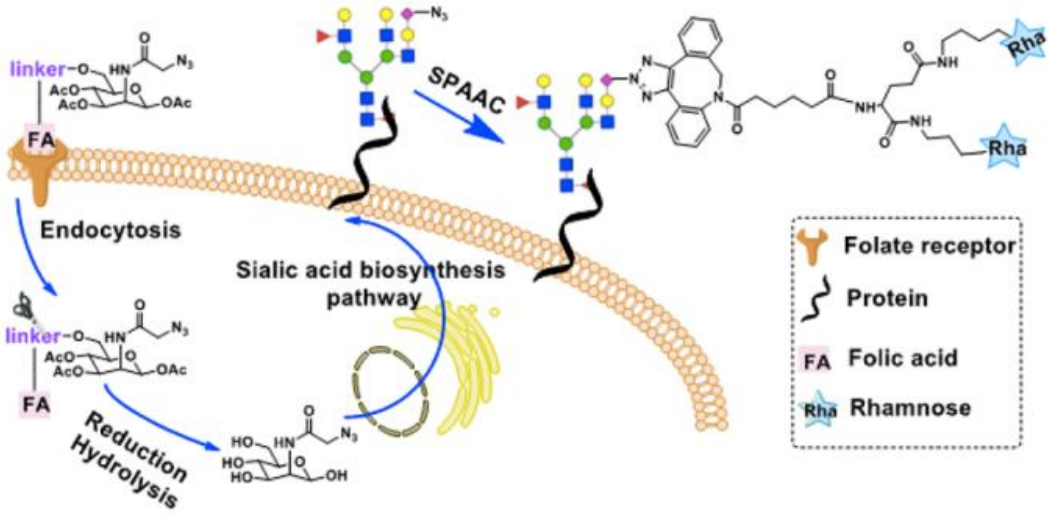

Figure 20 *Strategy to selectively tag the FR-modified carbohydrate into cell surface and recruit anti Rha antibodies. SPPAC: Strain-Promoted-Azide-Alkyne Click Chemistry (adapted from Wang and co-workers, ACS Chem. Biol. 2018).*[99]

The reaction between aza-dibenzocyclooctyne(DBCO) and an azido group is an example of the fastest Strain-Promoted-Azide-Alkyne Click Chemistry (SPAAC) reaction, widely used to avoid Cu toxicity, developed by Bertozzi and Boons. The cyclooctyne is able to react readily with an azide, in the absence of metal catalyst since its intramolecular strain with high yields at ambient temperature.[100-102] For a subsequent *in vitro* cytotoxic evaluation, KB cells, a folic receptor (FR) expressing cell line, and FR^+ KB cells, a 3-fold more FR over-expressing cell line than KB, were chosen as the target cell. MCF7, a breast cancer cell line, and HEK-293, a human embryonic kidney cell line, which do not express FR were used as negative controls. Cells were incubated with FA-PEG-Mz and labeled by DBCO-Rha Subsequently, cells were treated with 20% human serum and human complement. Around 50% of the labeled FR+ KB cells and 20% of KB cells were destroyed by CDC, while no effect occurred with MCF7 and HEK-293 cells.

I.5.A.II. "Large" semi-synthetic conjugates (TBM conjugated with Antibody)

This second ARM approach relies on the combination of small molecules as TBM and antibody as ABM into one unique therapeutic ARM. At the beginning of the 2000s it was demonstrated the power of combining small molecules with immunobiologics, studying the first "chemically programmed aldolase antibodies" targeting device based on the formation of a reversible or irreversible covalent bond between antibody and a TBM. The first example dates back to 2003 from Barbas group.[103, 104] This strategy relies on the utilization of SCS-873 molecule, an high specificity integrin targeting Arg-Gly-Asp (RGD) peptidomimetic, that possess a β-diketone moiety able to react with the reactive lysine of aldolase antibody m38C2 forming a reversible covalent enaminone bond (Figure 21 A). A long spacer between RGD peptidomimetic and β-diketone group was inserted to allow recognition of both moieties at the same time. The combination between mAbC32 and SCS-873 formed the conjugate cp38C2 (Figure 21 B). This construct showed: 1) to increase the serum half-life of SCS-873; 2) to mediate CDC (up to 60% killing) and ADCC (up to 30% killing) against human M21 melanoma cells; 3) to inhibit metastasis of M21 tumor cells in mice and in and Karposi's sarcoma.[105]

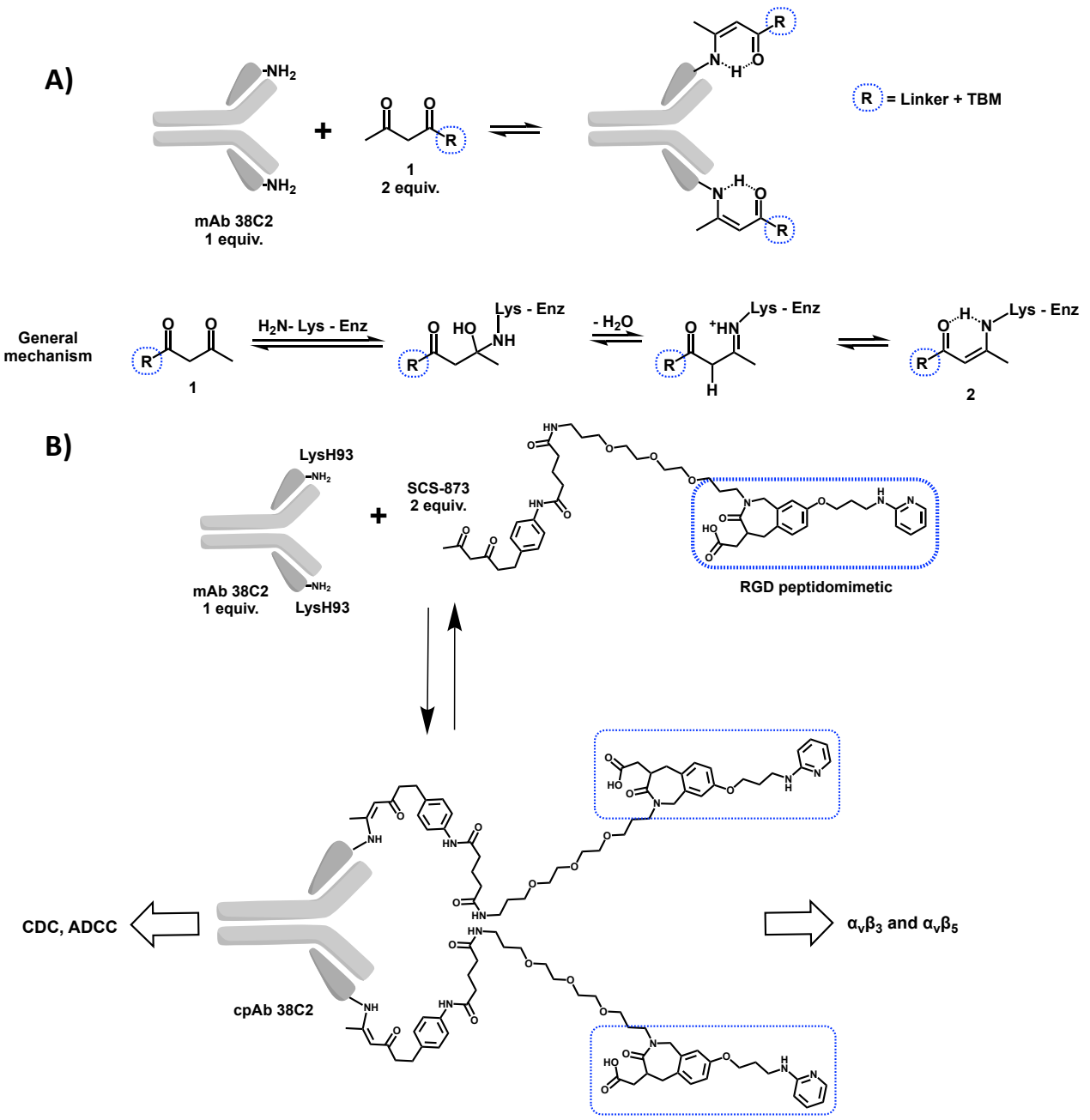

Figure 21 ***A)*** *mAb 38C2 chemical programmed antibody using a reactive β-diketone moiety linked to a targeting module 1. General mechanism of aldolase-catalyzed aldol-addition reaction (Enz: enzyme). The formation of the stable covalent enaminone 2 can be detected at λ= 316 nm.* ***B)*** *mAb 38C2 can be chemically programmed through formation of a reversible covalent bond between a β-diketone and a reactive lysine residue in the anti-body combining site. The resulting chemically programmed mAb 38C2 manifests double targeting (adapted from Barbas and co-workers, Proc Natl Acad Sci USA. 2003).*[103]

The same strategy was applied for targeting and blocking endothelin receptor, in order to develop strong antitumoral antagonists. The endothelin family (vasoconstrictor peptides) and their G protein coupled receptors ET_A and ET_B are found on smooth muscle cells where have a key role

in vasoconstriction and/or proliferative disorders. They play a role in tumor growth, proliferation, apoptosis, angiogenesis, and bone metastasis.[106] In this contest, in 2007, several aryl sulfonamide-based endothelin antagonists were synthesized and covalently linked to the reactive lysine of the m38C2 antibody to create a series of bispecific antibodies, called overall Cov-X-bodies (Cov means covalently and X represented one pharmacophore)(Figure 22).[107] Some of these conjugates exhibited up to a 45% efficacy in growth inhibition of murine xenograft model of human prostate cancer. To date, the CovX-body containing a peptide-based angiopoietin-2 inhibitor (Cov-X-060) is currently used in patients with advanced renal cell carcinoma.

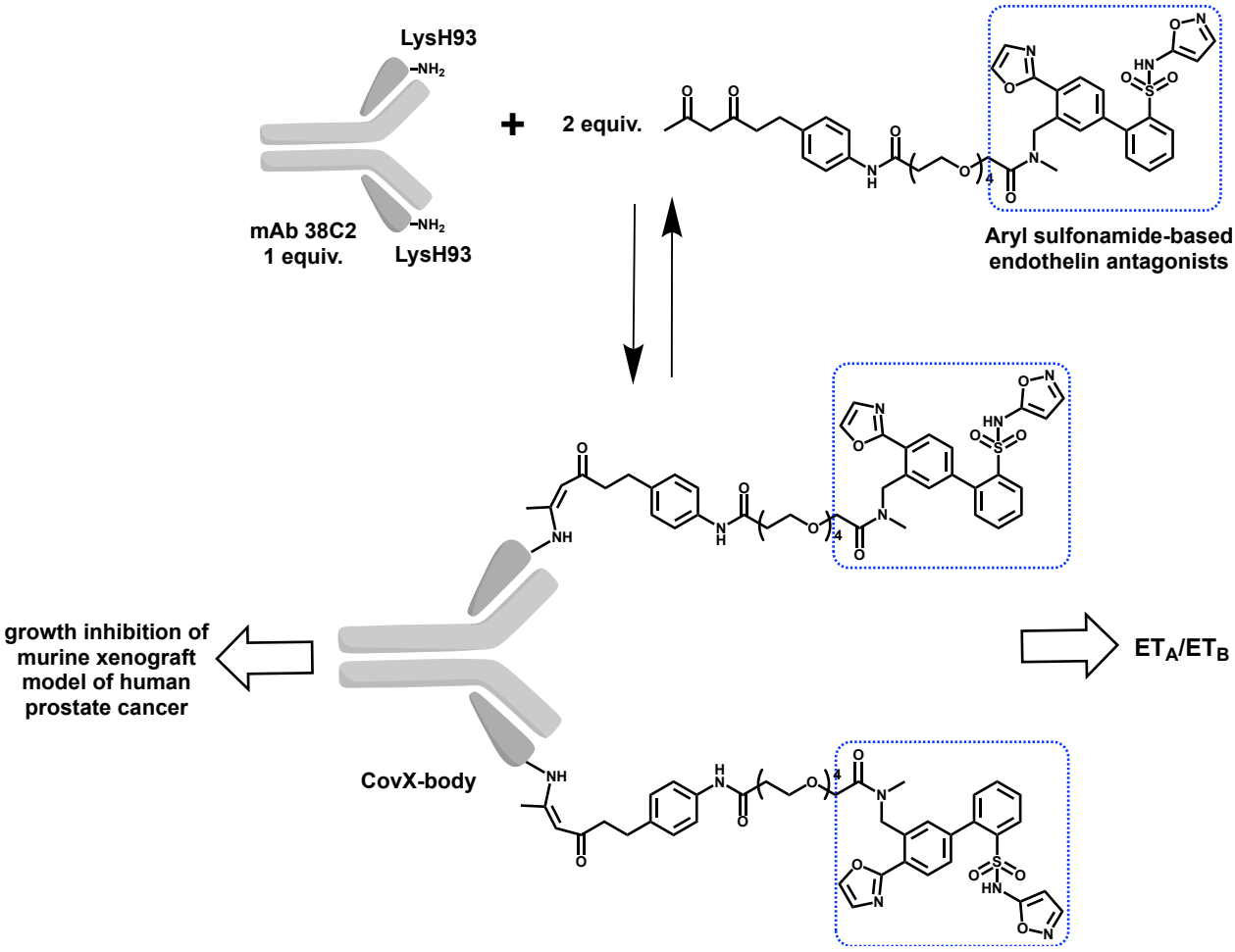

Figure 22 *CovX-body, composed by Aryl sulfonamide-based endothelin antagonists, targets cancer cells via ET_A and ET_B recognition on cell surfaces (adapted from Barbas and co-workers, Bioorg. Med. Chem. Lett. 2007).*[107]

Other example from the same group showed how chemically programmed aldolase antibody 38C2 can be conjugated *via* amide bond formation between the catalytic site lysine H93 and β-lactam equipped with aptamers (as TBM) (Figure 23).[108] Aptamers are structured nucleic acid ligands with excellent binding properties for proteins.[109] It was demonstrated that they can also benefit from antibody conjugation. For this study, the thiol-modified aptamer ARC245 was chosen

due its binding and inhibitory properties for Vascular Endothelial Growth Factor (VEGF), one of the most commonly overexpressed protein in human tumors.[110] Since ARC245 suffers from low *in vivo* stability and poor pharmacokinetic properties, his conjugation with mAb 38C2 lead to serum half-life increase from minutes to 21 h. As a result, a strong inhibition of angiogenesis and tumor growth occurred (Figure 24).[111]

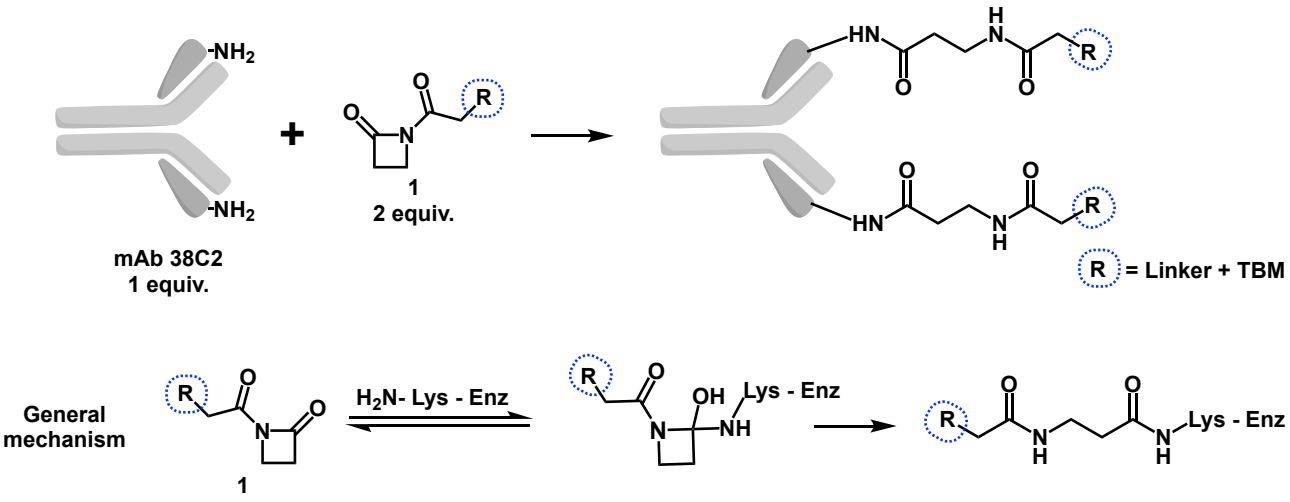

Figure 23 *β-lactam-based approach for the chemical programming of Aldolase Antibody 38C2 (adapted from Barbas and co-workers, Bioorg Med Chem Lett. 2009).*[109]

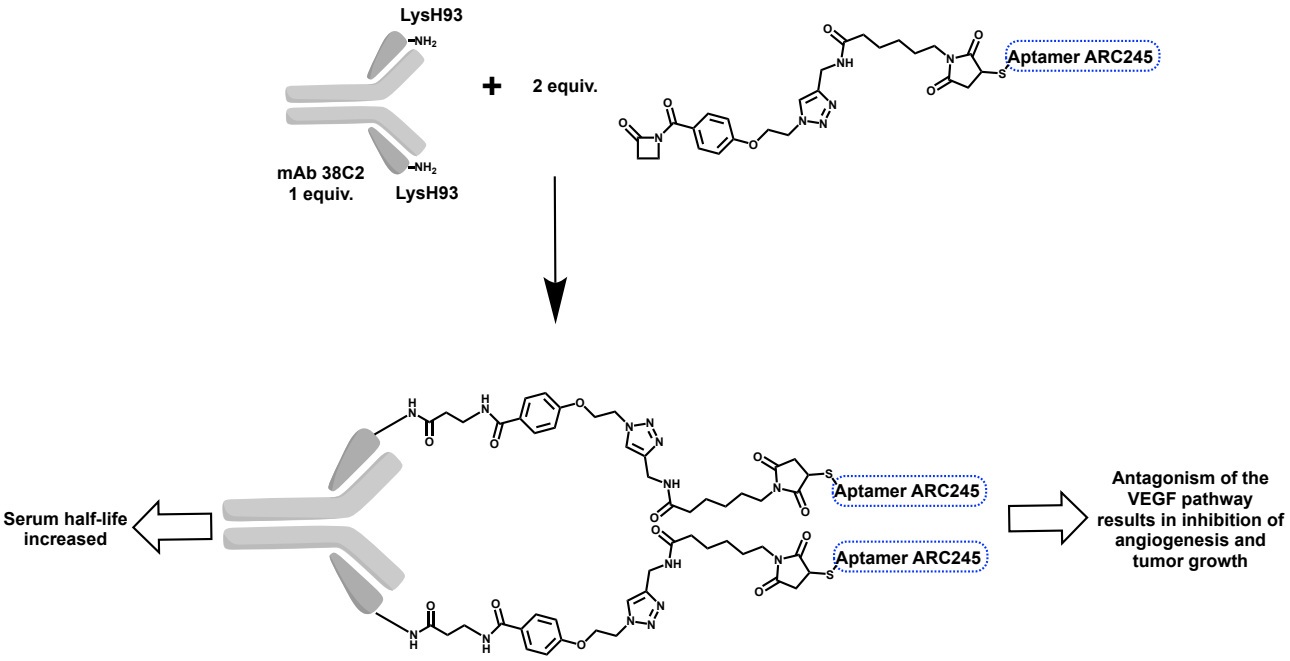

Figure 24 *mAb 38C2 can be chemically programmed through formation of an irreversible covalent bond between a β-lactam and a reactive lysine residue in the anti-body combining site. The resulting chemically programmed mAb 38C2 is composed by aptamer ARC245, strong VEGF inhibitor (adapted from Barbas and co-workers, Angew Chem Int Ed Engl. 2010).*[111]

Another approach involving the simultaneous targeting of two different receptors for a synergistic double strike against tumors has been developed. In 2009, the catalytic antibody mAb 38C2 conjugated with integrin $\alpha_v\beta_3$ and $\alpha_v\beta_5$ and the luteinizing hormone releasing hormone (LHRH) receptor targeting molecules has been reported. Through FACS analysis, it was demonstrated that the bispecific antibody enhanced the binding ability to integrin and LHRH as compared with antibody targeting single receptor. This study opens a new perspective for targeting diverse cell-types in multiple diseases. [112,113]

Other strategies relied on nanobodies (Nbs) that are proteins containing the smallest functional fragments of Fab. With their small size (12–15 kDa), smaller than whole Fab (~50 kDa) fragments, their commonly nanomolar-range affinity binding, high thermal and chemical stability, high water-solubility and low tendency for aggregation, Nbs are very attractive proteins for tumor targeting applications.[114,115] In 2016, the Spiegel and McNaughton groups have developed an ARM, called DNP-5F7, harnessing the nanobody multiple properties and incorporating DNP moiety (Figure 25).[116] DNP-5F7 was found to be specific for the human EGFR 2 (or HER2), a protein overexpressed on the surface of ~20–30% of breast cancers and ~20% of gastric cancers)[117,118] with a dissociation constant of ~510 pM and was able to mediate ADCC (20% cytotoxic value) on high HER2-expressing cells.

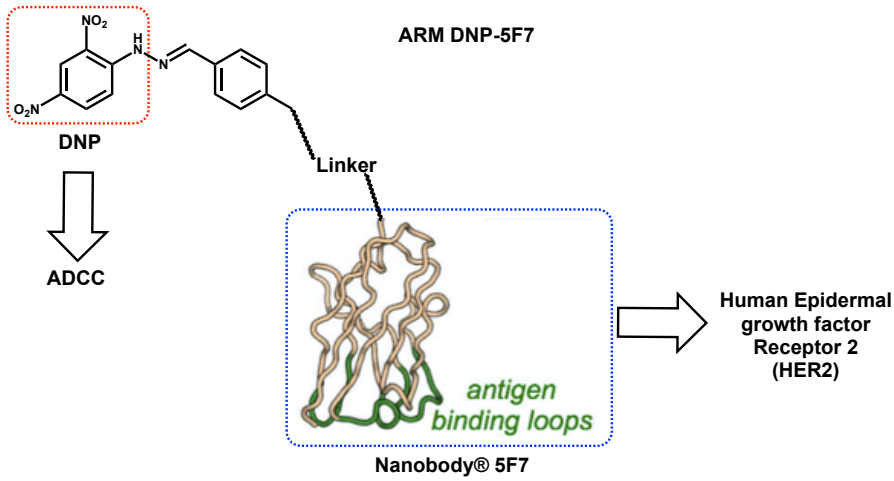

Figure 25 *ARM DNP-5F7, harnessing the nanobody properties, able to provoke ADCC on cancer cells overexpressing HER2 receptor protein (adapted from Spiegel and co-workers, ChemBioChem. 2016).*[116]

In conclusion, several ARM strategies have been developed over the last twenty years. Both "small molecules" and "TBM conjugates with antibodies" have showed encouraging effects in cellular assays and *in vivo* studies, resulted in average 40% of tumor-killing efficacy. These reports clearly highlight the potential of ARMs for cancer immunotherapy.

I.5.B Antibody Recruiting Molecules to treat pathogens

The World Health Organization (WHO) has estimated that infectious agents are responsible for approximately 25% (15 million) of global deaths each year and are one of the predominant cause of mortality in developing nations. Great varieties of ARM-based strategies to fight bacteria and virus have been reported and are currently available.

I.5.B.I. Overview of bacteria

Bacteria are microorganisms composed of one cell, ~0.5-5 μm in length, which normally are characterized by a lack of a nucleus structure and membrane-bound organelles. They could survive in almost all the environment, such as in human.[12/16/20 5:42:00 PM] There are two types of bacteria, the probiotic and pathogenic bacteria. Probiotics, like *Lactobacillus*, are beneficial to our health, primarily aiding in a healthy digestive system. These commensal bacteria are harbored in many different tissues through the body, which means the host immune system has to naturally adapt to these no-self-cells. An imbalance of the host immune response can lead to a number of serious diseases.[119]

The immune system has developed precise modes of detecting, responding, and clearing pathogens. Likewise, pathogens, due to their high adaptability to different environments and their high mutation rate, continue to evolve countermeasures and infection often requires the intervention of therapeutic agents such as antibiotics. Conventional antibiotics act by targeting vital bacterial functions such as cell wall synthesis, protein synthesis, RNA transcription, and DNA replication. Inhibitors against cell wall biosynthesis represent the largest class of antibiotics since cell wall it's absent in human. However, bacteria have been evolving mechanisms of resistance such as drug modification or degradation, efflux pumps, decreased permeation of drugs, and drug target alteration.[120-122] Today, resistant pathogenic bacteria are already responsible for thousands of deaths and billions of additional health care costs each year.[123] Recent estimates project that by 2050 more people will die from antimicrobial resistant infections than from all forms of cancer combined.[124] Importantly, the clinical management of multidrug-resistant (MDR) infections is complicated by the lack of currently approved antimicrobials that retain sufficient activity against MDR strains, particularly the so-called ESKAPE microorganisms (eg *Enterococcus faecium*, *Staphylococcus aureus*, *Klebsiella pneumoniae*, *Acinetobacter baumannii, Pseudomonas aeruginosa, and Enterobacter spp)*.[125]

I.5.B.II. ARMs to treat bacteria

Since the external surface of bacterial pathogens presents many diverse antigenic targets, the most important alternatives to the use of antibiotics are vaccines or administration of monoclonal antibodies (mAb) or, simply, harness our immune system. The vaccination induces a

specific immune response and protection of individuals against later exposure to the same pathogen. Conversely, mAb provide immediate protection to combat infections associated with emergency interventions. The only available Bezlotoxumab is licensed for use against *Clostridium difficile*.[126] The last option relies on natural antibodies that can either neutralize bacterial toxins or can form a complex with a bacterium cell (opsonization) and triggers the activation of CDC or the recruitment of effector cells as described in the previous part. For this reason, the employment of ARMs has the potential to elicit antibody dependent immune effector responses. Here again, simultaneous binding of ARMs with antibodies and surface-exposed escaped bacterium results in the formation of ternary complexes that can potentially lead to bacterial killing through mechanisms above-described.

The first example, described by Bertozzi, C. R. and Bednardski, M. D. in 1992, relies on the utilization of a biotinylated C-mannoside (BCM).[127] This latter was able to interact with *Escherichia coli* which express type 1 pili, known to be characterized by fimbrial FimH adhesin[128] from one side, and with an avidin from the biotinylated side. The resulting aggregate was then exposed to anti-avidin antibodies. Localization of anti-avidin antibodies on the bacterial cell was assayed by transmission electron microscopy using a protein A colloidal gold label (Figure 23 A). This complex lead to a complement- and macrophage-dependent cytotoxicity (about 75 % killing at 1 µM).[129] Other comparable studies by Li *et al*. have shown the ability polymers presenting mannose and Galα1→3Gal to bind human anti-Gal antibodies, by means of an ELISA inhibition assay, and to prevent the agglutination of yeast by *E. coli* (Figure 23 B).[130]

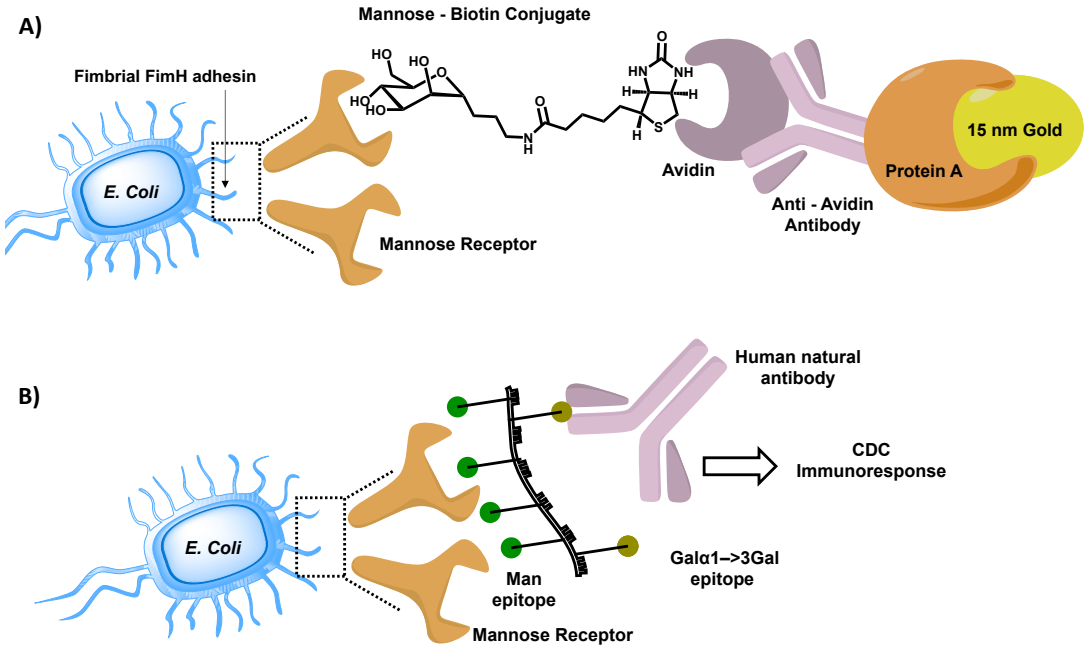

Figure 26 A) *Schematic representation of the Mannose – Biotin conjugate (BCM) that binds the mannose receptors on the bacterial pili through the FimH adhesin, and an avidin motif through a biotin residue. The full complex was able to recruit anti-avidin antibodies, revealed through the protein A conjugated to 15-nm*

gold particles (adapted from Bertozzi and co-workers, J. Am. Chem. Soc. 1992).[127] ***B)*** *Bacteria targeted by human natural anti-Gal antibody thought a-Gal and mannose containing glycopolymer mediator (adapted from Li and co-workers, Bioorg Med Chem. 1999).*[130]

More recently, Whitesides and co-workers developed ARMs by utilizing vancomycin, an antibiotic which interacts with D-Ala–D-Ala residues of the peptidoglycan to the surface of Gram-positive bacteria *S. aureus*, *S. epidermidis*, and *S. pneumoniae*. On the other side, the fluorescein ABM promoted the recruitment of anti-fluorescein antibodies. As a result, the authors demonstrated by FACS analysis that this antibody-recruiting polymer could mediate the formation of a ternary complex and the phagocytosis of opsonized bacterium through macrophages (cultured J774 cells from mouse), after preimmunization (Figure 27).[131,132]

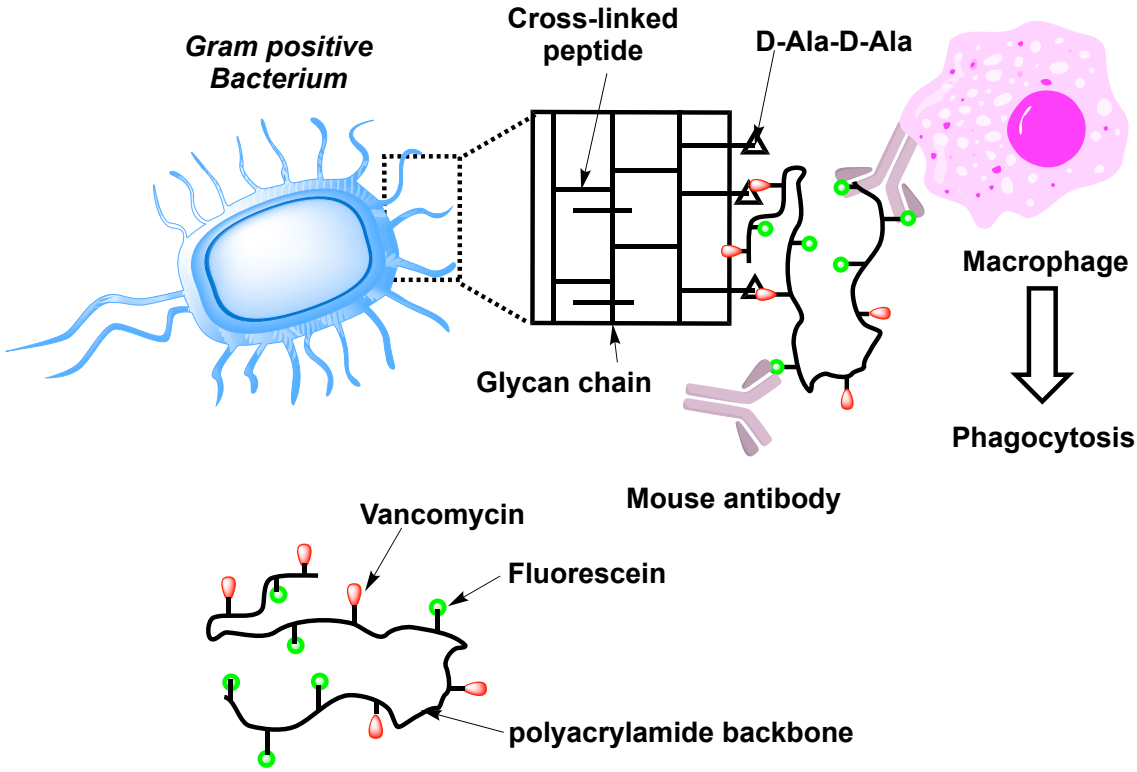

Figure 27 *The opsonization by antibodies and phagocytosis of a Gram-positive bacterium directed by a bifunctional polymer (adapted from Whitesides and co-workers, Journal of the American Chemical Society 2003).*[131]

In 2014, the Pires laboratory pioneered the use of a novel immunomodulation strategy based on the peptidoglycan remodeling strategy called “D-amino acid Antibody Recruitment Therapy” (DART).[133-135] This strategy relies on the utilization of DNP-conjugated D-amino acid recognizable by endogenous antibodies, in order to elicit a greater immune response in labelled bacteria. This

choice of unnatural amino acids is due to the fact that bacterial D,D-transpeptidases involve in processes of incorporation of cell wall building blocks and possess the unique ability to accept unusual D-amino acids.[136] In addition, it was observed the ability of PBP transpeptidases to incorporate D-amino acids possessing diverse C-terminus modifications. In particular, the Pires group demonstrated that exogenous D-amino carboxamide variant D-Lys(DNP)-$CONH_2$ is more readily incorporated into the peptidoglycan than the natural carboxylic acid D-Lys(DNP)-CO_2H, allowing a strong immune response in *B. subtilis* and *E. faecalis* bacteria (Figure 28).

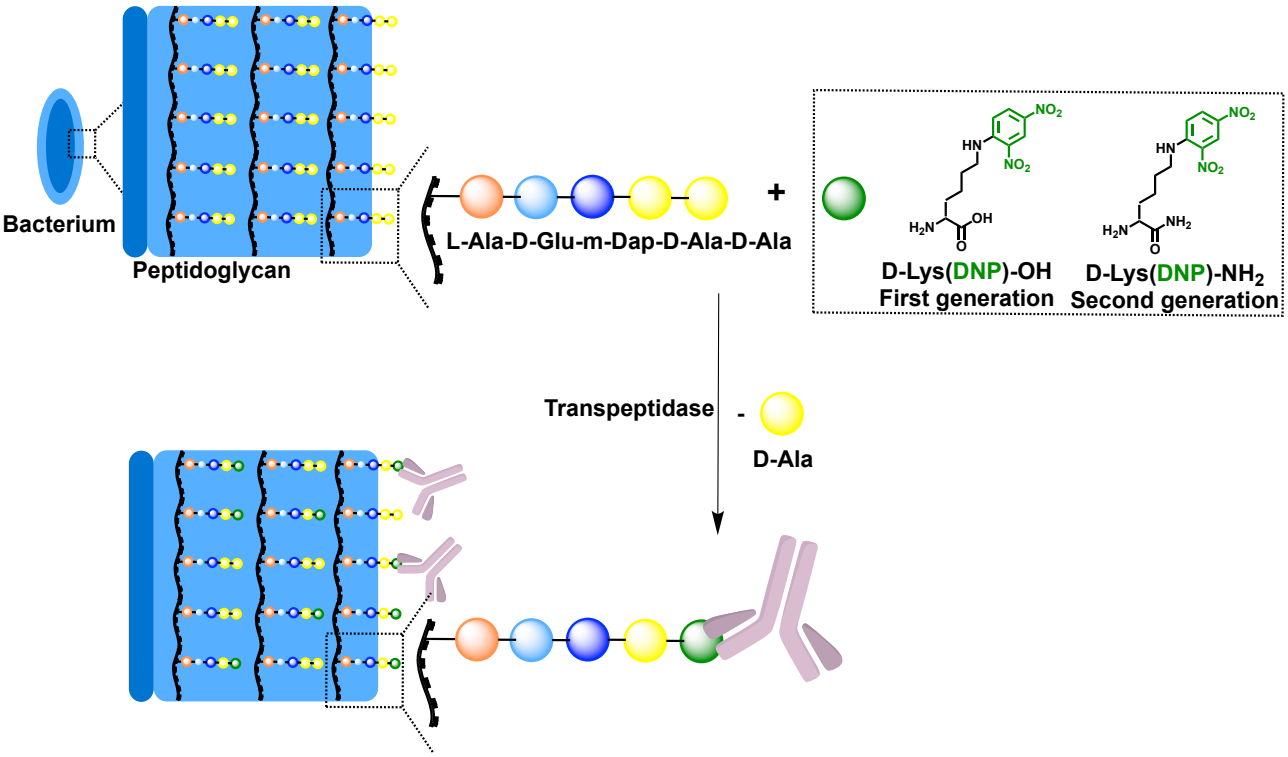

Figure 28 *Representation of the "one-step" labelling strategy upon surface remodeling with D-amino acid derivatives (adapted from Pires and co-workers, Biopolymers 2015).*[134]

Another enzyme involved in the peptidoglycan remodeling is the sortase A (SrtA). This enzyme can decorate the surfaces of Gram-positive bacteria with a diverse array of proteins. It is located on the extracellular face of the membrane, where it recognizes the pentapeptide motif LPXTG in secreted proteins (wherein X can be any amino acid). The enzyme cleaves between the Thr and Gly of this motif and then attaches the LPXT peptide to the peptidoglycan wall through the lipid II and thus the anchored protein will eventually be presented at the cell surface. Through this mechanism, *S. aureus* cell wall was modified with fluorescein labelled small-molecule through L(Fluor)PXTG and antifluorescein antibodies were subsequently recruited to the surface of the cell wall, resulting in the bacteria cell immune injury (Figure 29).[137]

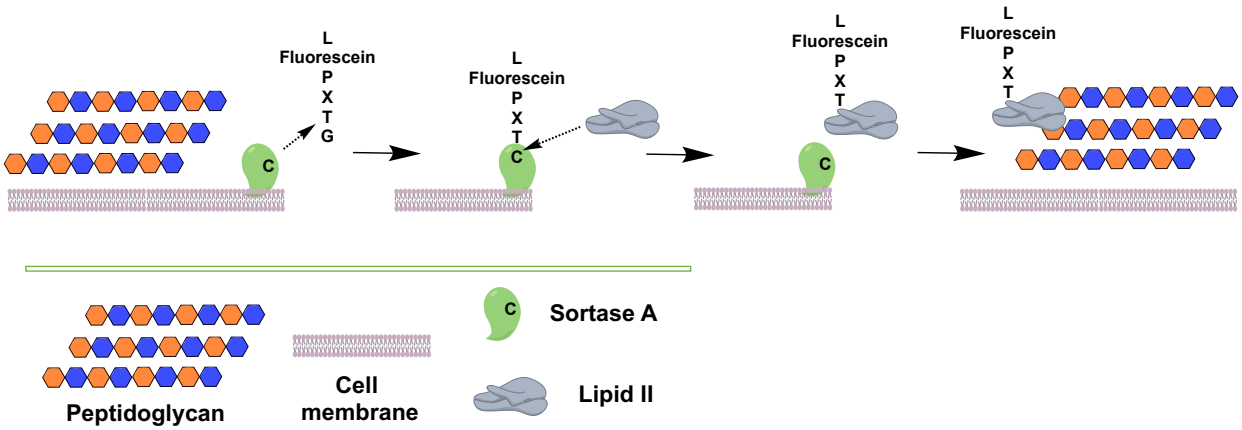

Figure 29 *Remodeling of Bacterial Surface via Sortase A. After this process, the fluorescein is inside the peptidoglycan strain and could be selectively targeted by anti-fluorescein antibodies. (adapted from Clubb and co-workers, Mol Microbiol. 2011).*[137]

To summarize, bacterial infections represent an important public health alarm, and new immunotherapy agents are needed. Using Gram-positive bacteria as a model, highly specific bifunctional ARMs composed by small molecules have been identified. These ARMs selectively bind mannose receptor on bacterial pili or specific amino acids present on peptidoglycan structure and recruit endogenous antibodies to bacteria surface, resulting in immune mediated clearance. In addition, "DART" or "sortase A" approaches represent other therapeutic strategies for treating bacteria disease with significant potential to combine with existing treatment strategies.

I.5.B.III. Overview of virus

A virus is an acellular microscopic entity that can multiply within the cells of other organisms. This infectious agent can infect all types of living systems such as animals, plants, micro-organisms (including bacteria) and other viruses.[138] The viral particles, also known as virions, are composed by two or three parts: (I) DNA or RNA (II) a protein coat, called capsid, which surrounds and protects the genetic material; and in some cases (III) a lipid sac that surrounds the protein coat when the virus is out of the host cell. Their size varies from 80 to 600 nm and their complex structures are also extremely variable. Among the strategies to eradicate viral infections, antivirals drugs, vaccines and monoclonal antibodies (mAb) are currently used for many years to fight a few human infectious with more or less efficiency (Human immunodeficiency virus or HIV, Hepatitis B virus or HBV, Hepatitis C virus or HCV, Human Cytomegalovirus or HCMV, Herpes simplex virus or HSV, Human papilloma virus or HPV, Respiratory syncytial virus or RSV, Varicella zoster virus VZV, influenza virus and Coronavirus or CoV), although more than 200 human viruses have been discovered.[139] However, all of these approaches have strong limitation. Available antiviral drugs, mainly reverse transcriptase, polymerase, protease, integrase, primase, and neuraminidase

enzymes inhibitors, have received limited attention due to rapid development of resistance and low efficacy.[140-142] Vaccines may be useful only against viruses causing acute, self-limited infections. In most of these cases, viruses have evolved to escape the immune system; therefore the immune response is not sufficient to eradicate the infection. Concerning mAb, their utility is limited for the "severe Respiratory Syncytial Virus" (RSV) infection. Palivizumab is the only safe and well tolerated mAb for the prophylactic use.[143,144]

I.5.B.IV. Overview of HIV virus

HIV and its replication cycle have been intensively studied. The first step is the binding and fusion between of its surface and the membrane of the target cell. The HIV surface is commonly composed by the envelope glycoprotein (Env), which consists of two noncovalently associated subunits (the gp120 external subunit and the gp41 transmembrane subunit) derived by the proteolytic cleavage of the gp160 biosynthetic precursor. The gp120 subunit is responsible for the binding of specific target cell receptors, while the gp41 subunit catalyzes the fusion reaction with the target cell, anchoring Env to the host membrane. The functional Env on the surface of the HIV particle or infected cells is organized as a trimer of three gp120-gp41 heterodimers. On the other hand, the CD4 antigen and the chemokine receptors, CCR5 or CXCR4, both located on the surface of the host cell are involved. HIV entry starts with the binding of gp120 to CD4 antigen. This generates some conformational changes in the env complex that cause the following CCR5 binding. Consequently, CCR5 binding activates gp41 to trigger membrane fusion; this reaction involves extension of the gp41 subunit to allow the insertion of its N-terminal "fusion peptide" into the target cell membrane, followed by its refolding process into an energetically favorable six-helix bundle that brings the two membranes together (Figure 30 A, B).[145,146]

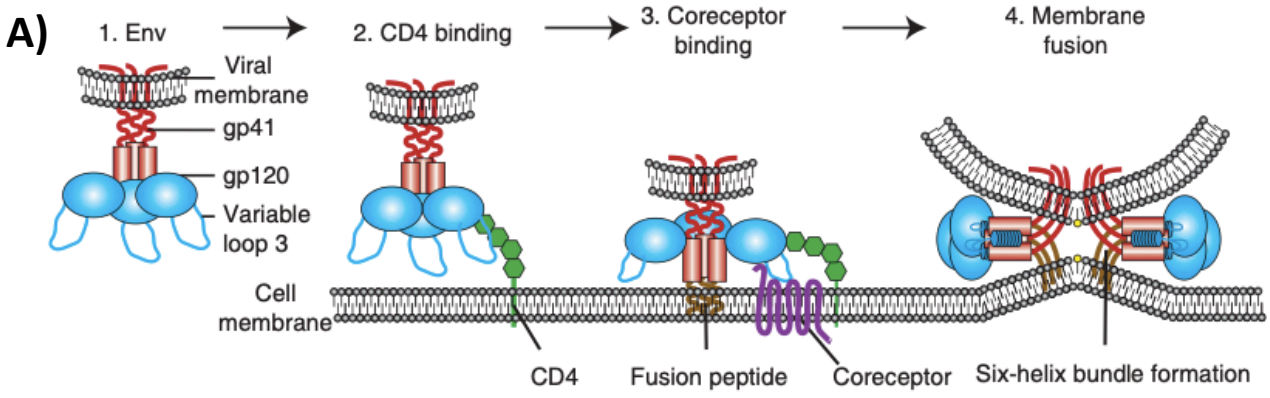

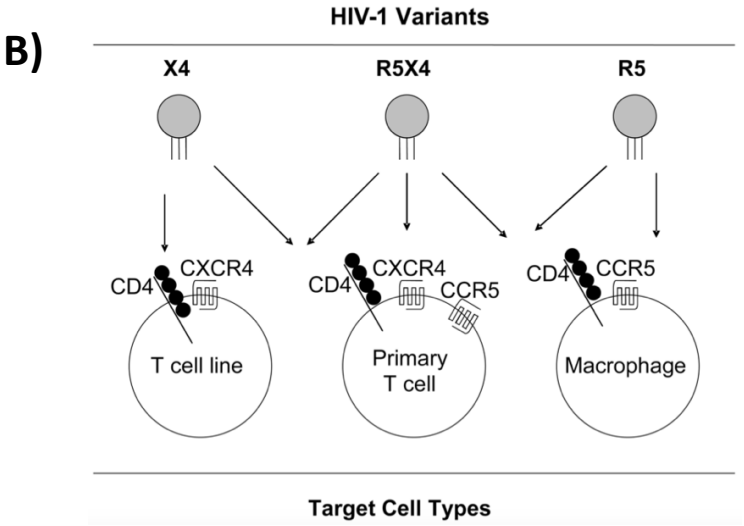

Figure 30 A) *Overview of HIV entry. HIV Env, comprised of gp120 and gp41 subunits (1), first attaches to the host cell, binding CD4 (2). This causes conformational changes in Env, allowing CCR5 or CXCR4 coreceptors binding, which are mediated in part by the V3 loop of Env (3). This initiates the membrane fusion process as the fusion peptide of gp41 inserts into the target membrane, followed by six-helix bundle formation and complete membrane fusion (4) (adapted from Doms and co-workers, Cold Spring Harb Perspect Med., 2012).*[145] ***B)*** *Coreceptor and HIV-1 tropism. X4-tropic strains are specific for CXCR4 and infect continuous CD4+ T cell lines and primary CD4+ T cells. R5-tropic strains are specific for CCR5 and can infect macrophages and primary CD4+ T cells. R5X4-tropic strains can utilize both CXCR4 and CCR5 (adapted from Alkhatib G., Curr Opin HIV AIDS. 2009).*[146]

I.5.B.V. ARM to treat HIV virus

The first example of ARM reported against HVH by Shokat and Schultz dates back to 1991. They demonstrated that anti-DNP antibodies could be redirected to immobilized proteins (gp120 and streptavidin) as a therapeutic strategy.[147] More recently, in 2004, Wang *et al.* reported an ARM containing two functional domains: the trisaccharide Galα1-3Galβ1-4Glcβ1-R that binds anti α-Gal IgG and IgM antibodies from human serum, and the peptide, called T20, able to bind the glycoprotein gp41 and inhibit its binding to the HIV envelope (Figure 31).The authors demonstrated that the trisaccharide epitope attachment to the *N*-terminus of T20 didn't change the peptide ability to bind to the gp41 region of the HIV envelope. As a result, the synthetic α-Gal T20 ARM complex allowed a strong CDC response.[148]

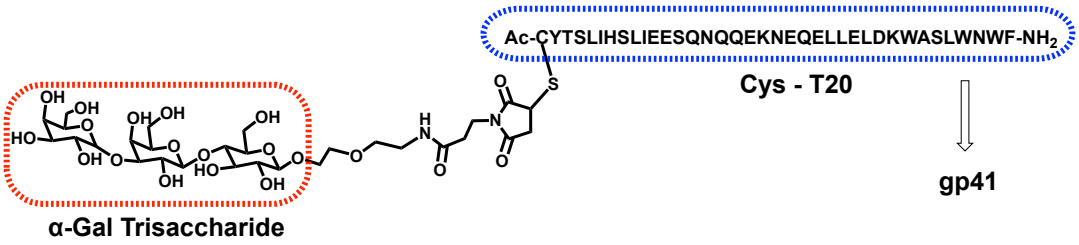

Figure 31 *A bifunctional molecule designed to redirect endogenous anti-α-Gal antibodies to HIV. This agent incorporated the α-Gal trisaccharide epitope at the ABM (red box) and was linked to the 36-amino-acid gp41 fusion inhibitory peptide, T-20, at the TBM (blue box)(adapted from Wang and co-workers, Org. Biomol. Chem. 2004).*[148]

Few years later, Valhne *et al.* developed a series of ARMs composed of a α-Gal disaccharide chemically linked to a series of 15 peptides able to block the CD4-gp120 interaction. Through ELISA assays, the authors demonstrated that this strategy allowed to address endogenous anti-α-Gal antibodies to immobilized cell-surface-expressed gp120, and to trigger both CDC and ADCC toward HIV-1 (Figure 32).[149]

Figure 32 *A series of ARMs designed to redirect endogenous anti-α-Gal antibodies to HIV. This agent incorporated the α-Gal disaccharide epitope at the ABM (red box) and was linked to the CD4-derived peptide, at the TBM (blue box) (adapted from Vahlne and co-workers, Proc Natl Acad Sci USA, 2008).*[149]

In 2009, the Spiegel laboratory has developed the first non peptidic-antibody-recruiting molecule targeting HIV (ARM-H).[150] This bifunctional molecule could both recruit anti-DNP antibodies and address them to gp120-expressing cells and inhibit the gp120-CD4 interaction. More specifically, the HIV-binding module is represented by the small molecule BMS-378806, a 7-azaindole inhibitor of the CD4-gp120 interaction. This component was linked *via* CuAAC to the DNP epitope. The final ARM-H (Figure 33 A) had the potential to interfere with the survival of HIV, forming a ternary complex and triggering complement-mediated killing of Env-expressing cells (the % cytotoxic rate was about 25% at concentrations ranging from 6 to 30 μM), without pre-immunization. Five years later, computational studies provided evidence that PEG linker at the C4 position of the azaindole in BMS-378806 inhibitor increases 300-fold the BMS-378806 inhibitory

activity, allowing the development of ARM-H2 (Figure 33 B), with an higher CDC activity (% cytotoxic rate was about 60%) than the previous ARM.[151]

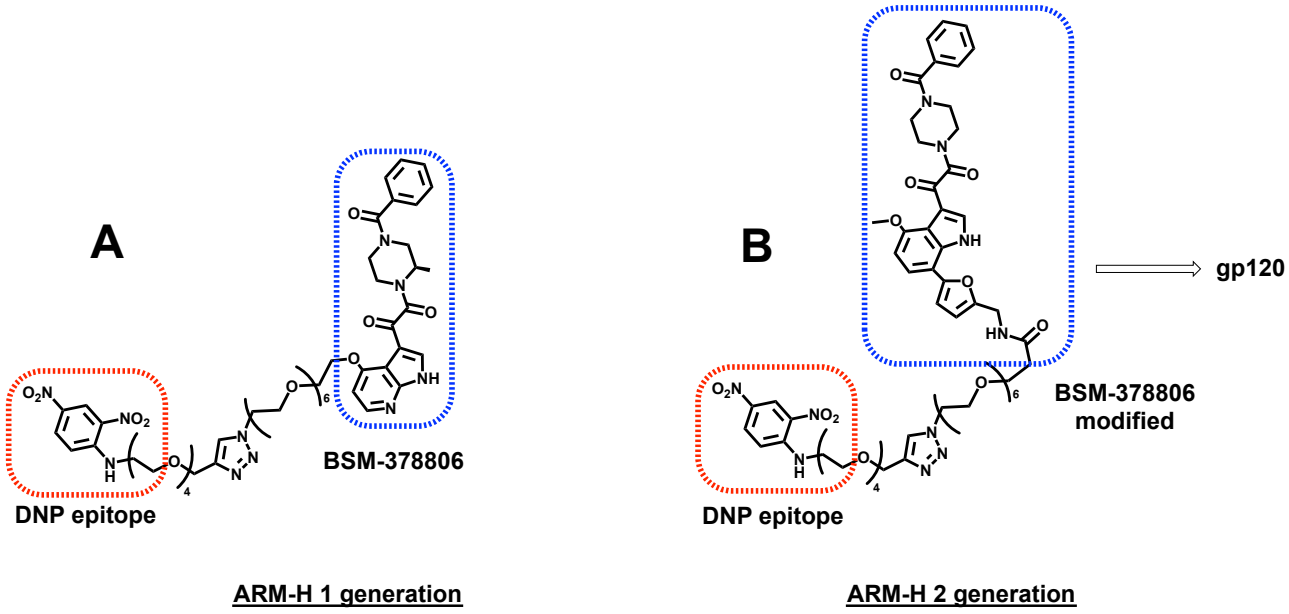

Figure 33 *HIV gp120–Ligand ARMs-H (**A** first generation and **B** second generation) (adapted from Spiegel and co-workers, Chem. Sci., 2014).*[151]

In conclusion, virus-neutralizing antibodies are generally directed against the viral surface structures, and in this way, they play an important role in suppressing, at least temporarily, virus replication in infected individuals. Here, we showed some ARMs developed to act against key points of the HIV infection and replication. However, the efficiency of an antibody response is limited by two main factors: the great variability of the virus envelope glycoprotein gp120 due to its high level of glycosylation, and the fact that the other conserved carbohydrate epitopes are exposed only after that the bind to the receptor occurs.[152,153]

I.6. My Project

As described above, Antibody Recruiting Molecules (ARMs) represent an important topic in chemical immunology, and are receiving increasing interest as bioactive components that can influence the immune system to treat current pathologies. In the contest of cancer and pathogen infections, several ARMs have been developed since the early 2000s, especially with the purpose of overcome the whole range of side effects and inefficiency of the other treatments, such as drugs, vaccines and monoclonal antibodies. To date, ARMs have demonstrated great potential in several *in vitro* and *in vivo* studies.

This project has the general objective to synthesize and screen ARMs, arising from the combinations of ABMs and TBMs into a whole single molecule, able to:

- interact with cancer cells. To do this, the ARM must have an excellent affinity for membrane proteins over-expressed in cancer cells.
- recruit endogenous antibodies to avoid pre-immunization since cancer patient are often immune-compromised.
- form a stable ternary complex between cancer cells and antibodies without promoting internalization to ensure the stimulation of the immune response against the cancer cell expressing the targeted membrane protein.
- trigger an strong immune response using human serum as the only source of immune effectors. We will thus focus on CDC only since human serum contains only the antibodies and other proteins (i.e. complement proteins) but not immune cells.

The general project started in 2015 and was divided into three parts (Figure 34 A). The first part, carried out by Dr. Eugenie Laigre, concerned the design, synthesis and biological evaluations of ABMs based on clusters of carbohydrates to improve recognition properties due to multivalent interactions. The second part, carried out by Dr. Benjamin Liet, concerned the design, synthesis and evaluation of TBMs to target tumoral membrane proteins with high affinity and selectivity. The third part, my Ph.D., schematically illustrated in yellow on Figure 34 B, concerned:

1. The synthesis of new molecular scaffolds and reproducible chemical processes to construct multimodal compounds called ARMs, combining several ABMs and TBMs within a single molecule;
2. The ARMs purification and the characterization by HPLC, ^{1}H-NMR and HRMS;
3. The development of a cell-based assay in order to form a ternary complex between cancer cells, ARM and human serum;
4. The assessment of the “antibody recruitment ability” of ARMs by FACS;
5. The localization of the ternary complex by confocal microscopy;

6. The valuation of ARM ability to mediate immune clearance of tumor and cytotoxic rate calculation.

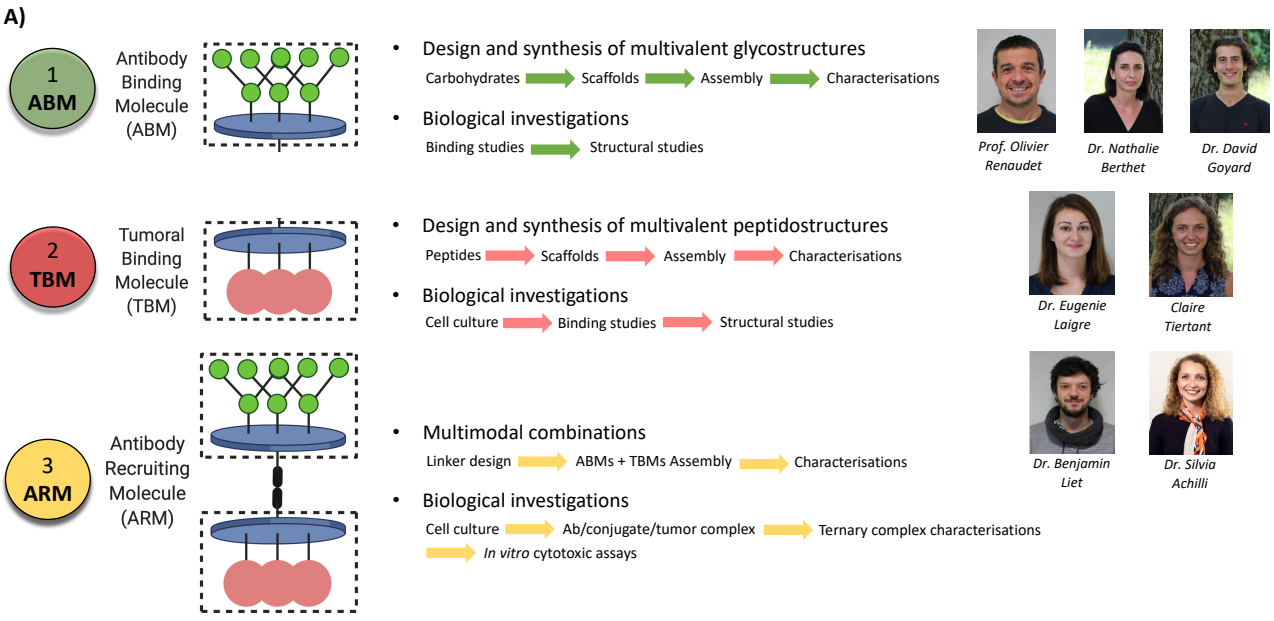

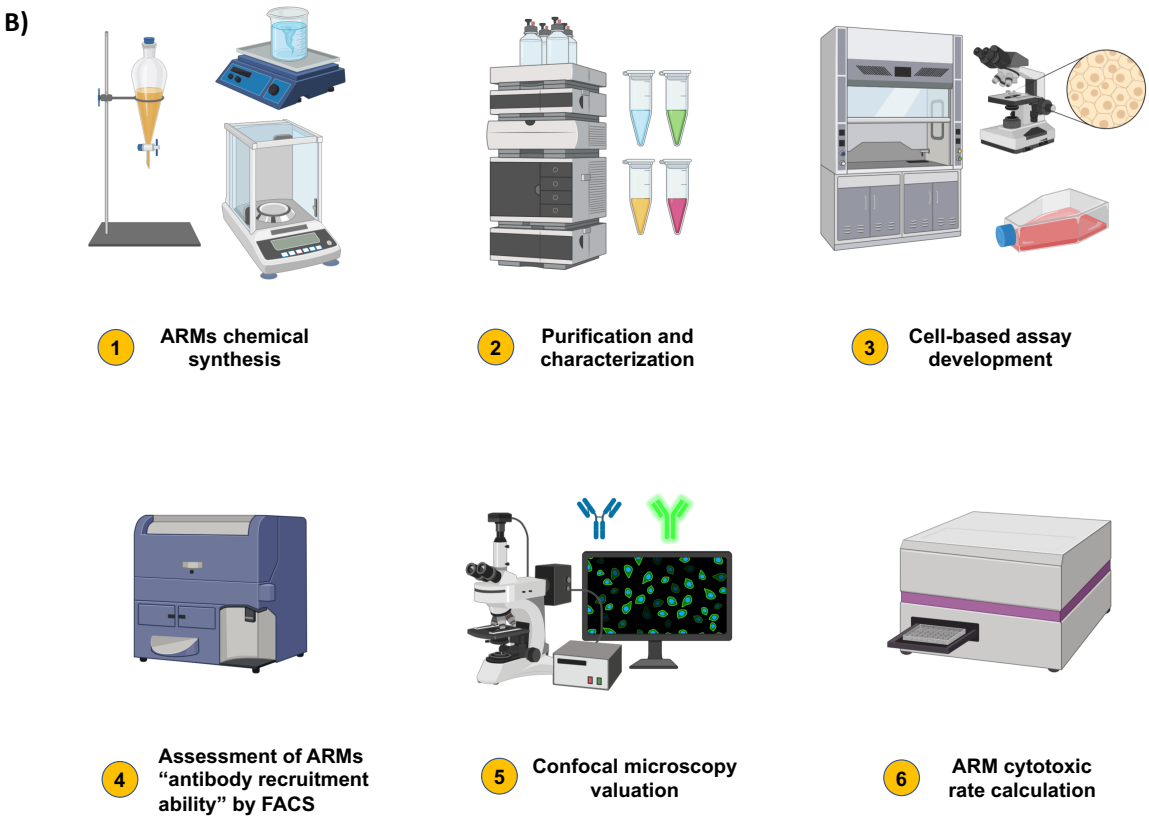

***Figure 34** A) General project; **B**) General scheme of my Ph.D. project.*

After a general introduction (Chapter 1) briefly describing cancer, immunotherapy, we highlighted the ARM approach through several structures developed over the last twenty years. Then the different steps of my thesis project are described in my manuscript.

In “Design and Synthesis of ARMs” (Chapter 2), we report the basis of our chemical strategies which relies on three successive steps: ABMs and TBMs were firstly chemically synthesized, and then assembled into a single molecule to provide ARM. Concerning the ABM part, different carbohydrate antigens have been modified to install an alkyne group in the anomeric position in order to be grafted on either azido-cyclodecapeptide or azido-dendron type platforms by CuAAC reaction. Concerning the TBM part, the same azido-platforms were functionalized with different peptides, modified with an alkyne group, by CuAAC reaction. Finally different ARMs were chemically synthesized, varying the combination of ABM and TBM, the architectures, the size, the length, the flexibility, the valence and nature of epitopes. Each molecule was characterized through HPLC, mass spectrometry (MALDI or ESI) and ^{1}H-NMR.

In “ARMs biological evaluation” (Chapter 3), each ARMs were assessed by FACS analysis and through a cytotoxic assay. By FACS analysis, we evaluated the ARM ability to form a ternary complex with the target cell and antibodies. Several conditions, such as ARM, cell, and human serum concentrations, incubation times, and different temperatures, were evaluated. Additional confocal microscopy analyses were done to confirm that the complex was not internalized inside the cell. Finally a cytotoxic test was used with ARMs on different cell lines to confirm that once the ternary complex is formed, a potent immunological response can be formed in the presence of human serum only. Once again, several parameters were assessed. We also discuss the correlation between the structure of ARMs and the observed biological effect.

After the “Conclusion and future outlooks” (Chapter 4) briefly describing the conclusion of this thesis and the short-term and long-term perspectives, the experimental part “Material and methods” (Chapter 5), and the bibliography are shown.

Chapter II.

Design and Synthesis of ARMs

II.1. Introduction

For the first part of this work, we synthesized different functionalized multivalent platforms and carbohydrate or peptides ligands to assemble them by chemoselective 'click' reactions, thus providing several ABMs and TBMs. Next, ABMs and TBMs have been combined within a single molecule to provide potential ARMs that will be studied in the second part of this work.

II.2. Chemoselective chemistry

II.2.A. General strategy

One of the main problems associated to the synthesis of complex supramolecular structures is their long multistep process including successive protections/deprotections and the utilization of often toxic chemical reagents. To circumvent these problems, our team has been interested for several years in the chemoselective approach based on click chemistry. They consist in synthesizing different functionalized building blocks, peptide scaffolds and sugars in our case, and assembling them by quick and effective coupling reactions to provide bioconjugates. Our peptide scaffold bearing 'clickable' functions are easily synthesized by solid phase peptide synthesis (SPPS). Carbohydrate building blocks are synthesized from commercial sugar moieties which are functionalized at the anomer position in order to install the complementary functions to allow ARM construction by click chemistry. Once synthesized, there are two main approaches to combine these building blocks as multivalent structures. Through a divergent approach (Figure 35 A), a central "core" peptide platform is grafted by another peptide platform to provide peripheral branching functions, which are finally functionalized with the sugar moiety. By a convergent assembly (Figure 35 B), peripheral peptide platform is previously functionalized with the sugar moiety, and then grafted on the central "core" platform, to give the same glycodendrimer. In our case, we decided to use a convergent strategy because, even if this strategy may be limited due to steric effects, it allows for an easier removal of impurities and partially reacted intermediates, usually providing pure glycostructure, as already demonstrated in our group.[154]

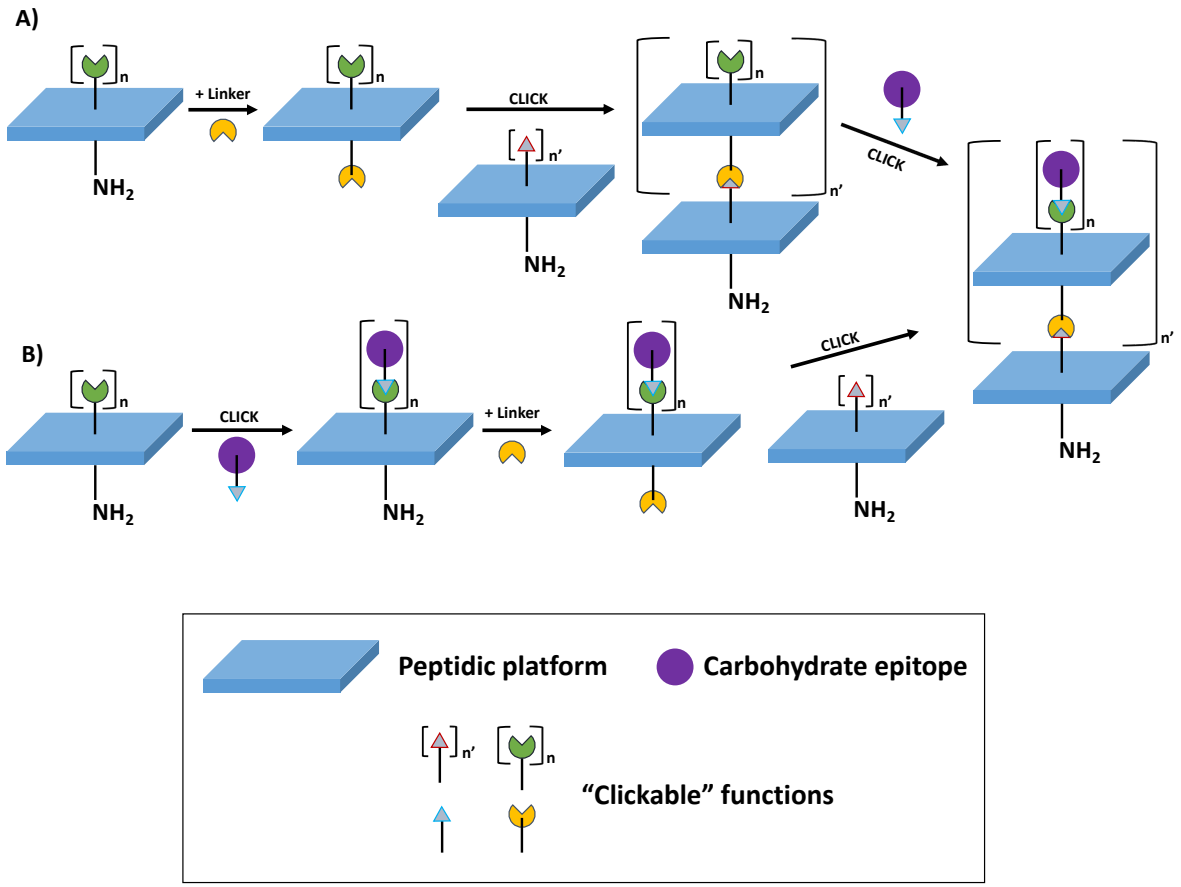

Figure 35 A) *divergent and* ***B)*** *convergent synthesis to obtain multivalent conjugates by click chemistry.*

II.2.B. Chemoselective "click" chemistry

II.2.B.I.General overview

"Click" chemistry was introduced by Sharpless *et al.* in 2001, defining the term such as "the development of an expanding set of powerful, selective, and modular blocks that work efficiently in both small- and large-scale application".[155] A reaction, in order to belong to the click chemistry family, must follow several criteria. Reagents and solvents must be commercially available and not toxic: in the ideal situation, the reaction occurs in aqueous solution, ambient temperature and near physiologic pH. The chemical reaction must be stereo-selective, rapid and efficient, have a high thermodynamic driving force, reproducible and give high reaction yields. The product must be stable under physiological conditions and easily isolated and if there are secondary products, they must be inoffensive and easily eliminated. Since their first description in the 2000s, click reactions have been the subject of many organic, medicinal and bio-chemistry articles, until providing new approaches to *in vivo* chemistry.[156] Moreover, several "click" reactions are orthogonal to each other, meaning different types of "click" reactions can happen in a one-pot approach or in a

sequential manner.[157] Among the most common reactions, we decided to use the copper(I)-catalyzed alkyne-azide cycloaddition (CuAAC).

II.2.B.II. Cu(I)-catalyzed azide-alkyne cycloaddition (CuAAC)

In 1967, the organic literature described for the first time the Huisgen 1,3-dipolar cycloaddition, cycloaddition performed between an azide and an alkyne moieties that leads to a mix of 1,4 + 1,2 -triazoles.[158] Approximately 30 years later, CuAAC reaction was presented by Sharpless (Scheme 1). CuAAC is a cycloaddition between an azide and an alkyne moiety performed at room temperature in the presence of copper as the catalyst. Cu(I) interacts in a specific manner with the reagents, resulting in the selective synthesis 1,4-triazoles only. Two mechanisms have been proposed in the literature. The first one hypothesizes the intervention of a unique Cu(I) ion (Figure 36 A), while much more recently second version suggests the intervention of a second Cu(I) ion in order to influence positively the energy profile of the reaction (Figure 36 B).[159-161]

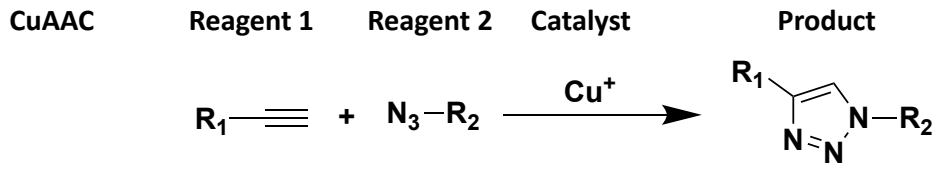

Scheme 1 *General Cu(I)-catalyzed azide-alkyne cycloaddition (CuAAC) reaction.*

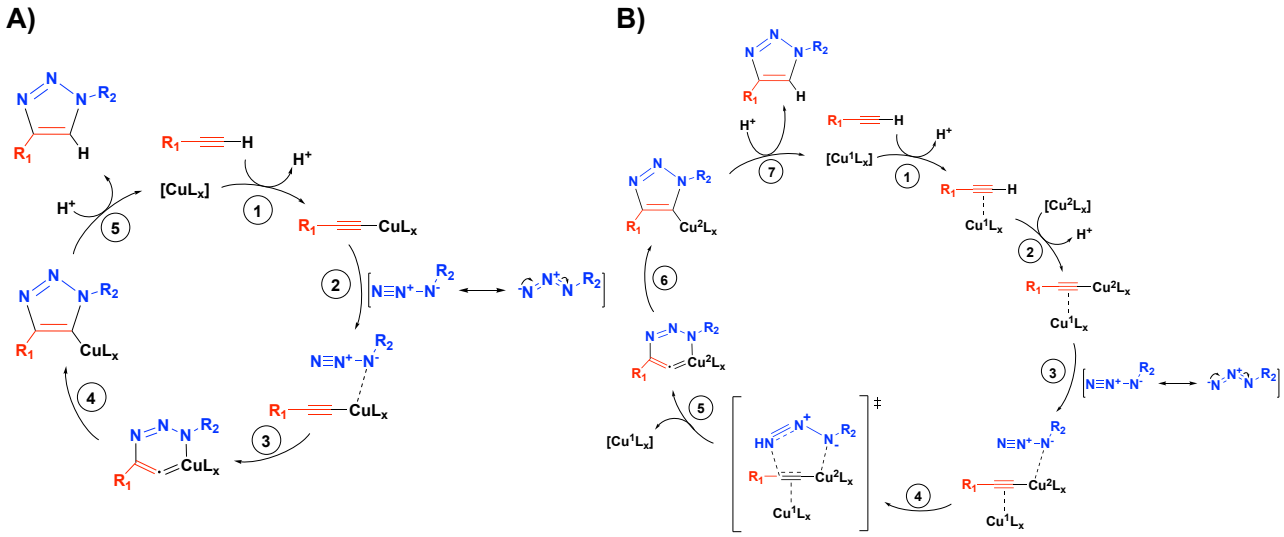

Figure 36 *Catalytic cycle of CuAAC* ***A)*** *catalyzed by one copper Cu(I) atom* ***B)*** *catalyzed by two copper Cu(I) atoms; Lx=H_2O (adapted from Fokin et co-workers, Chem. Soc. Rev., 2010).*[160]

A large variety of Cu(I) sources has been employed: CuX halides complex (where X is F, Cl, Br, or I), metallic copper or by a mixture of a Cu(II) salt and a reducing agent. Since the most

important factor is maintaining the Cu(I) at this oxidative step at all times during reaction, the preferred source of Cu(I) is use a Cu(II) salt with addition of a reducing agent in a large excess. $CuSO_4$ remains one of the most preferred options in case of aqueous solvent due to its ease of handling, to ease of workup and purity of product. Several molecules can be used as reducing agents, such as quinone, hydroquinone, vitamin K, glutathione, cysteine but sodium ascorbate being by far the most popular.[162,163] The reaction is degassed with an inert gas to avoid the re-oxidation of Cu(I) to Cu(II). Furthermore, several Cu(I) ligands have been carried out, notably the ligands tris(hydroxypropyltriazolylmethyl)amine (THPTA), 3-(4-((Bis((1-(tert-butyl)-1H-1,2,3-triazol-4-yl)methyl)amino)methyl)-1H-1,2,3-triazol-1-yl)propane-1-sulfonic acid (BTTES) and 2-(4-((Bis((1-(tert-butyl)-1H-1,2,3-triazol-4-yl)methyl)amino)methyl)-1H-1,2,3-triazol-1-yl)acetic acid (BTTAA), to overcome the problems of re-oxidation, to stabilize Cu(I) ion and to dramatically boost the CuAAC kinetics in aqueous solution (Figure 37).[164]

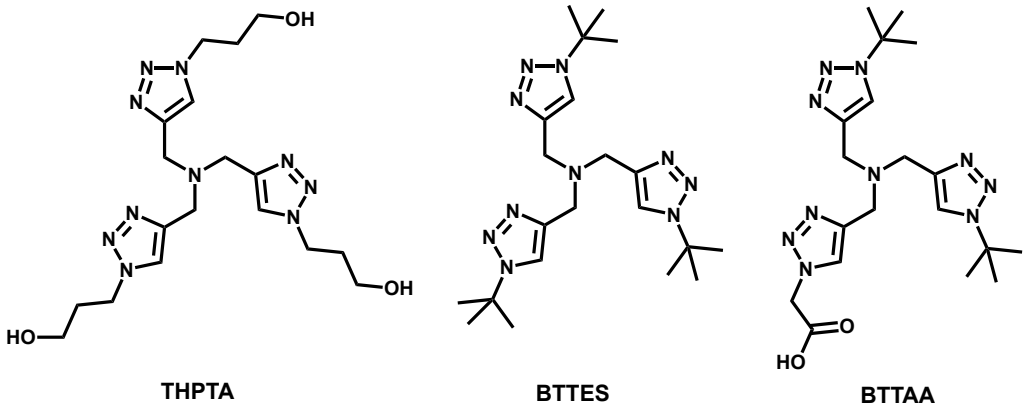

Figure 37 *THPTA, BTTES and BTTAA are a water-soluble, very effective ligand for Cu (I)-catalyzed Alkyne-Azide click chemistry reactions (CuAAC). They serve a dual purpose: acceleration of the CuAAC reaction by maintaining the Cu(I) oxidation state of copper sources and protection of biomolecules from oxidative damage during the labeling reaction.*

One of the biggest problematic of this reaction is that the triazole could chelate the Cu(I), which can remain trapped into the glycoconjugate and induce toxicity *in vivo*.[165] Chelating resin, dialysis, microfiltration, or high performance liquid chromatography (HPLC) are generally used to avoid these problems before biological tests with bioconjugates. Next, although CuAAC usually results in almost quantitative conversion, the secondary structure of long peptides or dendrimers may affect the efficiency of the reaction and decrease the yield. In this case, microwave irradiation has been shown to improve the reaction yields and purity.[166]

II.2.C. Solid phase peptic synthesis (SPPS)

Solid phase peptic synthesis (SPPS), described for the first time in 1963 by Merrifield *et al.*,[167] is a synthetic strategy which relies on the sequential coupling of amino acids, alternating selective deprotection and coupling steps, without intermediate purifications (Figure 38).

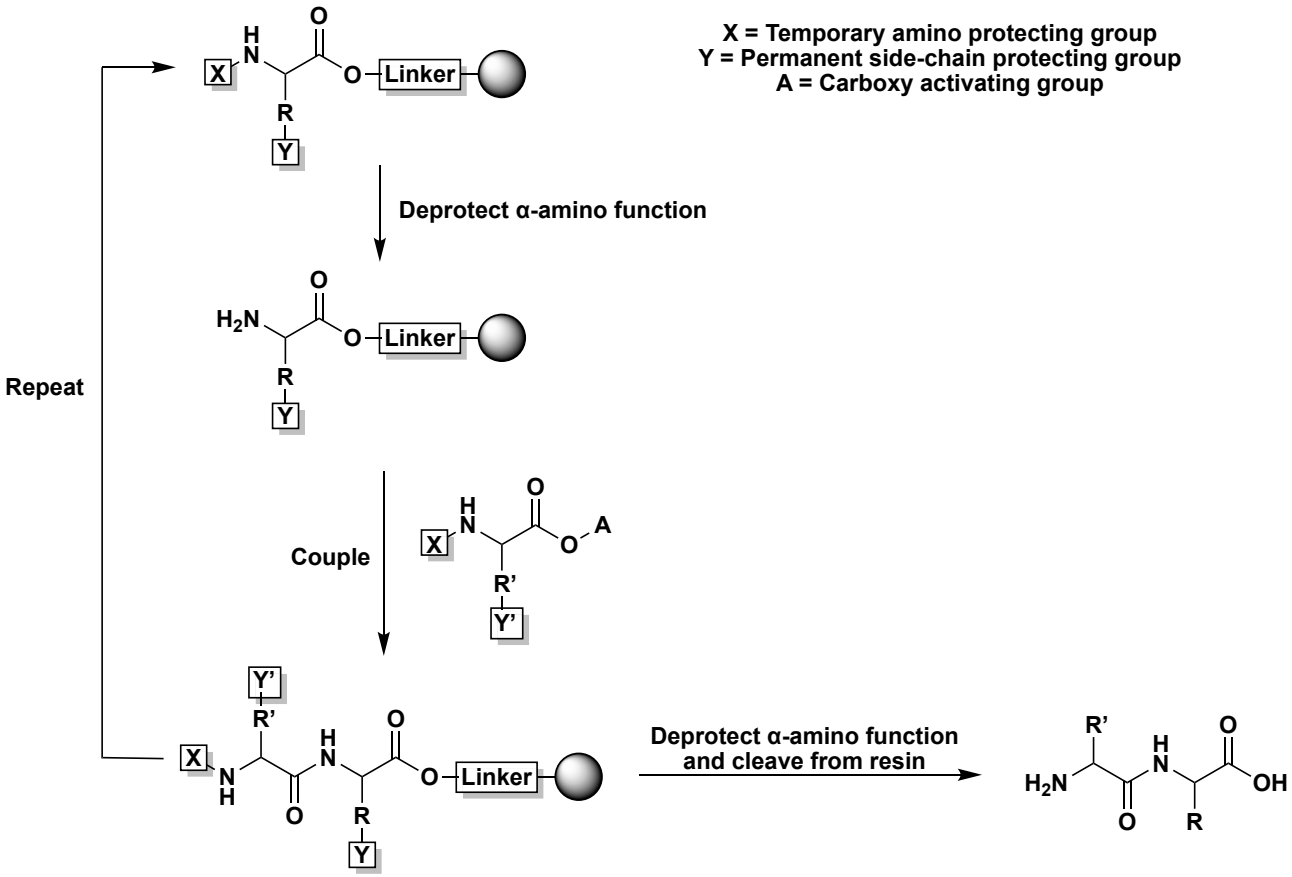

Figure 38 *The solid phase peptide synthesis (SPPS) principle.*

It is compatible with a large number of reaction conditions in terms of solvents, coupling reagents, orthogonal protective groups, etc. In addition, the solution containing the reactive species is easily removed by filtration, since the synthesis is carried out on functionalized resin beads, in a glass or plastic reactor. In SPPS, two strategies can be used. The first is called -Boc/-Bn strategy and it involves the use of amino acids having a -Boc protecting group on the amine function (temporary group), as well as the use of protecting groups on the side chains, adapted to acid conditions of -Boc deprotection, such as benzyl (permanent groups) (Figure 39 A). The The -Fmoc/-tBu strategy uses a -Fmoc protective group as the temporary group and often acido labile permanent group, thus requiring synthesis conditions softer and the possibility to monitor by spectrometry the deprotection/coupling steps harnessing the aromatic -Fmoc group (Figure 39 B). The -Fmoc/-tBu strategy is preferred and commonly used in our laboratory.

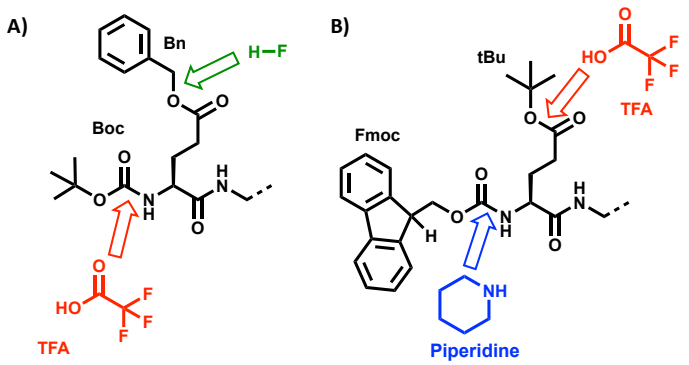

Figure 39 A) *-Boc/-Bn strategy based upon the graduated acid lability of the side chain protecting group.* ***B)*** *-Fmoc/-tBu based on an orthogonal protecting group strategy.*

After defining the strategy, 1) the solid support, 2) the temporary and permanent protective groups and 3) the coupling reagents should be carefully chosen.[168]

1) There are two essential conditions to select the right **solid support or resin**. First of all, it is crucial to check that the conditions for the peptide detachment from the support do not impact to the permanent protecting groups present on the lateral chains of the peptide. Next, it is fundamental to know which functional residue one wants on the terminal amino acid. A first resin category allows the release a carboxyl function on the final peptide structure, which are particularly suitable for the synthesis of cyclic peptides. Merrifield resin and Wang resin require strong acid conditions, such as hydrofluoric acid or trifluoroacetic acid (>90%) respectively, while Sasrin and Chlorotrityl resins involve milder conditions with dilute 1-0.5% trifluoroacetic acid solutions (Figure 40).

Resin	Structure	Cleavage condition	Strategy
Merrifield	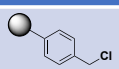	Hf or HBr/TFA	Boc/Bn
Wang	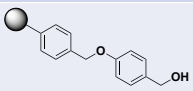	95% TFA	Fmoc/^{t}Bu
Sasrin	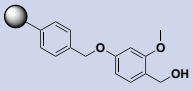	1% TFA	Fmoc/^{t}Bu
Chlorotrityle	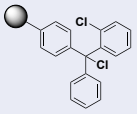	0.5% TFA or Acetic acid/TFE	Fmoc/^{t}Bu

Figure 40 *List of most common resins which release carboxyl function after cleavage. In the picture are indicated the name and the resin's structures, then the cleavage and the strategy conditions.*[169]

A second resin category allows the release of an amide group, often appropriate for the synthesis of linear peptides. Among the resins in this category, the Sieber resin, which requires mild acid conditions (2% TFA solution), the Rink amide and BHA/MBHA resins, that require highly concentrated TFA or HF solutions (>90%), are the most widely used (Figure 41).

Resin	Structure	Cleavage condition	Strategy
Sieber	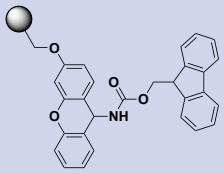	2% TFA	Fmoc/^{t}Bu
Rink amide	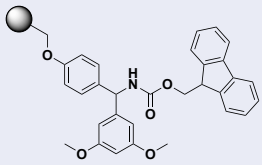	95% TFA	Fmoc/^{t}Bu
BHA MBHA	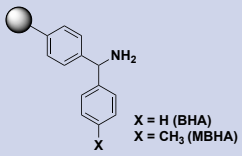	HF	Boc/Bn

Figure 41 *List of most common resins which release amide function after cleavage. In the picture are indicated the name and the resin's structures, then the cleavage and the strategy conditions.*[169]

2) Next, it is very important to choose the right **temporary and permanent protecting groups** that are eliminated only after synthesis ended. In the case of the strategy -Fmoc/-tBu, permanent protecting groups are different depending the amino acid. For amino functions, the most common are the -Boc, -Cbz (or -Z) and trityl (-Trt) groups, which require acidic conditions, the -Dde group, which needs the use of hydrazine, and the -Alloc group, which necessitates palladium catalyzed deprotection (Figure 42 A). For carboxyl groups, the permanent protective groups that can be used are -tBu, -Bn and cyclohexyl (-cHx) groups, that require TFA or HF solutions, the chlorotrityl group, which needs only 1% TFA solutions, and the allyl (-Al) group which requires the same deprotection condition than the -Alloc group (Figure 42 B). For hydroxyl groups, the usual protecting groups are the -Trt, -tBu and -Bn, already mentioned above (Figure 42 C).

A)

Protector group	Deprotection conditions
Fluorenylmethoxycarbonyl (Fmoc) 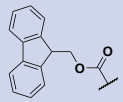	20% piperidine/DMF or 50% morpholine/DMF
Tert-Butyloxycarbonyl (Boc) 	25-50% TFA or HCl (4M)/dioxane or $MeSO_3H$ (2M)/dioxane
Benzyloxycarbonyl (Z) 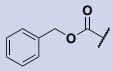	H_2 (cat) or HBr/AcOH or HF
Trityl (trt) 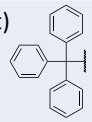	1% TFA/DCM or 3% TCA/DCM
2-(1-ethylidene)-5,5-dimethylcyclohexane-1,3-dione (Dde) 	2% $N_2H_4{\cdot}H_2O$/DMF
5,5-dimethyl-2-(3-methyl-1-butylidene)cyclohexane-1,3-dione (ivDde) 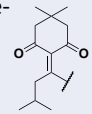	2% $N_2H_4{\cdot}H_2O$/DMF
Allyloxycarbonyl (Alloc) 	$Pd(PPh)_4$ (0.1 eq.) $PhSiH_3$ (25 eq.) in DCM

B)

Protector group	Deprotection conditions
Tert-Butyl (^{t}Bu) 	90% TFA/DCM or HCl (4M)/dioxane
2-ChloroTrityl (2-Cl-trt) 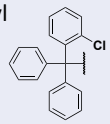	1% TFA/DCM
Benzyl (Bn) 	H_2 (cat) or HF
Cyclohexyl (cHx) 	HF
Allyl (Al) 	$Pd(PPh)_4$ (0.1 eq.) $PhSiH_3$ (25 eq.) in DCM

C)

Protector group	Deprotection conditions
Tert-Butyl (^{t}Bu) 	90% TFA/DCM or HCl (4M)/dioxane
Trityl (trt) 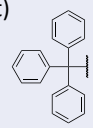	1% TFA/DCM or 3% TCA/DCM
Benzyl (Bn) 	HF

Figure 42 *Temporary and permanent protective groups used for **A)** amino, **B)** carboxyl and **C)** alcohol functions.*[169]

3) Finally, the choice of the **coupling reagent** is essential for the activation (enhance the electrophilicity) of the carboxylate function. The coupling agent is temporarily attached to this carboxylate group forming a highly electrophilic intermediate, making nucleophilic attack by the terminal amino group on the growing peptide more efficient.[170,171]

Among the variety of commercial coupling reagents, the most commonly families used in peptidic synthesis are:

➢ Carbodiimides family, for example N,N'-dicyclohexylcarbodiimide (DCC) or N,N'-diisopropylcarbodiimide (DIC). DCC is very useful in solution phase reactions, but is not suitable for reactions on resin since the dicyclohexylurea, the byproduct formed from DCC, is nearly insoluble in most organic solvents and precipitates from the reaction mixture as the reaction progresses. DIC is used instead in SPPS since the urea byproduct is more soluble and will remain in solution. The drawback of carbodiimide activation of amino acid derivatives is that often it causes a partial racemization, that can be reduced adding an equivalent of 1-hydroxybenzotriazole (HOBt) (Figure 43).

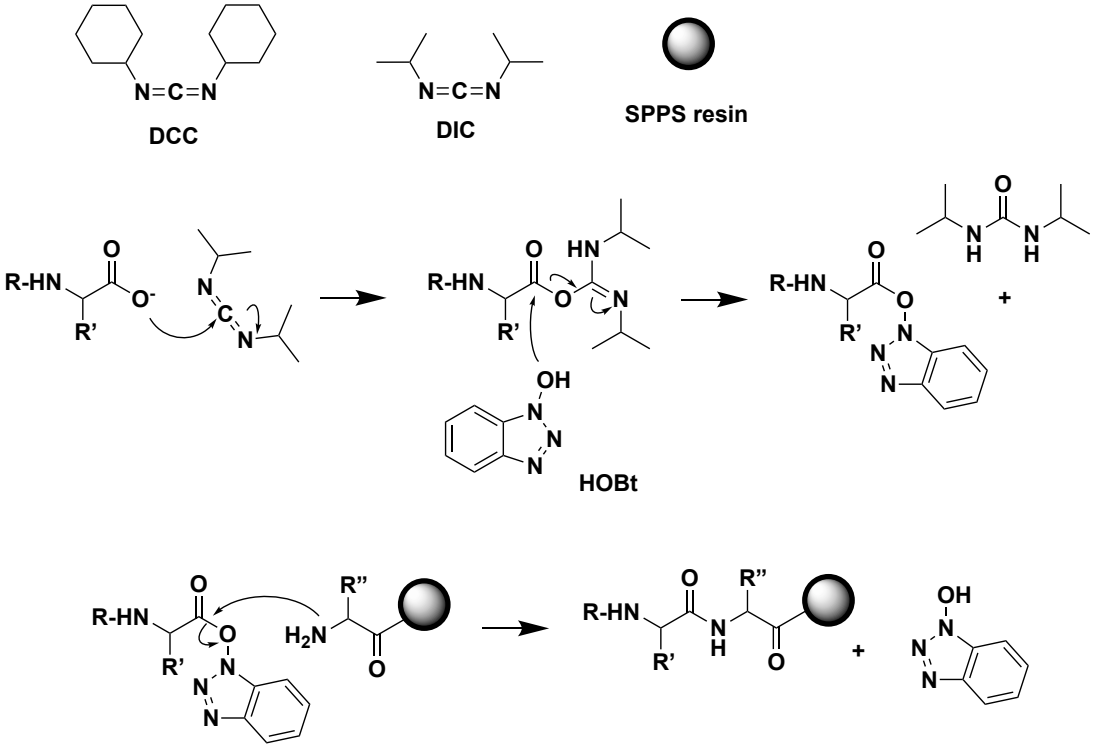

Figure 43 *Coupling reagents from the carbodiimides family. At the bottom it's showed the DIC mechanism of action.*

➢ Benzotriazole HOBt family, such as phosphonium derivatives and aminium/uranium derivatives (first and second generations):

- Phosphonium derivatives (PR_4^+), such as (7-Azabenzotriazol-1-yloxy)tripyrrolidino phosphonium hexafluorophosphate (PyAOP) and (Benzotriazol-1-yloxy)tris(dimethylamino) phosphonium hexafluorophosphate (PyBOP). These reagents are able to directly generate OBt esters *in situ* allowing a more rapid coupling kinetics than carbodiimide derivatives and minimizing the racemization and other side reactions occurring with the carbodiimide reagents (Figure 44 A).

- The most common aminium/uranium derivatives from the first generations (2002) are O-(7-Azabenzotriazol-1-yl)-N,N,N',N'-tetramethyluronium hexafluorophosphate (HATU) and O-

(Benzotriazol-1-yl)-N,N,N',N'-tetramethyluronium hexafluorophosphate (HBTU).[172] Both are very efficient peptide coupling reagents particularly useful for peptide cyclization and fragment condensations with insignificant levels of racemization and very rapid kinetics. Importantly, these reagents must be used in equal molar amounts relative to the carboxylic acid component of the coupling reaction since the excess of HATU and HBTU can react with the unprotected N-terminal of the peptide and form a guanidine moiety that blocks further elongation of the peptide (Figure 44 B).

- The most common aminium/uronium derivatives from the second generations (2007) are HDMA and HDMB derived from the replacement of one of the two dimethylamino groups by a morpholine group on the carbon skeleton of HATU and HBTU, allowing an increased reactivity and reduction of racemization. They are used in difficult coupling, such as coupling N-methylamino acids, where other coupling reagents are inefficient (Figure 44 C).

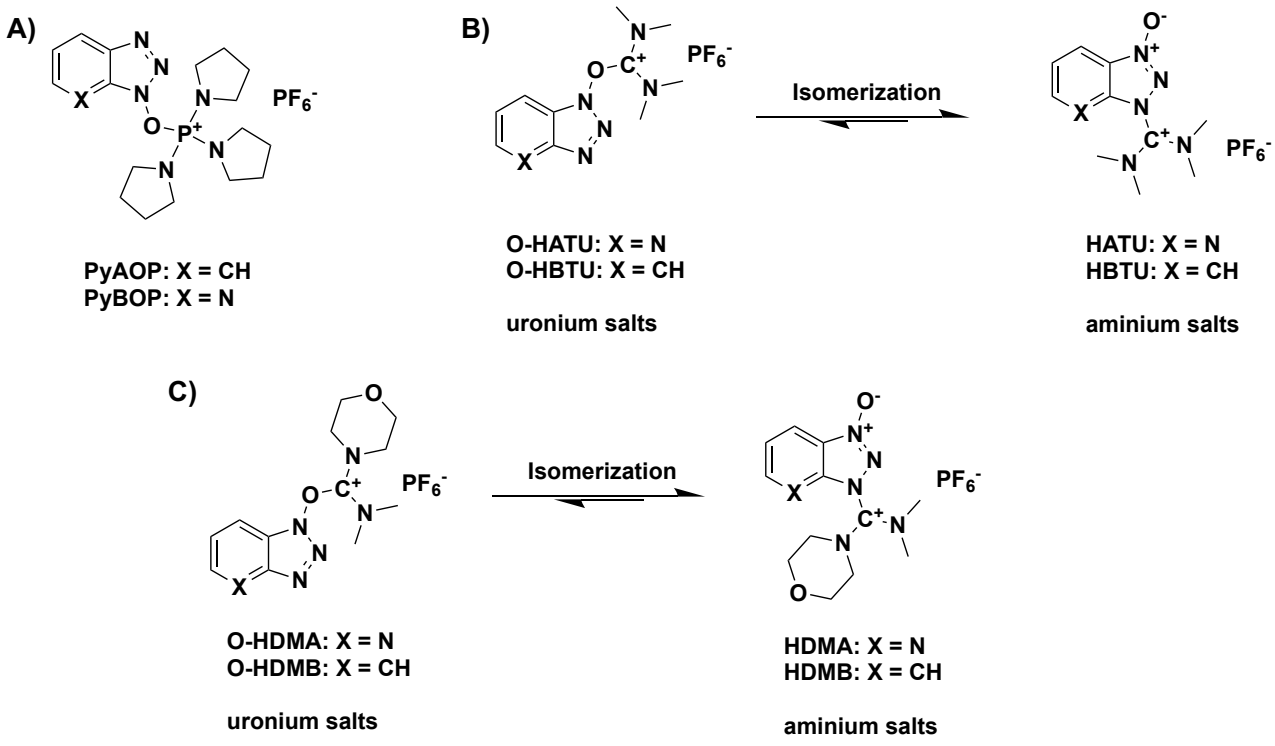

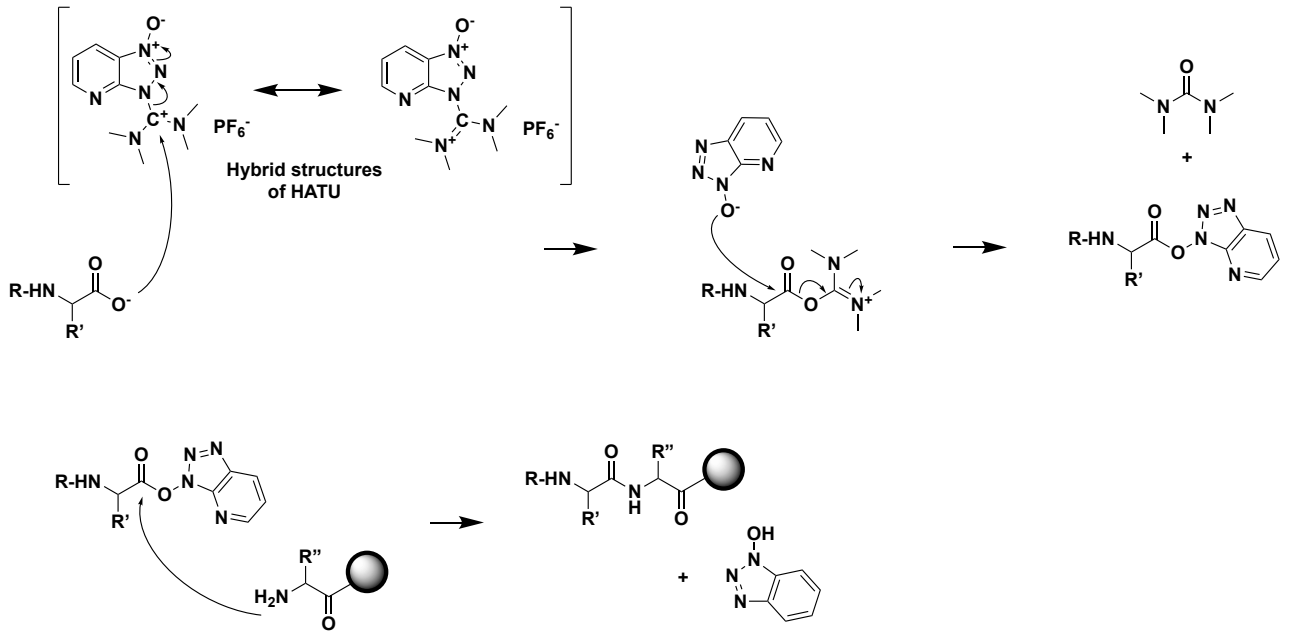

Figure 44 *Coupling reagents from the Benzotriazole HOBt family;* ***A)*** *phosphonium derivatives,* ***B)*** *first generations of aminium/uranium derivatives,* ***C)*** *second generations of aminium/uranium derivatives. At the bottom it's showed the HATU mechanism of action.*

- Oxyme family, such as the OxymaPure derivatives (first generation) and Oxyma-B (second generation).

- Since the discovery of the explosive properties of HOBt derivatives (2009), the ethyl cyanohydroxyiminoacetate (OxymaPure) derivatives, such as the dimethylmorpholineuronium salt (COMU), were reported as a safer and very efficiently coupling molecules (without racemization) than the benzotriazole HOBt derivatives (Figure 45 A).[173]

- More recently (2014) it has been reported the 5-(hydroxyimino)-1,3-dimethylpyrimidine-2,4,6(1H,3H,5H)-trione (Oxyma-B) as an excellent additive to prevent racemization during SPPS, showing superior performance than OxymaPure and HOBt. The uronium-type coupling reagents involving Oxyma-B as a leaving group, called TOMBU and COMBU, allowed to a better stability but slightly lower coupling yields than COMU (Figure 45 B).[174]

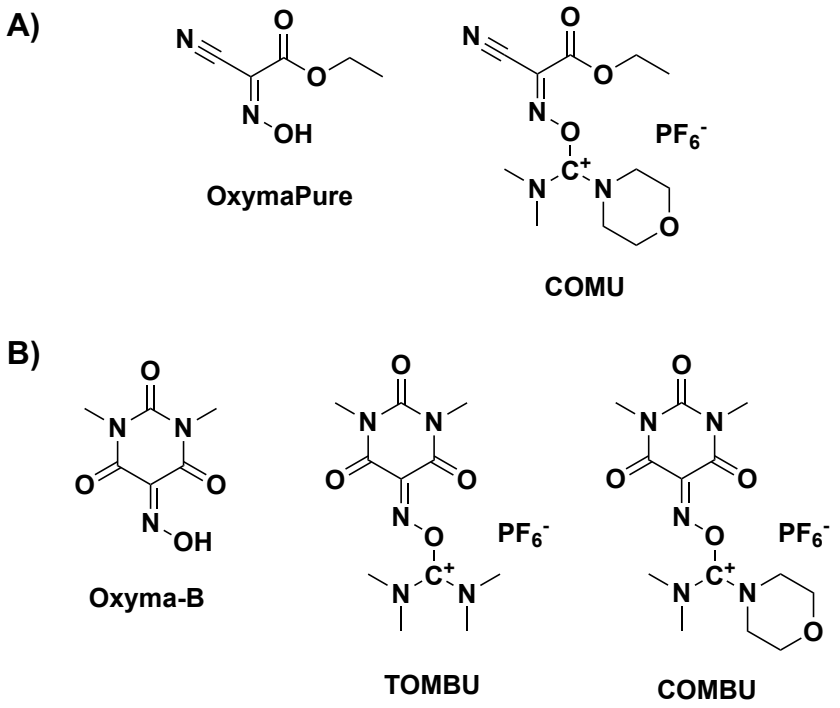

Figure 45 *Coupling reagents from the Oxyme family;* ***A)*** *OxymaPure derivatives,* ***B)*** *Oxyma-B derivatives.*

After successive cycles of deprotection of the temporary group and coupling steps, it is possible to obtain linear peptide sequences, which can be either cyclized and/or modified in solution.

II.2.D. Multivalent platforms

II.2.D.I General overview

In nature, biological processes harness multivalent interactions to increase ligands affinity and selectivity for their targets but also to make cluster receptors for certain cellular signal transmissions. The concept of multivalent effect, or glycoside cluster effect for glycoconjugate, has been introduced for the first time in 1995 by R. T. Lee.[175] According to this, the apparent affinity of a multivalent ligand for its target is superior than the affinity of the same ligand presented alone. Obviously, this effect could be observable only if the multivalent ligand has the valence, geometry and size to maximize interaction, whose several mechanisms depend on the number and geometry of the receptor recognition sites. Chelate mechanism consists in the simultaneous binding of a multiligand to the same multimeric form protein (Figure 46 A). It is also possible to observe this phenomenon when two monomeric receptors come in contact: this clustering phenomenon is observable especially in the case of membrane receptors (Figure 46 B). A chelate

effect is also possible when a multiligand involves a secondary site in addition to the active interaction site, allowing a better selectivity (Figure 46 C). Finally, the last interaction mechanism is linked to statistical re-association due to the local concentration near to the interaction site of a monomeric binding site (Figure 46 D). These properties can be explained by thermodynamic processes. Ligand affinity for a target is controlled by the binding energy. When multivalent ligand is presented on the multimeric form receptor, the main energy cost used for the binding of the first ligand, allows also the binding of the others without additional energy. Note that the multivalent effect observed for a multivalent ligand/multimeric receptor couple is usually dependent on a combination of interaction mechanisms.[176]

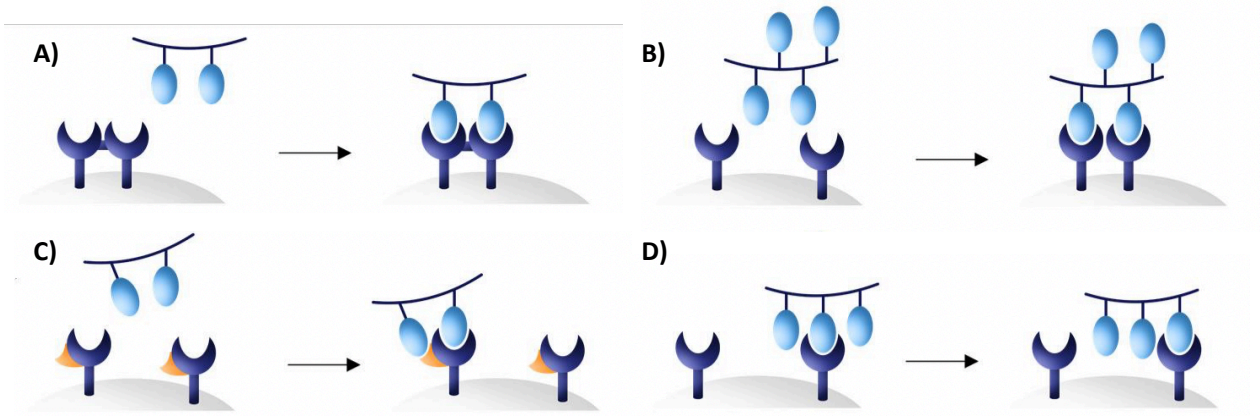

Figure 46 *Different mechanisms of multivalent interaction* ***A)*** *chelate mechanism;* ***B)*** *clustering mechanism;* ***C)*** *chelate mechanism involving secondary site* ***D)*** *statistical re-association (adapted from Kiessling and co-workers, Curr Opin Chem Biol., 2000).*[176]

II.2.D.II The RAFT platform

Among the diversity of multivalent platform described in the literature,[177] our group uses the RAFT (Regioselectively Addressable Functionalized Template) since more than a decade (Figure 47 A).[178-179] Discovered for the first time in the late 1990s by Mutter group and developed later by Renaudet, Dumy and others, it is a cyclodecapeptide that contains two Gly-Pro antiparallel ß turn able to stabilize the conformation of the cycle in solution. The presence of 4 Lys in the upper face allows the multiple conjugations with sugars, peptides or other platforms while the functionalization of the 1 or 2 Lys towards the lower side can be used as anchor point for fluorescent tags, biosensor or other peptidic platform depending on the targeted biological application (Figure 47 B). In our case, one of this last Lys is replaced by Ala since the presence of a second lysine is not required. In addition, RAFT is easily chemically accessible and due its cyclic structure, it is stable *in vivo* and non-immunogenic therefore suitable for applications *in vivo*.[180-183]

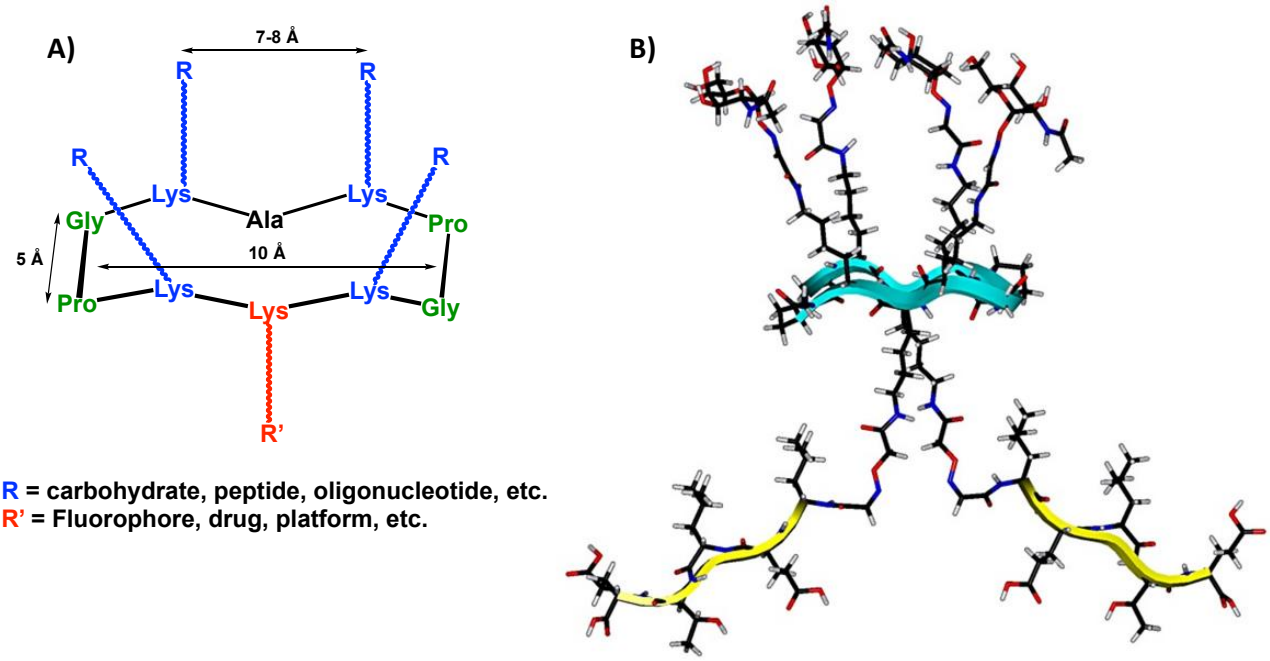

Figure 47 A) *General structure of RAFT developed by Mutter, Dumy and co-workers.* ***B)*** *3D model representation with four sugar residues in the upper domain and two peptide sequences in the lower domain.*

First of all, we synthesized the scaffold $R(N_3)_4$ **5** which contains 4 azide groups in the upper domain in order to graft 4 sugars or peptides previously functionalized with alkyne groups. The platform $R(N_3)_4$ **5** is obtained by multi-steps synthesis combining SPPS and reactions in solution (Scheme 2). SPPS on Fmoc-Gly-SASRIN resin leads to the protected linear peptide with sequence alternating Lys(N_3) **1** at four position. Once assembled on the solid support, the linear peptide **2** is cleaved from the resin by successive resin treatments with a 1% TFA solution in DCM (general procedure **B1**). The reaction mixture is then filtered into a flask and the TFA/DCM mixture is evaporated. Without further purification step, the linear peptide **3** is next cyclized in dilute DMF/DCM solution (0.5 mM), to avoid intermolecular reactions, in the presence of PyBOP and DIPEA (pH 8-9). The reaction is followed by analytic HPLC. After 2 hours stirring at room temperature, the cycling peptide **4** is subsequently concentrated and precipitated in Et_2O (general procedure **C**). Finally, a TFA/DCM (3:2) mixture affords to the cyclic peptide $R(N_3)_4$ **5,** subsequently concentrated, precipitated and purified by semi-preparative RP-HPLC, with an overall yield of 40%.

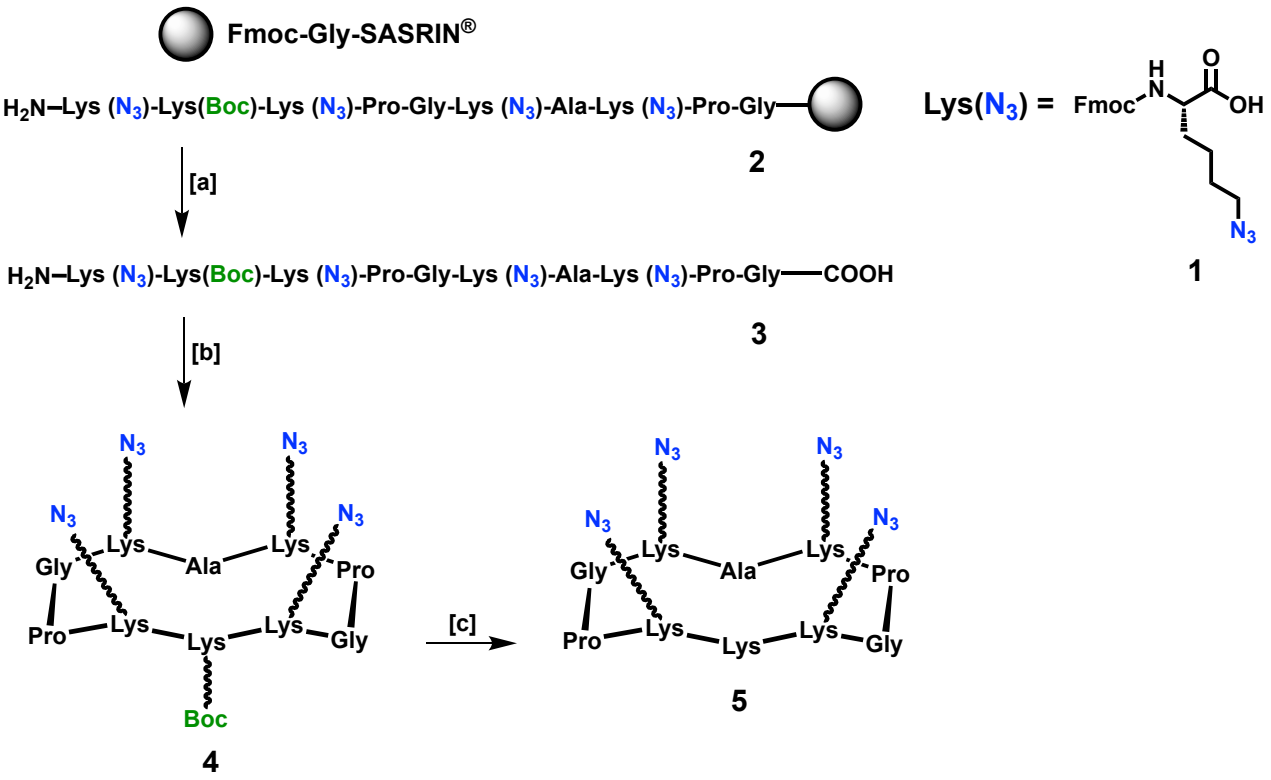

Scheme 2 *Synthesis of cyclopeptide* ***5****. Conditions:* ***[a]*** *1% TFA, CH_2Cl_2, 10x10 min ;* ***[b]*** *PyBOP (2.0 eq.), DIPEA (2 eq.), DMF/CH_2Cl_2 (1:1), 0.5 mM, r.t., 2 h.;* ***[c]*** *TFA/TIS/H_2O (95/2,5/2,5), 2x2h, r.t.; 40% overall yield.*

II.2.D.III The polylysine dendrimer platform

The word dendrimer is composed of the Greek terms “δέντρο” dendri- (tree-branch-like) and meros (part of), and was coined by Tomalia *et al.* in 1984.[184] Dendrimers are defined as repetitively branched macromolecules composed of a “core” functionalized with repeating arms, called dendrons. Unlike polymers, dendrimers are synthesized step-by-step, affording reproducible, well-defined and monodisperse structures often with spherical three-dimensional morphologies.[255] In the context of our work, we found this platform particularly attractive for its advantageous feature, which include the possibility to tailor and “grow” the epitope valency in a controlled fashion. From now, the terms glycodendrimer and peptido-dendrimer will refer to monodisperse, dendrimer-like, branched structures decorated with a peripheral carbohydrates or peptides moieties.

We selected the scaffold $D(N_3)_4$ **8** composed of a tri-peptide Lys-Ala-Lys core, subsequently conjugated with other 2 Lys bearing azide moieties, in order to graft 4 alkyne sugars or peptides. It is obtained by SPPS on Rink amide resin using a similar protocol to that previously used for $R(N_3)_4$ **5**. After -Fmoc deprotection of the amino lysine, two additional azido groups were introduced to **6** using the activated ester N_3-AcA-OSu **27** in presence of DIPEA (pH 8-9). The branched peptide **7**

was then cleaved from the resin and subsequently deprotected by a TFA/TIS/H_2O mixture (general procedure **B2**). The resulting $D(N_3)_4$ **8** platform is finally obtained with an overall yield of 65%, after precipitation and semi-preparative HPLC purification (Scheme 3).

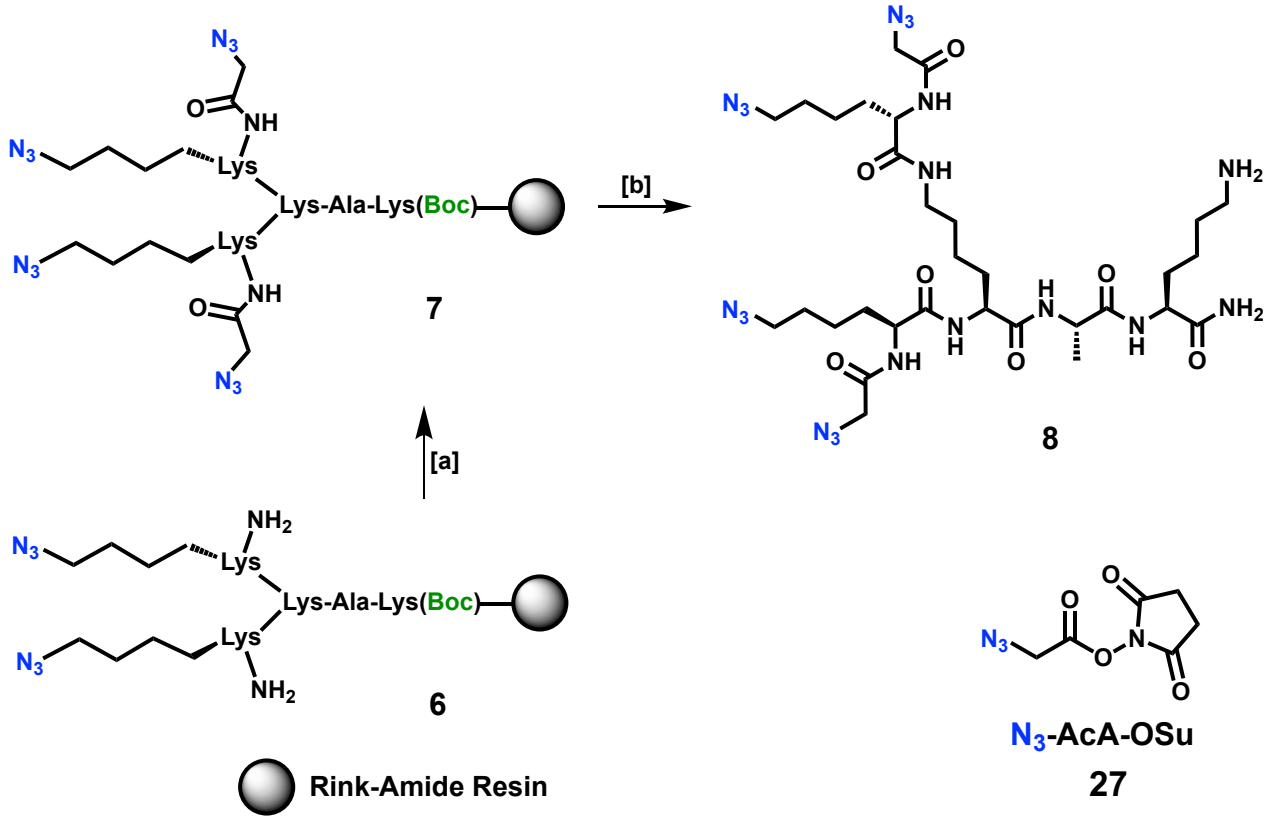

Scheme 3 *Synthesis of tetravalent dendrimer* ***8****. Conditions:* ***[a]*** *23 (5.5eq.), DIPEA (3.1 eq.), DMF, r.t., 1 h.;* ***[b]*** *TFA/TIS/H_2O (96:2:2), r.t., 2h (2 times); 65% overall yield.*

II.2.E. Carbohydrate ligands

The key parameter to consider in choosing carbohydrate ligand is the recognition of natural circulating antibodies on the human serum. High-throughput analyses of human sera by carbohydrate antigen arrays, done for the first time in 2009 by Jeffrey C. Gildersleeve research group, have allowed the characterization of the individual carbohydrate recognition patterns.[186] Among the others, L-Rhamnose (α-L-Rha, Figure 48 A), α-D-Galactose (α-D-Gal, Figure 48 C) and α-D-N-Glycolylneuraminic acid (Neu5Gc, Figure 48 D) have been identified as suitable carbohydrate moieties for our project, since the presence of high level of antibodies present in human serum against these antigen as well as the commercial availability of the free monosaccharide precursors and their reasonable simple chemical structure.[187-189] β-D-Galactose (β-D-Gal, Figure 48 B) was selected as negative control due to the absence of anti- β-D-Gal antibodies in the human serum. Regarding the trisaccharide α-D-Galactose, we decided to work

only with the nonreducing terminal carbohydrate residue, since it's the most important antigenic part.

Our strategy relies on the introduction of an alkyne functional group in the anomer position of these different carbohydrate in order to functionalize our azido-platforms by CuAAC. I was in charge to modify the commercial L-Rha in order to obtain the Propargyl α-L-Rha (compound **12**, Figure 48), while Propargyl α/ß-D-Gal (compound **29** and **30**, Figure 48) and Propargyl α-D-Neu5Gc (compound **31**, Figure 48) sugars were provided by Dr. David Goyard.

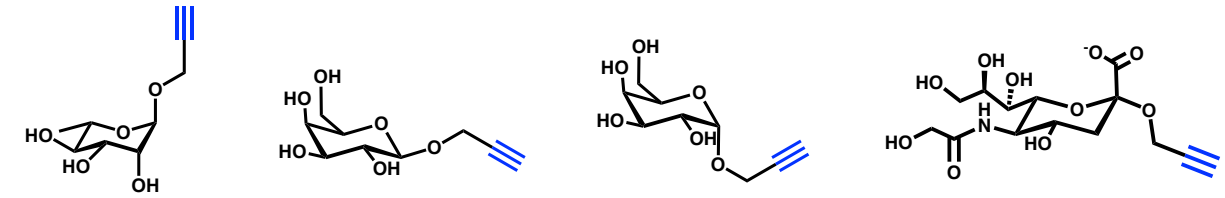

Figure 48 A) *Propargyl α-L-Rhamnose (**12**),* ***B)*** *Propargyl ß-D-Galactose (**29**),* ***C)*** *Propargyl α-D-Galactose (**30**) and* ***D)*** *Propargyl α-D-N-Glycolylneuraminic acid (**31**) are the modified carbohydrates ready to be conjugated with azido-platforms by CuAAC.*

Propargyl α-L-Rhamnopyranoside 12 is obtained in 3 steps, harnessing a protocol already described in literature.[190,191] Hydroxyl groups of commercial L-Rhamnose **9** are acetylated with a mixture of pyridine/acetic anhydride (2:1), with a quantitative yield. The α/β anomers mixture obtained is next activated at the anomeric position by treatment with propargyl alcohol in presence of boron trifluoride etherate (BF_3•Et_2O) as the promoter, afforded to the α-product **11,** with a yield of 75% after separation from the β anomer (3:1). The glycosylation for the α anomer is highly stereoselective due to the presence of the acetyl participating group at C_2. Finally, **11** is deprotected by a transesterification using a mixture of sodium methanoate and methanol to obtain Propargyl α-L-Rhamnopyranoside **12** (Scheme 4).

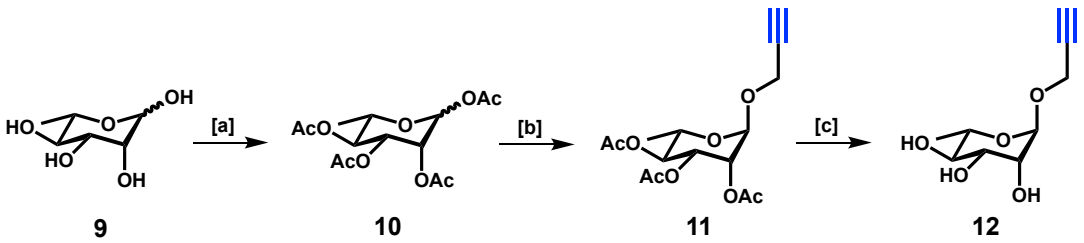

Scheme 4 *Synthesis of Propargyl α-L-Rhamnopyranoside **12**. Conditions: **[a]** Pyridine/Ac_2O solution (2:1), r.t., 24h; **[b]** Propargyl alcohol (4.0 eq.), $BF_3.Et_2O$ (2.5 eq.), anhydrous DCM, r.t., 24h; **[c]** NaOMe, MeOH, pH 9-10, r.t., 3h; 58% overall yield.*

II.2.F. Peptide ligands

As mentioned in the introduction, there are several proteins overexpressed on the surface of several type of cancer cells and, among them, $\alpha_v\beta_3$ integrin and EGFR represent key targets for antitumoral therapy nearly 30-odd years. In this thesis, we worked with 3 different peptides:

1. The cyclic Arg-Gly-Asp-(D-Phe)-Lys pentapeptide (cRGD) is an excellent ligand of the $\alpha_v\beta_3$ integrin overexpressed in many tumor cells; it is extensively studied by our research team and has been used for cell imaging and drug delivery.[192-196]
2. The linear Leu-Ala-Arg-Leu-Leu-Thr hexapeptide (LT), ligand of an extracellular region of EGFR (affinity and K_D are unknown), recently studied as a candidate for diagnostic applications.[197,198]
3. The linear Arg-Lys-Asp-His-His-Val-His-Leu-Pro-Asn-Asn-Gly dodecapeptide (HVH), ligand of EGFR identified by Phage Display on Jurkat cells (T cell leukemia cells) in 2017 and, next, conjugated to a fluorophore and evaluated by *in vitro* experiments on cancer cells expressing EGFR protein by our team.[199]

In the contest of this work, these peptides were synthesized, functionalized with an alkyne and thus employed as TBM.

The peptide cRGD was synthesized using a well-known SPPS procedure from the Fmoc-Gly-SASRIN® resin, Fmoc-protected amino acids and Fmoc-Lys(N-4-Pentynoic acid)-OH **13**.[200] After cleavage under mild acidic conditions, the linear peptide **15** is cyclized in solution (general procedure **C**) and then deprotected (general procedure **D**) to give the **Alk-cRGD 17**, with overall yield of 36% (Scheme 5).

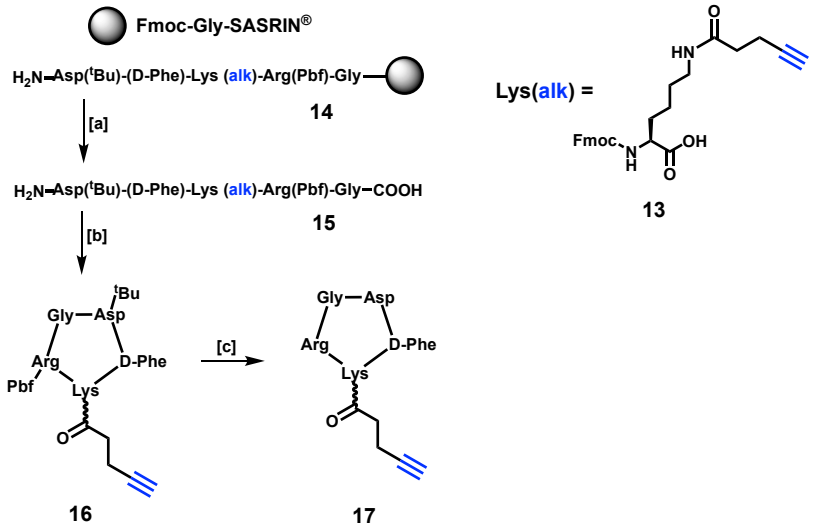

Scheme 5 *Synthesis of key penta-peptide Alk-cRGD **17**. Conditions: [**a**] 1% TFA, CH_2Cl_2, 10x10 min [**b**] PyBOP (2.0 eq.), DIPEA (2 eq.), DMF/CH_2Cl_2 (1:1), 0.5 mM, r.t., 2 h.; [**c**] TFA/TIS/H_2O (95/2,5/2,5), 2x2 h, r.t.; 36% overall yield.*

The linear hexapeptide LT is also synthesized by SPPS on the MBHA Rink amide resin on which the peptide cleavage and side chains deprotection is performed simultaneously. A pent-4-ynoic acid **18** is added at the end of SPPS on the N-terminal side in presence of PyBOP and DIPEA (pH 8-9). Semi-preparative HPLC purification result in **Alk-LT 21** (75% overall yield).

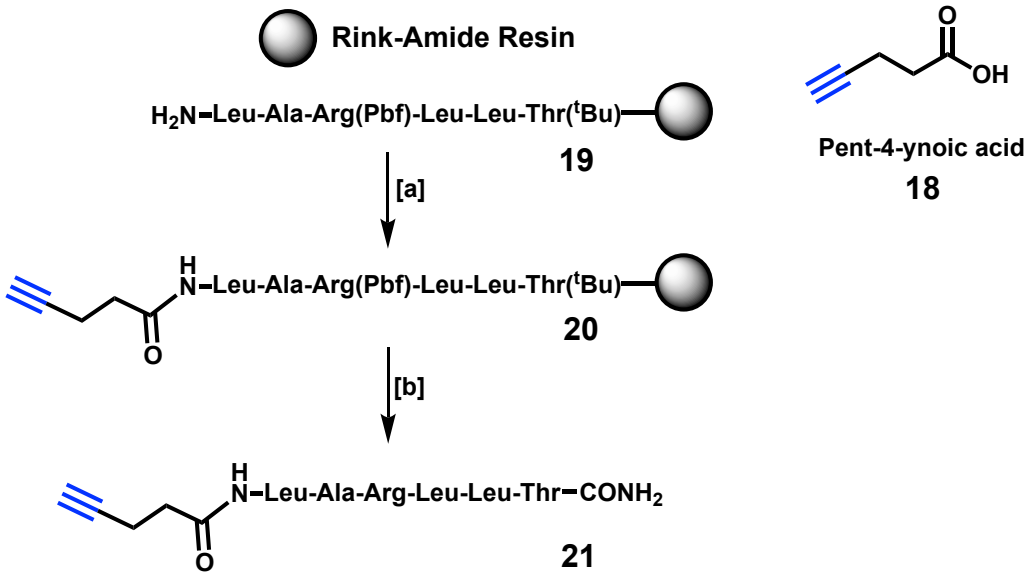

Scheme 6 *Synthesis of linear peptide Alk-LT **26**. Conditions: [**a**] SPPS + **18** (2.0 eq); [**b**] TFA/TIS/H_2O (96:2:2), r.t., 2x2h; 75% overall yield.*

The linear peptide HVH **22** is synthetized by SPPS on Rink amide resin. Instead of inserting Fmoc-Lys(N-4-Pentynoic acid)-OH **13** as the last amino acid of the sequence during SPPS , it is added as at the C-terminal end) in order to present HVH peptide at the same manner as expressed on the surface of the bacteriophages during Phage Display screening. Cleavage results in **Alk-HVH 23**, after semi-preparative HPLC purification in 48% overall yield (Scheme 7 A).

Subsequent RAFT conjugation with 4 HVH peptides will lead to the tetra peptidoconjugate, presenting 9 free amino group (2 for each HVH peptide and another on the RAFT Lys), and thus impossible to be next selectively modified (Scheme 7 A). For this reason, during SPPS, instead of Fmoc-Lys(Boc)-OH amino acid at position 3, Fmoc-Lys(NH-Alloc)-OH was added as the first amino acid of the sequence and Fmoc-Acetyl-Gly-OH (or Fmoc-Ac-Gly-OH) instead of Fmoc-Gly-OH as the last residue to afford peptide **24**. Successive cleavage from the resin afforded to the linear protected peptide **Alk-[Ac-HVH(Alloc)] 25** with 44% overall yield (Scheme 7 B).

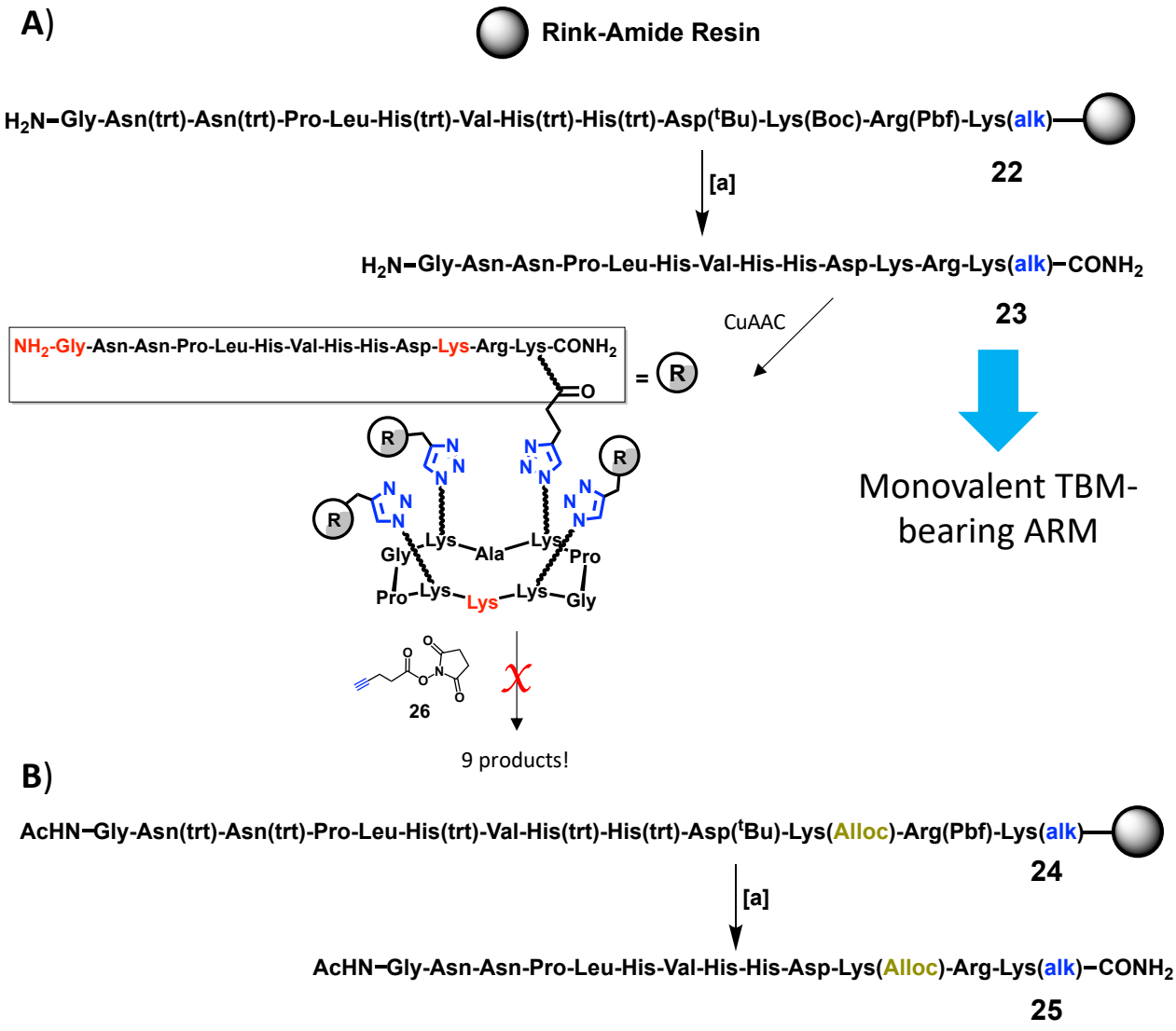

***Scheme** 7 **A)** Synthesis of linear peptide Alk-HVH **23** and **B)** Alk-[Ac-HVH(Alloc)] **25**. Condition: **[a]** TFA/TIS/H_2O (96:2:2), r.t., 2x2h; 48% and 44% yield, respectively.*

II.3. Antibody Binding Modules (ABMs)

II.3.A. Synthetic strategy

Our ABMs are peptidic scaffolds conjugated with carbohydrates known to bind endogenous antibodies, as already showed. We have prepared two kind of platform presenting either 4 or 16 copies of the same carbohydrate epitope thus providing tetravalent or hexadecavalent glycoconjugates. The synthesis of tetravalent ABM is carried out by CuAAC between a carbohydrate with a propargyl (or alkyne) function and a RAFT or dendrimer platform functionalized with four azide functions (**5** or **8**) in presence of catalytic amounts of $CuSO_4$. To solubilize copper and improve its catalytic activity, THPTA was also added. Finally, sodium ascorbate (NaAsc) was used to reduce Cu(II) to Cu(I). Concerning the solubility of the different partners, we observed that DMF/PBS (1:2) at pH 7.5 is generally optimal.. It's worth noting that the resulting click product is also soluble in this solvent mixture. The progress of the reaction was followed by UPLC-MS and a total conversion was generally observed after few hours of reaction. Finally, before purifying the resulting product, copper has to be removed from the reaction medium due to its *in vivo* toxicity and oxidizing power. For these reasons, the ion exchange Chelex resin® is added to the solution and a gentle agitation is maintained for at least 60 minutes. This latter is rinsed several times with water in order to recover all the product, then the solution is purified by semi-preparatory HPLC and lyophilized to afford the white fluffy solid (Figure 49).

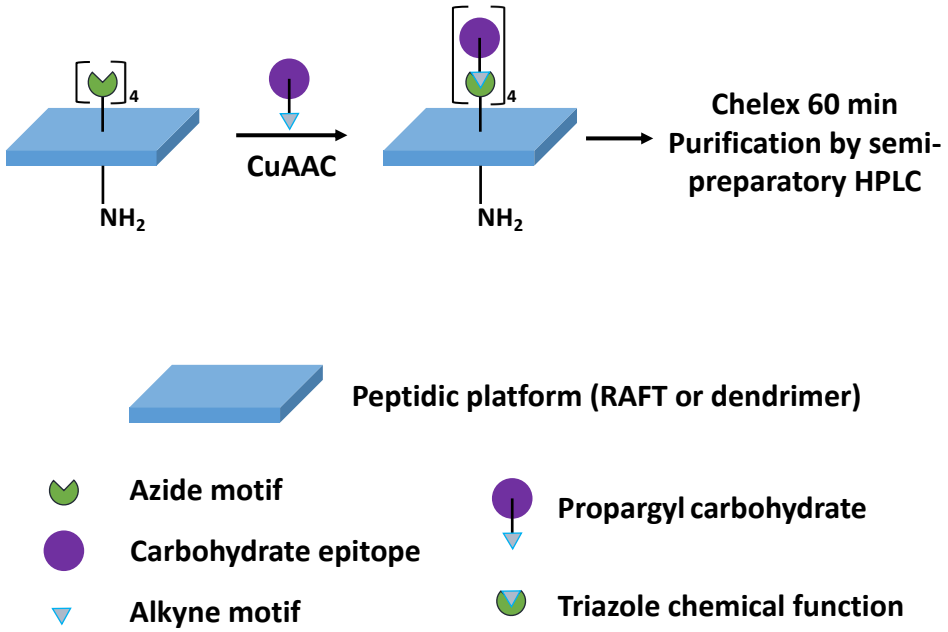

Figure 49 *Synthesis of tetravalent ABM is carried out by the CuAAC reaction, followed by Chelex resin treatment for 1 hour in order to remove copper. The crude is then purified by semi preparative HPLC.*

Once prepared, these tetravalent ABMs could be modified on free lysine present on RAFT and dendrimer (Figure 50):

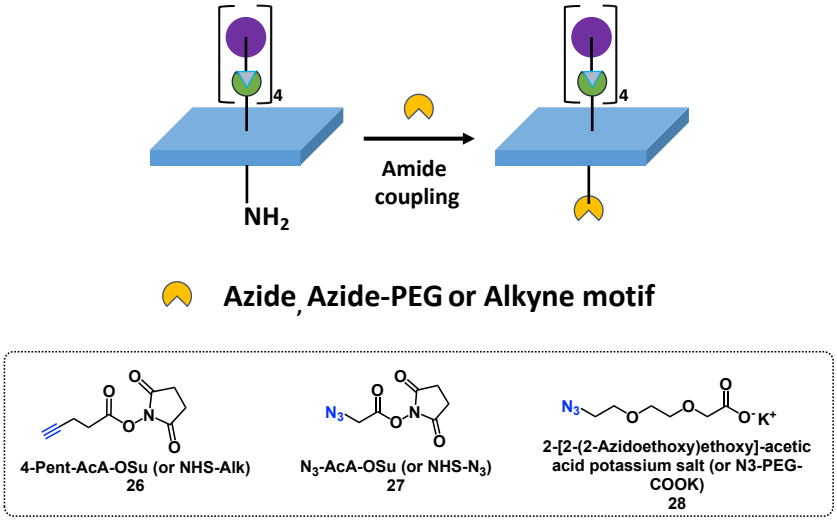

Figure 50 *Key reaction to modify the free lysine on RAFT or dendrimer scaffold. The reaction is performed by addition of* ***26, 27*** *or* ***28*** *to insert an alkyne, an azide or an azide-PEG moiety, respectively, to the remaining amine group.*

- By addition of an alkyne motif (-Alk): this group was introduced with 4-Pentynoic acid succinimidyl ester **26** under basic conditions to give alkyne-tetravalent ABMs.
- By addition of an azide motif (-N_3): this group was introduced by means of the activated ester azidoacetic succinimidyl ester **27** under basic conditions. We can obtain, in this way, azido-tetravalent ABMs ready to be conjugated with alkyne-TBMs.
- By addition of an azide-PEG motif (-PEG-N_3): this group was introduced by means of the 2-[2-(2-Azidoethoxy)ethoxy]-acetic acid potassium salt **28** activated by PyBOP to afford azide-PEG-tetravalent ABMs. We have decided to do this modification only with RAFT scaffold **5**.

Next, four copies of this tetravalent clusters are conjugated by CuAAC RAFT or dendrimer scaffold, in order to obtain four categories of hexadecavalent ABM in a convergent way:

1. "RR" ABM (**39, 52, 56)**, obtained from four copies of alkyne-tetravalent RAFT ABM on one 4-azido moieties bearing RAFT core.

2. "DR" ABM (**43**), obtained from four copies of alkyne-tetravalent RAFT ABM on one 4-azido moieties bearing dendrimer core.

3. "RD" ABM (**45**), obtained from four copies of alkyne-tetravalent dendrimer ABM on one 4-azido moieties bearing RAFT core.

4. “DD” ABM (**47**), obtained from four copies of alkyne-tetravalent dendrimer ABM on one 4-azido moieties bearing dendrimer core.

Once prepared, these hexadecavalent ABMs could be modified on the free remaining lysine by addition of an azide motif (-N_3) or an azide-PEG motif (-PEG-N_3), in order to obtain azido-hexadecavalent ABMs (**40**, **42**, **44**, **46**, **48**, **53**, **57**) ready to be conjugated with alkyne-TBMs (Figure 51).

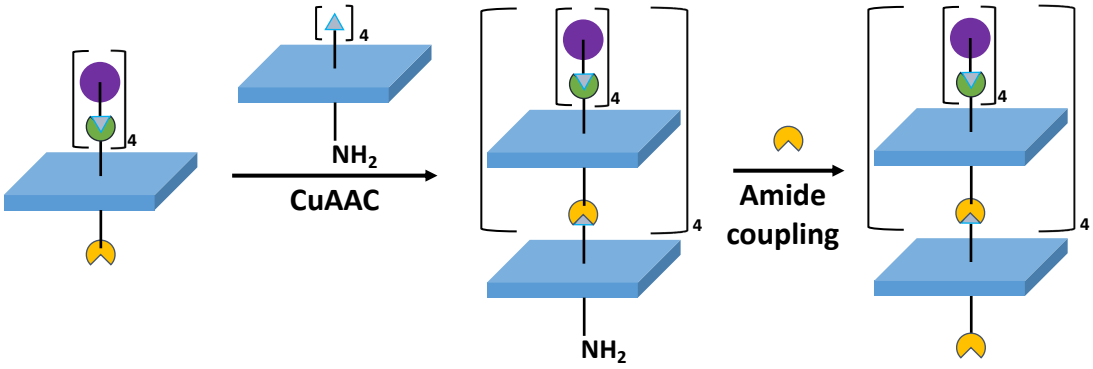

Figure 51 *Convergent synthetic strategy to chemically built hexadecavalent glycostructures, followed modified on the free amine. As shown in Figure 13, the blue parallelepiped could be RAFT or dendrimer scaffold.*

II.3.B. Synthesis of the α-L-Rhamnosylated ABMs

We decided to prepare tetra- and hexadecavalent platforms using combinations of both RAFT and dendrimer for α-L-Rha. A total of 8 α-L-Rha azido-ABMs are obtained (**33**, **35, 37**, **40**, **42**, **44**, **46**, **48**), ready to be conjugated with alkyne-TBMs. First, the tetravalent glycoconjugate α-L-Rhamnose ABM on RAFT **32** is prepared to be subsequently modified with an azide (**33**), an alkyne (**34**) or an azide-PEG (**35**) moieties as explained above (Scheme 8 A). The same synthetic procedure is applied to prepare the tetravalent α-L-Rhamnose ABM analogue with the dendrimer core **38**. It is then modified with an azide (**39**) or an alkyne (**40**) moiety (Scheme 8 B).

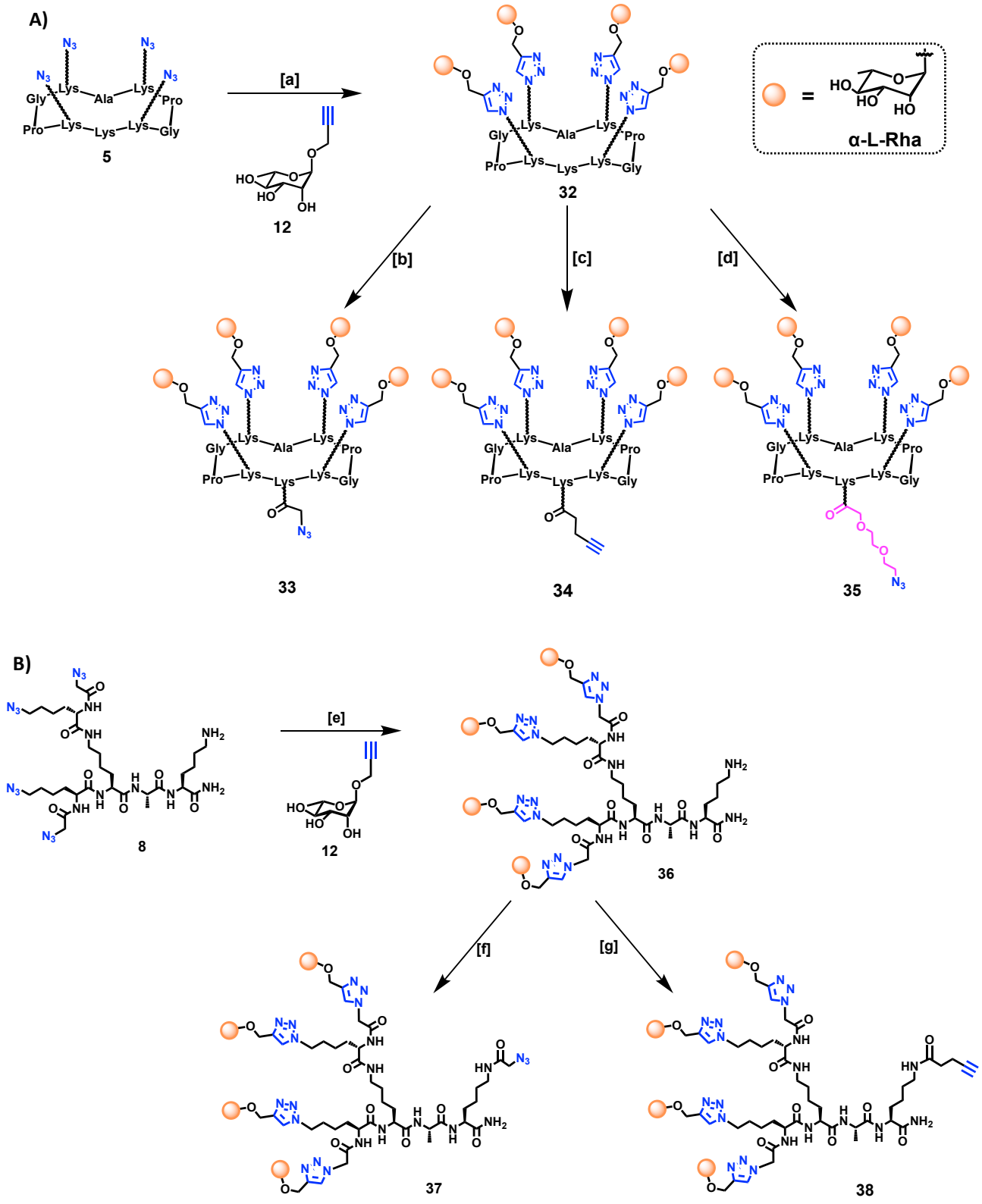

Scheme 8 A) *CuAAC synthesis of tetravalent glycoconjugate* ***32*** *and its conjugation with different linker moieties. Conditions:* ***[a]*** ***12*** *(4.4 eq.),* $CuSO_4$ *(0.5 eq.), THPTA (1.0 eq.), NaAsc (3.0 eq.), DMF/PBS (1:2), pH 7.5, r.t., 1 h, 82%.* ***[b]*** ***27*** *(1.5 eq.), DIPEA (1.0 eq.), DMF, pH 9-10, r.t., 45 min, 92%.* ***[c]*** *26 (1.5 eq.), DIPEA (1.0 eq.), DMF, pH 9-10, r.t., 45 min, 89%.* ***[d]*** ***28*** *(2.0 eq.), PyBOP (2.0 eq.), DIPEA (1.0 eq.), DMF, pH 9-10, r.t., 1 h, 73%.* ***B)*** *CuAAC synthesis of tetravalent glycoconjugate* ***36*** *and its conjugation with*

different linker moieties. Conditions: ***[e]*** ***15*** *(4.4 eq.), $CuSO_4$ (0.5 eq.), THPTA (1.0 eq.), NaAsc (3.0 eq.), DMF/PBS (1:2), pH 7.5, r.t., 1 h, 88%.* ***[f]*** ***27*** *(1.5 eq.), DIPEA (1.0 eq.), DMF, pH 9-10, r.t., 45 min, 90%.* ***[g]*** ***26*** *(1.5 eq.), DIPEA (1.0 eq.), DMF, pH 9-10, r.t., 45 min, 96%.*

In order to obtain the hexadecavalent platforms RR and DR, four copies of alkyne-tetravalent α-L-Rhamnose **34** are conjugated by CuAAC on RAFT **5** to give **39** (Scheme 9 A) or dendrimer **8** to give **43** (Scheme 9 B). Next, as before, these platforms (**39** and **43**) are modified with an azide or an azide-PEG linker in order to prepare RR and DR hexadecavalent α-L-Rhamnose ABMs **40**, **42** and **44** ready to be conjugated with alkyne-TBMs. In addition, the molecule **41** is also prepared.

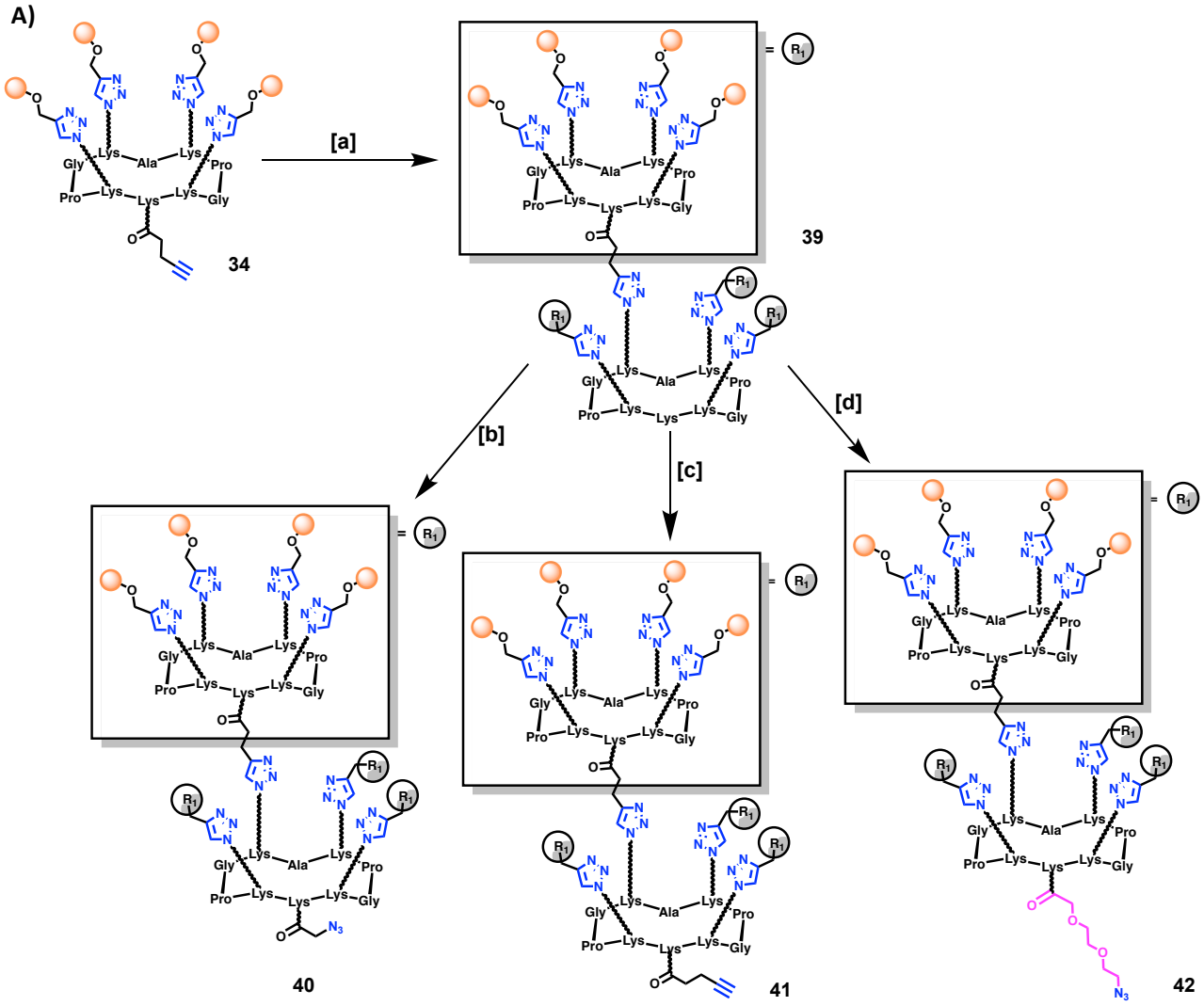

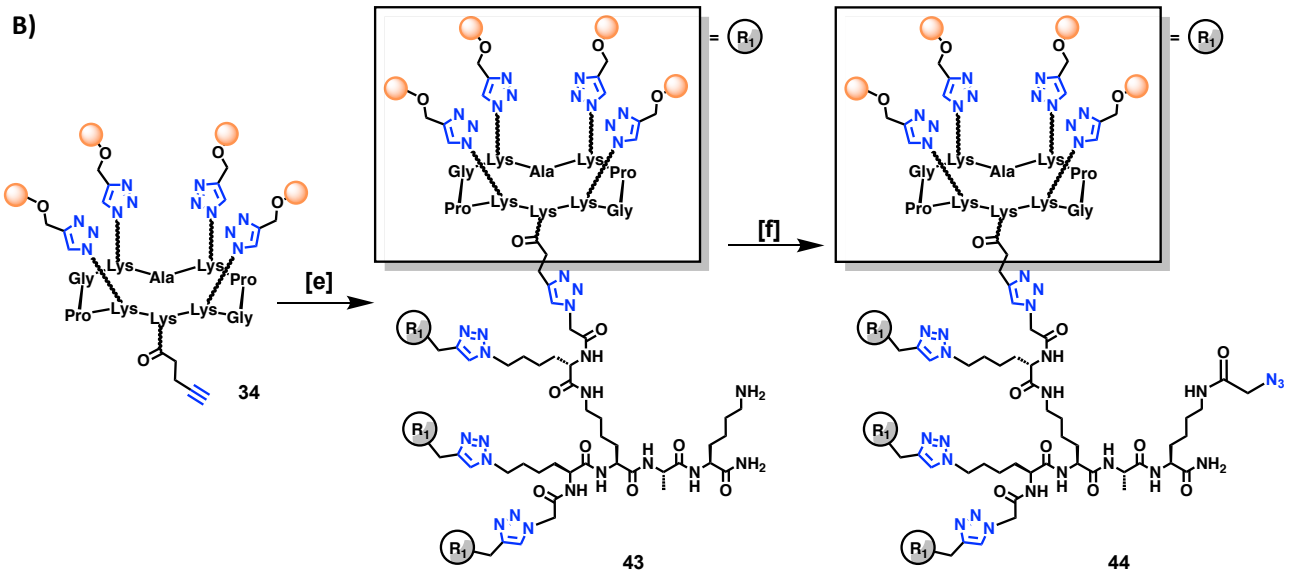

Scheme 9 A) *CuAAC synthesis of the hexadecavalent glycoconjugate* ***39*** *and its conjugation with different linkers. Conditions:* ***[a]*** ***5*** *(4.4 eq.), $CuSO_4$ (0.5 eq.), THPTA (1.0 eq.), NaAsc (3.0 eq.), DMF/PBS (1:2), pH 7.5, r.t., 1 h, 74%.* ***[b]*** ***27*** *(1.5 eq.), DIPEA (1.0 eq.), DMF, pH 9-10, r.t., 45 min, 77%.* ***[c]*** ***26*** *(1.5 eq.), DIPEA (1.0 eq.), DMF, pH 9-10, r.t., 45 min, 91%.* ***[d]*** ***28*** *(2.0 eq.), PyBOP (2.0 eq.), DIPEA (1.0 eq.), DMF, pH 9-10, r.t., 1 h, 92%.* ***B)*** *CuAAC synthesis of the hexadecavalent glycoconjugate* ***43*** *and its conjugation with azido linkers. Conditions:* ***[e]*** ***8*** *(4.4 eq.), $CuSO_4$ (0.5 eq.), THPTA (1.0 eq.), NaAsc (3.0 eq.), DMF/PBS (1:2), pH 7.5, r.t., 1 h, 82%.* ***[f]*** ***27*** *(1.5 eq.), DIPEA (1.0 eq.), DMF, pH 9-10, r.t., 45 min, 88%.*

We obtained the hexadecavalent platforms RD and DD following the same approach from **38** and **5** and **8** to give **45** and **47** (Scheme 10 A-B). As before, these platforms (**45** and **47**) are modified with an azide moiety to obtain **46** and **49**.

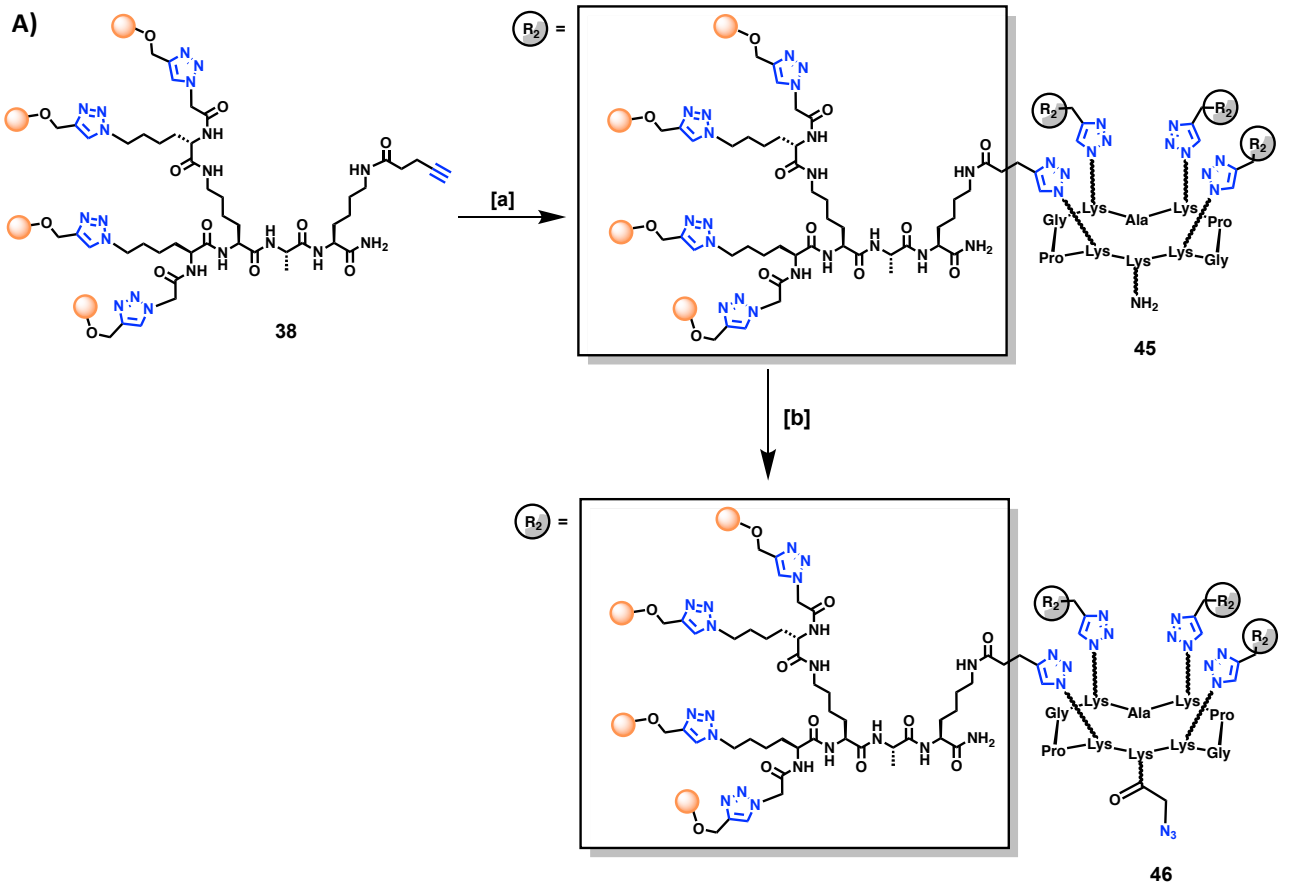
A)
38
[a]
45
[b]
46

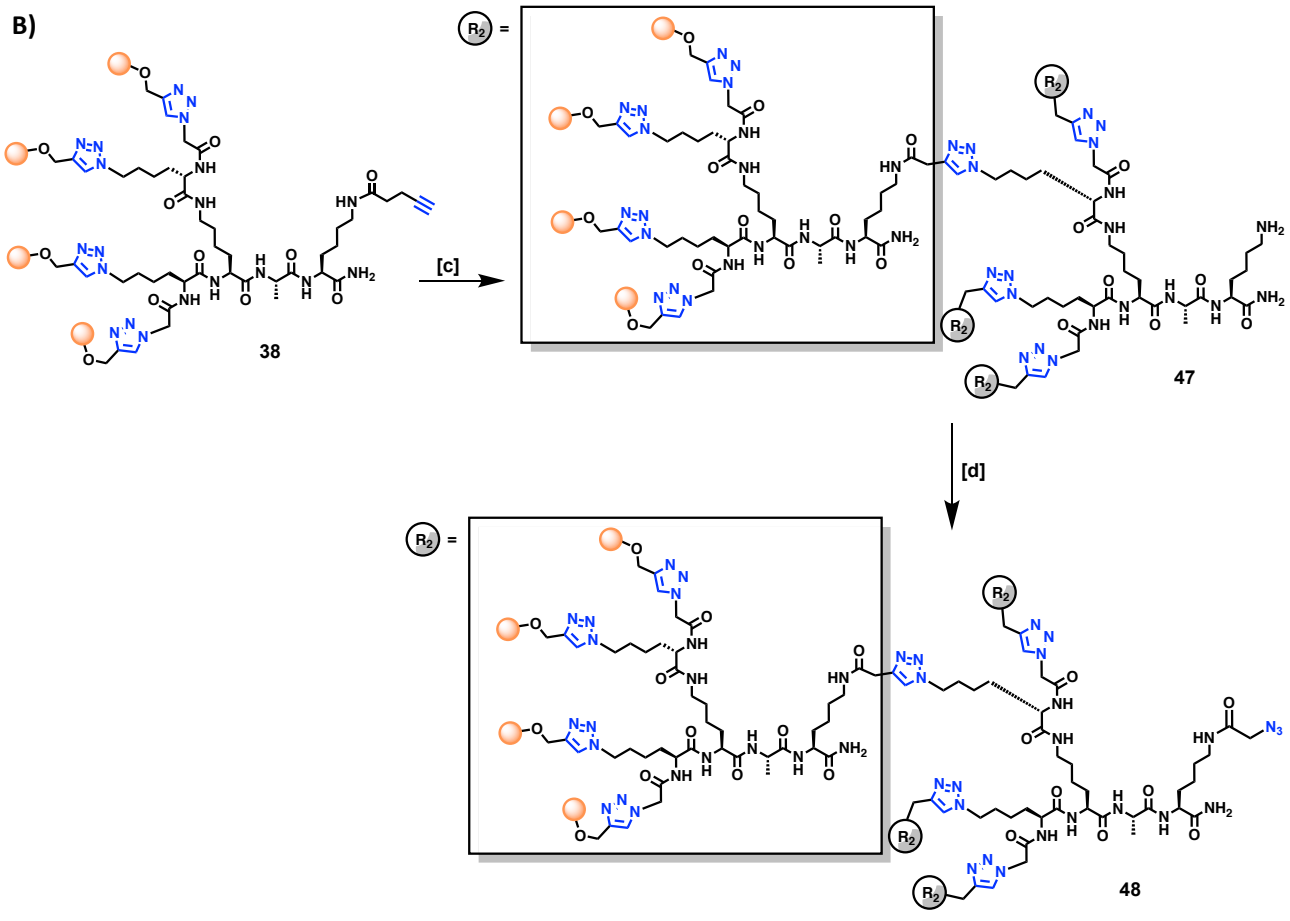
B)
38
[c]
47
[d]
48

Scheme 10 A) *CuAAC synthesis of the hexadecavalent glycoconjugate* ***45*** *and its conjugation with azido linkers. Conditions:* ***[a]*** ***5*** *(4.4 eq.), $CuSO_4$ (0.5 eq.), THPTA (1.0 eq.), NaAsc (3.0 eq.), DMF/PBS (1:2), pH 7.5, r.t., 1 h, 83%.* ***[b]*** ***27*** *(1.5 eq.), DIPEA (1.0 eq.), DMF, pH 9-10, r.t., 45 min, 88%.* ***B)*** *CuAAC synthesis of the hexadecavalent glycoconjugate* ***47*** *and its conjugation with azido linkers. Conditions:* ***[c]*** ***8*** *(4.4 eq.), $CuSO_4$ (0.5 eq.), THPTA (1.0 eq.), NaAsc (3.0 eq.), DMF/PBS (1:2), pH 7.5, r.t., 1 h, 83%.* ***[d]*** ***27*** *(1.5 eq.), DIPEA (1.0 eq.), DMF, pH 9-10, r.t., 45 min, 88%.*

Each final compound is characterized by MS and NMR and the purity is analyzed by RP-HPLC. ^{1}H-NMR spectra of ABM **39** were recorded in D_2O (Figure 52).

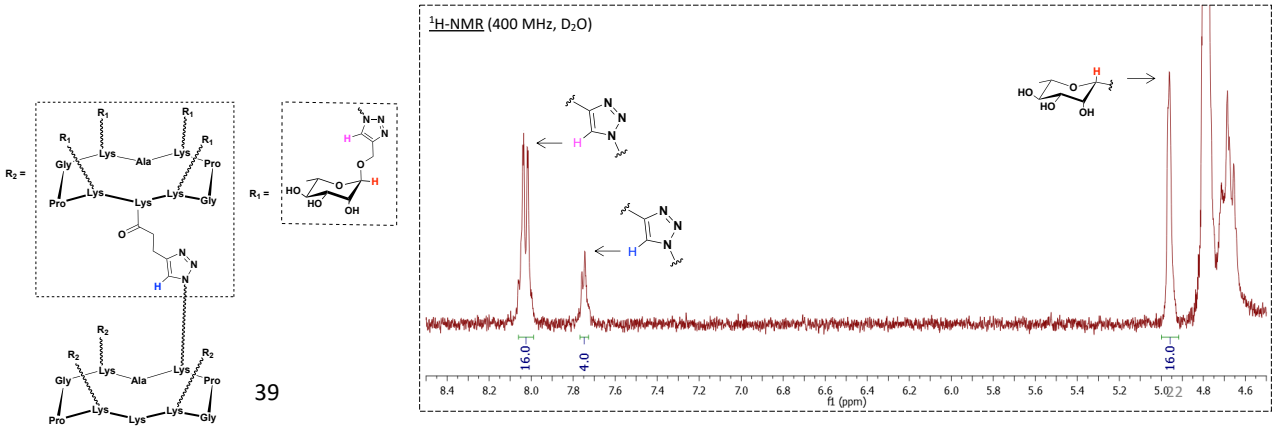

Fig. 52 *^{1}H-NMR (400 MHz, D_2O) zoom of compound* ***39****.*

The ^{1}H-NMR spectra showed the presence of characteristic rhamnose α anomeric protons at 5.0 ppm and characteristic triazole protons between 7.0 and 8.0 ppm. Regarding the anomeric protons (depicted in red), we expected a doublet signal due to the α anomeric protons coupling with C_2 protons (J= 2-3 Hz). Due to the small coupling constant value (for the α anomer) and since the relative asymmetry of this glycoconjugate, we can finally observe a singulet signal around 5.0 ppm, corresponding to 16 doublet signals overlapped. Regarding the triazole protons (depicted in violet and blue), we expected two singulet signals. Conversely two doublet signals (integration ratio of 16 and 4, respectively) are observed probably due to the relative asymmetry of the molecule once again. Integration ratio between triazole protons (H = 20) and the saccharide protons (H = 16) is consistent with target molecule ABM **39**.

II.3.C. Synthesis of the α- and ß-D-Galactosylated ABMs

With the same strategy, we prepared the tetravalent R and hexadecavalent RR with α-D-Gal and ß-D-Gal (this latter as negative control). Compounds **49** is prepared to be next modified with an azide (**50**) or an alkyne (**51**) moieties. Four copies of this latter are next conjugated by CuAAC with **5** to give the hexadecavalent platform **53** (Scheme 11).

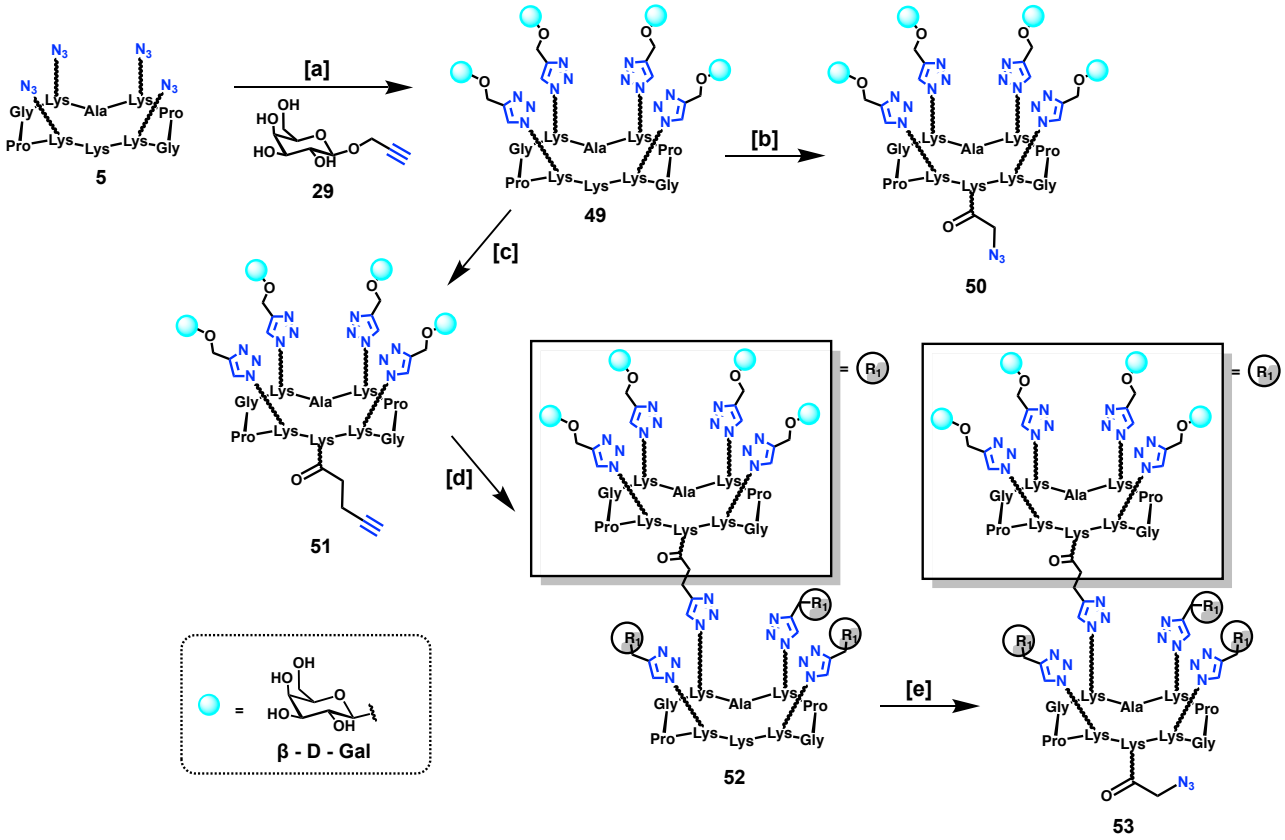

Scheme 11 *Synthesis of ß-D-Galactose ABMs. Conditions:* ***[a]*** ***29*** *(4.4 eq.), $CuSO_4$ (0.5 eq.), THPTA (1.0 eq.), NaAsc (3.0 eq.), DMF/PBS (1:2), pH 7.5, r.t., 1 h, 64%.* ***[b]*** ***27*** *(1.5 eq.), DIPEA (1.0 eq.), DMF, pH 9-10, r.t., 45 min, 90%.* ***[c]*** ***26*** *(1.5 eq.), DIPEA (1.0 eq.), DMF, pH 9-10, r.t., 45 min, 90%.* ***[d]*** ***5*** *(4.4 eq.), $CuSO_4$ (0.5 eq.), THPTA (1.0 eq.), NaAsc (3.0 eq.), DMF/PBS (1:2), pH 7.5, r.t., 1 h, 68%.* ***[e]*** ***27*** *(1.5 eq.), DIPEA (1.0 eq.), DMF, pH 9-10, r.t., 45 min, 93%.*

The same synthetic procedure is applied to prepare the tetravalent **54** and the hexadecavalent glycoconjugate **56**, then modified with an azide moiety (**57**) (Scheme 12).

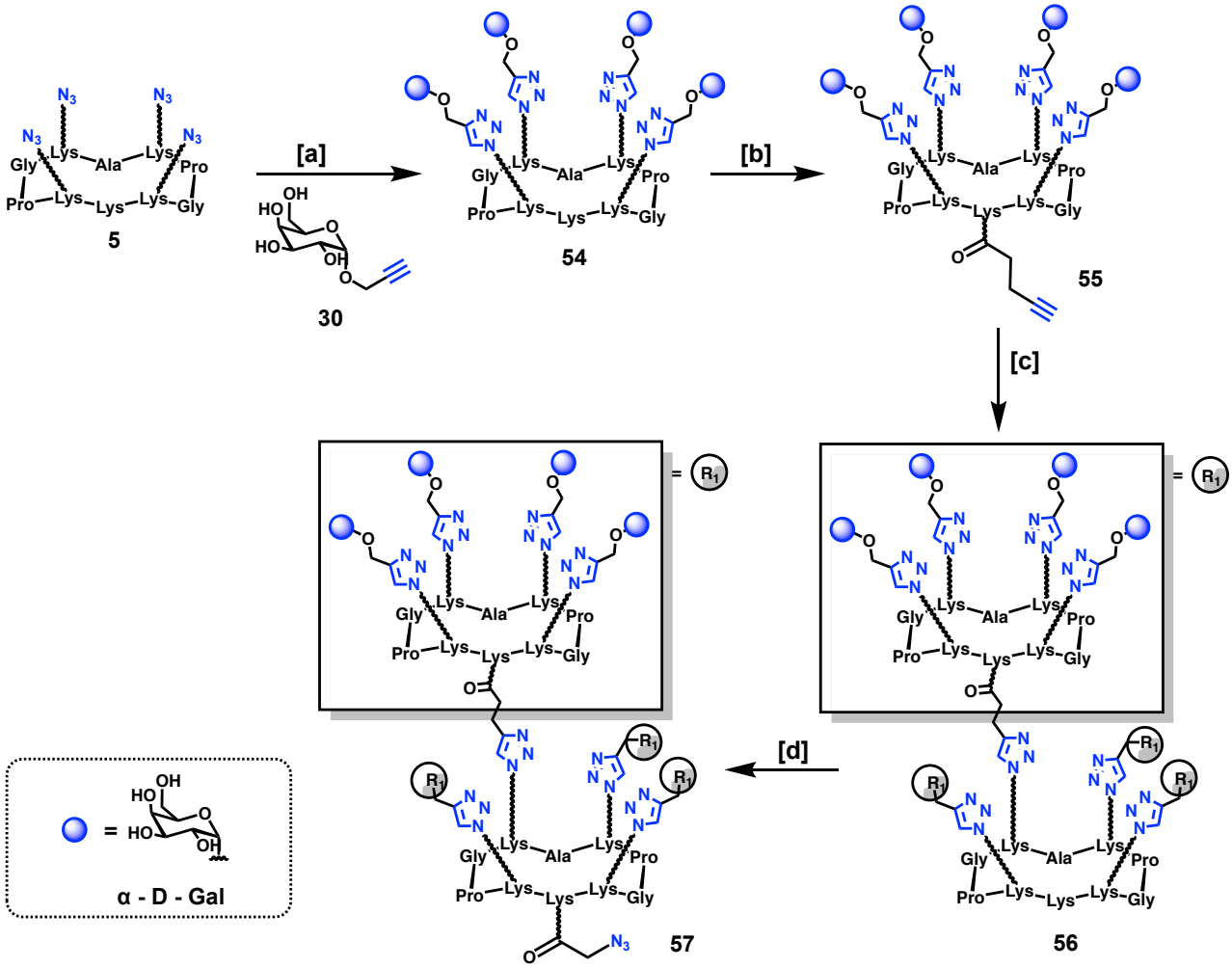

Scheme 12 *Synthesis of α-D-Galactose ABMs. Conditions:* ***[a]*** ***30*** *(4.4 eq.), $CuSO_4$ (0.5 eq.), THPTA (1.0 eq.), NaAsc (3.0 eq.), DMF/PBS (1:2), pH 7.5, r.t., 1 h, 80%.* ***[b]*** ***26*** *(1.5 eq.), DIPEA (1.0 eq.), DMF, pH 9-10, r.t., 45 min, 96%.* ***[c]*** ***5*** *(4.4 eq.), $CuSO_4$ (0.5 eq.), THPTA (1.0 eq.), NaAsc (3.0 eq.), DMF/PBS (1:2), pH 7.5, r.t., 1 h, 59%.* ***[d]*** ***27*** *(1.5 eq.), DIPEA (1.0 eq.), DMF, pH 9-10, r.t., 45 min, 96%.*

II.4. Tumoral Binding Modules (TBMs)

Our TBMs are composed by RAFT and dendrimer scaffolds conjugate with molecules able to recognize specific protein overexpressed on cancer cell surface. We decided to synthesized platform presenting 4 copies of the same epitope to afford tetravalent peptidoconjugates. One tetravalent glycoconjugate will be also prepared. Such structures should allow to evaluate the influence of a multimeric presentation for the TBM binding as previously observed with cRGD.

The TBM epitopes studied in this part are cRGD, LT, Ac-HVH peptides already presented.The tetravalent **58**, **60** and **62** have thus been prepared. On the other hand, we wanted to prepare a TBM composed by 4 ß-D-Glucose (ß-D-Glc) carbohydrate moieties. Since glucose transporter 1 (GLUT-1) is the most common glucose transporter in humans and due to its over-expression in many cancer cells, the development of ARMs targeting this protein remains an important topic in this context.[201] The synthesis of tetravalent ß-D-Glucose conjugate **65** is carried out by the classical CuAAC conditions described before. The reaction has been performed between the propargyl ß-D-Glucoside **64** (prepared by Dr. David Goyard) and platform **5**. Once prepared, the tetravalent TBMs have been functionalized on free remaining lysine present on RAFT by addition of an alkyne motif. As before, this group was introduced by means of the activated pentynoic succinimidyl ester **26** under basic conditions to afford alkyne-tetravalent TBMs (**59**, **61, 63** and **66)**.

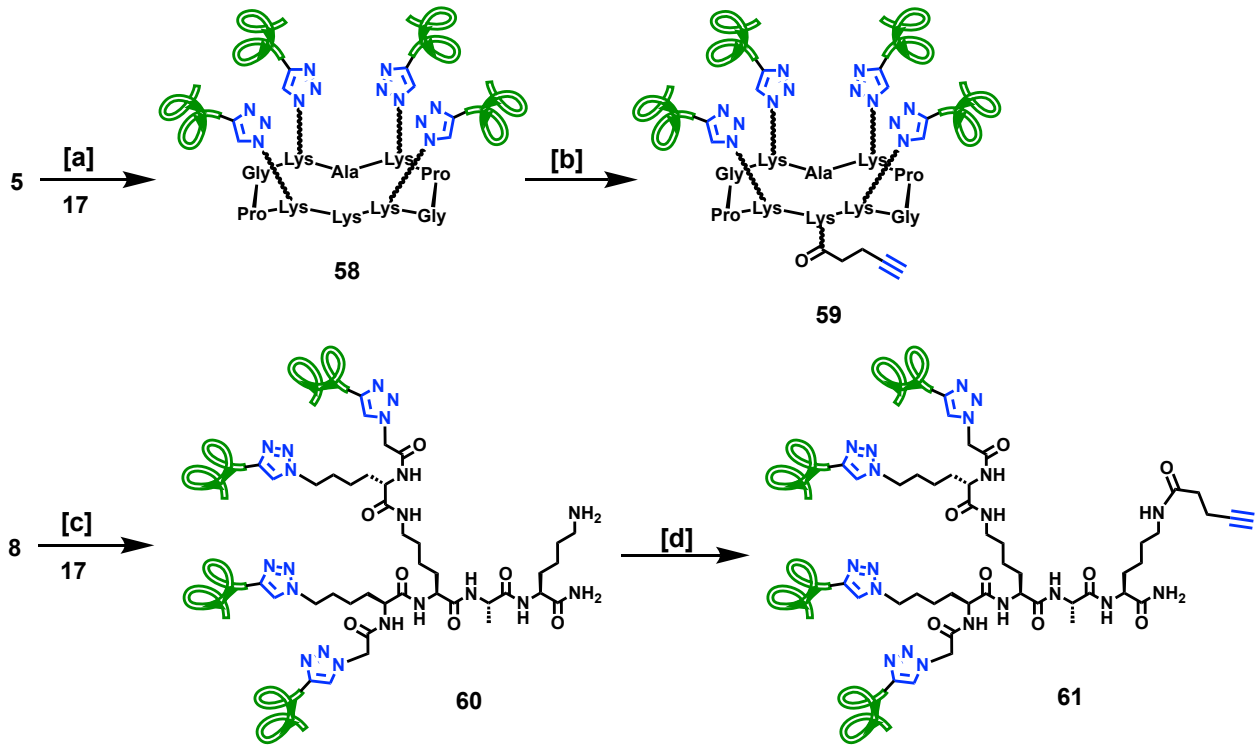

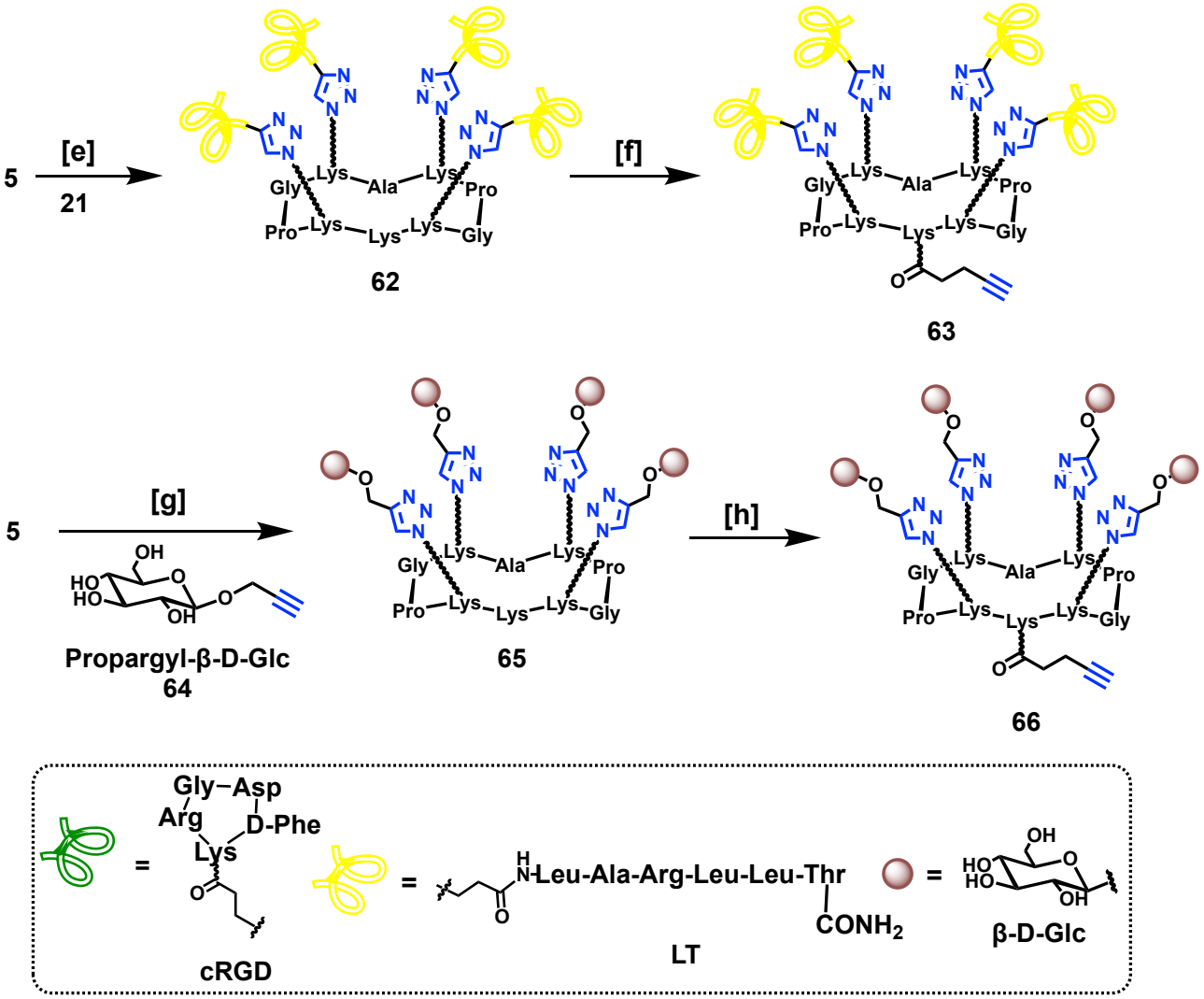

Scheme 13 *Synthesis of* ***59, 61, 63, and 66*** *TBMs. Conditions:* ***[a]*** ***17*** *(4.7 eq.), $CuSO_4$ (0.5 eq.), THPTA (1.0 eq.), NaAsc (3.0 eq.), DMF/PBS (1:1), pH 7.5, 60°C, then r.t., 3 h, 64%.* ***[b]*** ***26*** *(2.0 eq.), DIPEA (1.0 eq.), DMF, pH 9-10, r.t., 45 min, 94%.* ***[c]*** ***17*** *(4.7 eq.), $CuSO_4$ (0.5 eq.), THPTA (1.0 eq.), NaAsc (3.0 eq.), DMF/PBS (1:1), pH 7.5, 60°C, then r.t., 3 h, 75%.* ***[d]*** ***26*** *(1.5 eq.), DIPEA (1.0 eq.), DMF, pH 9-10, r.t., 45 min, 97%.* ***[e]*** ***21*** *(4.6 eq.), $CuSO_4$ (0.5 eq.), THPTA (1.0 eq.), NaAsc (3.0 eq.), DMF/PBS (1:1), pH 7.5, r.t., 2 h, 38%.* ***[f]*** ***26*** *(1.5 eq.), DIPEA (1.0 eq.), DMF, pH 9-10, r.t., 45 min, 52%.* ***[g]*** ***64*** *(4.4 eq.), $CuSO_4$ (0.5 eq.), THPTA (1.0 eq.), NaAsc (3.0 eq.), DMF/PBS (1:2), pH 7.5, r.t., 1 h, 84%.* ***[h]*** ***26*** *(1.5 eq.), DIPEA (1.0 eq.), DMF, pH 9-10, r.t., 45 min, 95%.*

Each final compound is characterized by MS and NMR and the purity analyzed by RP-HPLC. Concerning the synthesis of tetravalent cRGD and LT TBMs, the experimental conditions are almost the same compared to the glycoconjugates described before. The only two differences are related to use of a larger excess of alkyne-substituted peptide and to work at 60°C in DMF since

peptides sometimes could have low solubility in water. However, even in these solvent and temperature conditions, the reaction time remains slower than for ABMs glycoconjugates.

Lastly, the tetravalent compound **67** is prepared using the same procedure and is subsequently modified with an alkyne moiety (**68**). Further cleavage of -Alloc leads to **69** (Scheme 14). This reaction occurs in presence of $PhSiH_3$ (25.0 eq./-Alloc group) and is catalyzed by $Pd(PPh_3)_4$ in dry DMF under Argon. After 1 hour, MeOH is added and the mixture stirred until CO_2 bubbling ceased. The Alloc-deprotected product is precipitated in DCM/ diethyl ether and dried under vacuum.

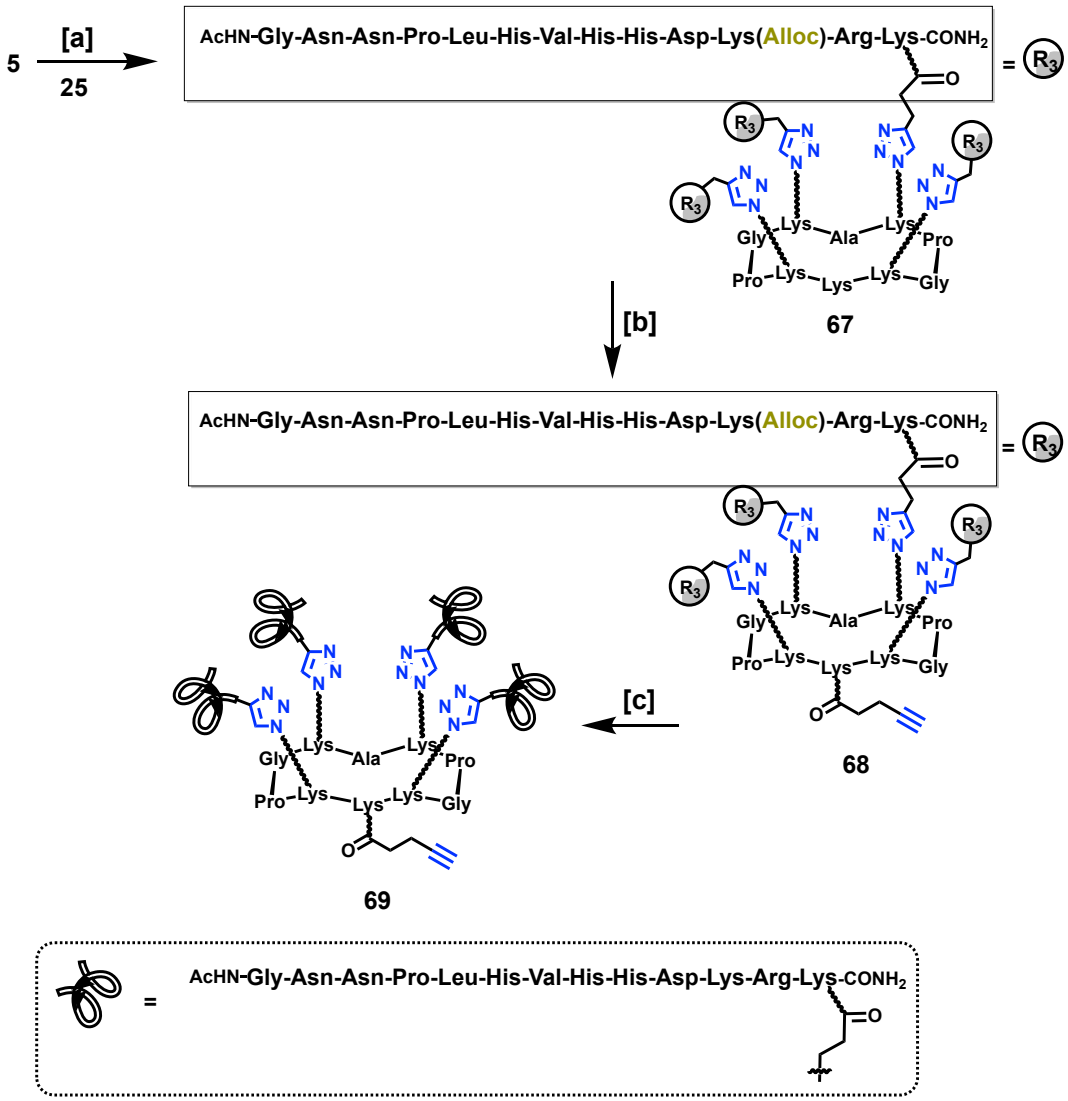

Scheme 14 *Synthesis of* ***69****. Conditions:* ***[a]*** ***25*** *(4.7 eq.), $CuSO_4$ (0.5 eq.), THPTA (1.0 eq.), NaAsc (3.0 eq.), DMF/PBS (1:1), pH 7.5, 40°C in order to solubilize, then r.t., 3 days, 61%.* ***[b]*** ***26*** *(1.5 eq.), DIPEA (1.0 eq.), DMF, pH 9-10, r.t., 2 h, 78%.* ***[c]*** *$Pd(PPh_3)_4$ (cat.), $PhSiH_3$ (100 eq.), dry DMF, r.t., 6 hours, then MeOH, 42%.*

The complete solubilization of alkyne-substituted protected peptide **25** requires agitation in DMF during 2h at 40°C. In addition, the reaction [a] was completed only with the use of large excess of peptide **25** and after 3 days with 60% of yield after purification by RP-HPLC. RP-HPLC profiles of compounds **25**, **67**, **68** and **69** (Figure 53) demonstrated their high purity after purification.

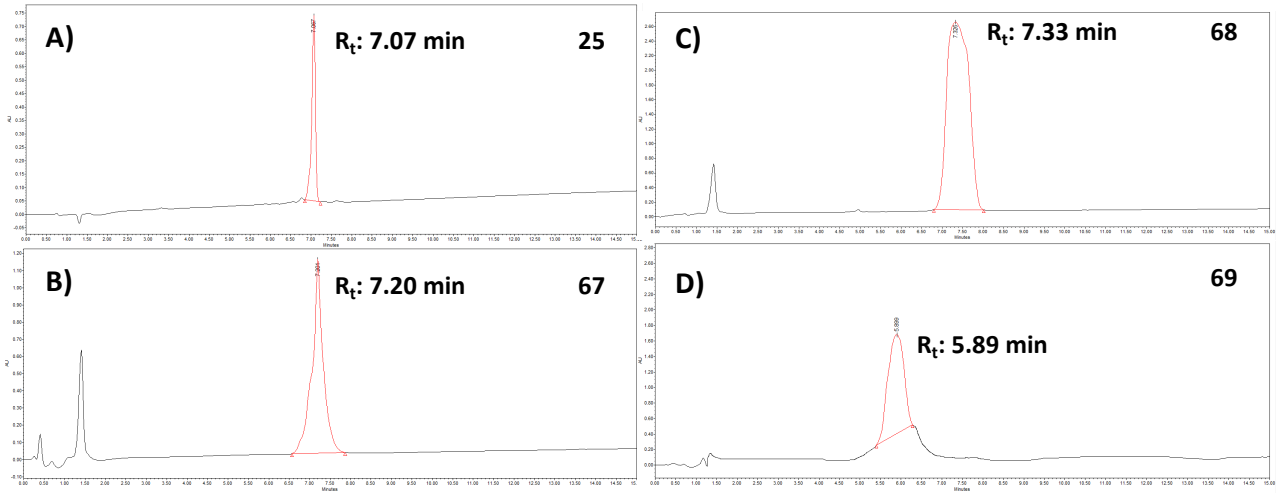

Figure 53 *RP-HPLC (C_{18}, λ = 214 nm, 5-60% B in 15 min) profiles of compounds* ***25***, ***67***, ***68*** *and* ***69***.

II.5. Antibody Binding Molecules (ARMs)

Nine ABMs and eleven TBMs were synthesized and are now combined to provide three classes of ARMs:

- The first class, called Rhamnose – cRGD ARMs, includes ARMs composed of Rhamnose (ABM) and cRGD (TBM);
- The second class, called X – cRGD ARMs, where X is an ABM involving a carbohydrate epitope different from Rhamnose;
- The third class, called Rhamnose – Y ARMs, where Y is a TBM involving a peptide epitope different from cRGD.

II.5.A. Synthesis of Rhamnose – cRGD ARMs

The first class of ARM is composed by Rhamnose as ABM and cRGD as TBM. 11 different combinations are synthesised (Scheme 15, ARMs **70**-**80**).

- ARM **70** (R-R): 4 Rha units displayed on a RAFT (R) and 4 cRGD units displayed on a RAFT (R);
- ARM **71** (RR-R): 16 Rha units displayed on a RAFT (R) bearing 4 RAFT (R) at the periphery and 4 cRGD units displayed on a RAFT (R);
- ARM **72** (RR-D): 16 Rha units displayed on a RAFT (R) bearing 4 RAFT (R) at the periphery and 4 cRGD units displayed on a dendrimer (D);
- ARM **73** (DR-R): 16 Rha units displayed on a dendrimer (D) bearing 4 RAFT (R) at the periphery and 4 cRGD units displayed on a RAFT (R);
- ARM **74** (RD-R): 16 Rha units displayed on a RAFT (R) bearing 4 dendrimers (D) at the periphery and 4 cRGD units displayed on a RAFT (R);
- ARM **75** (DD-R): 16 Rha units displayed on a dendrimer (D) bearing 4 dendrimers (D) at the periphery and 4 cRGD units displayed on a RAFT (R);
- ARM **76** (R-R PEG): 4 Rha units displayed on a RAFT (R) and 4 cRGD units displayed on a RAFT (R), separated by a PEGylated azide linker.
- ARM **77** (RR-R PEG): 16 Rha units displayed on a RAFT (R) bearing 4 RAFT (R) at the periphery and 4 cRGD units displayed on a RAFT (R), separated by a PEGylated azide linker.
- ARM **78** (R-c): 4 Rha units displayed on a RAFT (R) and 1 cRGD unit (c);
- ARM **79** (RR-c): 16 Rha units displayed on a RAFT (R) bearing 4 RAFT (R) at the periphery and 1 cRGD unit (c);
- ARM **80** (D-R): 4 Rha units displayed on a dendrimer (D) and 4 cRGD units displayed on a RAFT (R);

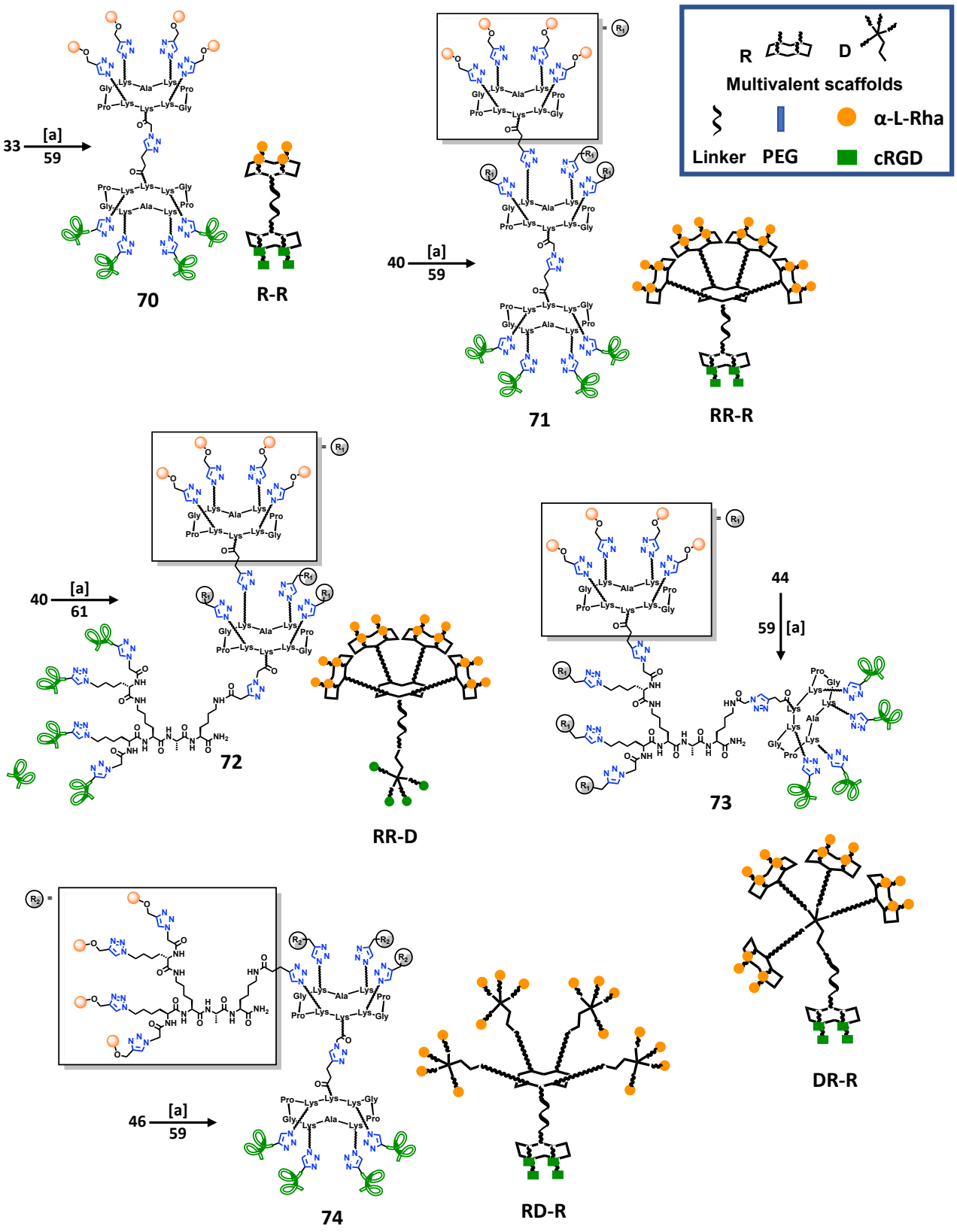
R
D
Multivalent scaffolds
Linker
PEG
α-L-Rha
cRGD
33
[a]
59
70
R-R
40
[a]
59
71
RR-R
40
[a]
61
72
RR-D
44
59
[a]
73
46
[a]
59
74
RD-R
DR-R

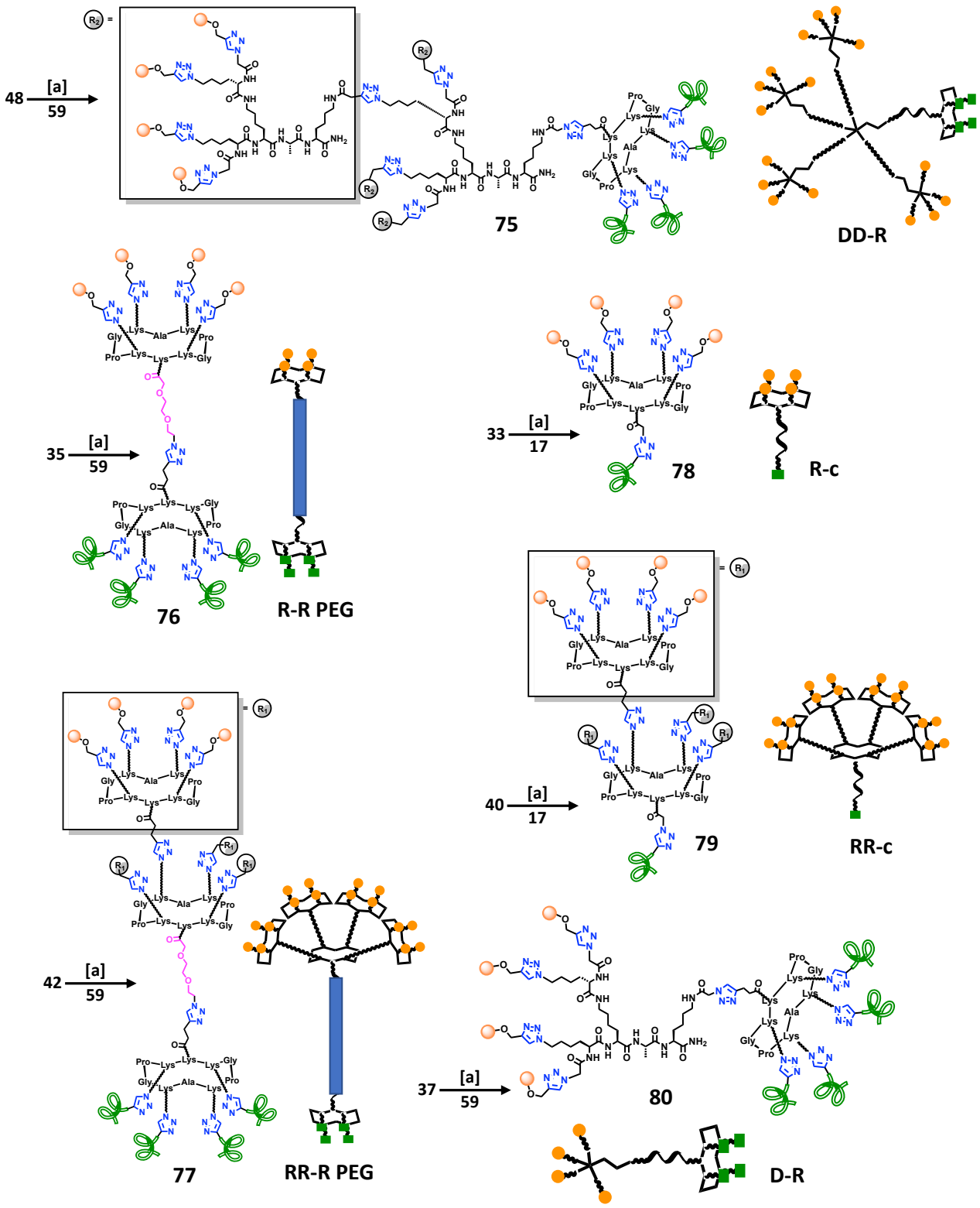

Scheme 15 *Synthesis of Rha-cRGD ARMs. Conditions: [**a**] $CuSO_4$ (1.0 eq.), THPTA (2.0 eq.), NaAsc (4.0 eq.), DMF/PBS (1:2), pH 7.5, r.t., 1 h. 78% for **70**; 78% for **71**; 54% for **72**; 69% for **73**; 56% for **74**; 78% for **75**; 87% for **76**; 77% for **77**; 80% for **78**; 85% for **79**; 50% for **80**.*

The CuAAC reactions are performed in 2 mL of a 1:1 mixture of DMF and PBS buffer (pH 7.5), at room temperature. Despite the structural complexity of different ARMs, no substantial

difference of reactivity is observed and all the reactions are completed within 1 hour, as confirmed by analytical RP-HPLC. After Chelex resin addition for 60 minutes, the crude is purified by semi-preparative RP-HPLC. All compounds are obtained with >50% yield. More precisely, ARMs composed by a combination between dendrimer and RAFT platforms (**72**, **73**, **74**) resulted in a lower yield than those composed by only RAFT or dendrimer (**71**, **75**); that's probably because the linker is less accessible due to the bigger size of ABM.

Finally, all ARMs are characterized by analytical HPLC, HRMS as well as ^{1}H-NMR. ^{1}H-NMR spectra of ARM **71** were recorded in D_2O (Figure 54).

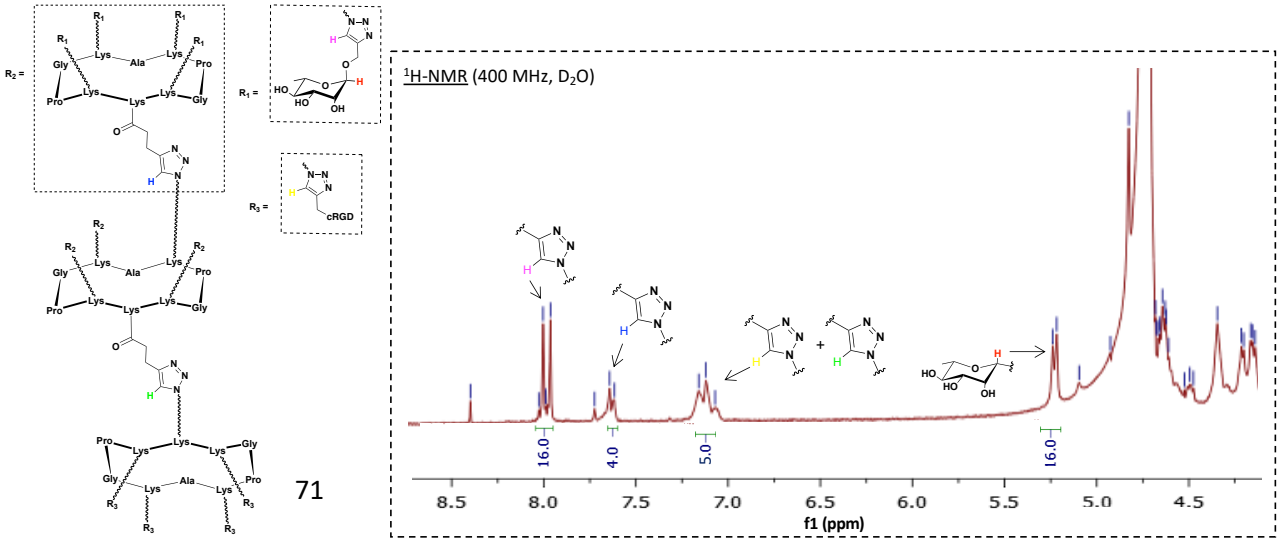

Fig. 54 *^{1}H-NMR (400 MHz, D_2O) zoom of ARM **71***

The ^{1}H-NMR spectra showed the presence of characteristic rhamnose α anomeric protons at 5.0 ppm and characteristic triazole protons between 7.0 and 8.0 ppm, already described in Figure 52. Comparing to the ^{1}H-NMR spectra of ABM **39** (Figure 52), the new presence of a multiplet signal around 7.2 ppm designates the presence of the triazole protons bearing cRGD (H = 4, depicted in yellow) and the linker triazole proton (H = 1, depicted in green). Integration ratio between triazole protons (H = 25) and the saccharide protons (H = 16) is consistent with target molecule ARM **71**. The RAFT asymmetrical structure and the different environments of the twenty-five triazole bonds influence chemical shift of these characteristic protons, resulting in peak broadening and signal shifting. These factors, together with the inherent complexity of **71**, make complete chemical shift assignment very hard without more powerful experiments involving high-field NMR, ^{13}C-NMR, or homonuclear 2D-NMR (COESY, NOESY, TOCSY).

RP-HPLC profiles of some example (compounds **71, 75, 76, 77** in Figure 55) demonstrated the good purity of ARMs after purification, despite the presence of some small signals on the HPLC profiles. Moreover the signal positions are analysed. First, it can observe the difference made by the different architectures. ARM **71**, for example, have a lower retention time (R_t: 4.90

min) than ARM **75** (R_t: 5.31 min); since both presents 16 carbohydrates residues on the ABM part, the polarity differences are due to the dendrimer platforms on ARM **75**, that make it less polar and thus right shifted (5.31 min). Next, it can observe the difference made by the different linker length comparing ARM **71** and ARM **77**. The long apolar PEG linker conjugated to a triazole very right shifts the signal of the molecule **77** (R_t: 5.30 min) than the simply triazole of the molecule **71**. Lastly, it can observe the difference made by the different amount of carbohydrates comparing ARM **76** and ARM **77**. 16 polar carbohydrate units are able to make the molecule **77** more polar (R_t: 5.30 min) than **76** (R_t: 5.49 min), shifting the signal on the left.

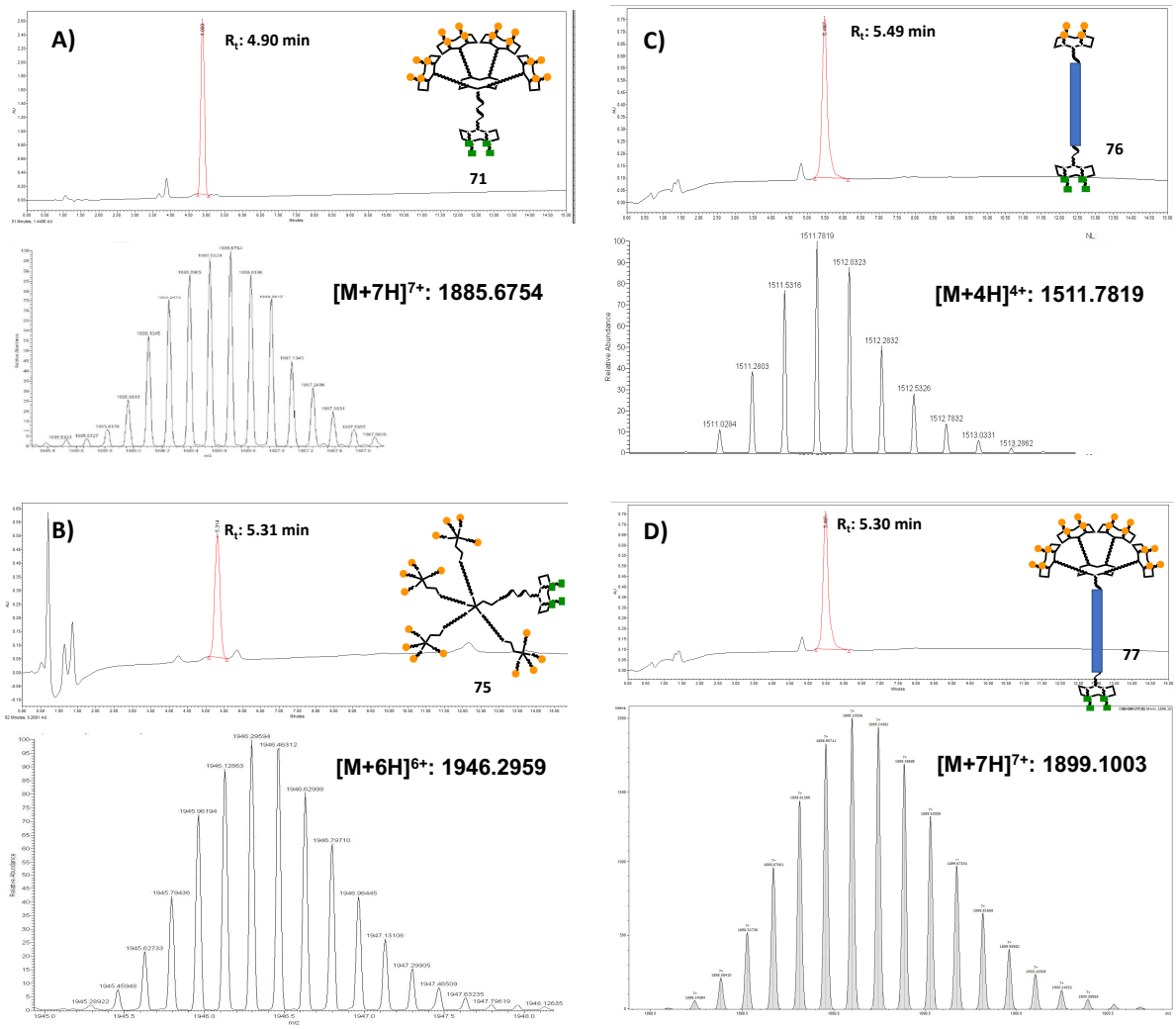

Figure 55 *RP-HPLC and HRMS characterizations.* ***A) ARM 71*** *RP-HPLC: R_t = 4.90 min (C_{18}, λ = 214 nm, 5-100% B in 15 min); HRMS (ESI⁺-TOF)* m/z*: calculated for $C_{581}H_{887}N_{177}O_{178}$ $[M+7H]^{7+}$: 1885.5187, found 1885.6754.* ***B) ARM 75*** *RP-HPLC: R_t = 5.31 min (C_{18}, λ = 214 nm, 5-100% B in 15 min;) HRMS (ESI⁺-TOF)* m/z*: calculated for $C_{501}H_{772}N_{162}O_{163}$ $[M+6H]^{6+}$: 1946.1279, found 1946.2959.* ***C) ARM 76*** *RP-HPLC: R_t = 5.49 min (C_{18}, λ = 214 nm, 5-100% B in 15 min); HRMS (ESI⁺-TOF)* m/z*: calculated for $C_{269}H_{407}N_{85}O_{76}$ $[M+4H]^{4+}$: 1511.0143, found 1511.7819.* ***D) ARM*** *77 RP-HPLC: R_t = 5.30 min (C_{18}, λ = 214 nm, 5-100% B in 15 min); HRMS (ESI⁺-TOF)* m/z*: calculated for $C_{585}H_{895}N_{177}O_{180}$ $[M+7H]^{7+}$: 1898.9571, found 1899.1003.*

II.5.B. Synthesis of X – cRGD ARMs

X – cRGD ARMs is our second ARM family. Instead of Rha, , X can be:

- ß-D-Gal epitope to afford ARM **81 (R-R (ß-D-Gal))** and ARM **82** (**RR-R (ß-D-Gal)**)
- α-D-Gal epitope to afford ARM **83** (**RR-R (α-D-Gal)**)
- α-L-Neu5Gc epitope to afford ARM **84** (**RR-R (α-D-Neu5Gc)**); this ARM was completely synthetized by Dr David Goyard;

4 different combinations are synthesised (Scheme 16, ARMs **81**-**84**).

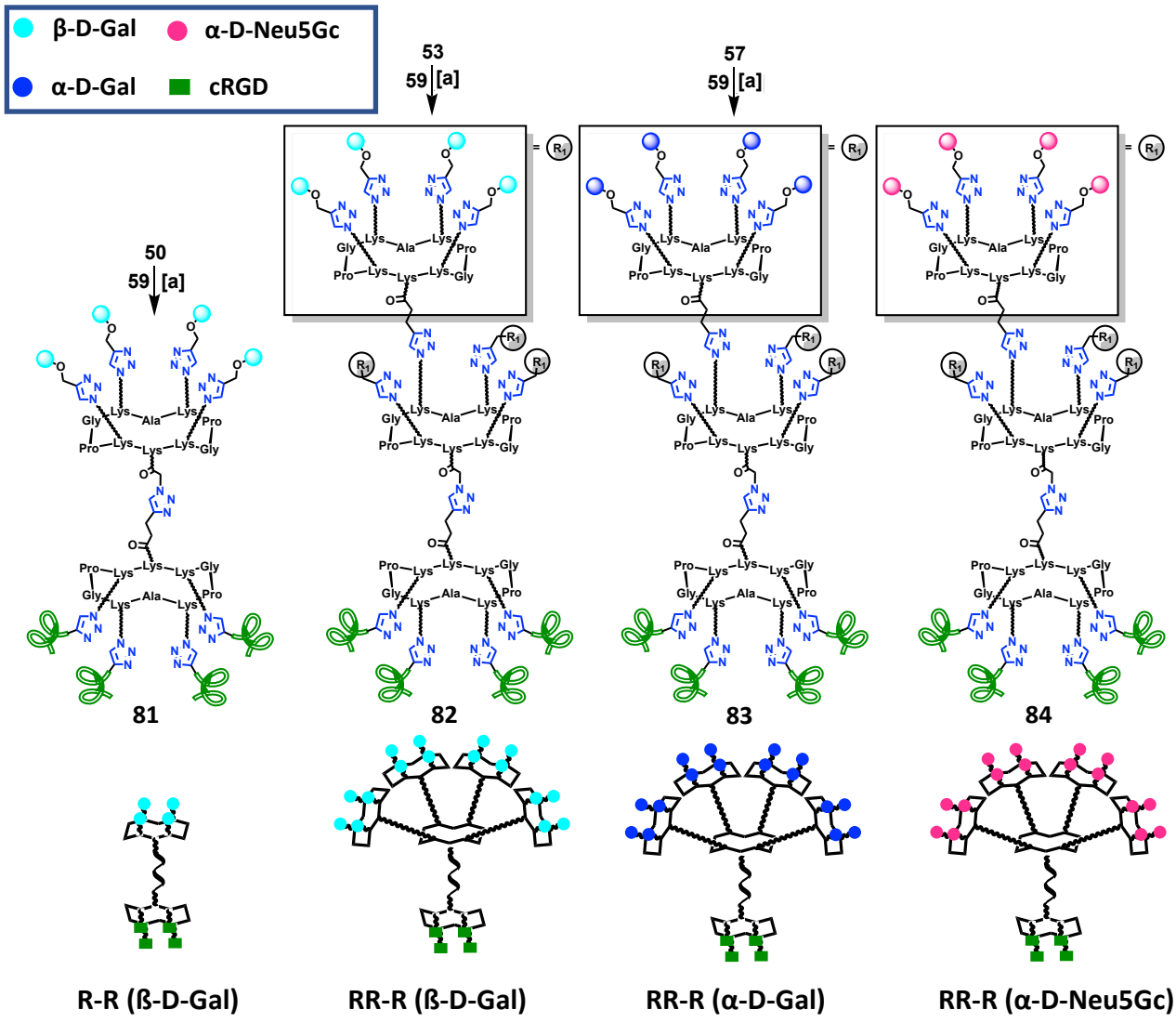

Scheme 16 *Synthesis of X-cRGD ARMs. Conditions: [**a**] $CuSO_4$ (1.0 eq.), THPTA (2.0 eq.), NaAsc (4.0 eq.), DMF/PBS (1:2), pH 7.5, r.t., 1 h. 78% for **81**; 78% for **82**; 73% for **83**.*

ARMs **81-84** are synthetized by CuAAC, harnessing the same condition described above, with a 73-78% yield after semi-preparative RP-HPLC. All ARMs are characterized by analytical HPLC, HRMS as well as ^{1}H-NMR. RP-HPLC and the HRMS profiles of some example (compounds **81** and **83**) show the high purity of ARMs after purification (Figure 56). MS analysis clearly confirmed the structure of each ARM without trace of truncated side-product.

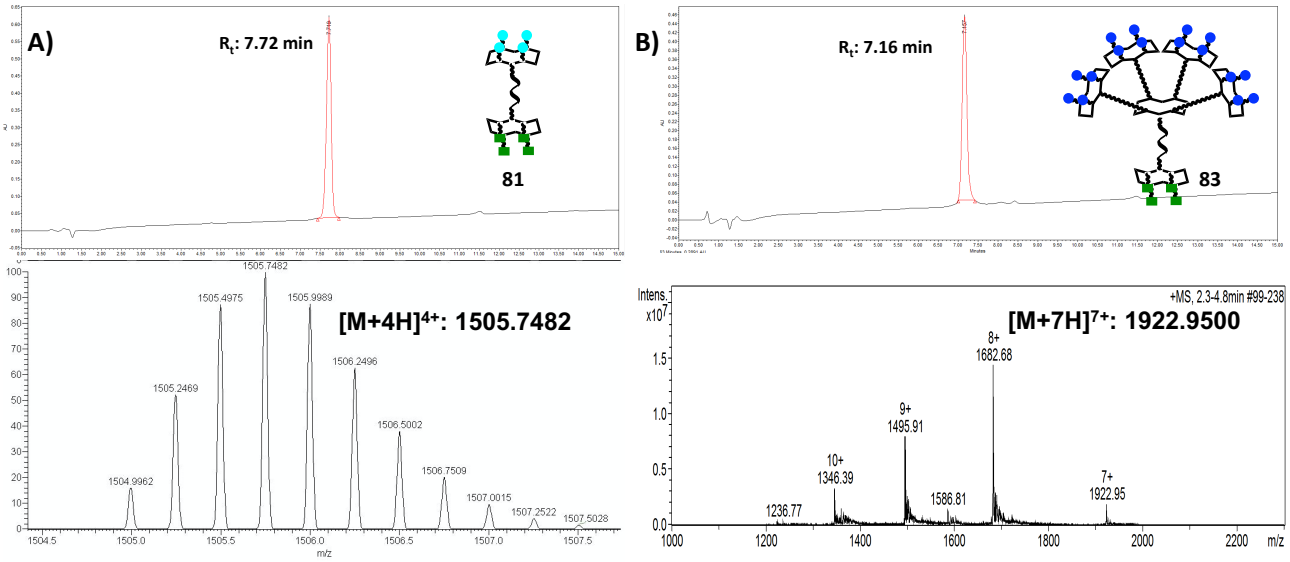

Figure 56 *RP-HPLC and HRMS characterizations.* ***A) ARM 81*** *RP-HPLC: R_t = 7.72 min (C_{18}, λ = 214 nm, 5-60% B in 15 min); HRMS (ESI^{+}-TOF) m/z: calculated for $C_{265}H_{399}N_{85}O_{78}$ $[M+4H]^{4+}$: 1504.9962, found 1505.7482.* ***B) ARM 83*** *RP-HPLC: R_t = 7.16 min (C_{18}, λ = 214 nm, 5-60 % B in 15 min); HRMS (ESI^{+}-TOF) m/z: calculated for $C_{581}H_{887}N_{177}O_{194}$ $[M+7H]^{7+}$: 1922.0785, found 1922.9500.*

II.5.C. Synthesis of Rha – Y ARMs

Rha – Y ARMs is our third ARM family, which are composed by a α-L-Rhamnose units as ABM and a non cRGD motif as TBM. In particular, Y can be:

- LT peptide to afford ARM **85** (**R-l (LT)**), ARM **86** (**RR-l (LT)**) and ARM **87** (**RR-R (LT)**)
- ß-D-Glucose epitope to afford ARM **88** (**R-g (ß-D-Glc)**), ARM **89** (**R-R (ß-D-Glc)**) and ARM **90** (**RR-R (ß-D-Glc)**).
- HVH peptide to afford ARM **91** (**R-h (HVH)**), ARM **92** (**RR-h (HVH)**) and ARM **93** (**RR-R (Ac-HVH)**).

9 different combinations are synthesized (Scheme 17, ARMs **85-93**).

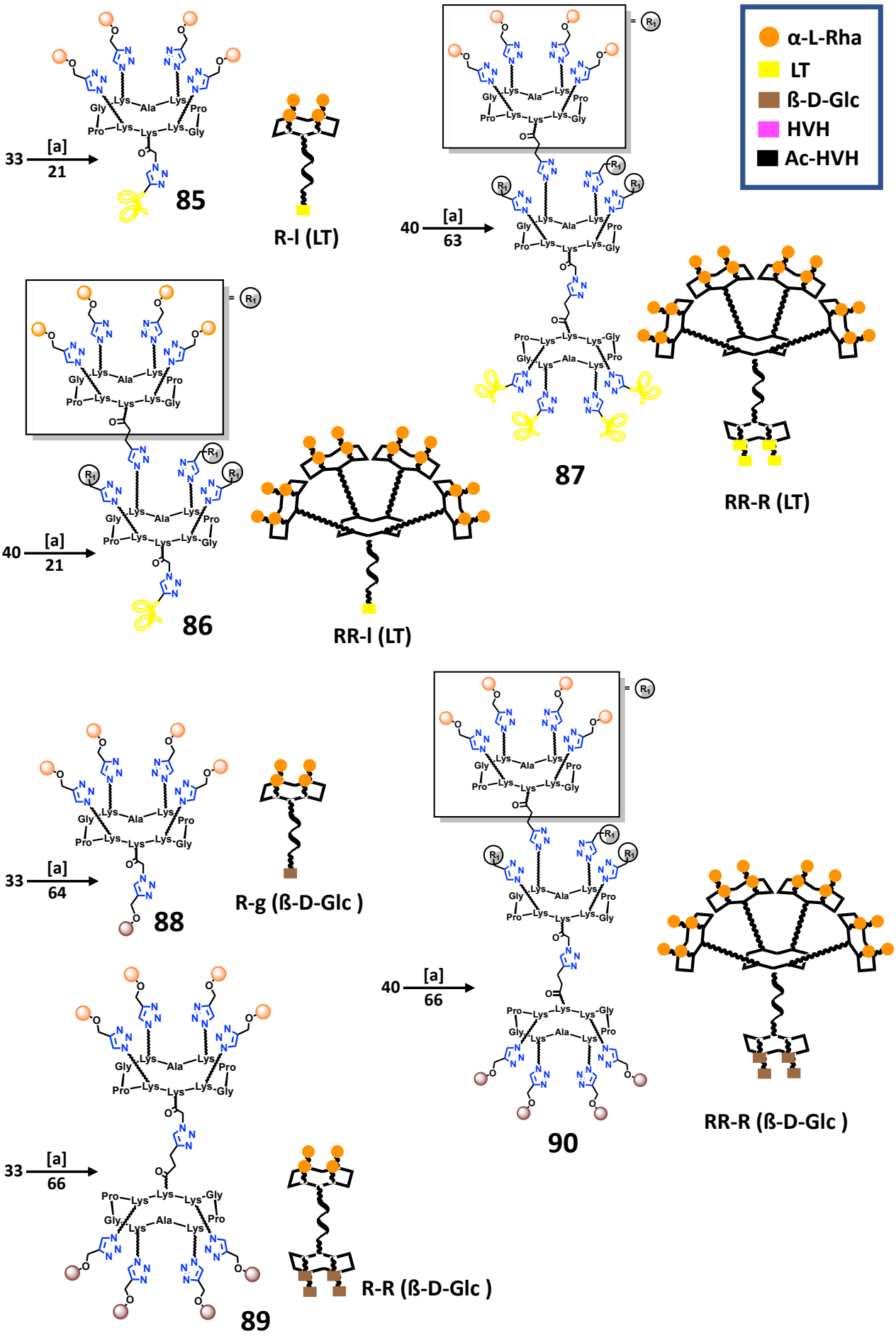
α-L-Rha
LT
ß-D-Glc
HVH
Ac-HVH
33
[a]
21
85
R-l (LT)
40
[a]
63
87
RR-R (LT)
40
[a]
21
86
RR-l (LT)
33
[a]
64
88
R-g (ß-D-Glc)
40
[a]
66
90
RR-R (ß-D-Glc)
33
[a]
66
89
R-R (ß-D-Glc)

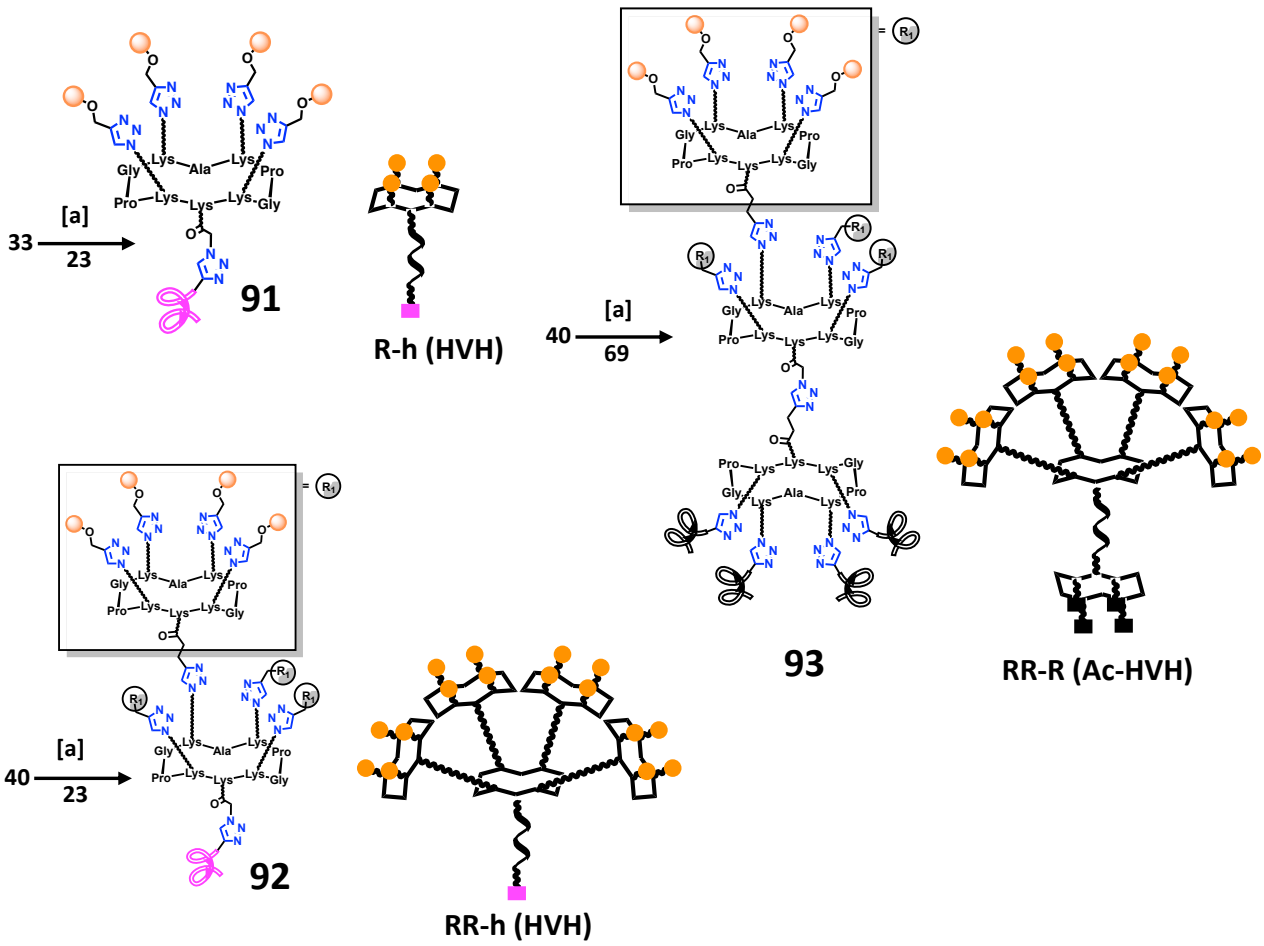

Scheme 17 *Synthesis of X-cRGD ARMs. Conditions: [**a**] $CuSO_4$ (1.0 eq.), THPTA (2.0 eq.), NaAsc (4.0 eq.), DMF/PBS (2:1), pH 7.5, r.t., 1 h. 70% for **85**; 83% for **86**; 31% for **87**; 75% for **88**; 88% for **89**; 87% for **90**; 51% for **91**; 38% for **92**; 30% for **93**.*

ARMs **85-93** are synthetized by CuAAC, harnessing the same condition described above, after semi-preparative RP-HPLC. It is worth noting that the yield is commonly influenced by the solubility, the nature of epitopes (peptide or carbohydrate), their amount and their length (in case of peptide). For LT peptide, for example, the yield is tremendously lower when the ARM valency increases: from 70-80% of yield with the mono LT (**85** or **86**) to 31% of yield with the tetravalent LT (**87**) ARM. A similar trend occurs for HVH peptide, but with even lower yield since HVH have a longer peptide sequence than LT: from 50% of yield for **91** to 38% and 30% of yield for **92** and **93**, respectively. Inverse tendency was found with ARM **88-90** (from 75% for **88** to 88-87% for **89** and **90**, respectively) since it can be assumed that there is direct correlation between the number of carbohydrate and the solubility of the whole molecule. It's worth noting the significant higher yield of these reactions than reactions involving peptide as TBM epitopes, due to the high solubility and small size of carbohydrate than peptide.

All ARMs are characterized by analytical HPLC, HRMS as well as ^{1}H-NMR. In figure 57 are shown the RP-HPLC and the HRMS profiles of some example (compounds **86, 89, 90** and **91**) that demonstrated the purity of ARMs after purification. RP-HPLC profiles confirm that, in general, the presence of one or more peptide sequences make less polar the final ARM, shifting on the right its signal.

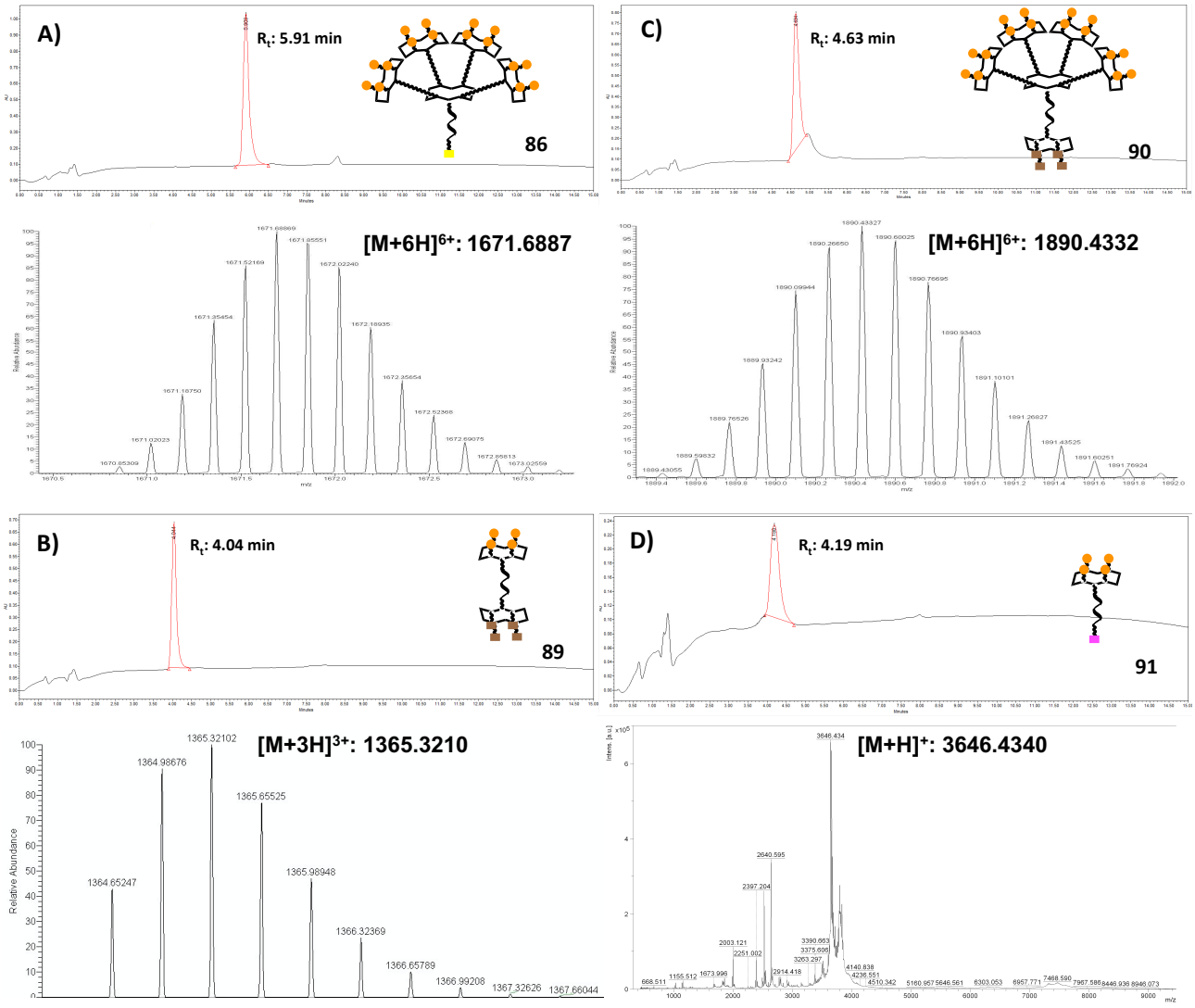

Figure 57 *RP-HPLC and HRMS characterizations.* ***A) ARM 86*** *RP-HPLC: R_t = 5.91 min (C_{18}, λ = 214 nm, 5-100% B in 15 min); HRMS (ESI$^+$-TOF) m/z: calculated for $C_{437}H_{696}N_{128}O_{143}$ $[M+6H]^{6+}$: 1671.6872, found 1671.6887.* ***B) ARM 89*** *RP-HPLC: R_t = 4.04 min (C_{18}, λ = 214 nm, 5-100% B in 15 min); HRMS (ESI$^+$-TOF) m/z: calculated for $C_{173}H_{271}N_{49}O_{66}$ $[M+3H]^{3+}$: 1364.6525, found 1365.3210.* ***C) ARM 90*** *RP-HPLC: R_t = 4.63 min (C_{18}, λ = 214 nm, 5-100% B in 15 min); HRMS (ESI$^+$-TOF) m/z: calculated for $C_{489}H_{769}N_{141}O_{170}$ $[M+6H]^{6+}$: 1890.2662, found 1890.4332.* ***D) ARM 91*** *RP-HPLC: R_t = 4.19 min (C_{18}, λ = 214 nm, 5-100% B in 15 min); MALDI-ToF m/z: calculated for $C_{156}H_{246}N_{53}O_{49}$ $[M+H]^{+}$: 3645.804, found 3646.4340.*

II.6. Conclusions of Chapter II

The first objective of this thesis work was to synthesize ARM molecules, combining several ABM and TBM, able to recruit and hijack natural circulating antibodies against cancer cells. In particular, we have synthesized:

- Peptidic platforms: RAFT (R), dendrimer (D) or combination of them (RR, DR, RD, DD);
- Propargylated carbohydrates: α-L-Rha, α-D-Gal, ß-D-Gal, α-D-Neu5Gc, ß-D-Glc;
- Propargylated peptides: cRGD, LT, HVH and Ac-HVH;
- Antibody Binding Modules (ABMs): glycoconjugates with 4 or 16 carbohydrate units to bind circulating endogenous antibodies;
- Tumoral Binding Modules (TBMs), glyco- or peptidoconjugates with 1 or 4 epitope units to interact with protein overexpressed on cancer cells surface;
- Antibody Recruiting Molecules (ARMs), molecules created by combining several ABM and TBM, to elicit an immune clearance response against cancer cells upon formation of a interacting (ternary) complex with antibodies and targeted cells.

ARMs were constructed following some key synthetic strategies. First of all, the use of CuAAC was extremely efficient to prepare these supramolecular bioconjugates by a convergent synthetic way, avoiding side molecules and difficult purifications. To evaluate the influence of the ligand structure multivalent platforms such as RAFT decapeptide platform and polylysine dendrimer scaffold were synthetized by SPPS and next decorated with multiple copies of carbohydrates or peptides in order to get ABM and TBM conjugates by CuAAC. ARMs were finally synthetized aiming to vary parameters such as the valency, the size, the flexibility, and the geometry of the molecules. In addition, ARMs were characterized by analytical HPLC, HRMS as well as ^{1}H-NMR.

In the next section, these ARMs have been tested biologically in order to have a preliminary evaluation of which structures could be the best to mediate an immune mediated clearance.

Chapter III.

ARMs biological evaluation

III.1. Introduction

As it was previously explained, the ultimate goal of my thesis project is to design original bimodal molecules able to selectively bind cancer cells and, at the same time, recruit endogenous antibodies from human serum. The formation of the ternary complex is a prerequisite to trigger an immunological reaction leading to cancer cell lysis, without pre-immunization.

The ability of ARMs to form binding complex with targeted cells and antibodies present in human serum has been evaluated by flow cytometry and is described in the first part of this chapter. In addition, confocal microscopy analysis have been performed to localize this ternary complex at cellular level. The immune-mediate cytotoxicity was next analysed for each ARM families using a cell viability assay. All the biological part of this work has been supervised by Dr. Nathalie Berthet.

III.2. Ternary complex assessment by FACS and confocal microscopy

The fluorescence-activated cell sorting (FACS) is a technique that defines physical and fluorescent features of cells or particles. In our experiments, it allowed to access to the size, the granularity and the fluorescence characteristics of cells. To do this, a cellular suspension is pushed into a cavity by a vector flux (liquid sheath) whose role is to pass the cells one by one in front of a light source (usually a laser). The light emitted by the irradiated cells is redirected to a set of detectors by a mirror and filter system with different angles relative to the incident beam. The light diffused at 90° informs about the shape and granularity of the cell: it is the parameter SSC (side scatter); for more complex and granular cells, the signals emitted perpendicularly will be stronger. The light diffused at 180° informs about the size of the cell: it is the parameter FSC (forward scatter); for bigger cells, the signals emitted will be stronger (Figure 58 A). Finally, cells can also be separated by whether they express a particular protein, usually stained by a fluorochrome, that emits light when excited by a laser with the corresponding excitation wavelength. Fluorescent labeled cells can be detected individually (Figure 58 B).

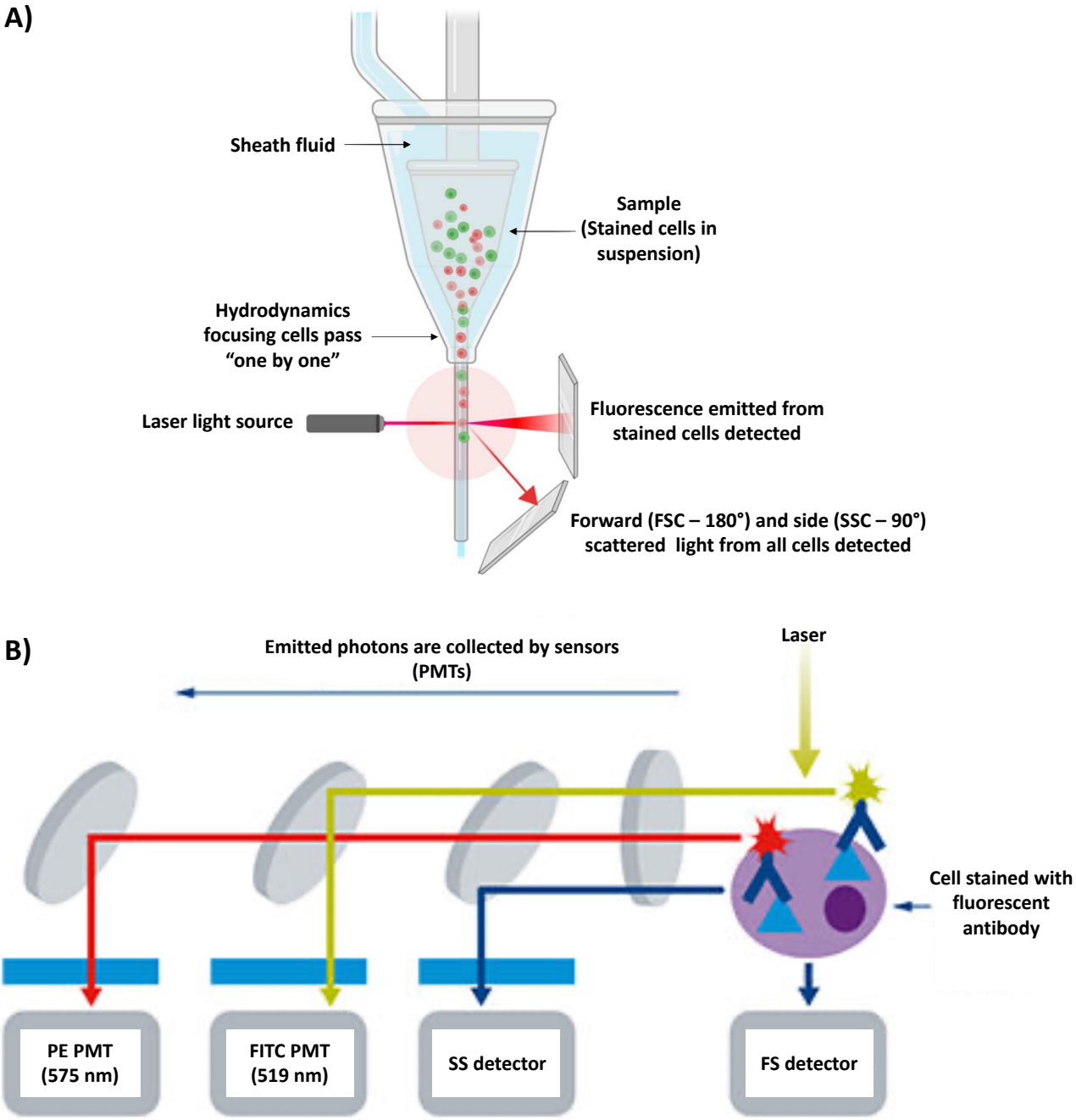

Figure 58 A) *Overview of the flow cytometer. Sheath fluid focuses the cell suspension, causing cells to pass through a laser beam one cell at a time. Forward and side scattered light is detected, as well as fluorescence emitted from stained cells.* ***B)*** *Fluorescent light is filtered so that each detector and the photo multiplying tube (PMT) detect a specific wavelength. The FITC (fluorescein isothiocyanate) channel PMT will detect light emitted from FITC at a wavelength of approximately 519 nm. The PE channel PMT will detect light emitted from PE (phycoerythrin) at 575 nm wavelength. Next, the PMTs convert the energy of a photon into an electronic signal. (abcam.com)*

As the fluorescing cell passes through the laser beam, it creates a peak or pulse of photon emission detected by the PMT and converted to a voltage pulse, known as an event. The measured voltage pulse area will correlate directly to the intensity of fluorescence for that event. When no fluorescing cells pass through the optics, no photons are emitted and no signal is detected. All the data are collected in a graphs in which each cell (or "event") appears as a point, with some value of FSC-A or SSC-A (the A meaning the area of the voltage signal). This makes it possible to distinguish between cellular fragments (Figure 59, Area A), damaged cells (Figure 59, Area C) and cells in good condition (Figure 59, Area B). The first step of an experiment is to select only the cells in good condition. Then, it has to select the single cells (singlets) (Figure 59, Area D) from those coupled (Figure 59, Area E), noting that doublet cells that pass at the same time at the beam level are counted as a single cell but with a fluorescence intensity twice of a normal single cell. Finally, the data appear as histograms shifted concerning on their fluorescence intensity (Figure 59, Area F). The greater is the right shift compared to the autofluorescence signal, the bigger is the number of fluorescent-labelled cells.

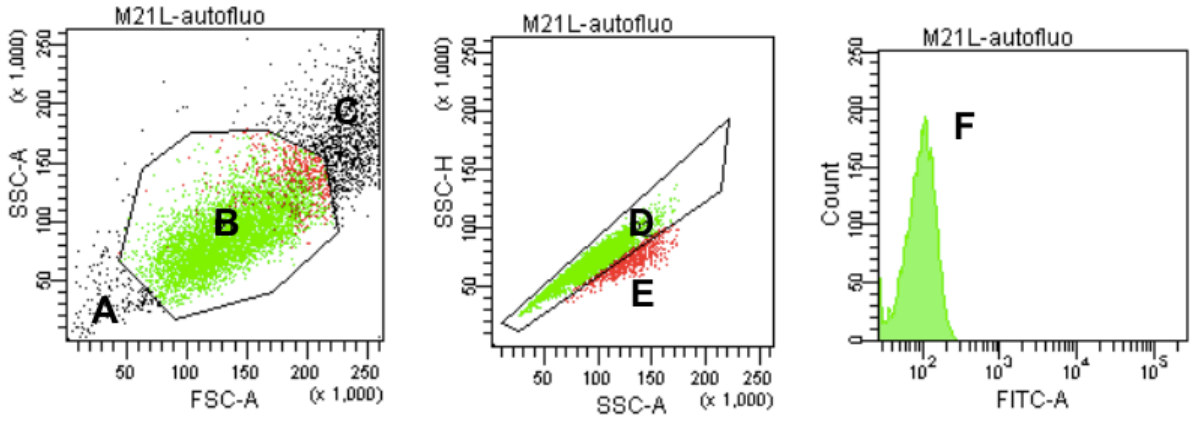

Figure 59 *Examples of fluorescent-labelled M21-L cell suspension analysed by flow cytometry. The graphs on the left show the SSC-A (granularity) and FSC-A (size) parameters for each cell (A: area). The graphs on the middle show the selection of good condition and singlet cells. The graphs on the right show the count or amount of FITC-labelled cells. A: crushed cells, B: healthy cells, C: damaged cells, D: singlet cells, E: doublet cells, F: histogram represented the fluorescence intensity of each cell. (abcam.com)*

In addition to FACS, we used confocal microscopy to obtain additional and important information about the location of fluorescent-labelled molecules at the cell level. It's worth noting that I didn't execute this procedure by myself, but all data derived from cooperation with Cécile Cottet, laboratory of Fundamental and Applied Bioenergetics (LBFA), Grenoble.

III.3. Previous results

The key step to evaluate an ARM efficiency to stimulate a cytotoxic immune response is the assessment of its ability to form a ternary complex between cancer cells and antibodies. The FACS condition, including cell lines typologies and human serum parameters, was already determined in our laboratory by Dr. Benjamin Liet. All ARMs have been tested on different cell lines: $\alpha_v\beta_3$ integrin over-expressing cell lines for ARMs containing cRGD TBM; EGFR over-expressing cell lines for ARMs containing LT and HVH moieties; GLUT-1 over-expressing cell lines for ARMs containing glucose moiety. Four types of tumor cell lines have thus been used:

- M21 are adherent human cells from melanoma tissue. These cells overexpress $\alpha_v\beta_3$ integrins on their surface (Figure 60 A).[202]
- M21-L (where L means low) are identical to M21 but do not have the gene encoding for the α subunit of the integrins (integrin subunit alpha v, IGTAV) resulting in a low expression of $\alpha_v\beta_3$ integrins (Figure 60 B).[203]
- MCF_7 (Michigan Cancer Foundation-7) are adherent human cells from mammary gland adenocarcinoma derived from metastatic site, known for having an high expression rate of EGFR on the surface (Figure 60 C).[204,205]
- HeLa are adherent human cells from cervical cancer tissue, known for having an high expression rate of GLUT-1 on the surface (data not shown).[206,207]

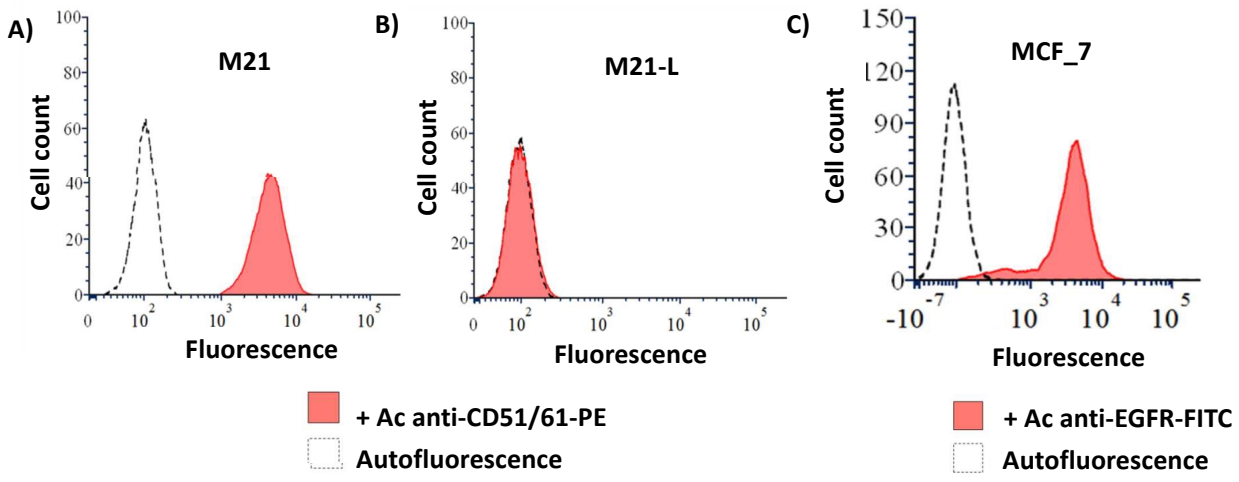

Figure 60 *Flow cytometry analysis indicating the $\alpha_v\beta_3$ integrin expression by M21 (**A**) and M21-L (**B**) cell lines and the EGF receptor amount on the MCF_7 (**C**) cell line. The studies A and B are done with a human CD55/CD61 antibody (or $\alpha_v\beta_3$ integrin, BD Pharmingen, 550037) coupled to phycoerythrin (PE), while the study (C) is done with an anti-EGFR mouse antibody coupled with fluorescein (FITC).*

M21, M21-L and HeLa cell lines were cultured in specific media and maintained at 37°C in a humidified atmosphere containing 5% CO_2 (see chapter V – materials and methods).

Previous work in our laboratory showed the ability of the tetravalent $R(cRGD)_4$ as TBM (compound **59**, Scheme 13) to bind M21 cell line. For the TBM binding to the $\alpha_v\beta_3$ integrins expressed at cell surface, M21 and the negative control M21-L cell lines were counted and resuspended at 1 million cells in 1 mL of Hank's Balanced Salt Solution containing Ca^{2+} and Mg^{2+} (HBSS*, * denotes the presence of these divalent cations). It allows the integrins to spread on the membrane and become active.[208]

The fluorescently-labelled TBM **94** (Figure 61 A) was incubated with M21 and M21-L cell suspensions at 5 µM to involve a maximum of $\alpha_v\beta_3$ integrins present on the cell surface. After one hour of incubation at 37°C, the fluorescence of the cells was analysed by flow cytometry, relating to autofluorescence (no compound). An interaction of **94** only with M21 was observed. Similar experiments were conducted to prove the $R(LT)_4$ binding to the MCF_7 cell surface. It was clearly showed that **95** interacts with MCF_7 (Figure 61 B).

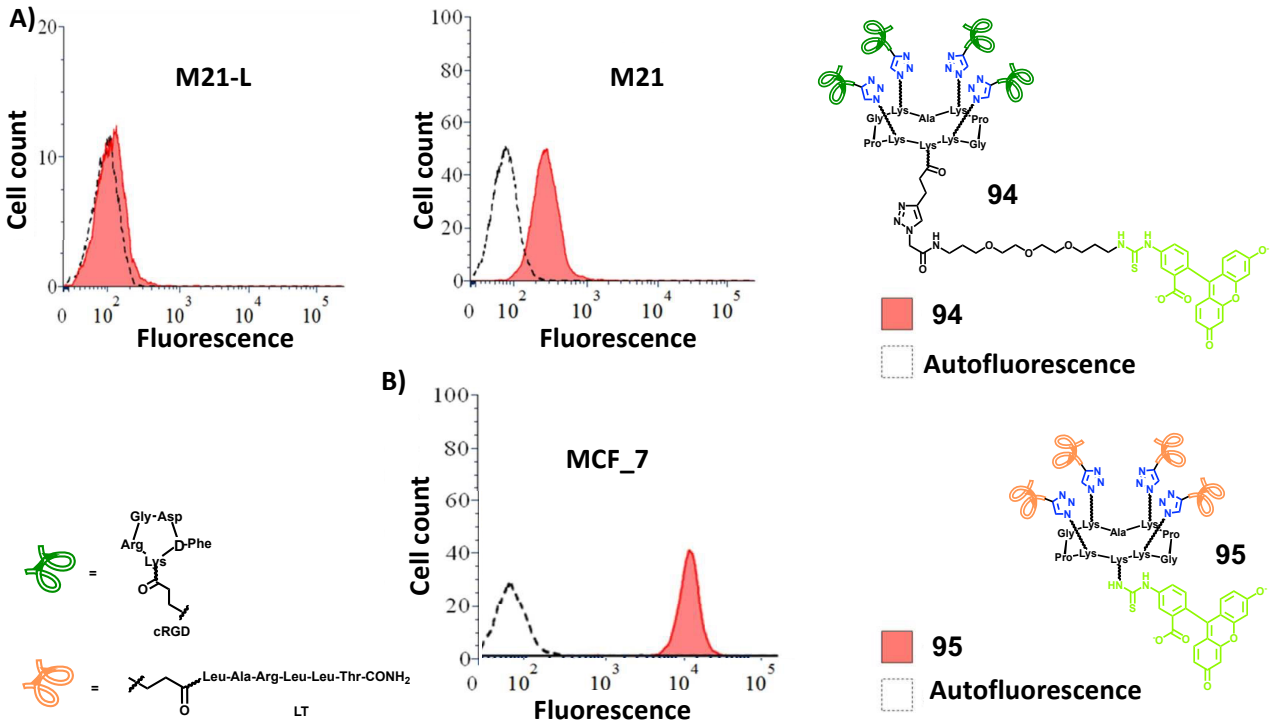

Figure 61 A) *Flow cytometry analysis representing the interaction of tetravalent **94** on M21-L and M21 cells.* **B)** *Flow cytometry test representing the interaction of tetravalent **95** on MCF_7 cells.*

The interaction of **94** with M21 and M21-L cells was also observed by confocal microscopy (Figure 62).

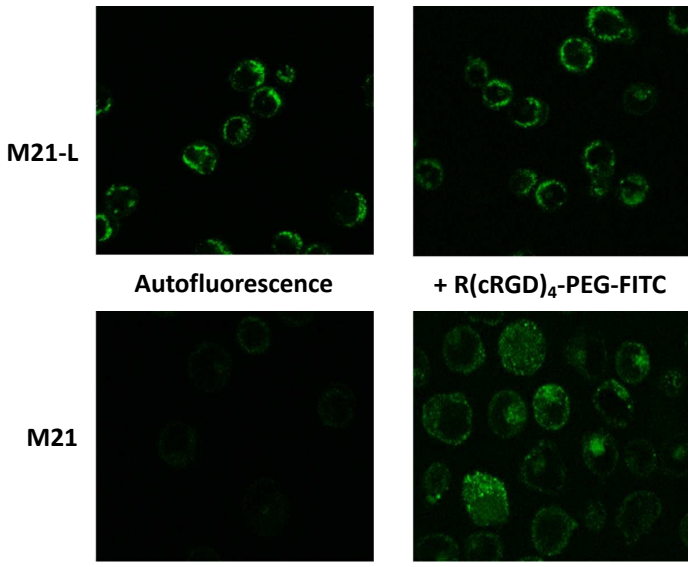

Figure 62 *Confocal microscopy showing the localization and the characteristics of fluorescent-labelled R(cRGD)$_4$-PEG-FITC* ***94*** *while interacts with M21 and M21-L cell lines. Autofluorescence is done in absence of fluorescent-labelled compound.*

Pictures of M21 cells incubated with this molecule showed a higher fluorescence intensity in the presence of the fluorescent compound compared to the autofluorescence. The M21-L cells, on the other hand, showed a significant autofluorescence making the analyses more delicate, but we were able to confirm the absence of increased fluorescence of the cells in the presence of **94**. The localization of cRGD peptides, and therefore of $\alpha_v\beta_3$ integrins, seems to be concentrated mainly at the cell membrane with some more intense areas, most certainly due to the well-known «clustering» of integrins upon binding with their ligand. For some cells, fluorescence was also observed in cytoplasm indicating an internalization process initiated by the integrins as soon as the interaction with the fluorescent compound **94** occurred. This phenomenon could be problematic for the intended application and will therefore require optimized conditions to minimize this risk.

Next, it was determined the amount of IgG and IgM antibodies in the human serum (HS) able to bind Rha moieties. The experiment was performed by a direct affinity test, incubating a polyacrylamide polymer functionalized with α-L-Rha (Lectinity Holding Inc., Moscow) with HS containing anti-α-Rha antibodies and secondary antibodies allowing fluorescence revelation, in 96 microplate wells (Figure 63 A). Using a dilution of the secondary anti-IgG and anti-IgM fluorescent antibodies, it was demonstrated that there is no anti-Rha IgG in HS, while IgM antibodies have a strong interaction with the immobilized α-L-Rha moiety, probably due to their pentameric structure (Figure 63 B).

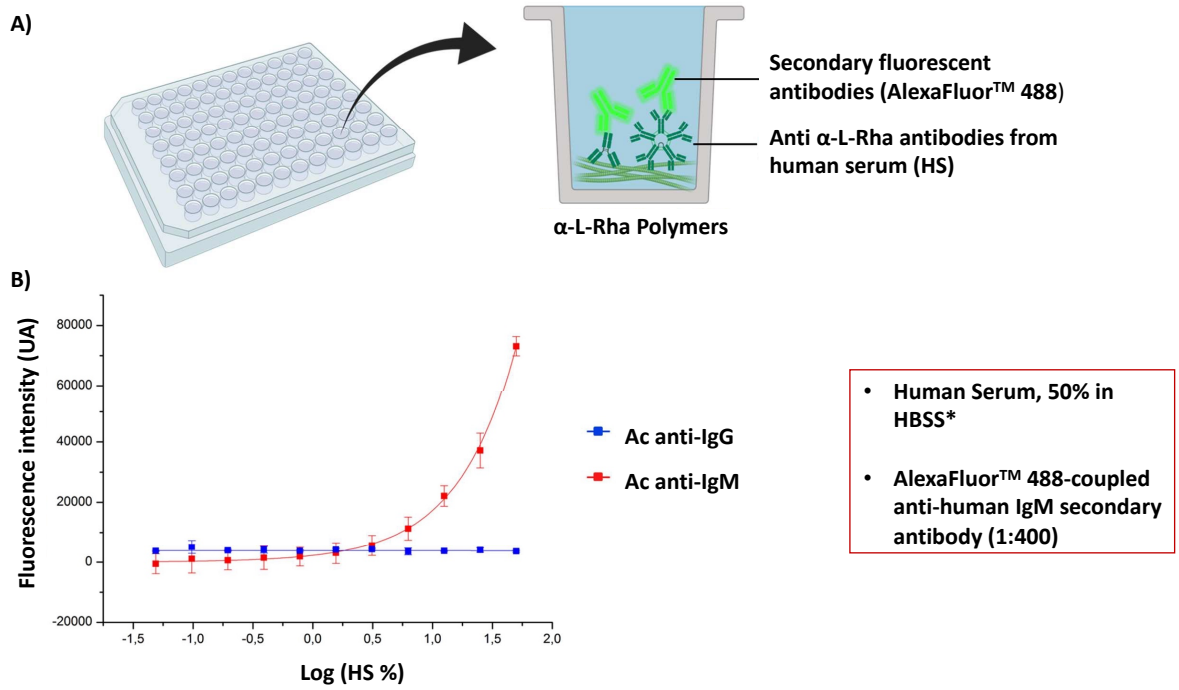

Figure 63 *Previous experiment conducted in our laboratory to demonstrate the amount of IgG and IgM antibodies in the human serum able to bound rhamnose.* ***A)*** *The experiment was performed in 96 microplate wells incubating a polyacrylamide polymer functionalized with α-L-Rha with HS and secondary fluorescent antibodies.* ***B)*** *The picture shows that, with the final condition for HS and secondary antibody listed in the red box, only IgM can interact with the α-L-Rha on the polymer.*

At the end, it was determined the ideal concentration of ARM to incubate with cells and HS, that is an essential parameter to assess when a ternary complex has to be formed, even if the situation could be different in cellular assays. As already described by Spiegel group (Chapter I), [79,89] the behaviour representing the ternary complex formation is described by a Gaussian curve: if ARM is added in small quantities, a lot of integrins will be free and the recruitment of antibodies will not be optimal, while if ARM is added in excess to saturate $\alpha_v\beta_3$ integrins, the unbound molecules will bind the antibodies leading to a competitive event. Thus, these latter cannot bind to the ARMs present on the cell surface. For this reason, the determine of the optimal concentration of ARM is essential. In the previous experiments carried out in our team by Benjamin Liet with the tetravalent ARM **70** and the hexadecavalent ARM **71** from the Rha – cRGD ARM family, it was chosen to keep fix the M21 cell concentration at 1 x 10^6 cells/mL in HBSS* and to vary the ARM concentration from a range of 20 µM to 10 nM. After several tests, it was found that, with these conditions, 100 nM concentration of ARM seems appropriate to observe the formation of the ternary complex.

III.4. FACS analysis of the ternary complex formation with the Rha – cRGD ARM family

Starting from conditions previously established, ARMs **70** and **71** were retested by FACS following the procedure described in chapter V – material and methods. The results are showed in Figure 64.

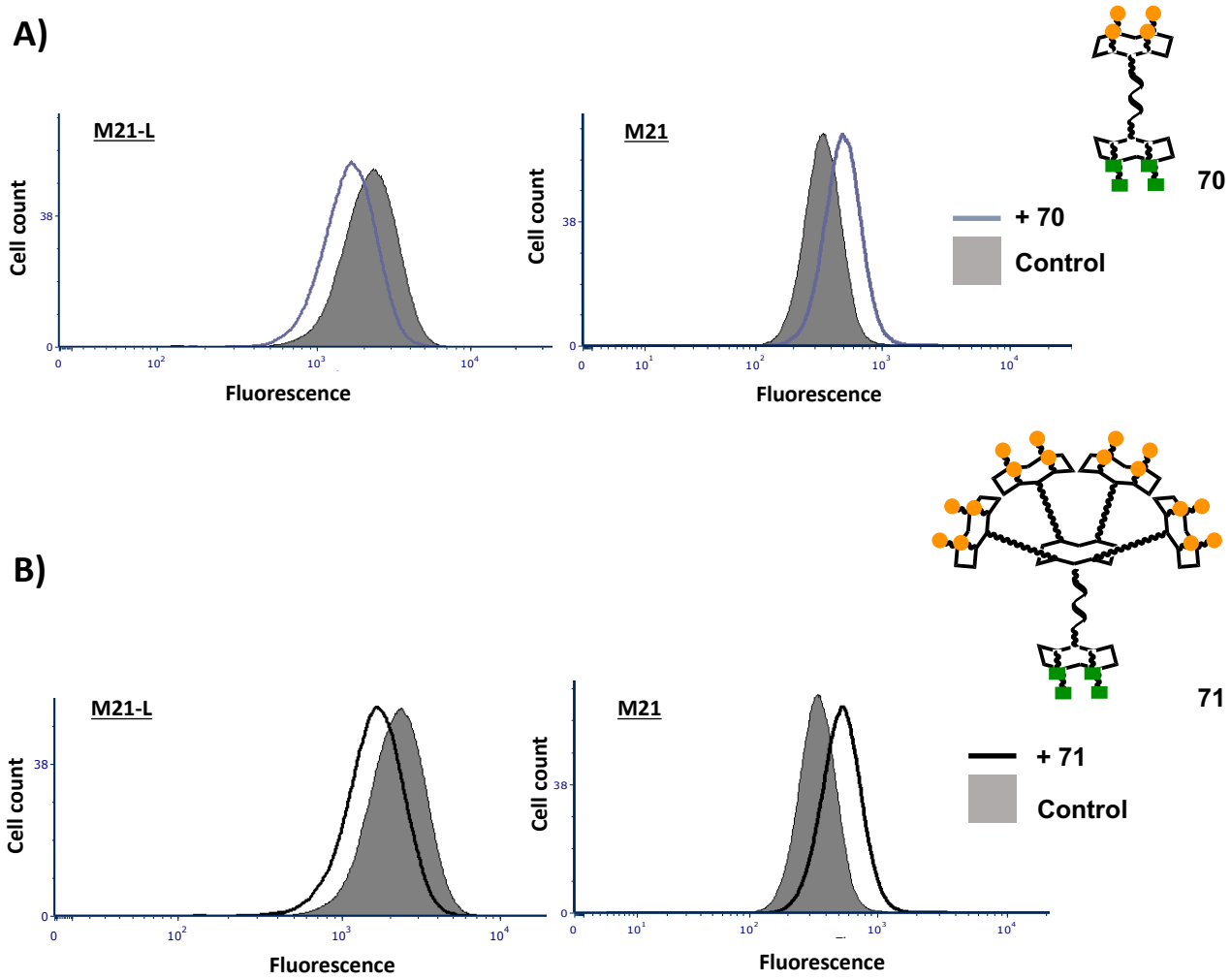

Figure 64 A) *Flow cytometry analysis of M21-L and M21 cell lines incubated with ARM* ***70*** *+ human serum + AlexaFluor™ 488-coupled anti-human IgM secondary antibody.* ***B)*** *Flow cytometry test representing M21-L and M21 cell lines incubated with ARM* ***71*** *+ human serum. Cells incubated with human serum (in absence of ARM) then treated with secondary anti-Rha conjugated AF-488 antibody was used as control (grey filled curve).*

In Figure 64, histogram analysis shows that the fluorescence signals of M21 cells treated with both ARMs are shifted to the right compared to the control, meaning that they are able to recruiting antibodies. Overlapping this two M21 signal (data not show), we can observe a higher

fluorescence value for the hexadecavalent ARM **71** than the tetravalent ARM **70**. A presentation of 16 units of α-L-Rha allows a better recruitment of antibodies than 4 units of α-L-Rha due to multivalent effect, confirming the results observed by E. Laigre and B. Liet in their Ph.D. thesis.[169, 209] Conversely, a decrease of fluorescence signal can be observed when both ARMs are incubated with M21-L control cells. This could be explained by unspecific interactions with proteins present in the human serum that can change the autofluorescence properties of the cancer cells.

Then, we decided to study the location of ARMs by confocal microscopy (Figure 65).

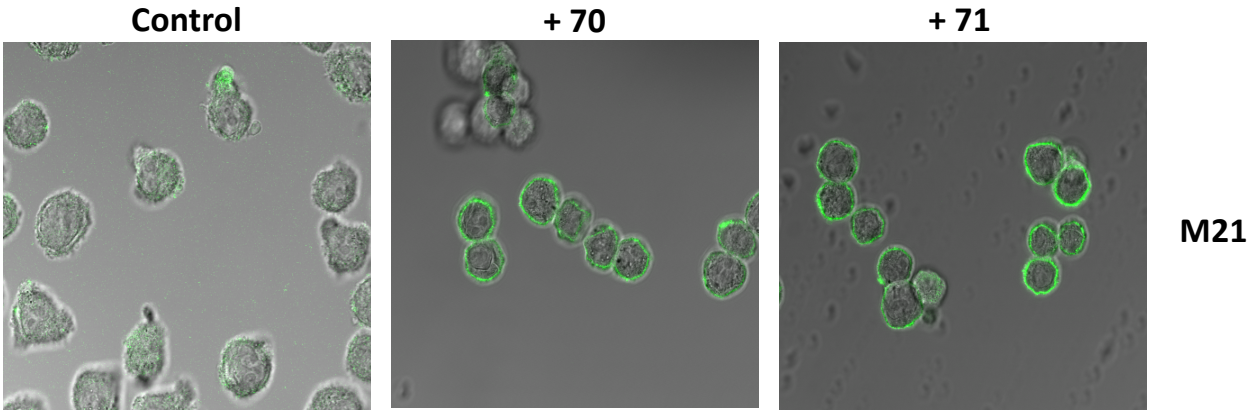

Figure 65 *Fluorescence pictures of M21 cell lines observed under confocal fluorescence microscopy, either incubated with ARM (**70** or **71**) plus human serum and secondary anti-IgM antibody coupled to Alexafluor™ – 488. The control denotes the incubation of cells with human serum and secondary anti-IgM antibody coupled to Alexafluor™ – 488, but in absence of ARM.*

The visualisation by confocal microscopy of the M21 cells incubated with ARM **70** or **71**, human serum and fluorescent secondary antibody localise ARMs at the cell surface (Figure 65). A slightly higher fluorescent halo was observed for cells incubated with the hexadecavalent ARM **71** compared to ARM **70**. These observations confirm the FACS results showing the best antibody recruitment for ARM **71** compared to ARM **70**. All these results clearly show the ARM accessibility at the cell surface to human serum antibodies.

Once established the potential of ARMs **70** (R-R) and **71** (RR-R) composed by RAFT platforms to recruit endogenous antibodies, we evaluated others architectures displaying the same valency (16 epitopes of Rha). Notably, ARMs **72** (RR-D), **73** (DR-R), **74** (RD-R) and **75** (DD-R) are composed by different combination of polylysine dendrimer and RAFT, while ARMs **76** (R-R PEG) and **77** (RR-R PEG) have longer linker (PEG) than our first prototypes **70** and **71**.

First ARMs were incubated with the control cell line M21-L (Figure 66).

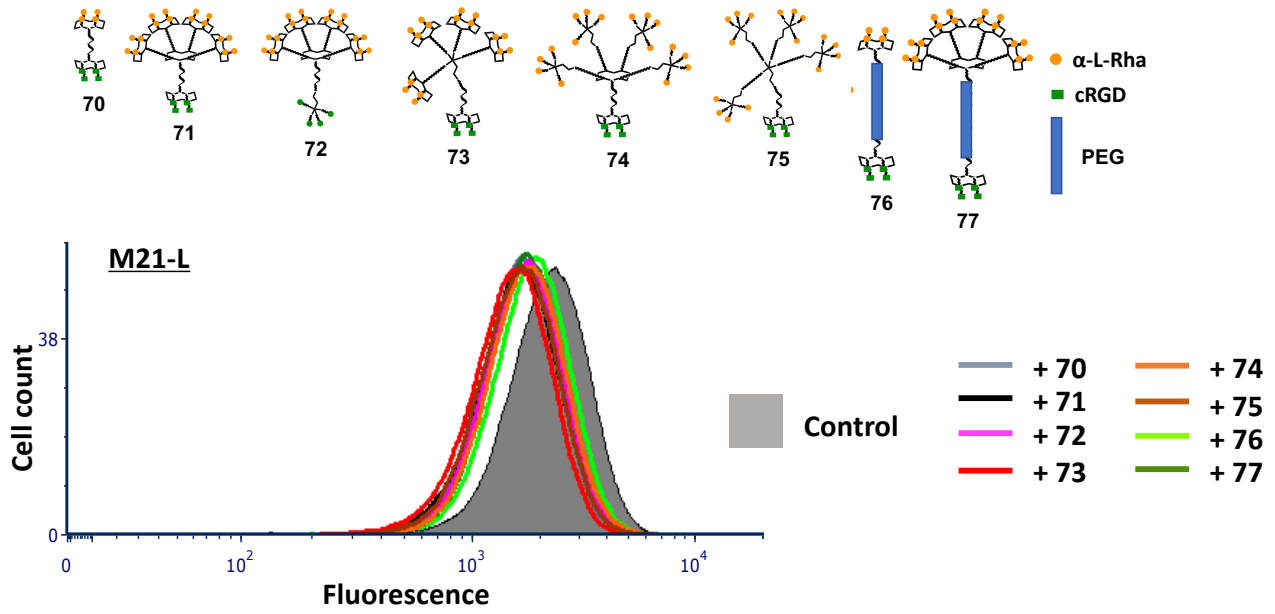

Figure 66 *Flow cytometry analysis representing M21-L cell line incubated with different ARMs (**70**, **71**, **72**, **73**, **74**, **75**, **76** or 77) + human serum + secondary anti-IgM antibody coupled to an Alexafluor™ – 488. M21-L cells incubated with human serum + secondary anti-IgM antibody, in absence of ARM was used as control (grey filled curve).*

As shown on Figure 66, the interaction between this cell line and our ARMs is described by a shared trend: the fluorescence signal for cells treated with all ARMs tested remains slightly lower than control denoting the absence of specific ARM binding and antibody recruitment at the cell surface. Here again, a decrease in the fluorescence signal is observed for cells treated successively with ARM, human serum and the fluorescent conjugated secondary antibody compared to the control in which cells were incubated only with serum and the fluorescent conjugated secondary antibody. This could be attributed to unspecific interactions, both to cells and some constituents of the serum, that may change the autofluorescence properties of the cell.

We next evaluated the ability of the same ARMs to form a ternary complex with M21 cell line and human serum antibodies. We first compared ARMs **72**-**75** with ARM **71** as a reference (Figure 67).

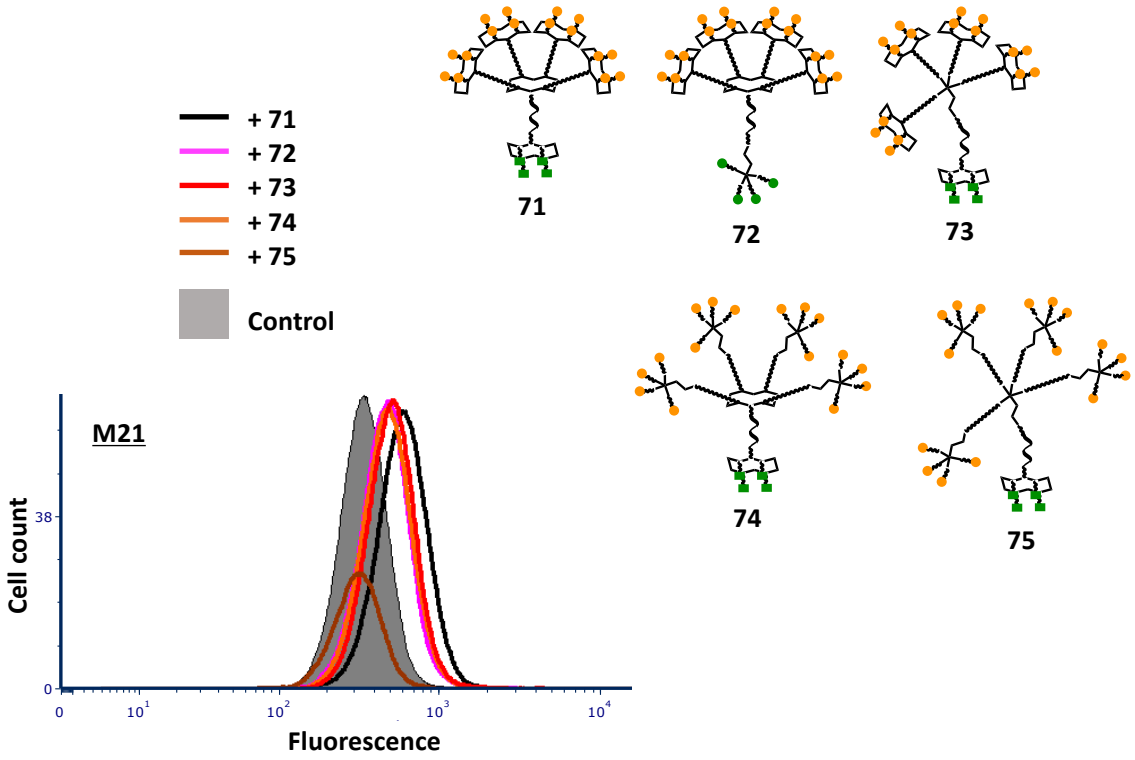

Figure 67 *Flow cytometry analysis representing M21 cell line incubated with different ARMs (**71**, **72**, **73**, **74** or **75**) + human serum + secondary anti-IgM antibody coupled to an Alexafluor™ – 488. The grey filled curve (control) denotes the interaction between cells and human serum + secondary antibody, in absence of ARM.*

Some relevant conclusions can be drawn from Figure 67. First of all, the higher fluorescence signal was observed for cells incubated with ARM **71**, showing its higher ability in recruiting antibodies than other ARMs. Indeed, ARMs **72, 73** and **74** showed lower potency to form ternary complex than ARM **71** but overlapped fluorescent signals suggest comparable effect for each compound. Conversely, ARM **75** does not seem able to recruit antibodies, since its curve is perfectly overlapped with the control experiment (without ARM).

The results have been analysed comparing molecules which differ by one structural parameter, such as the TBM or ABM architectures or the central “core” or of the peripheric layer. For example, ARM **71** and ARM **72** differ each other from the platform that displays the cRGD peptides: from the FACS result, it could be assumed that the 4 peptides are better presented to the cell by a RAFT platform (ARM **71**) than by a dendrimer platform (ARM **72**). This result is in good agreement with previous results, which confirms that the presence of ABM does not influence the binding with the integrins. ARM **71** is thus more efficient to recruit antibodies.

Regarding the ABM part, we compared molecules with the same “core” architecture, such as ARM **71** and **74** (same “core” RAFT but different peripheric platform) or ARM **73** and **75** (same “core” dendrimer but different peripheric platform). We observed that the recruitment ability decreases when the carbohydrate epitopes are presented by a peripheric dendrimer (ARM **74** and **75**). On the other hand, the “core" architecture is also an important parameter, since comparing ARM **71** and **73** (same peripheric RAFTs layer but different “core” platform), it results into lower ability to recruit antibody when the central “core” is a dendrimer architecture. We can do the same observation with ARMs **74** and **75**: in both cases, the 16 sugars are presented by a dendrimer platform but these molecules have either a RAFT (ARM **74**) or dendrimer (ARM **75**) “core”. In the latter case, we again observed a lower intensity signal and a lower antibody recruitment ability. These results indicate that, both the “core” and the peripheric architecture are key parameters to form the ternary complex. In addition, the RAFT platform seems to be more suitable for the ligand presentation for ABM, TBM as well as the central core than the dendrimer platform presumably due to a higher rigidity.

Next, we evaluated the influence of PEG motif as a linker between ABM and TBM parts. It is important to consider that a longer linker could not only increase the distance between ABM and TBM parts but also modify the flexibility of the whole molecule leading to a different ARM ability in antibodies recruitment. Two FACS analysis were performed with M21 cell line using the procedure described previously. First cells were incubated with the two tetravalent Rha – cRGD ARMs **70** (R-R) and **76** (R-R PEG) (Figure 68 A) then with the two hexadecavalent Rha – cRGD molecules **71** (RR-R) and **77** (RR-R PEG) (Figure 68 B).

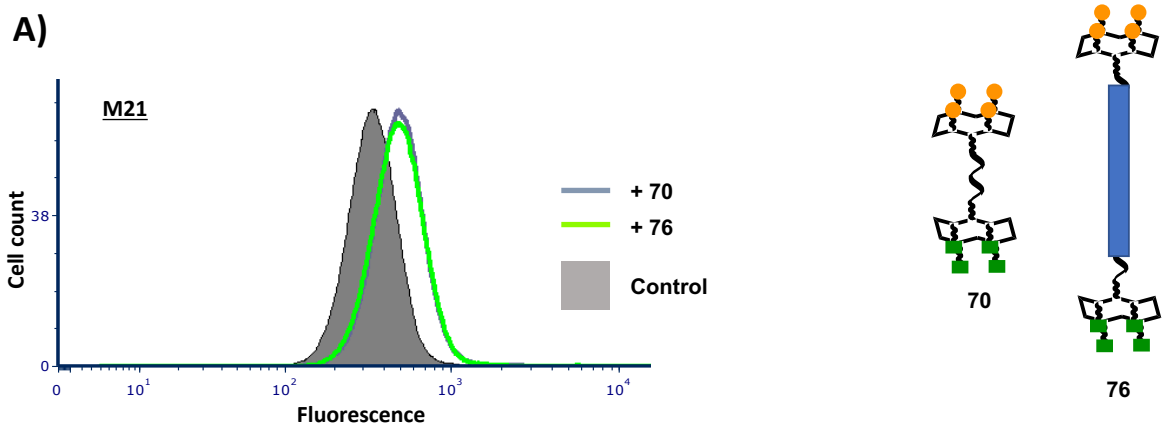

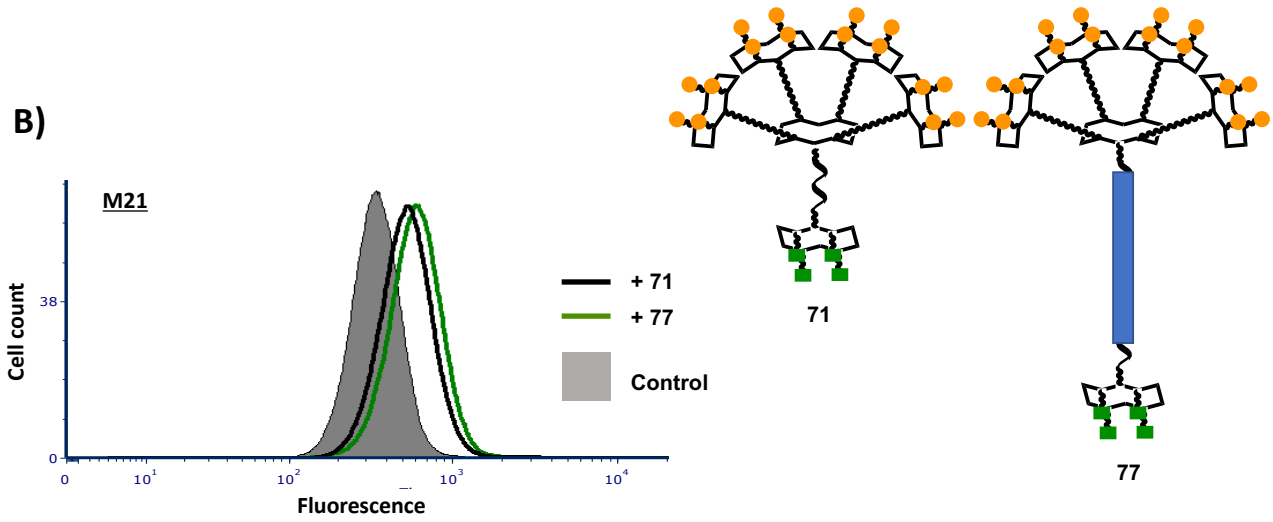

Figure 68 A) *Flow cytometry analysis representing M21 cell line incubated with ARMs **70** or **76** + human serum + secondary anti-IgM antibody coupled to an Alexafluor™ – 488.* ***B)*** *Flow cytometry analysis representing M21 cell line incubated with ARMs **71** or 77+ human serum + secondary anti-IgM antibody coupled to an Alexafluor™ – 488. Cells incubated with human serum and secondary antibody, in absence of ARM was used as control (grey filled curve).*

The fluorescent signal of the cells treated with the tetravalent ARM **76** (R-R PEG) is basically overlapped to the same molecule without PEG (ARM **70**), showing that in this case the linker doesn't affect the ability of the compounds to recruit anti-Rha antibody. Conversely, for the hexadecavalent compounds, the fluorescent value for cells treated with ARM **77** (RR-R PEG) is higher than for the reference ARM **71** (RR-R), meaning an improvement in the ability to recruit antibody. This effect is probably due to the fact that the 16 units of α-L-Rha are more available at the cell surface to interact with antibodies. It might have been also expected a rise in fluorescence with ARM **76** (R-R PEG), longer than ARM **70** (R-R). This, instead, doesn't happen because, even if the 4 copies of α-L-Rha are more accessible in the environment, the valency of ARM **76** is probably not enough to increase the recruitment ability of antibodies. In other words, multivalent effect for the rhamnose presentation at the cell surface seems to be a more important parameter than length linker between ABM and TBM.

In view of the FACS results, confocal microscopy was done with the hexadecavalent molecules ARM **71** and **77** (Figure 69).

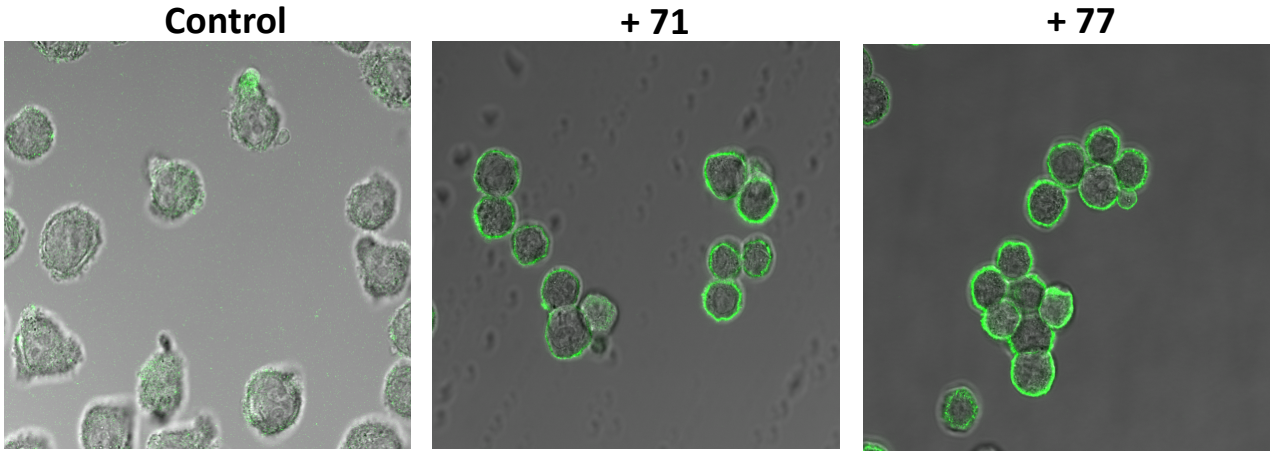

Figure 69 *Fluorescence pictures of M21 cell line observed under confocal fluorescence microscopy, either incubated with ARM (**71** or **77**) and HS and secondary anti-IgM antibody coupled to an Alexafluor™ – 488. Control denotes the incubation of cells with human serum and secondary anti-IgM antibody coupled to Alexafluor™ – 488, but in absence of ARM.*

Figure 69 shows that incubation of M21 cells with these ARMs results in a more intense signal than control. More importantly, a stronger signal located at the M21 cell surface is clearly visible when the cells are incubated with ARM 77 than ARM 71. Thus, confocal microscopy pictures was in agreement with FACS results.

III.5. Cytotoxicity assay

III.5.A. Selection of the cytotoxicity assay

Once demonstrated that ARMs are able to form a ternary complex with the targeted cells and the anti-Rha antibodies, we evaluated whether this complex can initiate an immune cascade leading to the cytotoxicity of the target cell. For this reason, a cytotoxic test was performed to assess the cell viability upon treatment with ARMs and human serum. Since this latter doesn't contain blood cells but only antibodies and other proteins, including complement proteins, we expect a CDC response only rather than ADCC or ADCP.

There are several cytotoxicity methods using microplates format to investigate the cell death. For example, bioluminescent quantification of intracellular ATP levels can be used. Adenosine triphosphate (ATP) is an energetic metabolite that plays a key role in active cells as the primary donor of free energy. As a result, cells need ATP to stay alive and perform their various metabolic and anabolic processes. When the cells run out of substrates or when the substrates initiate death, cytoplasmic ATP decrease over time. The measurement of intracellular ATP is thus a dosage of choice for studying the viability of a cell population. Over the past decades of research, the determination of ATP has been developed and is now widely used to determine cell proliferation. This method relies on the determination of a bioluminescent product, oxyluciferin, which is produced by the transformation of luciferin by the enzyme luciferase. This reaction involves the intervention of various co-factors, such as the dioxygen, the divalent cation Mg^{2+} as well as the ATP. Thus, bioluminescence will only be detected if ATP is present in the system, and therefore if cells are alive.[210]

Intracellular ATP is not the only metabolite or cell component present at high doses in eukaryotic cells. Some enzymes have a constant activity in active cells, such as dehydrogenase. Their intracellular activity could be monitored, for example, through colorimetric tests. The most widely used experiment in recent years is the colorimetric determination of formazan crystals formed by the transformation of a tetrazolium salt, 3-(4,5-dimethylthiazol-2-yl)-2,5-diphenyl tetrazolium bromide (MTT) by mitochondrial dehydrogenase. To be detected by UV, the crystals must be solubilized in an organic solvent (dimethyl sulfoxide, DMSO).[211]

However, we decided to use for our study another well-known cytotoxicity assay, already optimized in our laboratory, that is based on the fluorescence released by death cells. This test relies on a chemical agent, the 2',7'-bis-(2-carboxyethyl)-5(6)-carboxyfluorescein acetoxymethyl ester (BCECF_AM), originally non-fluorescent,[212] which is able to cross the plasmatic membrane. Once internalized, it is enzymatically hydrolysed by esterase to the fluorescent 2',7'-bis-(2-carboxyethyl)-5(6)-carboxyfluorescein (BCECF). Due to its high polarity, BCECF cannot cross

back the plasmatic membrane, thus it is trapped inside the cell. After incubation with an ARM and human serum, if the cell is killed and the plasmatic membrane damaged, BCECF can finally come out in the culture medium and the fluorescence can be measured. (Figure 70). A high fluorescence value indicates a high cell death due to immune mediated cytotoxicity by ARM.

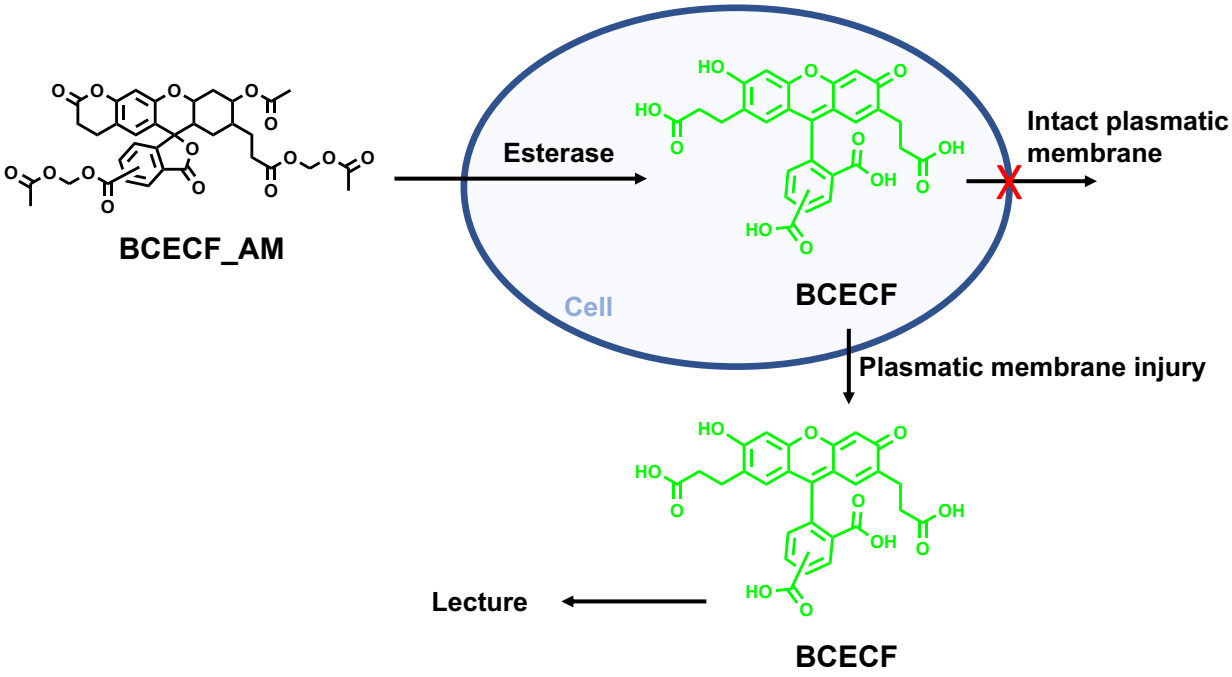

Figure 70 *Principe of the BCECF cytotoxicity test. Acetoxymethyl ester of 2',7'-bis-(2-carboxyethyl)-5(6)-carboxyfluorescein (BCECF_AM) cross the cellular membrane and, only inside the cell, it is hydrolyzed by esterase. This molecule (2',7'-bis-(2-carboxyethyl)-5(6)-carboxyfluorescein or BCECF) cannot cross the health and undamaged cellular membrane. Excitation: 450 nm. Emission: 531 nm.*

After the best conditions have been determined, the ARM cytotoxicity was calculated from the following equation:

$$\text{Cytotoxic rate \%} = \frac{(\text{sample} - \text{BG}) \cdot 100}{(\text{max} - \text{BG})}$$

Where:

sample = fluorescence released by ARM's

BG = spontaneous release of fluorescence by cells not treated

max = highest fluorescence value obtained by cells treated with Triton 1%

100 = % factor

In particular, cells marked with BCECF_AM give “BG” value; cells marked with BCECF_AM, then treated with ARM and HS, give “sample” value; cells marked with BCECF_AM, then treated with ARM and HS, then incubated with a cellular lysis agent (usually a detergent) give the “max” value, corresponding to 100% cytotoxic rate (Figure 71).

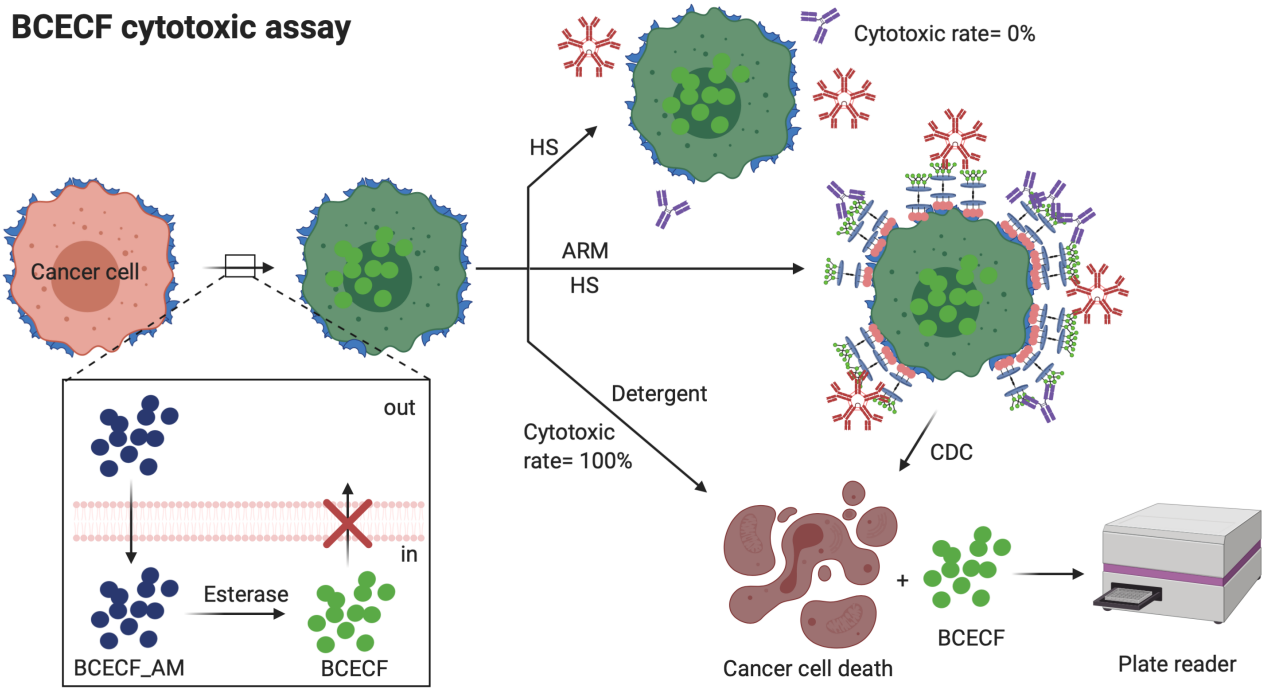

Figure 71 *Cytotoxicity BCECF test used to assess the ability of ARM conjugates to kill the tumor cells in presence of human serum (HS). CDC: complement-dependent cytotoxicity.*

At this point, some key parameters were assessed in order to optimize the protocol. First of all several concentration of the chemical agent BCECF_AM (range from 2 µg/mL to 0.2 µg/mL) and incubation time (2 hours to 30 minutes) were tested. Next, different lysis agents, such as TRITON,[213] RIPA,[214] BD Pharma Lyse[215] at different concentration and several incubation times (2 hours to 30 minutes) with cells were evaluated. We found that the best conditions to obtain the maximum readable fluorescence are:

- 30 min of BCECF_AM 2 µg/mL to obtain the maximum number of marked cells.
- 30 min of non-ionic detergent TRITON 1% to obtain the maximum number of lysed cells (Figure 72).

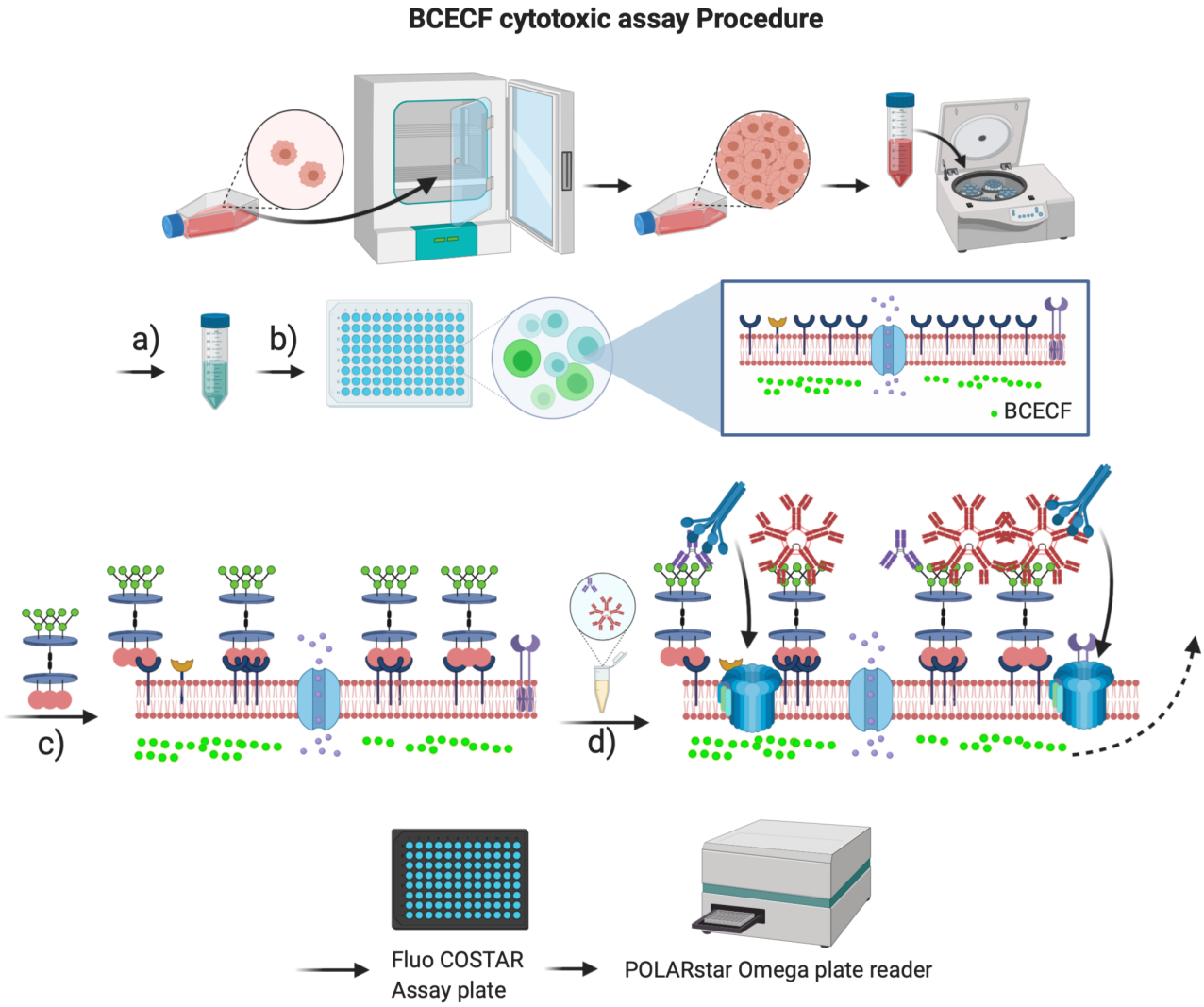

Figure 72 *Test procedure developed to assess the cytotoxic degree of ARM Detailed procedure is described in Chapter V. a) BCECF_AM (2 µg/mL) for 30 min at 37 °C , washing step. The cell are diluted to 1x10^5 cells/mL in HBSS* binding buffer. b) 60 min, 0°C. 1x10^4 cells are added to the rinsed wells. c) 2 washing steps, then incubation with 100 nM ARM, 1h, r.t. d) 1 washing step, then incubation with human serum 50% in HBSS*, 2 h, r.t. For maximum cell lysis, 1% (w/v) of the non-ionic detergent TRITON is added to certain selected wells without ARM after 1h30 of HS incubation.*

III.5.B. Cytotoxicity results of Rha – cRGD ARM family

We first defined the best conditions to use in our cytotoxic test in 96-wells microplate format. The density of cells per well (125x10^3, 80x10^3, 40x10^3, 10x10^3 cells/well) and the ARM concentration (10nM, 100 nM) were thus varied and the cytotoxicity measured (Figure 73).

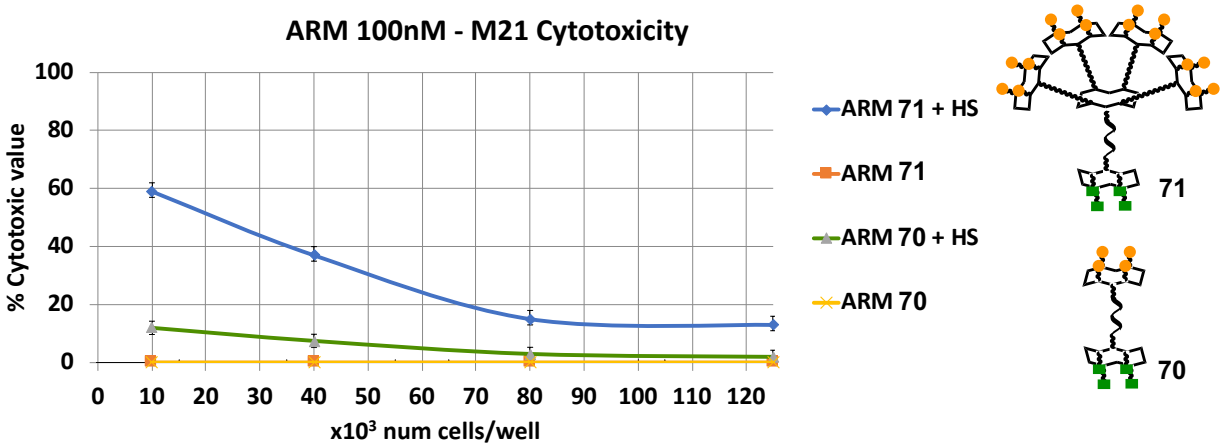

Figure 73 *Cell cytotoxicity varying the number of cells/well (M21 cell lines).*

Figure 73 shows the cytotoxicity of ARM **70** and **71** at 100 nM on various amounts of M21 cells in with or without human serum. First of all, we observe that in absence of human serum (orange and yellow curves) ARMs don't trigger any cytotoxic effect, meaning that our ARMs aren't cytotoxic themselves and that they are functional only in the presence of HS. Next, a cytotoxic effect on M21 cells is observed when treated with ARM **70** and **71** and HS. In contrast with FACS experiments where we obtained almost the same binding effect with both compounds, here we observe a large difference of cell death rate, with less than 20% of cytotoxic effect provided by the tetravalent ARM **70** and 60% by the hexadecavalent ARM **71**. As expected, the highest cytotoxic value for cells treated with both ARMs was obtained for the lower density of cells: $10x10^3$ cells per well. It's worth noting that by reducing the number of cells too much, the intensity of the fluorescence could decrease until making the signal undetectable. In addition, working with $300x10^3$ cells, i.e. the best condition for FACS experiment, no cytotoxicity was observed for each ARMs. A possible explanation is that with $10x10^3$ number of cells, they have a better accessibility inside the well. With higher amounts however, the cells are overlapped to each other into multiple layers, decreasing their accessibility to ARMs and HS.

Once all parameters for the test were optimised, the cytotoxicity of each ARM was evaluated following the procedure described in chapter V – material and methods. This cytotoxic test was performed several times in order to evaluate the influence of different valency (test 1), the influence of different ARMs architecture with same valency (test 2) and the influence of different linker (test 3) on the ability to mediate an immune-mediated clearance on M21 cell line. In addition, it has been also assessed the ARM properties with other cell lines than M21 (test 4).

- **Test 1: % cytotoxic rate evaluation of ARMs with different valency**

The first cytotoxic test was carried out with our ARMs prototype **70** (R-R) and **71** (RR-R) from Rha – cRGD family. In addition, β-D-Gal tetravalent (**81**) and hexadecavalent (**82**) ARMs were

used as negative control. Each ARMs are assessed at two concentrations (10 and 100 nM) and with or without serum. Considering that the presence of TRITON lysis agent leads to the 100% of cellular death (positive control), it is possible to calculate the cytotoxic degree of each ARMs. Each experiment was repeated several times (at least 4 times for each ARM) and the analysis of the cytotoxicity values was reported by histograms, using the Software GraphPad PRISM 8 (Figure 74).

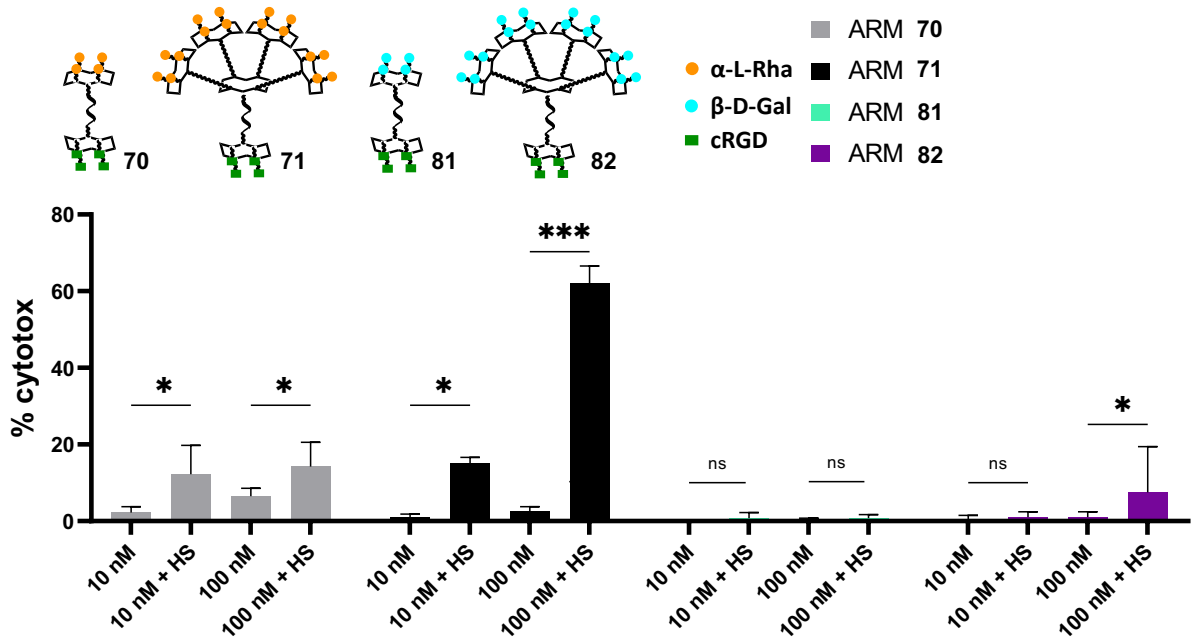

Figure 74 *Comparison of ARMs cytotoxicity on M21 tumor cell line; each ARMs were tested at 10nM and 100 nM, in presence or absence of human serum. ARM* ***81*** *(R-R ß-Gal) and ARM* ***82*** *(RR-R ß-Gal) were used as negative control. Data points represent mean values of at least 4 experiments. Error bars represent 95% confidence intervals. T-test comparisons at 95% confidence were performed using GraphPad Prism 8.0 (not significant or ns: p < 1, *: p < 0.1, **: p < 0.01, ***: p < 0.001).*

First of all, we observed that no ARMs (concentrated both at 10 or 100 nM) are cytotoxic in absence of HS (all percentage of cytotoxicity are <5%) which indicates that the supramolecular constructs are safe compounds. In addition, we observed that the hexadecavalent ARM **71** at 100 nM is very active cause it's able to kill about 60% of tumor cells in the presence of HS, while ARM **70** is considered inactive at the same concentration (% cytotoxic rate: 14%). Therefore, the presentation of multiple copies of carbohydrates on ARM **71** seems to increase the cytotoxic effect. The percentage of cytotoxicity of tetra and hexadecavalent **81** and **82**, tested as negative control, resulted <10% at both concentrations and with/without HS, confirming that the ARM cytotoxic effect is due to the rhamnose in the ABM.

- **Test 2: % cytotoxic rate evaluation of ARMs with different architectures but the same valency**

We assessed the cytotoxic effect of ARMs presenting different architectures (**72-75**) and displaying the same number of Rha epitopes. All ARMs have been tested with M21 cell line under the conditions described above (Figure 75).

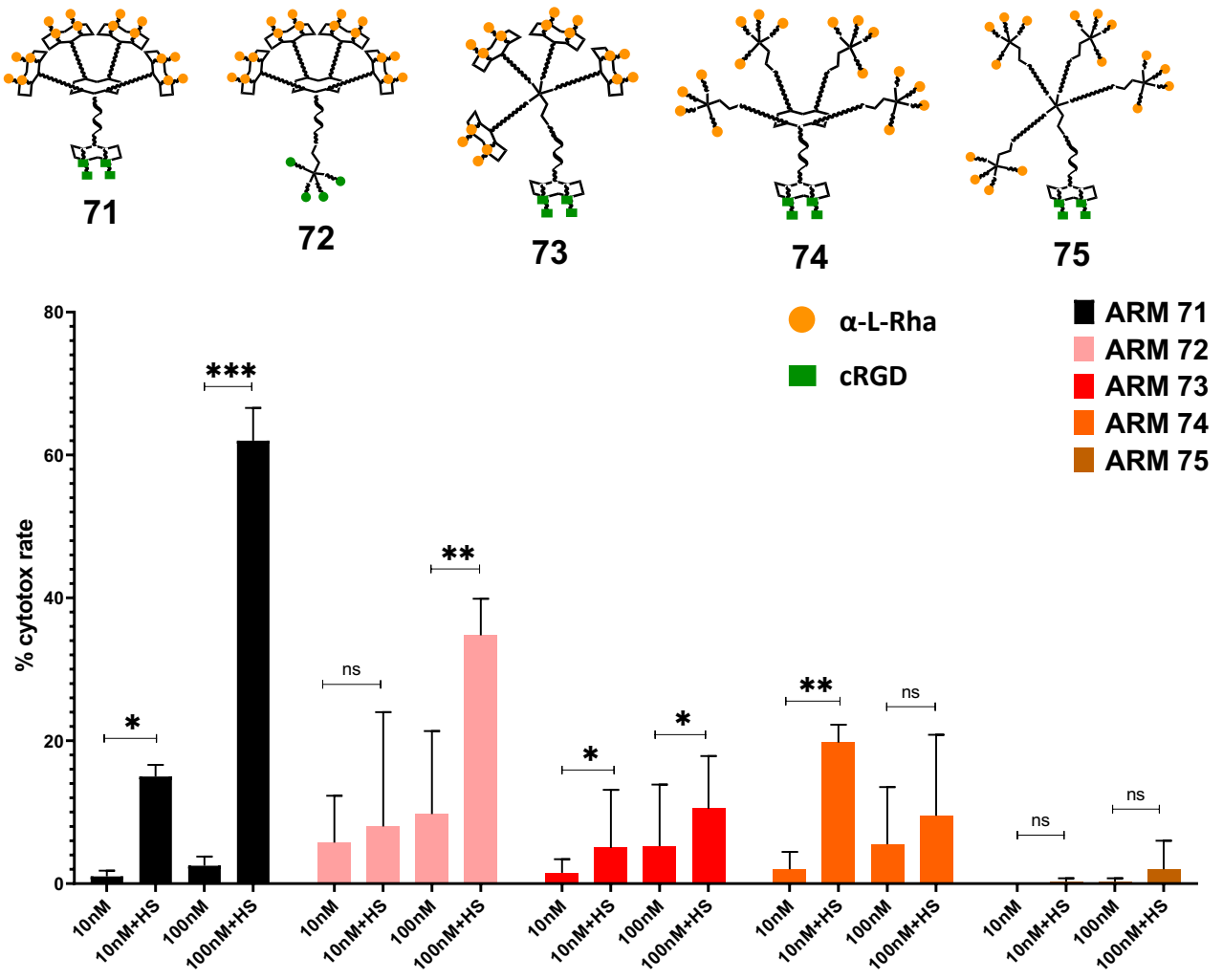

Figure 75 *Comparison of cytotoxicity. Experiments are done on M21 tumor cell line. Data points represent mean values of at least 4 experiments. Error bars represent 95% confidence intervals. T-test comparisons at 95% confidence were performed using GraphPad Prism 8.0 (not significant or ns: $p < 1$, *: $p < 0.1$, **: $p < 0.01$, ***: $p < 0.001$).*

As shown in Figure **75**, 10 nM and 100 nM ARMs without HS have a negligible cytotoxic effect. In presence of HS, an extremely weak cytotoxicity (% cytotoxic rate: 19%) was observed for 10 nM ARMs **74** (RD-R) while no cytotoxicity appears for the other compounds.

As for FACS experiments, the results have been analysed by comparing molecules which differ by one structural parameter. ARM **71**, presenting 4 cRGD with a RAFT platform, resulted in a higher % cytotoxic rate than ARM **72**, composed of the same ABM but presenting cRGD to the cell with a dendrimer platform (from 39% cytotoxic rate of ARM **72** to 60% cytotoxic rate of ARM **71**). As observed by FACS, this result indicates that cRGD are better presented to the $\alpha_V\beta_3$ integrins in ARM **71** than with the more flexible dendrimeric TBM found in ARM **72**.

Regarding the ABM part, comparison between ARM **74** and **71** showed an important increase of the ability to mediate an immune response when the peripheric layer varies from dendrimer to RAFT architecture (from 19% cytotoxic rate of ARM 74 to 60% cytotoxic rate of ARM **71**). The same observation can be done for the ARMs **75** and **73**: both possess the dendrimer "core" but varying the peripheric layer from dendrimer to RAFT, which results in an higher cytotoxic value (from 2% cytotoxic rate of ARM **75** to 10% cytotoxic rate of ARM **73**).

On the other hand, the influence of the "core" structure is clearly visible with, ARM **73** and **71** or ARM **75** and **74**. Both couples showed that the cytotoxic rate increases when the "core" varies from dendrimer to RAFT architecture (from 12% cytotoxic rate of ARM **73** to 60% cytotoxic rate of ARM **71** and from 2% cytotoxic rate of ARM **75** to 19% cytotoxic rate of ARM **74**).

Therefore, both the "core" and the peripheric architecture resulted once again key parameters not only to recruit antibody but also to mediate an immune response. To this aim, the RAFT platform has proved to be more suitable architecture than the flexible dendrimer platform.

- **Test 3: % cytotoxic rate evaluation of ARMs with different linker**

Next, we assessed the cytotoxic effect of ARM **76** (R-R PEG) and ARM **77** (RR-R PEG) presenting a PEG-triazole linker between ABM and TBM, in comparison with ARM **70** and **71**, presenting only a triazole linker. Once again, all ARMs tested with M21 cell line are tested in the same conditions (Figure 76).

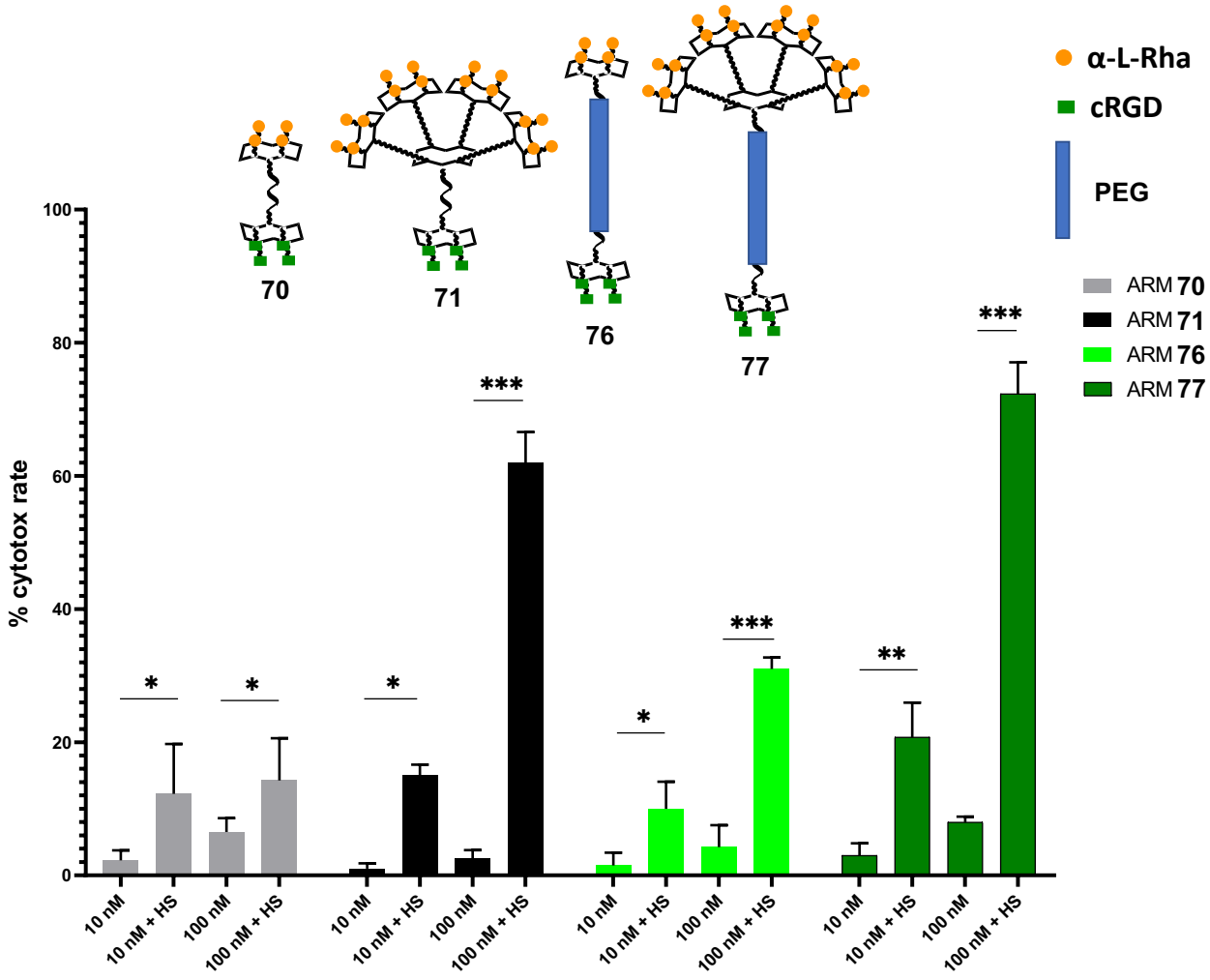

Figure 76 *Comparison of cytotoxicity regarding ARMs with different linkers. Experiments are done on M21 tumor cell line. Data points represent mean values of at least 4 experiments. Error bars represent 95% confidence intervals. T-test comparisons at 95% confidence were performed using GraphPad Prism 8.0 (not significant or ns: $p < 1$, *: $p < 0.1$, **: $p < 0.01$, ***: $p < 0.001$).*

As it can be seen from Figure 76, both ARMs **76** and **77** are no cytotoxic without HS and weakly active at 10 nM in presence of HS. Comparing the two tetravalent ARMs **70** and **76** at 100 nM and in presence of HS, it can observe a moderate gain of cytotoxicity when the linker is present (the % cytotoxic rate varies from 18% of ARM **70** to 35% of ARM **76**). Similar trend was found comparing the two hexadecavalent ARMs **77** and **71** (with and without PEG, respectively). ARM **77**, achieving a 72% of cytotoxic rate, seems to be more cytotoxic than the reference ARM **71** (60% of cytotoxic rate). The result regarding these two latter molecules confirms what was observed by FACS: ARM **77** containing a longer linker than a simple triazole of ARM **71** is probably more inclined toward recruiting antibodies, forming a ternary complex and achieving a greater % cytotoxic rate. In contrast to the results by the group of James C. Paulson,[52] we

observed that longer linkers can probably increase even more this cytotoxic effect by increasing the access of both ABM and TBM for antibodies and tumor markers. However, this observation could probably not be considered as a general rule for the design of the next generation of ARMs.

We next decided to perform the same assay with human serum from several donors (provided by the EFS at Grenoble) in order to evaluate whether this ARM **77** could be active for different serum composition (Figure 76).

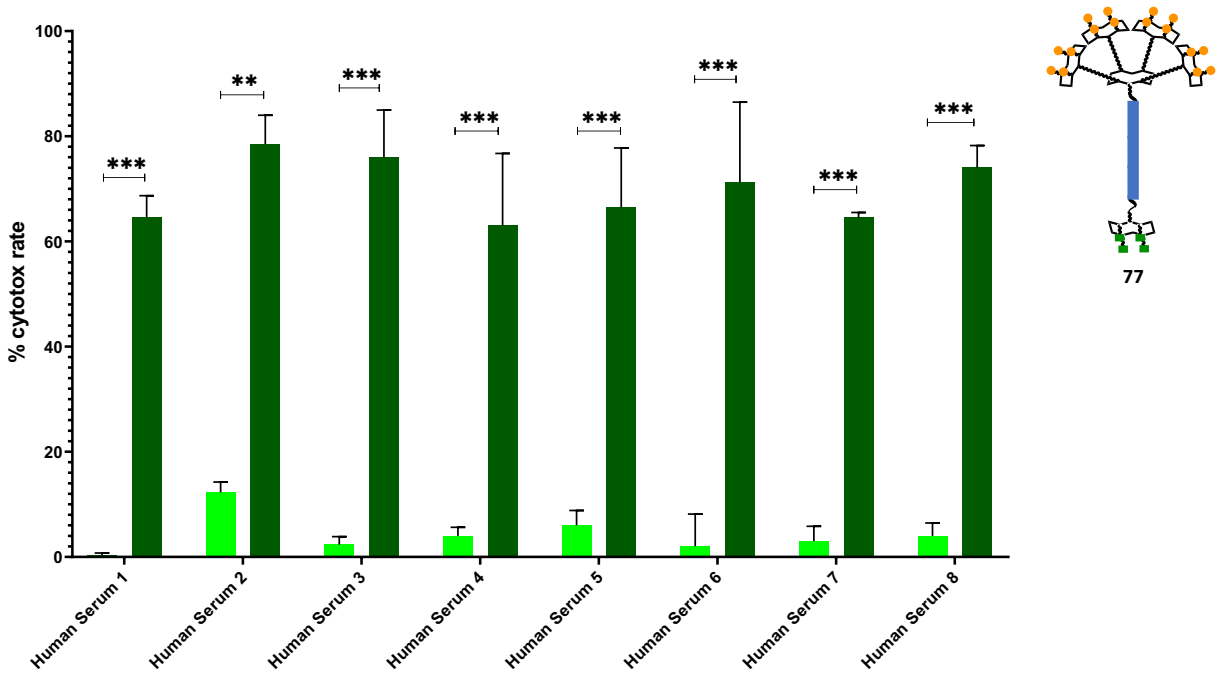

Figure 76 *Comparison of ARM 77 cytotoxicity values on M21 cell line from different Human Serum; control (without Human Serum) in light green, treated (with Human Serum) in dark green. Data points represent mean values of at least 4 experiments. Error bars represent 95% confidence intervals. T-test comparisons at 95% confidence were performed using GraphPad Prism 8.0 (not significant or ns: $p < 1$, *: $p < 0.1$, **: $p < 0.01$, ***: $p < 0.001$).*

Interestingly, significant cytotoxic percentage ranging from 63% (HS 4) to 78.5% (HS 2) was observed with different serum. While percentage variability (probably due to different amount of IgM) is observed, this experiment confirms that ARM **77** can be active for different donor without pre-immunization.

- **Test 4: % cytotoxic rate evaluation of ARMs on different cell lines**

The Rha-cRGD ARM family was tested on different cell lines following the same procedure. In addition to M21, HeLa and MCF_7 cell lines have been employed (Figure 78).

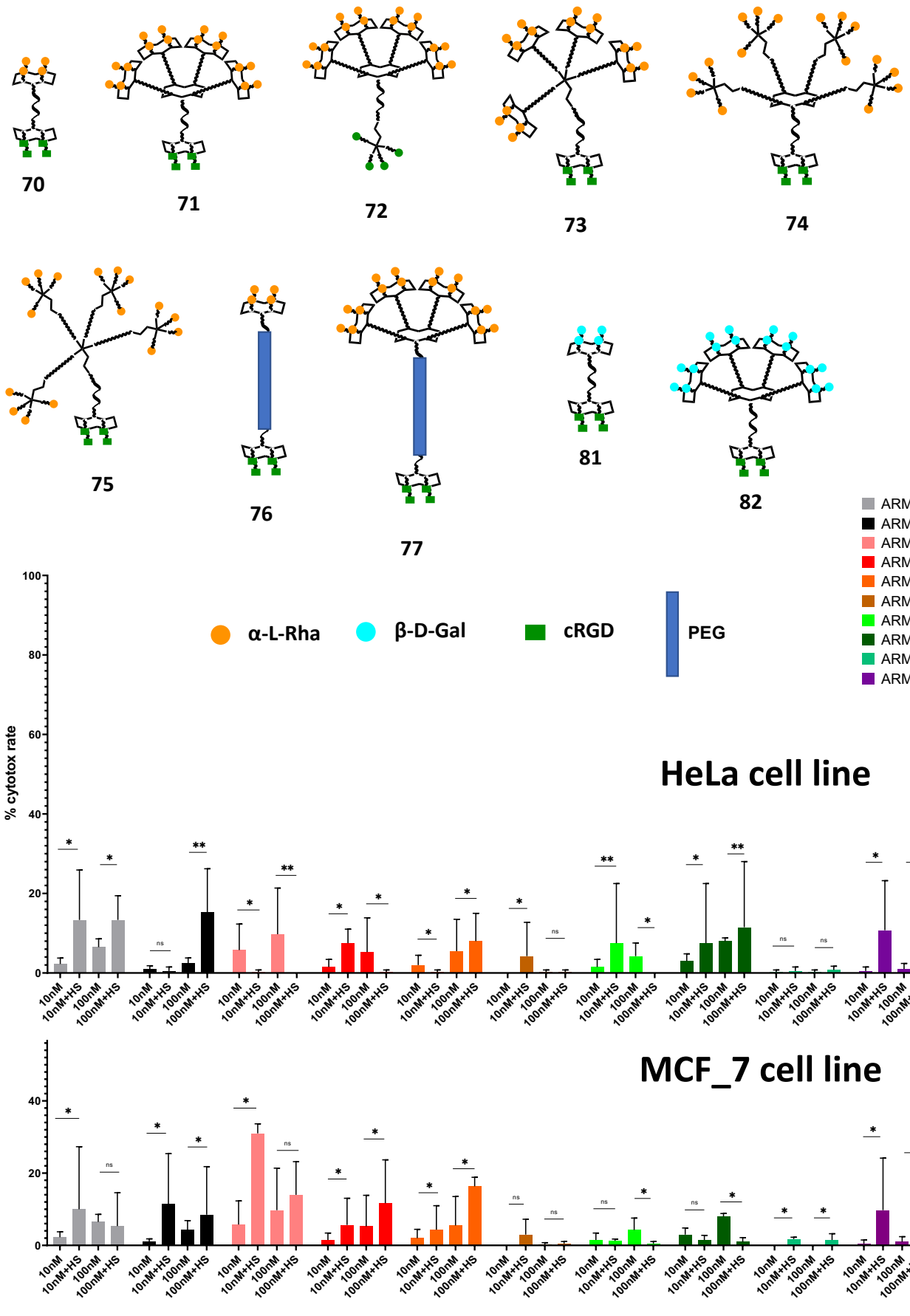
70
71
72
73
74
75
76
77
81
82
α-L-Rha
β-D-Gal
cRGD
PEG
ARM 70
ARM 71
ARM 72
ARM 73
ARM 74
ARM 75
ARM 76
ARM 77
ARM 81
ARM 82
% cytotox rate
HeLa cell line
MCF_7 cell line
10nM
10nM+HS
100nM
100nM+HS

Figure 78 *Comparison of ARMs cytotoxicity for HeLa and MCF_7 tumor cell lines. Data points represent mean values of at least 4 experiments. Error bars represent 95% confidence intervals. T-test comparisons at 95% confidence were performed using GraphPad Prism 8.0 (not significant or ns: $p < 1$, *: $p < 0.1$, **: $p < 0.01$, ***: $p < 0.001$).*

First of all, ARMs induce low cytotoxicity with HeLa cell line. While $\alpha_v\beta_3$ integrins are reported to be overexpressed in those cells,[216,217] additional FACS assays would be essential to determine the amount of $\alpha_v\beta_3$ integrins on these cells and to explain the low but different biological effect observed here. Similarly, no cytotoxicity was observed with MCF_7 cell line, except for ARM **72** at 10 nM in presence of HS that showed 30% of cytotoxicity rate. By contrast with the result obtained with M21 cell line (i.e. 39% for ARM **72** and 60% for ARM **71** (Figure 75), the cytotoxic value of ARM **72** seems higher (30%), probably because the 4 cRGD epitopes presented by the dendrimer TBM (in ARM **72**) interact better with the MCF_7 cells than when presented in ARM **71**. This result might be explained by the higher ability of a dendrimeric than cyclopeptide TBM to promote $\alpha_v\beta_3$ integrins clustering on MCF_7. However, additional experiments by FACS and confocal microscopy would be necessary to confirm this hypothesis.

III.5.C Cytotoxicity results of the cRGD ARMs varying by the ABM

In this section, the cytotoxicity of ARMs with cRGD as TBM and in which ABM is based on clusters of 16 copies of other carbohydrates than Rha is evaluated with the approach described previously. More precisely, the cytotoxicity of ARM **83** (16 copies of α-D-Gal) and **84** (16 copies of α-D-Neu5Gc) was assessed comparing to ARM **71**. Once again, the ARM cytotoxic values are investigated on M21, MCF-7 and HeLa cell lines (Figure 79).

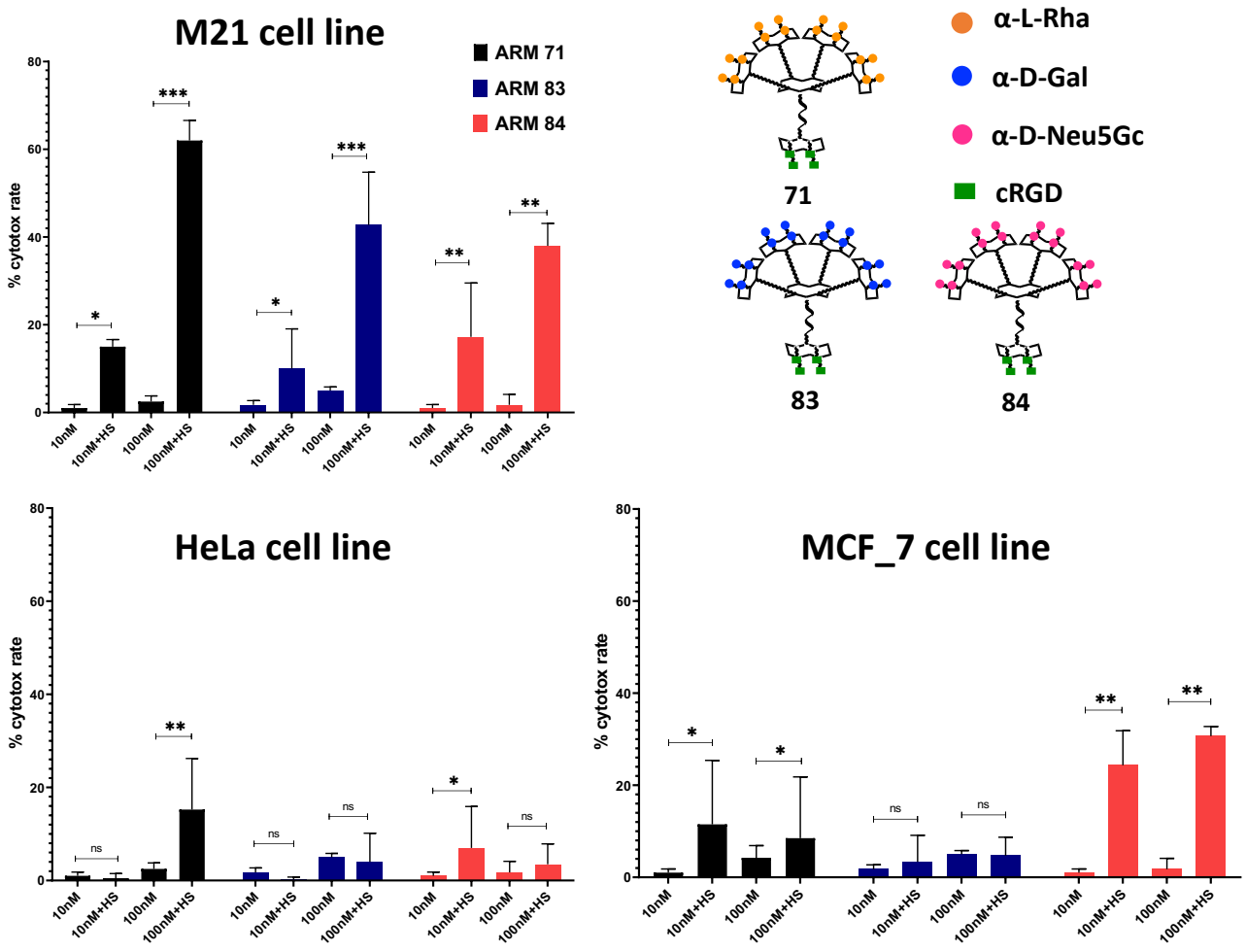

Figure 79 *Comparison of Rha – cRGD (ARM **71**), α-Gal – cRGD (ARM **83**) and α-D-Neu5Gc – cRGD (ARM **84**) cytotoxicity from M21, HeLa and MCF_7 tumor cell lines; for each ARMs there were reported 10nM, 10nM+HS, 100nM, 100nM+HS cytotoxic values. Data points represent mean values of at least 4 experiments. Error bars represent 95% confidence intervals. T-test comparisons at 95% confidence were performed using GraphPad Prism 8.0 (not significant or ns: $p < 1$, *: $p < 0.1$, **: $p < 0.01$, ***: $p < 0.001$).*

On M21 cell line, a maximum 20% of cytotoxic effect for ARMs at 10 nM whatever its structure. Conversely, ARM **83** and **84** at 100 nM induced about 40% of cytotoxic rate on M21 cells while ARM **71** results in 60% of cytotoxicity. These effects are lower when the same ARMs are

tested with HeLa or with MCF_7, except for ARM **84** which showed % cytotoxic rate of about 25% at 10 nM and 34% at 100 nM), i.e. higher than the reference ARM **71**, with MCF_7. This could be due to a more favourable presentation of ABM in ARM **84** than in ARM **71** upon binding with the MCF_7. It's worth noting that no FACS data are reported for the α-D-Gal and Neu5Gc ARM families but a FACS analysis would be necessary to confirm these results.

III.5.D. Cytotoxicity results of the cRGD ARMs varying by the TBM

In this last section, cytotoxic assays with ARMs presenting Rha but with other TBM than cRGD peptide were investigated. In particular the TBM chosen in this work was LT and HVH peptides, targeting EGFR overexpressing cells, and β-D-Glucose, targeting GLUT-1 overexpressing cells. All ARMs were tested on M21, HeLa and MCF_7 cell lines.

- **% cytotoxic rate evaluation of α-L-Rha – LT ARM family**

As already described on chapter II, our Rha – LT family is composed by three ARM molecules. That final molecules should be able to recruit anti α-L-Rha antibodies from HS and hijack them selectively against that cells. Here the % cytotoxic rates of ARM **85** and **86** (1 copy of LT) and **87** (4 copies of LT) are compared to that of ARM **70** and **71** (Figure 80).

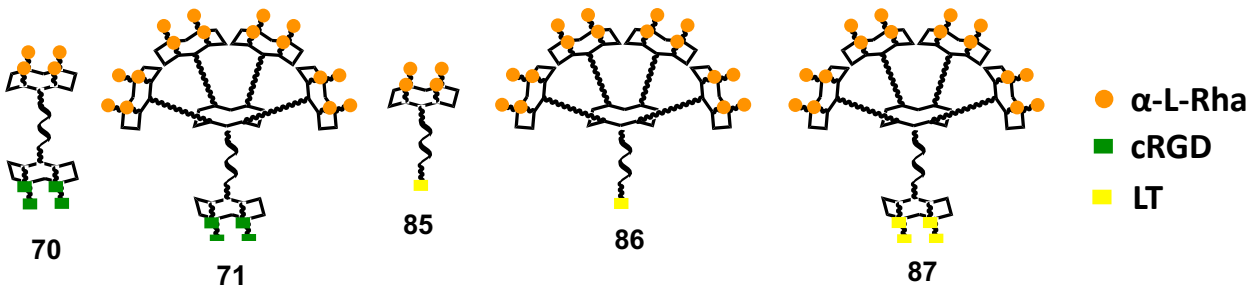

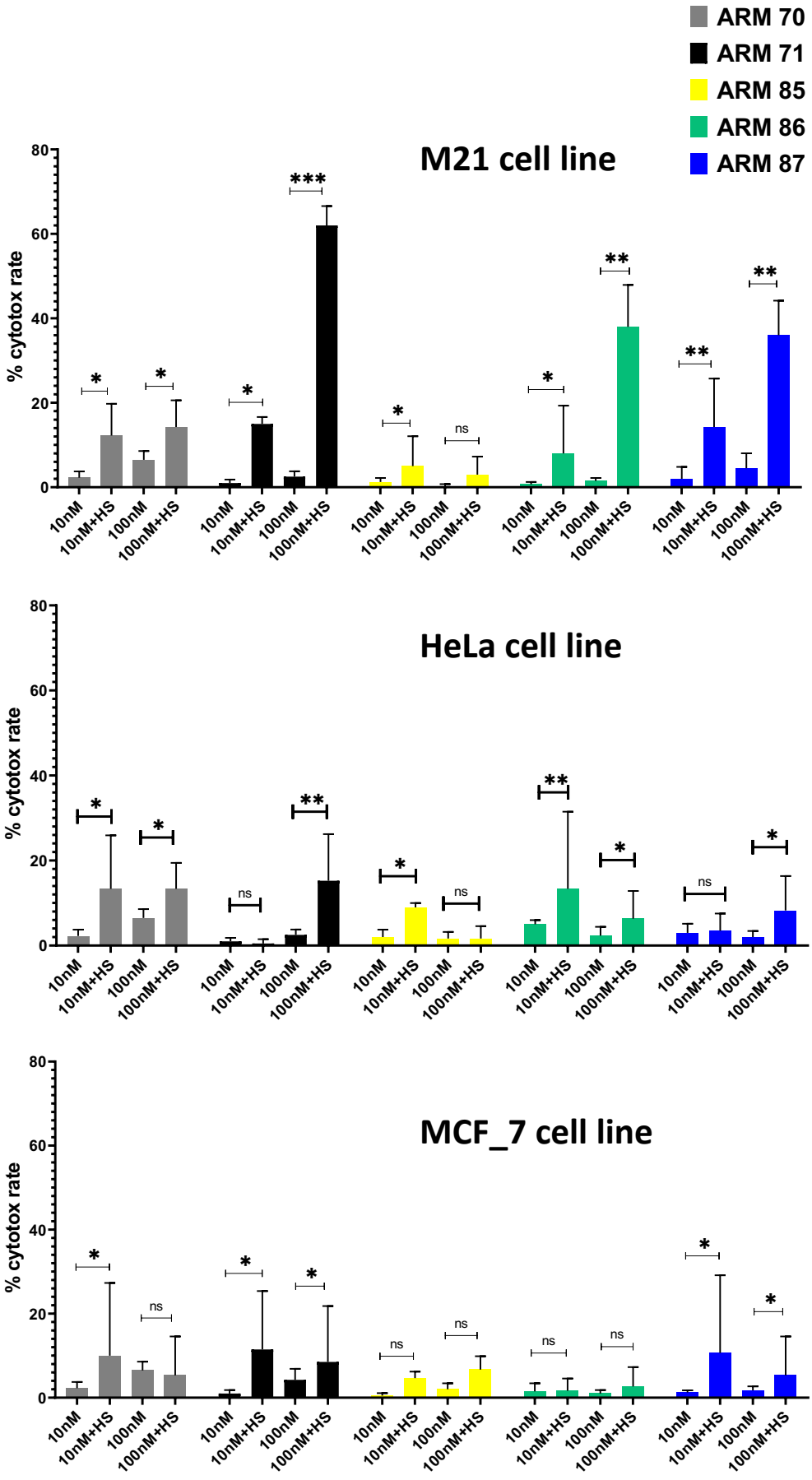
ARM 70
ARM 71
ARM 85
ARM 86
ARM 87
M21 cell line
HeLa cell line
MCF_7 cell line
% cytotox rate
0
20
40
60
80
10nM
10nM+HS
100nM
100nM+HS
*
**
***
ns

Figure 80 *Comparison of Rha - LT and Rha – cRGD ARMs cytotoxicity rates from M21, HeLa and MCF_7 tumor cell lines; for each ARMs there were reported 10nM, 10nM+HS, 100nM, 100nM+HS cytotoxic values. Data points represent mean values of at least 4 experiments. Error bars represent 95% confidence intervals. T-test comparisons at 95% confidence were performed using GraphPad Prism 8.0 (not significant or ns: $p < 1$, *: $p < 0.1$, **: $p < 0.01$, ***: $p < 0.001$).*

For all cell lines, ARMs exhibit less than 10% of toxic effect without HS. Next, we observed the absence of cytotoxicity on HeLa and MCF_7 with all ARMs even at the higher concentration (100 nM) in presence of human serum. Conversely, different % of cytotoxic rate is observed on M21 cell line with 100 nM ARMs. The multivalent effect between ARM **85** and **86** is significant since there is an important rising of cytotoxic rate (from 5 to 40%) probably due to a higher recruitment of antibodies. By contrast, the multimerization of LT peptide does not influence the cytotoxicity since ARM **86** (1 LT peptide moiety) and ARM **87** (4 LT peptide moieties) have in fact the same % cytotoxic rate. It can be assumed that our conjugate does not present suitable structure in term of flexibility, valency and/or size to promote EGFR clustering at the cell membrane surface.[218]

- **% cytotoxic rate evaluation of α-L-Rha – β-D-Glc ARM family**

As already described on chapter II, our α-L-Rha – β-D-Glc ARM family is composed by three molecules targeting GLUT-1 overexpressing cells through β-D-Glc. Here the % cytotoxic rates of ARM **88** (1 copy of β-D-Glc), **89** and **90** (4 copies of β-D-Glc) are compared to that of ARM **70** and **71** (Figure 81).

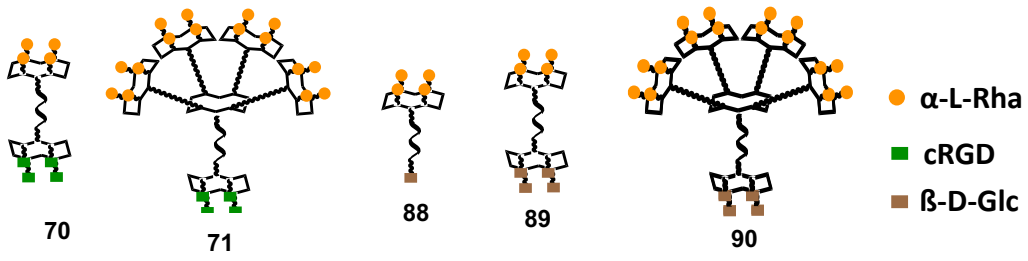

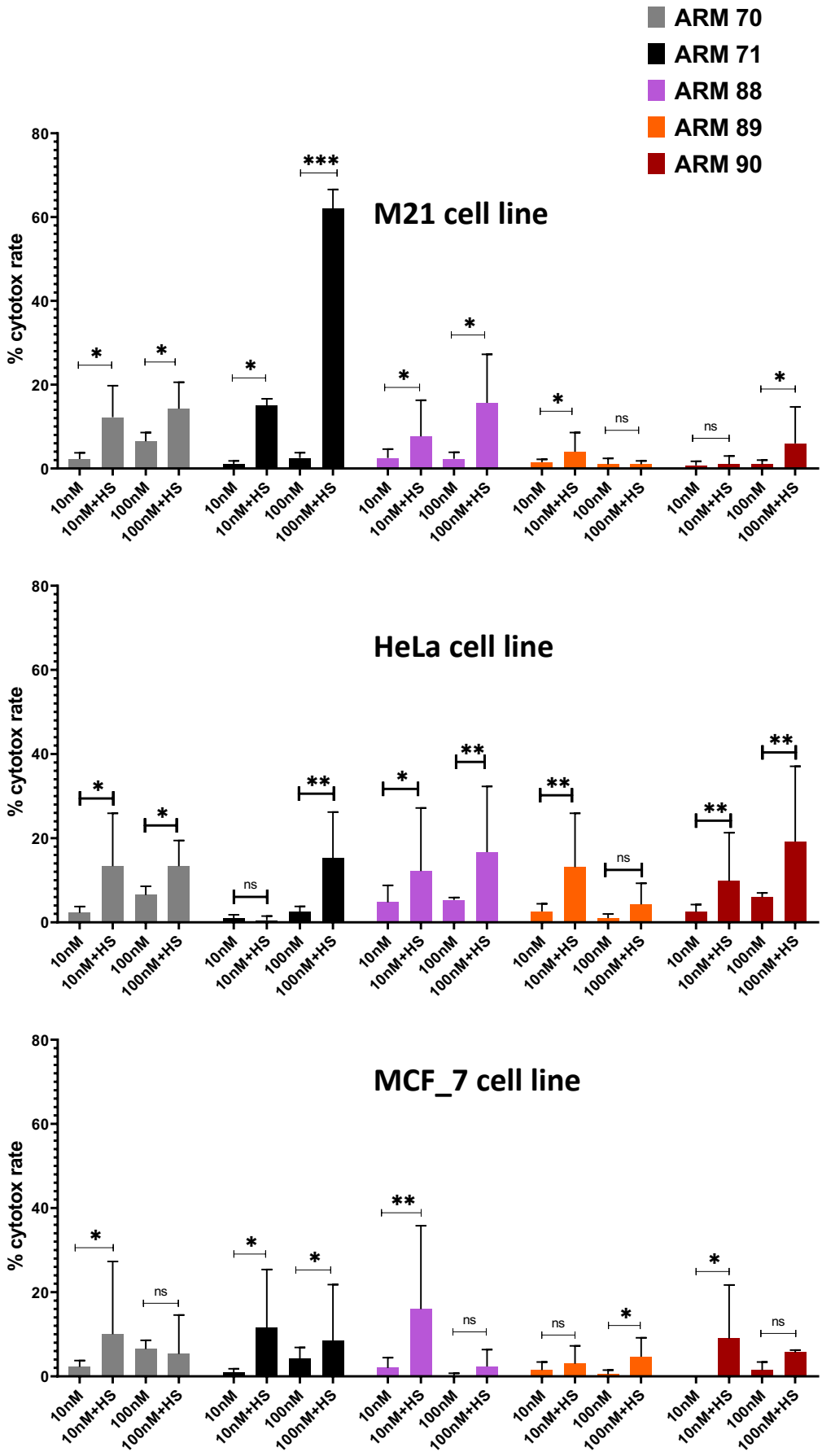
ARM 70
ARM 71
ARM 88
ARM 89
ARM 90
M21 cell line
HeLa cell line
MCF_7 cell line
% cytotox rate
0
20
40
60
80
10nM
10nM+HS
100nM
100nM+HS
*
**
***
ns

Figure 81 *Comparison of Rha - ß-D-Glc and Rha – cRGD ARMs cytotoxicity rates from M21, HeLa and MCF_7 tumor cell lines; for each ARMs there were reported 10nM, 10nM+HS, 100nM, 100nM+HS cytotoxic values. Data points represent mean values of at least 4 experiments. Error bars represent 95% confidence intervals. T-test comparisons at 95% confidence were performed using GraphPad Prism 8.0 (not significant or ns: p < 1, *: p < 0.1, **: p < 0.01, ***: p < 0.001).*

From Figure 81, there is low evidence of cellular death when ARMs **88**-**90** are incubated with M21 and MCF_7 cell lines. However, we can observe some very weak cytotoxic effect when 100 nM ARMs **88** and **90** are incubated with HeLa cell line. Beside structural consideration mentioned above (i.e. valency, flexibility of the scaffold etc), we hypothesized that changing the sugar unit with a C-6 functionalized glucose instead of the C-1 as found in ARM **88**-**90** could strongly improve the binding with GLUT-1.[219, 220]

- **% cytotoxic rate evaluation of α-L-Rha – HVH ARM family**

As already described on chapter II, our Rha – HVH ARM family is composed by three molecules targeting EGFR overexpressing cells through HVH peptide. Here the % cytotoxic rates of ARM **91** and **92** (1 copy of HVH) are compared to that of ARM **70** and **71** (Figure 82).

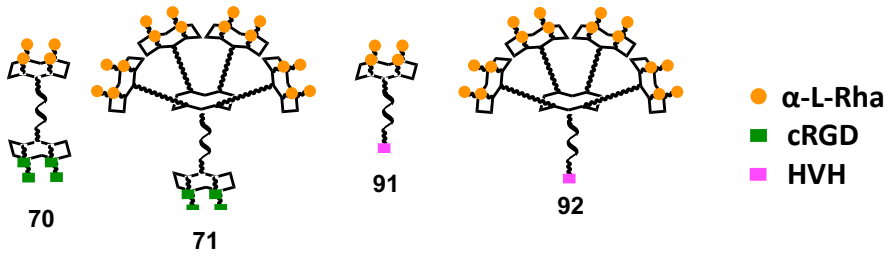

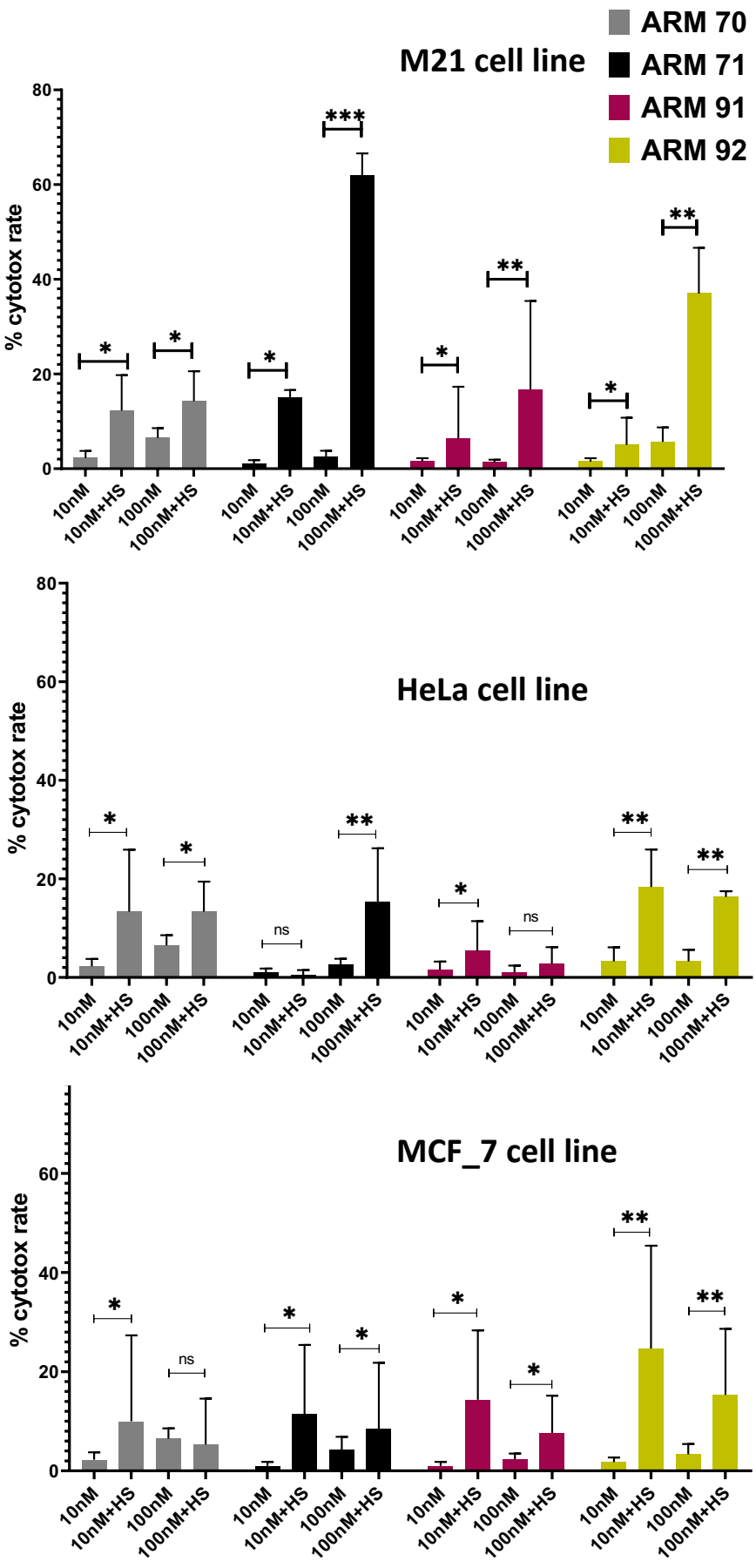
M21 cell line
ARM 70
ARM 71
ARM 91
ARM 92
% cytotox rate
HeLa cell line
MCF_7 cell line
10nM
10nM+HS
100nM
100nM+HS
ns

Figure 82 *Comparison of Rha - HVH and Rha – cRGD ARMs cytotoxicity rates from M21, HeLa and MCF_7 tumor cell lines; for each ARMs there were reported 10nM, 10nM+HS, 100nM, 100nM+HS cytotoxic values. Data points represent mean values of at least 4 experiments. Error bars represent 95% confidence intervals. T-test comparisons at 95% confidence were performed using GraphPad Prism 8.0 (not significant or ns: p < 1, *: p < 0.1, **: p < 0.01, ***: p < 0.001).*

As it can be observed in Figure 80, HVH – ARMs showed interesting cytotoxic trend only with M21. Firstly, all ARMs didn't show any cytotoxic effect without HS or at 10 nM in presence of HS. Next, ARM **91** (displaying 4 copies of Rha such as ARM **70**) was not able to recruit enough antibodies to exhibit a significant cytotoxic response (cytotoxic rate < 20%) at both concentrations. Conversely, ARM **92** (displaying 16 Rha epitopes) at 100 nM showed significant cytotoxic effect (cytotoxic rate: 38%). Even if this value is lower than that of the hexadecavalent ARM **71**, it's worth noting that ARM **92** display only one copy of HVH peptide. Thus, we can hypothesized e that an increase of this TBM valence may likely result in higher cytotoxic rate. For this reason, ARM **93** is already synthesized and the cytotoxic tests are ongoing in our laboratory.

III.6. Conclusions of Chapter III

After the observation of the previous results obtained in our group, all our Rha – cRGD ARM conjugates were tested by FACS in order to evaluate their ability to form a ternary complex with cell and antibodies from human serum. The formation of this ternary complex is the prerequisite to promote the subsequent immune response to the target cell. In addition, confocal microscopy experiments were performed to visualize the localization of this ternary complex at the cell surface. This is indeed essential to confirm the absence of internalization of ARM since this phenomenon would prevent the stimulation of the immune mediated clearance of the target cell. We have demonstrated the influence of 1) the "core" and the peripheric architecture, 2) the valency and 3) the linker length to form the ternary complex.

Subsequent cytotoxic assay was perform to confirm that the ability to form ternary complex lead to cytotoxicity. We firstly confirmed that the cell toxicity occurs only in presence of ARM and serum. Next, even if all ARMs (except ARM **76**) were able to recruit antibodies towards M21, we discovered that only few ARMs induced high cytotoxicity (60% and 72% for ARMs **71** and **77**, respectively). These two similar molecules are composed by the same architecture (RAFT), have the same valency for ABM (16 Rha epitopes) as well as for TBM (4 cRGD epitopes) but differ from their linker. In addition, performing the same assay with human serum from several donors, we demonstrated that ARM **77** resulted active with all, suggesting its potential efficiency for a large population of patients.

ARM family with different ABM epitopes (α-D-Gal and Neu5Gc carbohydrates) were evaluated. A moderate cytotoxic effect was found only for α-D-Gal ARM **83** at 100 nM on M21 cell line and for Neu5Gc ARM **84** at 100 nM on M21 and MCF_7 cell lines. Next, ARM family with different TBM epitopes (β-D-Glc carbohydrate and LT and HVH peptides) did not show significant cytotoxic effects except for a modest cytotoxic effects for ARM **86**, **87** at 100 nM on M21. This could be attributed to structural parameters such as flexibility, valency and size of TBM task that do not allow multivalent interactions with the targeted receptors. Concerning HVH peptide bearing ARMs, some encouraging results have been showed and additional experiments will be performed.

Chapter IV.

Conclusions and future outlooks

My work was conducted at the Département de Chimie Moléculaire, under the supervision of Prof. Olivier Renaudet and supported by Dr. Nathalie Berthet, Dr. David Goyard, Claire Tiertant and Dr. Silvia Achilli. The objective to develop bifunctional molecules (ARMs) that can recruit endogenous antibodies and trigger an immune response against cancer cells.

For this purpose, we first synthesized 4- and 16-valent structures to target endogenous antibodies (ABM part). Several carbohydrates, such as α-L-Rhamnose or α-D-Galactose have been synthesized as ligands and presented as clusters on either cyclopeptide and/or polylysine-dendron. Previous ELISA-type assay have indeed shown that multimeric presentation of α-L-Rhamnose ensures more efficient binding with IgM due to the glycoside cluster effect. Next, we focused on the synthesis of several well-known peptides ligands, such as cRGD, LT and other peptides discovered by phage display in our group (TBM part). The peptides (mono- and tetra-valent structures to evaluate the importance of a multivalent display) were labeled with Fluorescein and studied by flow cytometry against cancer cells. This study allowed the selection of a few peptides as TBM.

After having confirmed the recognition potency of ABMs and TBMs, we next combined them covalently to provide different ARMs. A total of 24 structures were synthetized and characterized by analytical HPLC, HRMS as well as ^{1}H-NMR. Different structural parameters were varied, such as the valency (presence of 1, 4 or 16 copies of carbohydrates and 1 or 4 copies of peptides), the length of the linker between ABM and TBM, and the flexibility (combination of different scaffolds) of the final molecules. The copper-catalyzed alkyne-azide cycloaddition (CuAAC) was chosen as the general synthetic strategy for the assembly because its efficiency, versatility and robustness. It requires a limited set of easily accessible building blocks and the resulting triazole linkage is generally well-tolerated and stable *in vivo*.

The last part of my PhD was dedicated to biological assays. We have evaluated the ability of ARMs 1) to form a ternary complex with the cancer cell over-expressing the target protein and the natural endogenous antibodies and 2) to mediate the subsequent immune destruction of that cancer cells. To demonstrate the ternary complex formation, each ARM was incubated with the selected cells in the presence of human serum as unique source of antibodies and adding a fluorescent secondary anti-IgM antibody to be detected by FACS. It's worth noting that the ARM concentration is a critical parameter to consider. ARM at high concentration may simultaneously saturate both antibodies and tumor surface proteins and unbound material may compete with the ternary complex. Once optimal concentration has been determined (100 nM), we observed that the antibodies recruiting ability is dependent on the rigidity and valency of the molecules. Cell viability assays were next performed to measure the immune-mediated cytotoxicity against M21, HeLa and MCF_7 cell lines. We thus identified the best ARM for each cell line:

- ARM **77** (Figure 83 A) at 100 nM triggered a high immune response on $\alpha_v\beta_3$-positive M21 cell line (cytotoxic value: 72%);
- ARM **90** (Figure 83 B) at 100 nM triggered the higher immune response on GLUT-1-positive HeLa cell line (cytotoxic value: 20%);
- ARM **84** (Figure 83 C) at 100 nM triggered the higher immune response on EGFR-positive MCF_7 cell line (cytotoxic value: 34%).

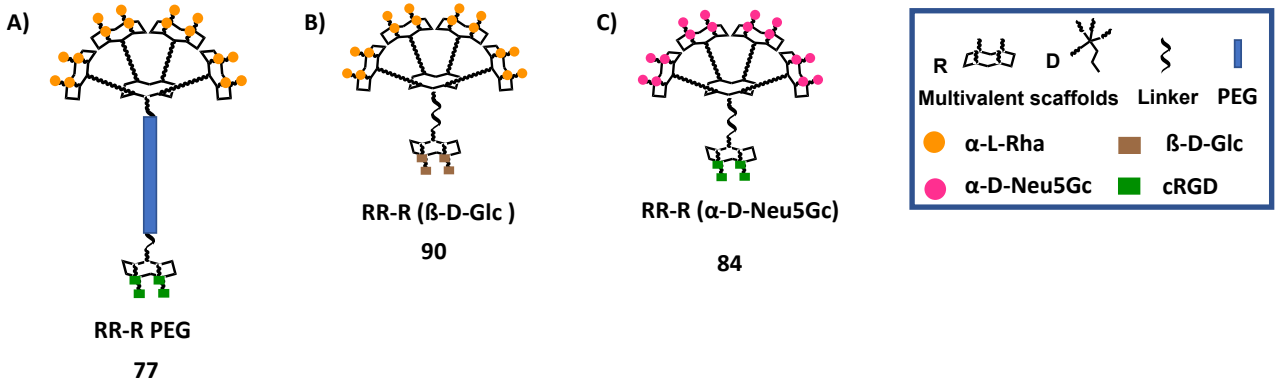

Figure 83 *Best ARMs candidate in this Ph.D. work.*

These three ARMs share the same architectures and the same valency since each of them display 16 copies of carbohydrates epitopes on RAFT platforms as ABM and 4 copies of peptides or carbohydrates epitopes on RAFT platforms as TBM. Special mention should be done for the PEG linker that probably improve the access of both ABM and TBM for antibodies and tumor markers, thus leading to a higher cytotoxic value (72%) in comparison to the that one of ARM **71** (60%). Thus, we can consider ARM **77** as a lead compound for subsequent test *in vivo*, as compared with results obtained by Kiessling ARM cytotoxic value of 60% (Figure 11 A) or by Spiegel ARMs cytotoxic value of 50-55% with ARM-P8 or ARM-U2 (Figure 13 B and 15). Conversely, regarding ARM **90** and **84**, it has clearly been demonstrated that the clusterization of the TBM ligand improve the cytotoxic rate. Structural modification of these conjugates regarding their flexibility, valency and size could allow multivalent interaction with their receptor. At the end of this thesis work, it's possible to consider certain future short-term and long-term outlooks in order to optimize the efficacy of ARMs.

Future short-term outlooks

- Additional FACS analysis seems essential to confirm the antibodies recruitment ability of Rha – X (ARMs **81** – **84**) and with Y – cRGD ARMs (ARMs **85** – **92**). In addition, FACS analysis and cytotoxic assays have to be carry out with the new conjugate **93**.
- Due the unusual result of ARM **72** (the unique ARM displaying 4 cRGD peptides by dendrimer rather than by a RAFT platform) on MCF_7, it is necessary to verify if the same result occurs by FACS and to study the $\alpha_v\beta_3$ integrins expression on the MCF_7 cellular membrane. It will be also interesting to synthetize new "polylysine – cRGD" TBMs in order to assess their cytotoxic values when incubated with MCF_7 cells.
- Since the cytotoxicity results of ARM **90** and **84** were the most successful ones on HeLa and MCF_7 respectively, it should be interesting to insert a longer linker (i.e. PEG linker) to evaluate the influence on the cytotoxicity rates.
- *In vivo* biological tests have to be performed on ARM **77** in order to identify the ARM efficacy and stability, the side effects and assess the several cytotoxic mechanisms that could lead to the immune mediated clearance on mice.

We have already demonstrated that passing from the tetravalent to the hexadecavalent structures and from the insertion of a PEG-triazole linker helps the recognition and improve the "killing" ability. Since the multivalence effect plays an important role in antibodies recruitment and in promotion receptor clustering at the cell membrane surface, it can therefore be supposed that the ARM efficacy could be increased by some structural modifications, such as enhancing the saccharide/peptide antigens density (Figure 84 A) as well as investigation other linkers (Figure 84 B), such as PEG_4 or PEG_8 or β-Ala. This latter have the advantage to be lot cheaper and more rigid than PEG. It's worth noting that the efficiency of our click-based synthetic strategy will allow to explore a large variety of TBM and ABM combination and identify the best ARM structure.

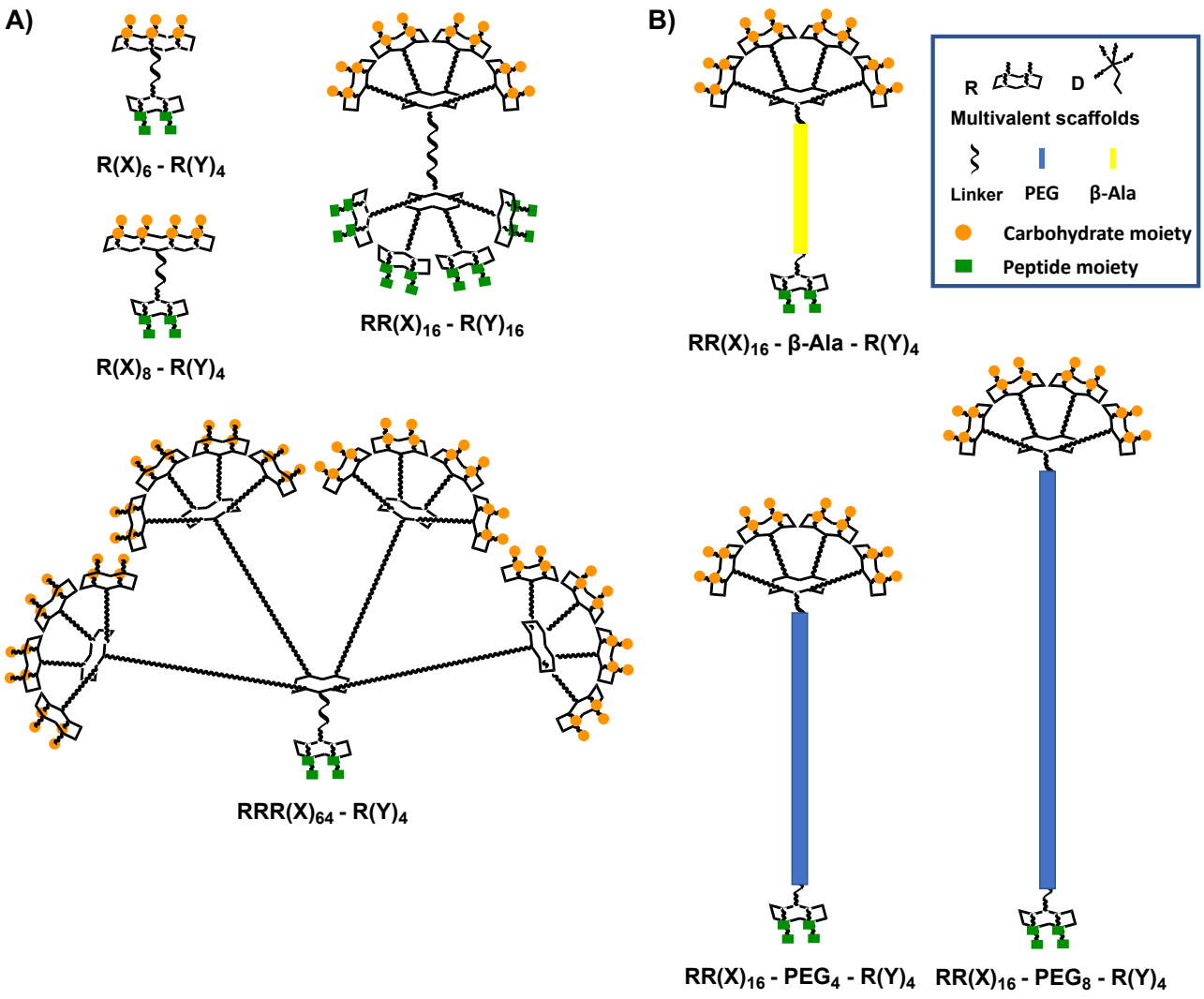

Figure 84 *Some structural modification about* ***A)*** *ABM and/or TBM platform valency,* ***B)*** *linker between ABM and/or TBM.*

Future long-term outlooks

- The synthesis of heteroglycoclusters as ABM would allow specific interactions with different natural antibodies and thus provide a higher efficiency in antibody recruitment (Figure 85 A). In addition, the identification of new tumor-associated markers can be of great impact for the conception of new generations of TBMs, in particular displaying ligands for different tumor markers. Since the phenotype of cancer cells is in continue evolution, it may therefore be suitable to present several ligands simultaneously (Figure 85 B). Therefore, the hetero-ARMs development, combining hetero-ABMs or TBMs (Figure 85 C), could be a very attractive to go one step further the development of an antitumoral immunotherapeutic approach.

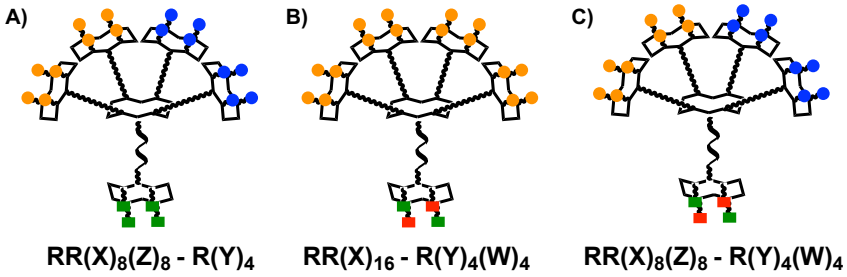

Figure 85 A) *ARM composed by an heteroglycocluster ABM,* ***B)*** *ARM composed by an heteropeptidocluster TBM,* ***C)*** *ARM composed by an heteroglycocluster ABM and an heteropeptidocluster TBM. X and Z are two different glycan epitopes, Y and W are two different peptide epitopes.*

- Since lots of proteins allow the internalization of the ligand, it should be interesting performed the synthesis of an azide-bearing antigen conjugated with a TBM moiety that selectively will interact with its corresponding overexpressed protein on cancer cells. This latter, once inside, will be then metabolized and carried on a surface protein. Here, the N_3 azido moiety should be able to react with the dibenzocyclooctyne ABM through SPAAC reaction, and then form a ternary complex (Figure 86).

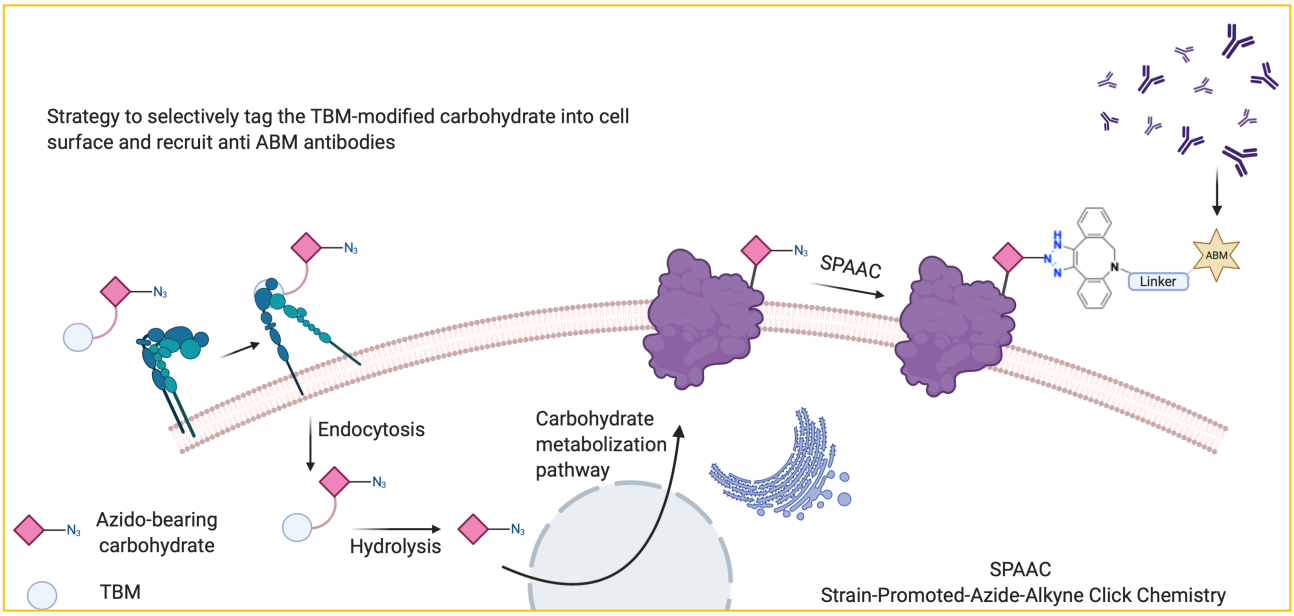

Figure 86 *New ARM strategy developed in order to avoid any risk of internalization of conjugate inside the cell membrane.*

Chapter V.

Materials and methods

V.1. Chemical synthesis

V.1.A. Products and reagents

All chemical reagents and solvents were purchased from Sigma–Aldrich (Saint Quentin Fallavier, France) or Acros (Noisy-Le-Grand, France) and were used without further purification. All protected amino acids, Fmoc-Gly-Sasrin resin and Rink amide resin were obtained from Advanced ChemTech Europe (Brussels, Belgium), Bachem Biochimie SARL (Voisins-Les-Bretonneux, France) and France Biochem S.A. (Meudon, France). PyBOP was purchased from France Biochem S.A. (Meudon, France). PEG were purchased from Iris Biotech GMBH (Marktredwitz, Deutschland).

V.1.B. Equipment

V.1.B.I. Analytical characterizations

For carbohydrates, the progress of reactions in organic solvents was monitored by thin layer chromatography using silica gel 60 F254 pre-coated plates (Merck). Spots were revealed with 10% H_2SO_4 in EtOH, with a para-anis-aldehyde reagent (solution of p-anis aldehyde, sulphuric acid and acetic acid in EtOH), with ninhydrin in EtOH or with a solution of $KMnO_4$. Silica gel 60 (0.063-0.2 mm or 70-230 mesh, Merck) was used for column chromatography.

^1H NMR spectra were recorded on BrukerAvance III 500 MHz spectrometer and chemical shifts (δ) were reported in parts per million (ppm). Spectra were referenced to the residual proton solvent peaks relative to the signal of $CDCl_3$ (δ 7.27 ppm), D_2O (δ 4.79 ppm).

ESI mass spectra were recorded by ICMG's mass platform service and were measured on an Esquire 3000 spectrometer from Bruker or on an Acquity UPLC-MS system from waters equipped with an SQ2 detector.

MALDI-TOF spectra were recorded by ICMG's mass platform service and were performed on an AutoFlex Speed Bruker after sample pre-treatment in an OligoR3 microcolumn (Applied Biosystems, USA) using 2,5-dihydroxybenzoic acid matrix (glycopeptides).

HRMS spectra were recorded by ICMG's mass platform service and were performed either on a Waters Xevo® G2-S QTof or on a Thermo Scientific MS-ESI/LTQ Orbitrap XL.

Analytical RP-HPLC was performed on a Waters alliance 2695 separation module, equipped with a Waters 2489 UV/visible detector. Analyses were carried out at 1.23 mL min^{-1} (Waters X-Bridge, C_{18}, 3.5 µm, 4.6 x 100mm) with UV monitoring at 214 nm and 250 nm using a linear A–B gradient (solvent A: 0.1% TFA in water; solvent B: 0.1% TFA in 90% acetonitrile – 10% water). The sample solutions were prepared in water, with an addition of acetonitrile or DMF if necessary.

Analytical RP-UPLC (coupled with ESI-MS) was performed on a Waters Acquity UPLC system. Analyses were carried out at 0.6 mL/min (Aeris^{TM}, C_{18}, 1.7 µm, 100 Å, 50x2.1 mm) with UV monitoring at 214 nm, using a linear C–D gradient (C: 0.1% CH_2O_2 in water; D: 0.1% CH_2O_2 in 90% acetonitrile – 10% water).

V.1.B.II. Purifications

Preparative RP-HPLC was performed on Gilson GX 281 equipped with a fraction collector, or on Waters equipment composed by a Waters 600 controller and a Waters 2487 Dual Absorbance Detector. Purifications were carried out at 22.0 mL·min^{-1} (Macherey-Nagel VP, C_{18}, 5 µm, 130 Å, 250x19 mm) with UV monitoring at 214 nm and 250 nm, using a linear C–D gradient (C: 0.1% CH_2O_2 in water; D: 0.1% CH_2O_2 in 90% acetonitrile – 10% water).

V.1.C. General synthesis methods and procedures

A) General procedure for solid-phase peptide synthesis (SPPS)

Assembly of all linear protected peptides was performed manually or automatically by solid-phase peptide synthesis (SPPS) using the standard 9-fluorenylmethoxycarbonyl/tert-butyl (Fmoc/^{t}Bu) protection strategy. Fmoc-Gly-Sasrin resin or Rink amide resin were chosen depending on the targeted peptide sequence. In manual SPPS, the device consisted in a 150 mL volume polypropylene syringe-shaped reactor (#5147808 Grace SA, USA), loadable up to 4 g of resin and equipped with a filter and a valve in the lower end, to removal solvent through filtration assisted by compressed air. A certain amount of Fmoc-protected resin, based on the quantity of willed final peptide, was weighed and then gently stirred thanks to an orbital laboratory agitator (IKA Vibrax VXR basic, USA), firstly with 10 mL·g^{-1} of DCM then with 10 mL·g^{-1} DMF, each for 10 min separately. After the swelling phase, in order to remove the -Fmoc protecting group, the resin was treated with a fresh 20% piperidine solution in DMF, two times for 10 min and one times for 5 min.

In order to know the real loading of the resin, the collected deprotection cocktail was transferred in a volumetric flask and the volume was adjusted with MeOH. Next, a little fraction of this solution was transferred in a quartz cuvette and the absorbance of the dibenzofulvene-piperidine adduct (product of the -Fmoc deprotection) was measured at 299 nm. In this way, the effective loading of the resin was indirectly calculated by measuring the moles of free amino groups per gram of resin according to the following formula:

$$n = \frac{A \cdot V \cdot d \cdot 1000}{l \cdot m \cdot \epsilon_{299}}$$

With:

n = free amino groups (mmol·g$^{-1)}$

A = absorbance value at 299 nm

V = volumetric flask volume (L)

d = dilution factor (100 µL of solution in 900 µL of MeOH)
1000 = factor conversion of mol to mmol
l = optical path length of the cell (cm)
m = sample weight of resin (g)
ε_{299} = molar attenuation coefficient of dibenzofulvene at 299 nm (7800 $L \cdot mol^{-1} \cdot cm^{-1}$)

Before proceeding the coupling phase, the resin was washed 10 times for 1 min with DMF and 1 times for 1 min with DCM, in order to remove piperidine traces. To confirm that, the pH of the DCM solution have to be neutral.

The first coupling phase was performed in 10 $mL \cdot g^{-1}$ DMF with N-Fmoc-protected amino acids (2.0 eq.), *in situ* activators PyBOP (2.0 eq.) and DIPEA (3.0 eq.). The solution's pH was checked equal to 9-10 and the reaction mixture was gently stirred for 60 min at room temperature. Then, the resin was washed 3 times for 1 min with DCM and 5 times for 1 min with DMF, until the neutrality of solution's pH.

TNBS test was made to evaluate the completeness of the coupling phase. This test relies on the utilization of a small portion of resin beads treated with a yellow solution containing 2,4,6-trinitrobenzene-sulphonic acid (1% w/v in DMF). If the coupling step is fully ended, there aren't free amino group available to react with acid and the resin beads remains colourless; conversely, if the coupling step is not complete, the acid reacts with free primary amino groups to form a visible orange-red trinitrophenylated derivative. In this case, the coupling step have to be repeated again.

After checking the completion of the coupling, the procedure for the peptide elongation was repeated from the Fmoc-deprotection step. After repeating this protocol for the following coupling steps, the final linear peptide sequence was obtained on beads.

The procedure could be stopped after the TNBS test, stirring the beads for 10 min in the presence of diethyl-ether, and it could be resumed from the swelling phase.

Automated synthesis of peptides were performed on a Syro II Synthesizer (Biotage, Uppsala, Sweden). The logic is the same as the manual synthesis, except for the -Fmoc deprotection times (3 times for 10 min) as well as the added reagent equivalents (40% piperidine in DMF, amino acid 4.0 eq.) and the coupling agent used (HBTU (hexafluorophosphate benzotriazole tetramethyl uronium) 4 eq.). In addition, it isn't possible get the TNBS test.

B) General procedure for peptide cleavage

The peptide cleavage is a procedure depending from the resin:

B1. Linear peptides synthesized on Gly-SASRIN™ resin were treated 10 times for 10 min. with a mixture of TFA/DCM (1/99). The collected solutions were gathered, neutralized with DIPEA, in order to avoid the deprotection of other protecting groups, and concentrated under reduced pressure. The resulting oil was dissolved in a minimum quantity of DCM and it was added drop by drop to a calibrated falcon filled with ice-cold diethyl ether to induce precipitation. After one centrifugation (4000 g, 3 min), the supernatant is discarded without disturbing the pellet and the precipitation process is repeated twice more. That procedure allows to wash the pellet from impurities soluble in diethyl ether. After desiccation, the resulting white solid was weighted, triturated to give a powder and analysed by UPLC-MS. The crude was then purified, if necessary, through preparative RP-HPLC and lyophilized.

B2. Linear peptides synthesized on Rink amide® resin were treated 2 times for 2 hours with a mixture of TFA/TIS/H_2O (95/2,5/2,5), resulting in acid-sensitive protecting groups remotion too. The collected solutions were gathered and concentrated under reduced pressure. The resulting oil was dissolved in a minimum quantity of DCM and it was added drop by drop to a calibrated falcon filled with ice-cold diethyl ether to induce precipitation. After one centrifugation (4000 g, 3 min), the supernatant is discarded without disturbing the pellet and the precipitation process is repeated twice more. That procedure allows to wash the pellet from impurities soluble in diethyl ether. After desiccation, the resulting white solid was weighted, triturated to give a powder and analysed by UPLC-MS. The crude was then purified, if necessary, through preparative RP-HPLC and lyophilized.

C) General procedure for peptide cyclization

Linear peptides were dissolved in DMF (0.5 mM; by means of this concentration we are able to maximize intramolecular reactions, minimizing intermolecular reactions) and the pH values were adjusted to 8-9 by addition of DIPEA. PyBOP (2.0 eq.) was added and the solution stirred at room temperature for 2 h. Solvent was removed under reduced pressure and the residue dissolved in a minimum of DCM. It was added drop by drop to a calibrated falcon filled with ice-cold diethyl ether to induce precipitation. After one centrifugation (4000 g, 3 min), the supernatant is discarded without disturbing the pellet and the precipitation process is repeated twice more. After desiccation, the resulting white solid was weighted, triturated to give a powder and analysed by UPLC-MS. The crude was then purified, if necessary, through preparative RP-HPLC and lyophilized.

D) General procedure for the removal of protecting groups

For routine synthesis, protecting group that are removed with TFA/TIS/H_2O (95/2,5/2,5), 2 hours for 2 times, are usually employed as this allows the peptide to be globally deprotected at the same time as it is cleaved or released from the support. Furthermore, a wide range of groups is

also available which can be selectively removed on the solid phase, thus enabling the selective modification of side-chain of individual residues within the peptide chain.

D1. Removal of -Boc protecting group on an amine moiety. The Boc-containing product was dissolved in a mixture of TFA/DCM (3:2) and the reaction mixture was stirred for 30 minutes at room temperature. The solvent mixture was removed and the residue dissolved into DCM; this solution was added drop-wise to ice-cold diethyl ether causing the precipitation of the Boc-deprotected product, which was filtrated and dried under vacuum. The crude was purified by semi-preparative RP-HPLC.

D2. Removal of -Alloc protecting group on an amine moiety. The Alloc-containing product and $Pd(PPh_3)_4$ (cat.) were dissolved in a dry DMF solution and, at this solution, $PhSiH_3$ (25.0 eq./-Alloc group) was added under Argon condition. The reaction mixture was stirred for 60 min at room temperature, so MeOH was added and the mixture stirred until CO_2 bubbling ceased. The solvent mixture was removed and the residue taken into DCM; this solution was added drop-wise to ice-cold diethyl ether causing the precipitation of the Alloc-deprotected product, which was filtrated and dried under vacuum.

E) General procedure for the preparation of glycoclusters by copper-catalyzed azide-alkyne cycloaddition (CuAAC)

Propargyl glycoside or alkyne-substituted glycoclusters (4.4 eq.) and azide-functionalized scaffold (1.0 eq.) were dissolved in a 1:2 mixture of DMF and PBS buffer (pH 7.5). A solution of $CuSO_4 \cdot 5H_2O$ (0.5 eq.) and THPTA (1.0 eq.) in PBS was added to a solution of sodium ascorbate (3.0 eq.) in PBS. This mixture was added to the solution containing the azide and alkyne which was degassed with argon and stirred at r.t. for at average 2 hours after which RP-HPLC showed completion of the reaction. Chelex® resin was then added to the reaction mixture which was stirred for 45 minutes. The resin was filtered off, rinsed with water and the filtrate purified by semi-preparative RP-HPLC. Fractions containing the product were combined and lyophilized.

F) General procedure for the preparation of peptidoclusters by copper-catalyzed azide-alkyne cycloaddition (CuAAC)

Alkyne-substituted peptide (4.6 eq.) and azide-functionalized scaffold (1.0 eq.) were dissolved in DMF (pH 7.5). A solution of $CuSO_4 \cdot 5H_2O$ (0.5 eq.) and THPTA (1.0 eq.) in PBS was added to a solution of sodium ascorbate (3.0 eq.) in PBS. This mixture was added to the solution containing the azide and alkyne which was degassed with argon and stirred from 2 hours to 24 hours, after which RP-HPLC showed completion of the reaction. It is recommended to heat up until 60°C. Chelex® resin was then added to the reaction mixture which was stirred for 45 minutes. The

resin was filtered off, rinsed with water and the filtrate purified by semi-preparative RP-HPLC. Fractions containing the product were combined and lyophilized.

G) General procedure for the preparation of ARM by copper-catalyzed azide-alkyne cycloaddition (CuAAC)

Azido-functionalized ABM (1.0 eq.) and alkyne-functionalized TBM (1.0 eq.) were solubilized in a 1:1 mixture of DMF and PBS buffer (pH 7.5). A solution of $CuSO_4$.•$5H_2O$ (1.0 eq.) and THPTA (2.0 eq.) in PBS was added to a solution of sodium ascorbate (4.0 eq.) in PBS. This mixture was added to the solution containing the azide and alkyne which was degassed with argon and stirred at r.t. for 2 hours after which RP-HPLC showed completion of the reaction. Chelex® resin was then added to the reaction mixture which was stirred for 45 minutes. The resin was filtered off, rinsed with water and the filtrate purified by semi-preparative RP-HPLC. Fractions containing the product were combined and lyophilized.

H) General procedure for the coupling of NHS-functionalized module

Free amine compound (1.0 eq.) was dissolved in dry DMF, DIPEA was added to reach pH ~ 9-10, then succinimide ester of pentynoic (**26**) or azidoacetic (**27**) acid (1.5 eq.) was added. The reaction mixture was stirred at r.t. for 1 hour after which RP-HPLC showed completion of the reaction. The mixture was diluted with water and purified by semi-preparative RP-HPLC. Fractions containing the product were combined and lyophilized.

J) General procedure for the coupling of PEG azide module

Free amine compound (1.0 eq.) was dissolved in dry DMF, DIPEA was added to reach pH ~ 9-10, then PEG azide (2.0 eq.) and PyBOP (2.0 eq.) were added. The reaction mixture was stirred at r.t. for 1 hour after which RP-HPLC showed completion of the reaction. The mixture was diluted with water and purified by semi-preparative RP-HPLC. Fractions containing the product were combined and lyophilized.

V.1.D. Synthesis and characterizations

V.1.D.I. Carbohydrate functionalized in anomeric position

1,2,3,4-tetra-O-acetyl-L-Rhamnopyranoside **10**

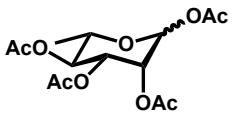

$C_{14}H_{20}O_9$

Mw: 332.31 g/mol

Commercial L-Rhamnose **9** (3.100 g, 17 mmol) was dissolved in a Pyridine/Ac_2O solution (2:1). The reaction was stirred for 24 hours at room temperature. The completion of the reaction was

monitored by TLC. The reaction mixture was then diluted in DCM (100 mL) and 1N HCl (100 mL) was carefully added at 0°C. After 20 min , the two phases were separated and the organic phase was washed 2 times with 1N HCl, 2 times with saturated $NaHCO_3$ solution, 1 time with H_2O, 1 time with NaCl and dried over anhydrous $MgSO_4$. Combined organic fractions were concentrated under reduced pressure. The crude was finally purified by flash chromatography (SiO_2, EtOAc/Pentane 30:70 to 40:60) to obtain **10** (4.984 g, 15 mmol) as a yellow oil in 88% yield. A mixture of anomers α/β was obtained. TLC (SiO_2): Rf = 0.46 (EtOAc/Pentane 40:60; revelation: UV and H_2SO_4 in EtOH). NMR data were in agreement with the literature.[191]

Propargyl 2,3,4-tris-O-acetyl-α-L-Rhamnopyranoside **11**

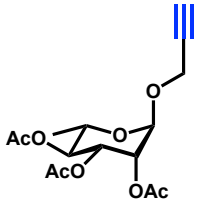

$C_{15}H_{20}O_8$

Mw: 328.32 g/mol

Compound **10** (4.984 g, 15 mmol) was dissolved in anhydrous DCM (100 mL) under argon and propargylic alcohol (3.5 mL, 60 mmol) was added. At 0°C, $BF_3.Et_2O$ (4.6 mL, 37.5 mmol) was added dropwise to the reaction mixture. The reaction was then stirred for 24 hours at room temperature. The completion of the reaction was monitored by TLC. At 0°C, saturated $NaHCO_3$ solution (100 mL) was carefully added (bubbles) and the organic layer was washed 3 times with saturated $NaHCO_3$ solution, with brine, and finally dried over anhydrous $MgSO_4$. The solvent was removed under pressure. The crude was finally purified by flash chromatography (SiO_2, EtOAc/Pentane 20:80 to 40:60) to obtain **14** (3.546 g, 10.8 mmol) as a colourless oil in 75% yield (3:1 for α: β). TLC (SiO_2): Rf = 0.56 (EtOAc/Pentane 40:60; revelation: UV and H_2SO_4 in EtOH). NMR data were in agreement with the literature.[191]

Propargyl α-L-Rhamnopyranoside **12**

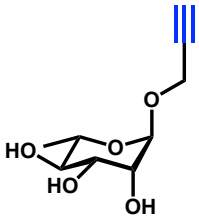

$C_9H_{14}O_5$

Mw: 202.21 g/mol

Compound **11** (3.546 g, 10.8 mmol) was dissolved in MeOH (30 mL) and NaOMe was added until having pH 9-10. The reaction was stirred for 3 hours at room temperature. The completion of the reaction was checked by TLC. The mixture was neutralized with activated amberlite resin (H^+), filtered and concentrated under pressure. The final product was precipitated in cold DCM to give α-L-Rha-Prop **15** (2.082 g, 10.3 mmol) as a white powder in 95% yield. TLC (SiO_2): Rf = 0.31 (DCM/MeOH 90:10; revelation: UV and H_2SO_4 in EtOH). NMR data were in agreement with the literature.[191]

VI.1.D.II. Peptide scaffolds

Scaffold $R(N_3)_4$ **5**

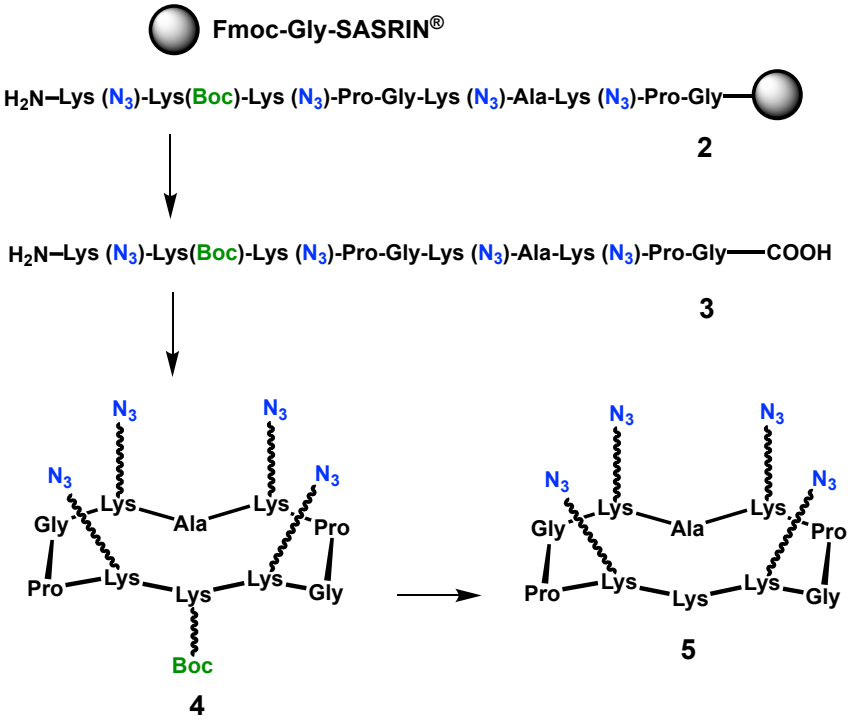

$C_{47}H_{77}N_{23}O_{10}$

Mw: 1124.26 g/mol

Peptide scaffold **2** was synthetized manually following the general procedure **A** on 1 g of Fmoc-Gly-SASRIN resin (loading = 0.6 mmol/g). Cleavage of the peptide **2** was realized using general procedure **B1** to obtain the -Boc protected linear peptide **3**. Next, it was cyclized (general procedure **C**) to obtain **4** and subsequent deprotected from -Boc protecting group following the general procedures **D1** afforded to scaffold $R(N_3)_4$ **5** in 40% overall yield. HRMS (ESI^+-TOF): m/z

calculated for $C_{47}H_{78}N_{23}O_{10}$ $[M+H]^+$: 1125.6302 (monoisotopic), found: 1125.6216. RP-HPLC: R_t = 12.28 min. (C_{18}, λ = 214 nm, 5-60% solvent B in 15 min).

Scaffold D$(N_3)_4$ **8**

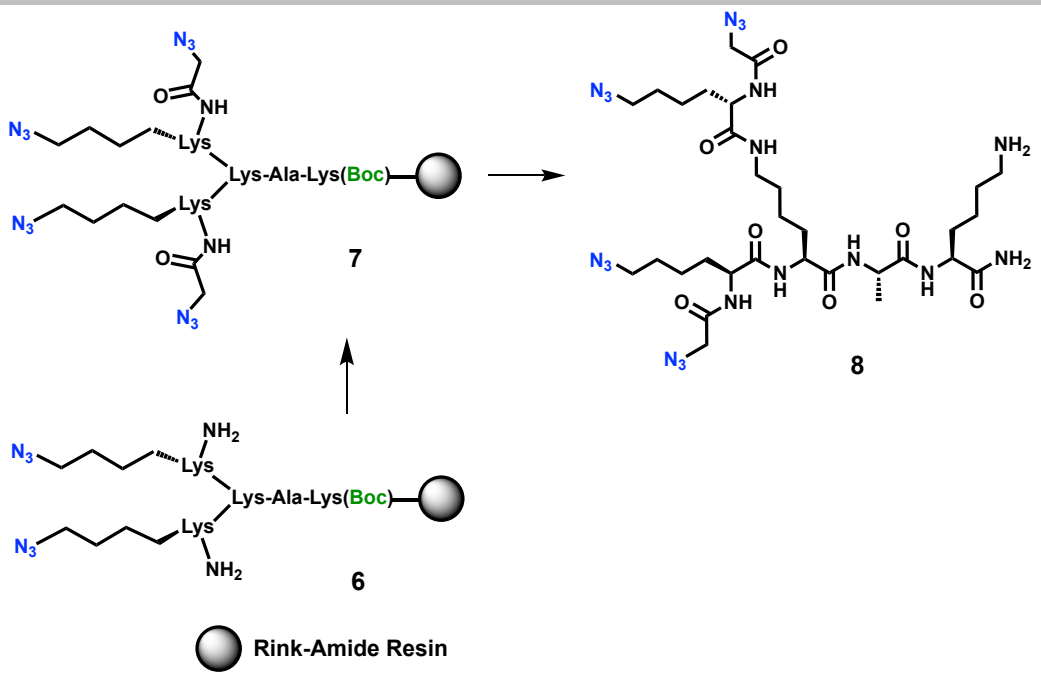

$C_{31}H_{54}N_{20}O_7$

Mw: 818.89 g/mol

Peptide scaffold **6** was synthetized manually following the general procedure **A** on 1 g of Rink amide resin (loading = 0.5 mmol/g) to obtain the linear sequence. N_3-AcA-OSu **27** (1.8 mmol, 4.0 eq.) and DIPEA (1.8 mmol, 4.0 eq.) were added to the reactor to graft the linker on the free amines of the structure **6** following the general procedure **H**, to obtain the -Boc protected linear peptide **7** on the resin. Cleavage was realized following the general procedure **B2** to get **8** after semi-preparative HPLC purification in 65% overall yield. HRMS (ESI^+-TOF): m/z calculated for $C_{31}H_{55}N_{20}O_7$ $[M+H]^+$: 819.4563 (monoisotopic), found: 819.4531. RP-HPLC: R_t = 6.96 min. (C_{18}, λ = 214 nm, 5-80% solvent B in 15 min).

Alk-cRGD **17**

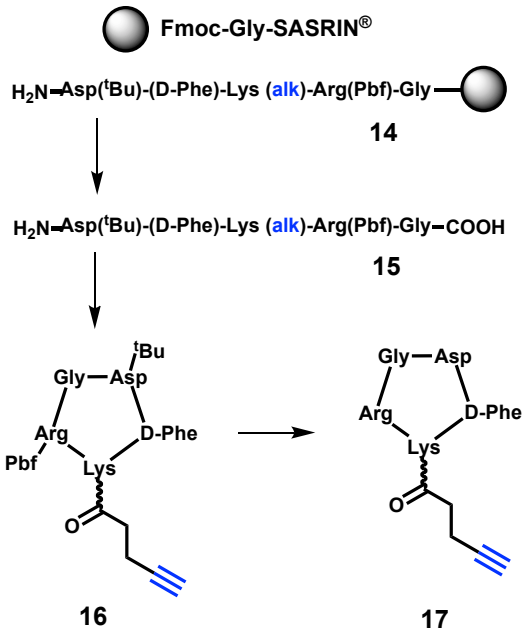

$C_{32}H_{45}N_9O_8$

Mw: 683.34 g/mol

Peptide scaffold **14** was synthetized manually following the general procedure **A** on 1 g of Fmoc-Gly-SASRIN resin (loading = 0.6 mmol/g). Cleavage of the peptide was realized in using general procedure **B1** to obtain the protected linear peptide **15**. Next, it was cyclized (general procedure **C**) to obtain **16** and subsequent deprotected following the general procedures **D1** afforded to **17** in 36% overall yield. HRMS (ESI^+-(ESI^+-TOF): m/z calculated for $C_{32}H_{45}N_9O_8$ $[M+H]^+$: 684,34639; (monoisotopic), found: 684,34555. RP-HPLC: R_t = 7.30 min. (C_{18}, λ = 214 nm, 5-60% solvent B in 15 min).

Alk-LT **21**

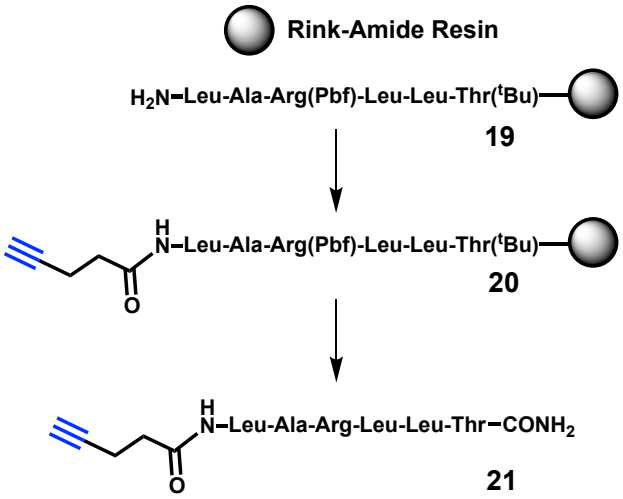

$C_{36}H_{64}N_{10}O_8$

Mw: 764.50 g/mol

Peptide scaffold **19** was synthetized manually following the general procedure **A** on 1 g of Rink amide resin (loading = 0.5 mmol/g), adding 4-Pentynoic acid as last amino acid in coupling phase afforded to **20**. Cleavage was realized in using general procedure **B2** to give **21** after semi-preparative HPLC purification in 75% overall yield. HRMS (ESI^+-TOF): m/z calculated for $C_{36}H_{65}N_{10}O_8$ $[M+H]^+$: 765.4981 (monoisotopic), found: 765.4976. RP-HPLC: R_t = 11.70 min. (C_{18}, λ = 214 nm, 5-60% solvent B in 15 min).

Alk-HVH **23**

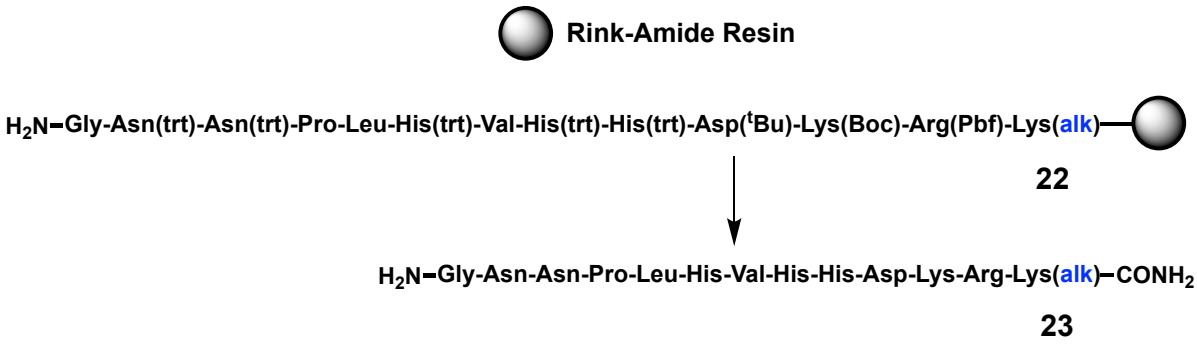

$C_{71}H_{111}N_{18}O_{27}$

Mw: 1629.86 g/mol

Peptide scaffold **22** was synthetized manually following the general procedure **A** on 1 g of Rink amide resin (loading = 0.5 mmol/g) adding Fmoc-Lys(N-4-Pentynoic acid)-OH as first amino acid in coupling phase. Cleavage was realized in using general procedure **B2** to give **23** after semi-preparative HPLC purification in 48% overall yield. HRMS (ESI^+-TOF): m/z calculated for $C_{71}H_{114}N_{18}O_{27}$ $[M+3H]^{3+}$: 544.2939, found: 544.2936. RP-HPLC: R_t = 5.24 min. (C_{18}, λ = 214 nm, 5-60% solvent B in 15 min).

Alk-[Ac-HVH(Alloc)] **25**

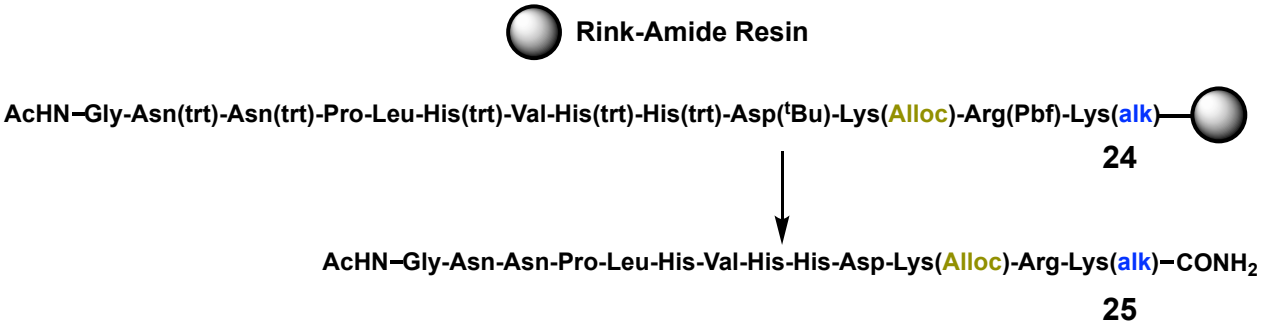

$C_{77}H_{117}N_{27}O_{21}$

Mw: 1756.89 g/mol

Peptide scaffold **24** was synthetized manually following the general procedure **A** on 1 g of Rink amide resin (loading = 0.5 mmol/g) adding Fmoc-Lys(N-4-Pentynoic acid)-OH as first amino acid and Acetil-Gly as last amino acid in coupling phase. Cleavage was realized in using general procedure **B2** to give **25** after semi-preparative HPLC purification in 44% overall yield. MALDI-ToF m/z: calculated for $C_{77}H_{118}N_{27}O_{21}$ $[M+H]^+$: 1756.89, found 1756.91;. RP-HPLC: R_t = 7.07 min. (C_{18}, λ = 214 nm, 5-60% solvent B in 15 min).

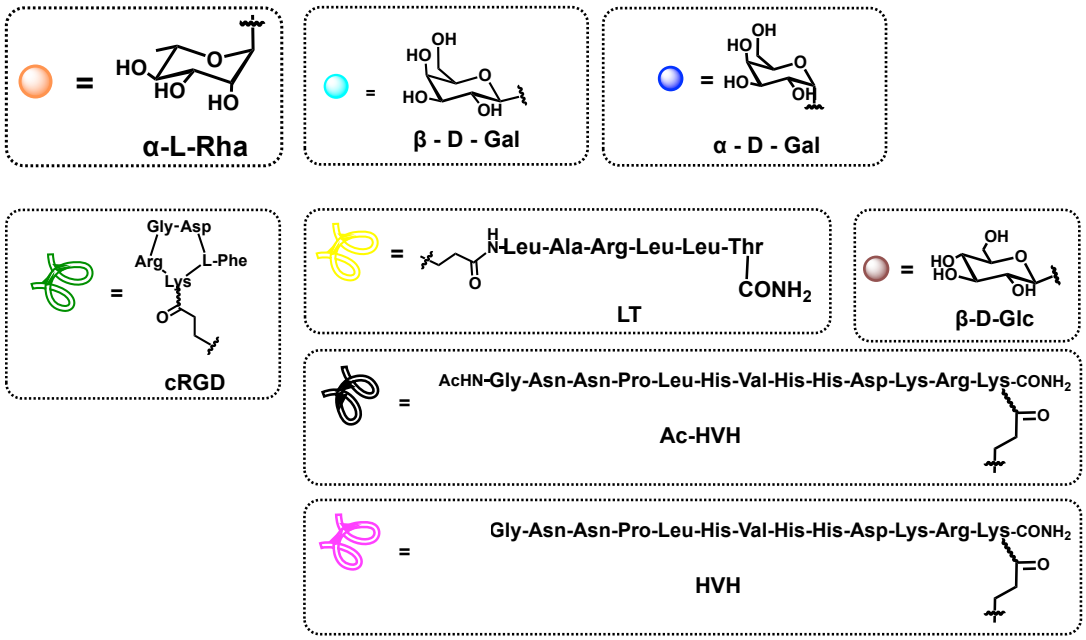

V.1.D.III. Antibody Binding Modules (ABMs)

R(α-L-Rha)$_4$ 32

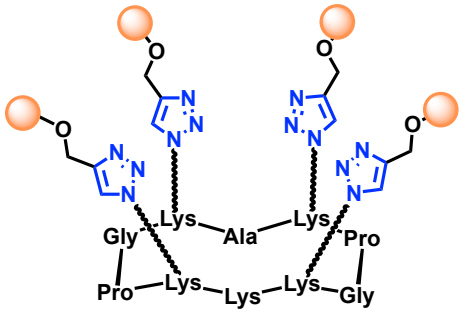

$C_{83}H_{133}N_{23}O_{30}$

Mw: 1933.08 g/mol

Prepared according general procedure **E** from propargyl α-L-Rhamnopyranoside **12** (11.5 mg, 57 µmol) and R(N_3)$_4$ **5** (14.5 mg, 13 µmol). The crude mixture was purified to afford the title compound as a white fluffy solid after lyophilization (20.5 mg, 11 µmol, 82%). HRMS (ESI$^+$-TOF) m/z: calculated for $C_{83}H_{134}N_{23}O_{30}$ $[M+H]^+$: 1933.9667, found 1933.9700; RP-HPLC: R_t = 12.78 min (C_{18}, λ = 214 nm, 0-20% B in 15 min).

N_3-R(α-L-Rha)$_4$ 33

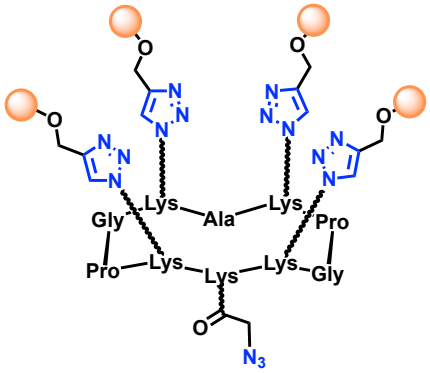

$C_{85}H_{134}N_{26}O_{31}$

Mw: 2015.48 g/mol

Prepared according general procedure **H** from **32** (32.0 mg, 16.6 µmol) and azidoacetic acid succinimide ester **27** (4.9 mg, 24.8 µmol). The crude mixture was purified to afford the title compound as a white fluffy solid after lyophilization (30.7 mg, 15.2 µmol, 92%). HRMS (ESI$^+$-TOF) m/z: calculated for $C_{85}H_{136}N_{26}O_{31}$ $[M+2H]^{2+}$: 1008.4927, found 1008.4916; RP-HPLC: R_t = 9.15 min (C_{18}, λ = 214 nm, 5-60% B in 15 min).

Alk-R(α-L-Rha)$_4$ **34**

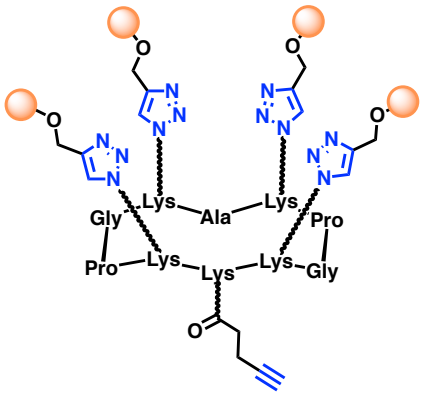

$C_{88}H_{137}N_{23}O_{31}$

Mw: 2012.48 g/mol

Prepared according general procedure **H** from **32** (27 mg, 14.0 µmol) and pentynoic acid succinimide ester **26** (4 mg, 20.9 µmol). The crude mixture was purified to afford the title compound as a white fluffy solid after lyophilization (25 mg, 12.4 µmol, 89%). HRMS (ESI$^+$-TOF) m/z: calculated for $C_{88}H_{137}N_{23}NaO_{31}$ $[M+Na]^+$: 2034.9749, found 2034.9777; RP-HPLC: R_t = 9.30 min (C_{18}, λ = 214 nm, 0-40% B in 15 min).

N_3-PEG-R(α-L-Rha)$_4$ **35**

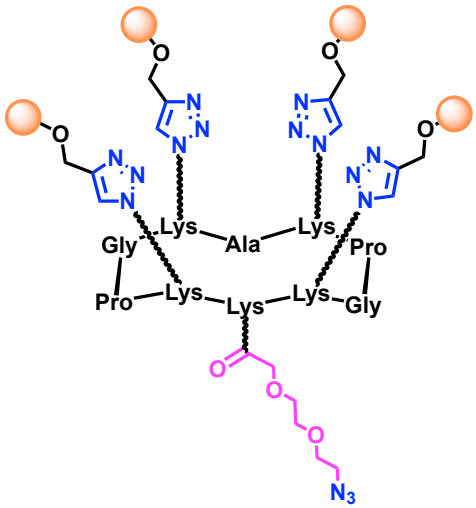

$C_{89}H_{142}N_{26}O_{33}$

Mw: 2103.51 g/mol

Prepared according general procedure **J** from **32** (27.9 mg, 14.4 µmol) and 2-[2-(2-Azidoethoxy)ethoxy]-acetic acid potassium salt **28** (6.6 mg, 28.8 µmol) and PyBOP (15.3 mg, 28.8 µmol). The crude mixture was purified to afford the title compound as a white fluffy solid after lyophilization (22.2 mg, 10.5 µmol, 73%). HRMS (ESI$^+$-TOF) m/z: calculated for $C_{89}H_{144}N_{26}O_{33}$ $[M+2H]^{2+}$: 1052.5189, found 1052.5207; RP-HPLC: R_t = 6.71 min (C_{18}, λ = 214 nm, 5-60% B in 15 min).

D(α-L-Rha)$_4$ **36**

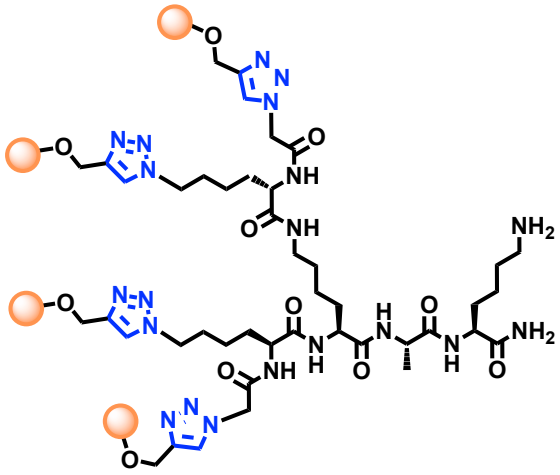

Prepared according general procedure **E** from propargyl α-L-Rhamnopyranoside **12** (43.3 mg, 214 µmol) and D(N$_3$)$_4$ **8** (39.9 mg, 48.7 µmol). The crude mixture was purified to afford the title compound as a white fluffy solid after lyophilization (70.0 mg, 43 µmol, 88%). HRMS (ESI$^+$-TOF) m/z: calculated for $C_{67}H_{112}N_{20}O_{27}$ $[M+2H]^{2+}$: 814.3997, found 814.3994; RP-HPLC: R_t = 4.05 min (C_{18}, λ = 214 nm, 5-60% B in 15 min).

$C_{67}H_{110}N_{20}O_{27}$

Mw: 1626.80 g/mol

N$_3$-D(α-L-Rha)$_4$ **37**

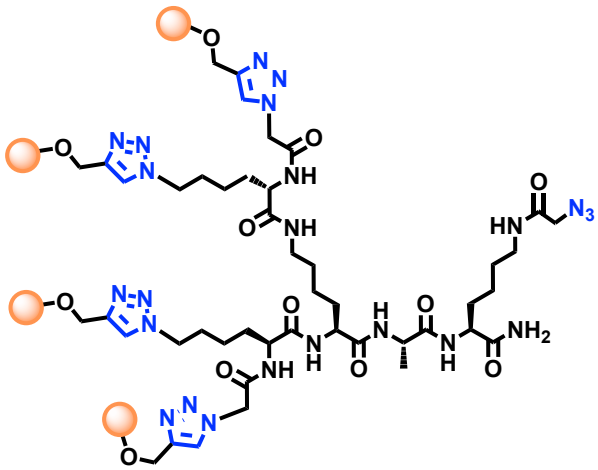

Prepared according general procedure **H** from **36** (24.2 mg, 14.9 µmol) and azidoacetic acid succinimide ester **27** (4.4 mg, 22.3 µmol). The crude mixture was purified to afford the title compound as a white fluffy solid after lyophilization (23.0 mg, 13.4 µmol, 90%). HRMS (ESI$^+$-TOF) m/z: calculated for $C_{69}H_{113}N_{23}O_{28}$ $[M+2H]^{2+}$: 855.9057, found 855.9055; RP-HPLC: R_t = 4.93 min (C_{18}, λ = 214 nm, 5-60% B in 15 min).

$C_{69}H_{111}N_{23}O_{28}$

Mw: 1709.80 g/mol

Alk-D(α-L-Rha)$_4$ **38**

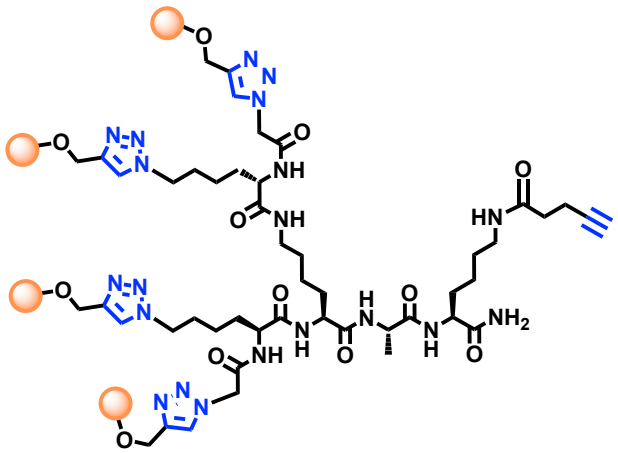

Prepared according general procedure H from **36** (79.3 mg, 48.7 µmol) and pentynoic acid succinimide ester **26** (14.3 mg, 73.0 µmol). The crude mixture was purified to afford the title compound as a white fluffy solid after lyophilization (79.9 mg, 46.8 µmol, 96%). HRMS (ESI$^+$-TOF) m/z: calculated for $C_{72}H_{116}N_{20}O_{28}$ $[M+2H]^{2+}$: 854.4128, found 854.4125; RP-HPLC: R_t = 4.92 min (C_{18}, λ = 214 nm, 5-60% B in 15 min).

$C_{72}H_{114}N_{20}O_{28}$

Mw: 1706.80 g/mol

RR(α-L-Rha)$_{16}$ **39**

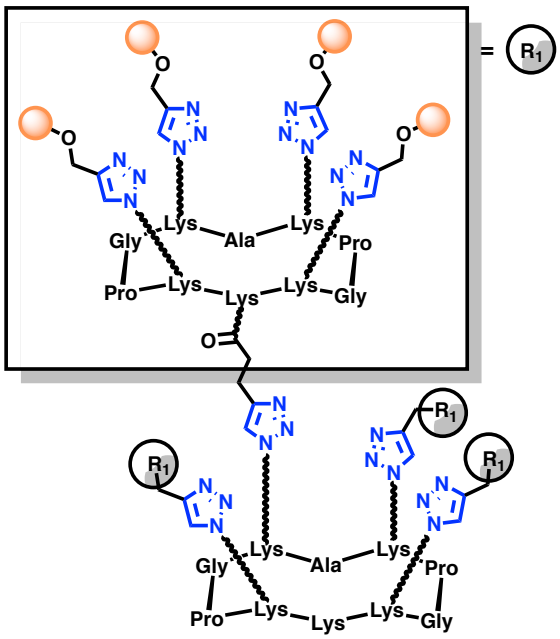

Prepared according general procedure **E** from **34** (25.0 mg, 12.1 µmol) and R(N$_3$)$_4$ **5** (3.0 mg, 2.7 µmol). The crude mixture was purified to afford the title compound as a white fluffy solid after lyophilization (18.6 mg, 2.0 µmol, 74%). HRMS (ESI$^+$-TOF) m/z: calculated for $C_{399}H_{630}N_{115}O_{134}$ $[M+5H]^{5+}$: 1835.3198, found 1835.3266; RP-HPLC: R_t = 10.16 min (C_{18}, λ = 214 nm, 0-40% B in 15 min).

$C_{399}H_{625}N_{115}O_{134}$

Mw: 9171.32 g/mol

N_3-RR(α-L-Rha)$_{16}$ **40**

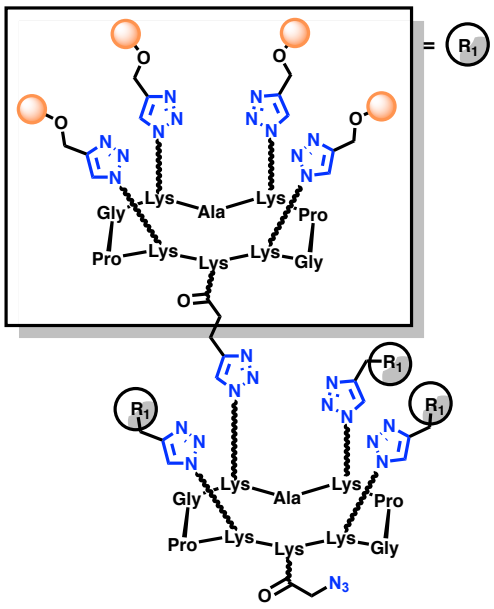

Prepared according general procedure **H** from **39** (24 mg, 2.6 µmol) and azidoacetic acid succinimide ester **27** (0.8 mg, 3.9 µmol). The crude mixture was purified to afford the title compound as a white fluffy solid after lyophilization (18.4 mg, 2.0 µmol, 77%). MALDI-ToF m/z: calculated for $C_{401}H_{627}N_{118}O_{135}$ $[M+H]^+$: 9254.6, found 9255.0; RP-HPLC: R_t = 4.97 min (C_{18}, λ = 214 nm, 5-100% B in 15 min).

$C_{401}H_{626}N_{118}O_{135}$

Mw: 9253.60 g/mol

Alk-RR(α-L-Rha)$_{16}$ **41**

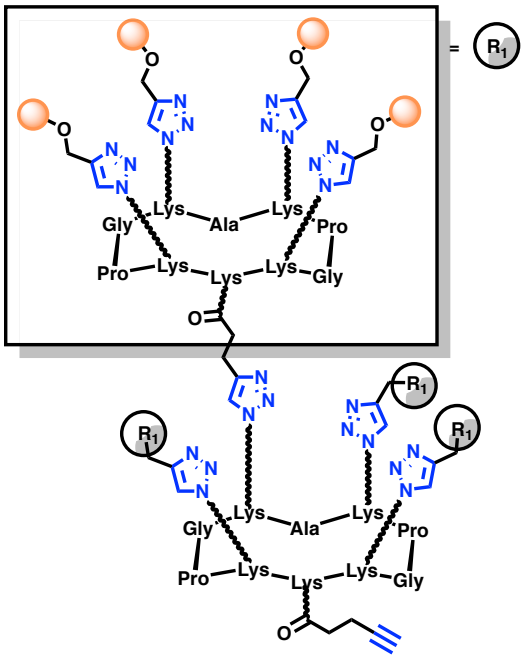

Prepared according general procedure **H** from **39** (91.3 mg, 9.9 µmol) and pentynoic acid succinimide ester **26** (2.9 mg, 14.9 µmol). The crude mixture was purified to afford the title compound as a white fluffy solid after lyophilization (83.4 mg, 9.0 µmol, 91%). HRMS (ESI$^+$-TOF) m/z: calculated for $C_{404}H_{634}N_{115}O_{135}$ $[M+5H]^{5+}$: 1852.1273, found 1852.1301; RP-HPLC: R_t = 6.94 min (C_{18}, λ = 214 nm, 5-60% B in 15 min).

$C_{404}H_{629}N_{115}O_{135}$

Mw: 9251.58 g/mol

N_3-PEG-RR(α-L-Rha)$_{16}$ **42**

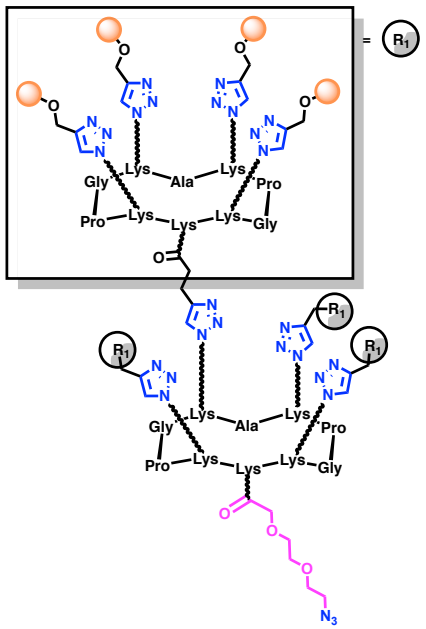

Prepared according general procedure **J** from **39** (7.0 mg, 0.7 µmol) and 2-[2-(2-Azidoethoxy)ethoxy]-acetic acid potassium salt **28** (0.3 mg, 9.5 µmol) and PyBOP (0.8 mg, 1.5 µmol). The crude mixture was purified to afford the title compound as a white fluffy solid after lyophilization (6.1 mg, 0.6 µmol, 92%). HRMS (ESI$^+$-TOF) m/z: calculated for $C_{405}H_{639}N_{118}O_{137}$ $[M+5H]^{5+}$: 1869.5327, found 1869.5446; RP-HPLC: R_t = 7.10 min (C_{18}, λ = 214 nm, 5-60% B in 15 min).

$C_{405}H_{634}N_{118}O_{137}$

Mw: 9342.63 g/mol

DR(α-L-Rha)$_{16}$ **43**

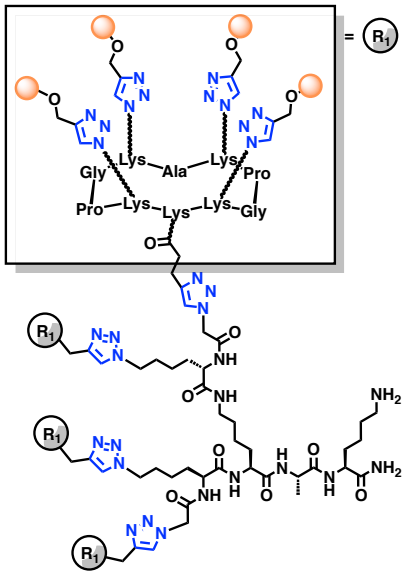

Prepared according general procedure **E** from **34** (36.9 mg, 18.0 µmol) and $D(N_3)_4$ **8** (3.4 mg, 4.0 µmol). The crude mixture was purified to afford the title compound as a white fluffy solid after lyophilization (29.0 mg, 3.3 µmol, 82%). HRMS (ESI$^+$-TOF) m/z: calculated for $C_{383}H_{602}N_{112}O_{131}$ $[M+5H]^{5+}$: 1775.0872, found 1775.0887; RP-HPLC: R_t = 8.76 min (C_{18}, λ = 214 nm, 5-40% B in 15 min).

$C_{383}H_{597}N_{112}O_{131}$

Mw: 8870.40 g/mol

N_3-DR(α-L-Rha)$_{16}$ **44**

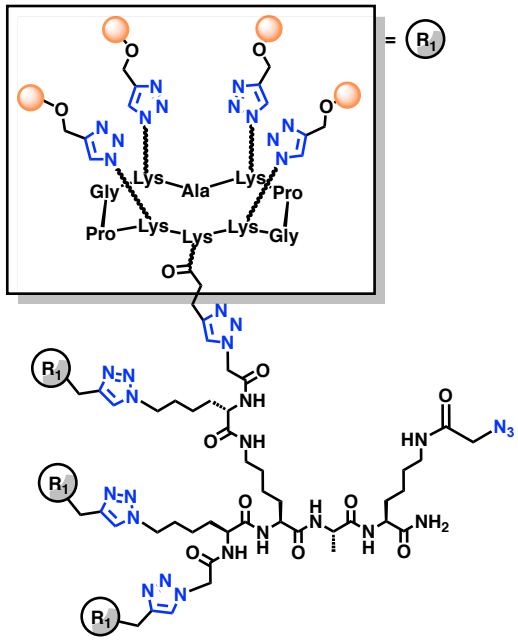

Prepared according general procedure **H** from **43** (21.5 mg, 2.4 μmol) and azidoacetic acid succinimide ester **27** (1.0 mg, 4.8 μmol). The crude mixture was purified to afford the title compound as a white fluffy solid after lyophilization (19.4 mg, 2.1 μmol, 88%). HRMS (ESI$^+$-TOF) m/z: calculated for $C_{385}H_{603}N_{115}O_{132}$ $[M+5H]^{5+}$: 1791.6896, found 1791.6916; RP-HPLC: R_t = 7.57 min (C_{18}, λ = 214 nm, 5-60% B in 15 min).

$C_{385}H_{598}N_{115}O_{132}$

Mw: 8953.45 g/mol

RD(α-L-Rha)$_{16}$ **45**

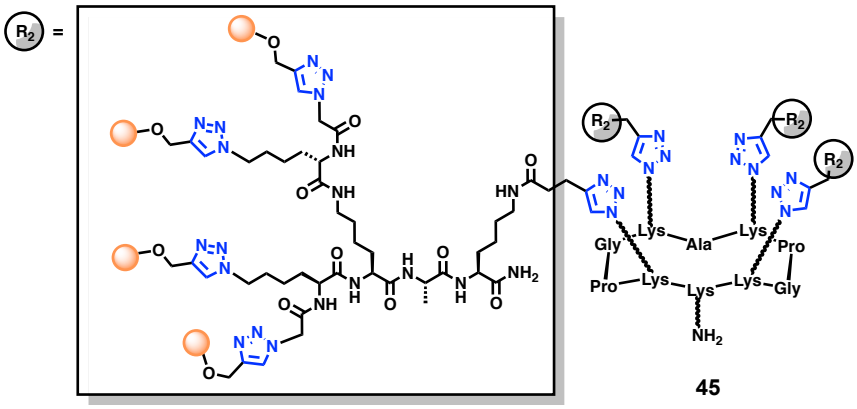

45

$C_{335}H_{533}N_{103}O_{122}$

Mw: 7950.88 g/mol

Prepared according general procedure **E** from **38** (7.9 mg, 4.6 μmol) and R(N$_3$)$_4$ **5** (1.2 mg, 1.0 μmol). The crude mixture was purified to afford the title compound as a white fluffy solid after lyophilization (6.6 mg, 0.8 μmol, 83%). HRMS (ESI$^+$-TOF) m/z: calculated for $C_{335}H_{537}N_{103}O_{122}$ $[M+4H]^{4+}$: 1988.7240, found 1988.7281; RP-HPLC: R_t = 5.62 min (C_{18}, λ = 214 nm, 5-60% B in 15 min).

N_3-RR(α-L-Rha)$_{16}$ **46**

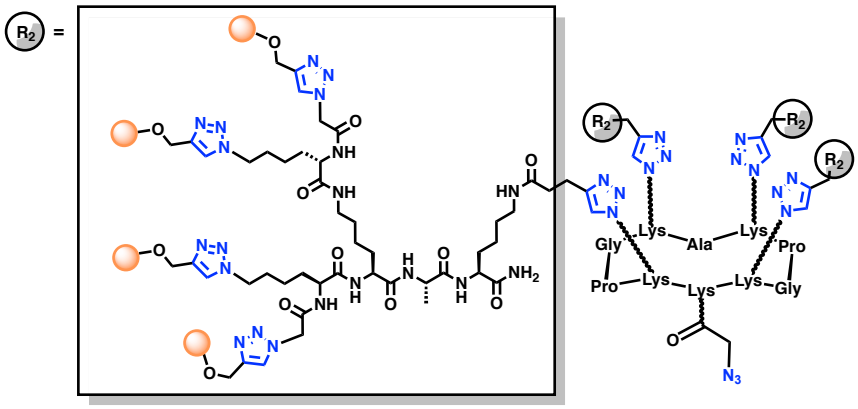

$C_{337}H_{529}N_{106}O_{123}$

Mw: 8037.90 g/mol

Prepared according general procedure **H** from **45** (21.5 mg, 2.7 µmol) and azidoacetic acid succinimide ester **27** (0.8 mg, 4.0 µmol). The crude mixture was purified to afford the title compound as a white fluffy solid after lyophilization (19.1 mg, 2.4 µmol, 88%). HRMS (ESI$^+$-TOF) m/z: calculated for $C_{337}H_{534}N_{106}O_{123}$ $[M+5H]^{5+}$: 1608.5852, found 1608.5903; RP-HPLC: R_t = 4.35 min (C_{18}, λ = 214 nm, 5-100% B in 15 min).

DD(α-L-Rha)$_{16}$ **47**

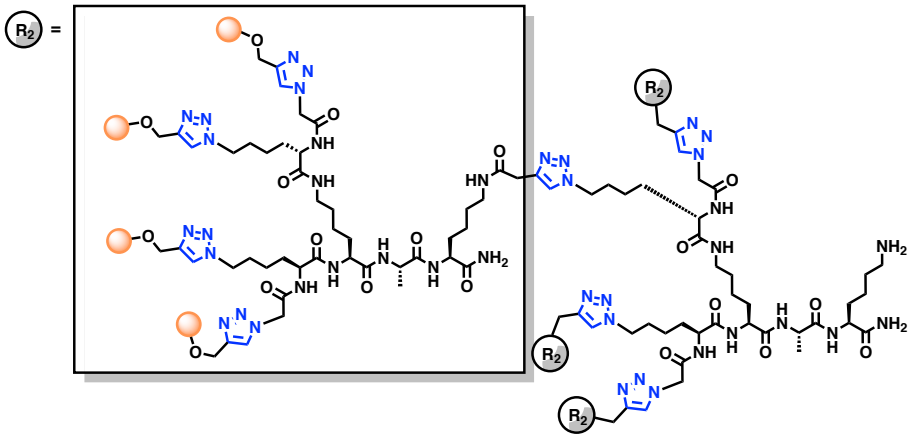

$C_{319}H_{510}N_{100}O_{119}$

Mw: 7645.72 g/mol

Prepared according general procedure **E** from **38** (38.7 mg, 22.7 µmol) and $D(N_3)_4$ **8** (4.2 mg, 5.1 µmol). The crude mixture was purified to afford the title compound as a white fluffy solid after lyophilization (29.4 mg, 3.8 µmol, 75%). HRMS (ESI$^+$-TOF) m/z: calculated for $C_{319}H_{514}N_{100}O_{119}$ $[M+4H]^{4+}$: 1912.4305, found 1912.4374; RP-HPLC: R_t = 5.41 min (C_{18}, λ = 214 nm, 5-60% B in 15 min).

N_3-DD(α-L-Rha)$_{16}$ **48**

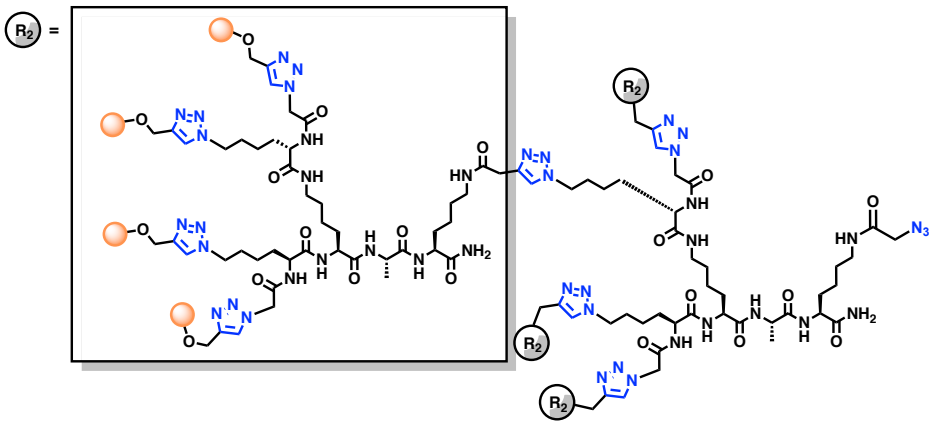

$C_{321}H_{511}N_{103}O_{120}$

Mw: 7728.73 g/mol

Prepared according general procedure **H** from **47** (39.2 mg, 5.1 µmol) and azidoacetic acid succinimide ester **27** (1.5 mg, 7.7 µmol). The crude mixture was purified to afford the title compound as a white fluffy solid after lyophilization (38.0 mg, 4.9 µmol, 96%). HRMS (ESI$^+$-TOF) m/z: calculated for $C_{321}H_{515}N_{103}O_{120}$ $[M+4H]^{4+}$: 1933.1835, found 1933.1879; RP-HPLC: R_t = 4.11 min (C_{18}, λ = 214 nm, 5-100% B in 15 min).

R(β-D-Gal)$_4$ **49**

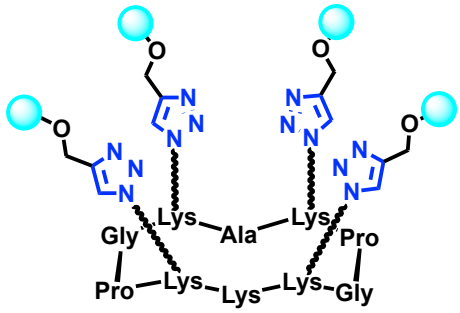

Prepared according general procedure **E** from propargyl β-D-galactopyranoside **29** (8.7 mg, 39.7 µmol) and R(N_3)$_4$ **5** (10.2 mg, 9.0 µmol). The crude mixture was purified to afford the title compound as a white fluffy solid after lyophilization (11.5 mg, 5.8 µmol, 64%). HRMS (ESI$^+$-TOF) m/z: calculated for $C_{83}H_{135}N_{23}O_{34}$ $[M+2H]^{2+}$: 998.9765, found 998.9779; RP-HPLC: R_t = 8.81 min (C_{18}, λ = 214 nm, 0-20% B in 15 min).

$C_{83}H_{133}N_{23}O_{34}$

Mw: 1995.95 g/mol

N_3-R(β-D-Gal)$_4$ **50**

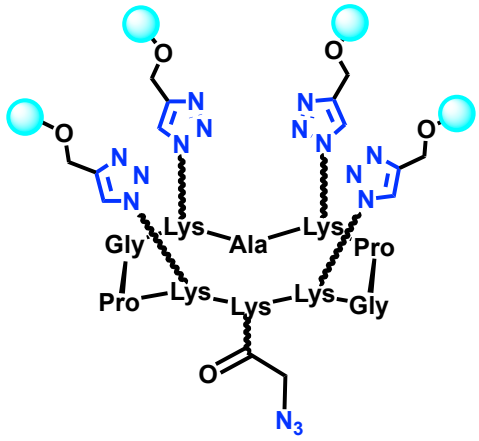

$C_{85}H_{133}N_{26}O_{35}$

Mw: 2078.96 g/mol

Prepared according general procedure **H** from **49** (10.0 mg, 5.0 µmol) and azidoacetic acid succinimide ester **27** (2.0 mg, 10.0 µmol). The crude mixture was purified to afford the title compound as a white fluffy solid after lyophilization (9.5 mg, 4.6 µmol, 90%). Maldi-ToF m/z: calculated for $C_{85}H_{134}N_{26}O_{35}$ $[M+H]^+$: 2079.9504, found 2077.1660; RP-HPLC: R_t = 4.88 min (C_{18}, λ = 214 nm, 5-60% B in 15 min).

Alk-R(β-D-Gal)$_4$ **51**

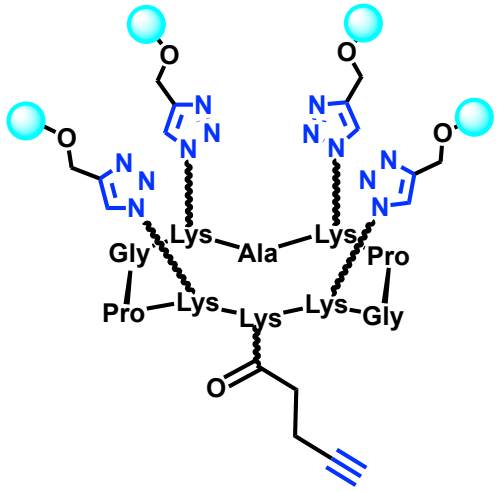

$C_{88}H_{139}N_{23}O_{35}$

Mw: 2075.97 g/mol

Prepared according general procedure **H** from **49** (13.2 mg, 6.61 µmol) and pentynoic acid succinimide ester **26** (1.9 mg, 9.92 µmol). The crude mixture was purified to afford the title compound as a white fluffy solid after lyophilization (12.4 mg, 5.95 µmol, 90%). HRMS (ESI$^+$-TOF) m/z: calculated for $C_{88}H_{139}N_{23}O_{35}$ $[M+2H]^{2+}$: 1038.9896, found 1038.9937; RP-HPLC: R_t = 5.80 min (C_{18}, λ = 214 nm, 5-40% B in 15 min).

RR(β-D-Gal)$_{16}$ **52**

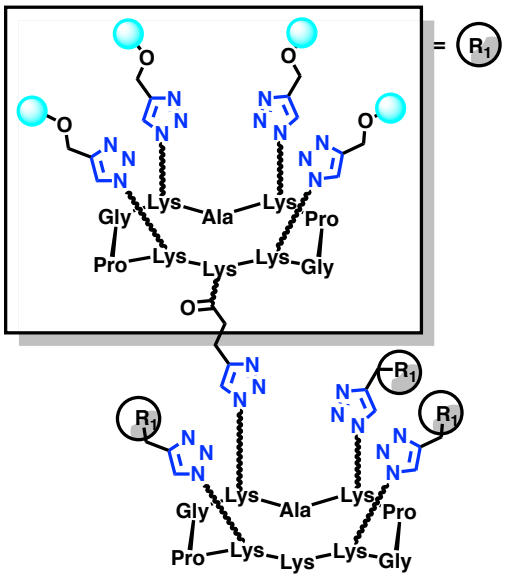

$C_{399}H_{630}N_{177}O_{178}$

Mw: 9432.52 g/mol

Prepared according general procedure **E** from **51** (11.0 mg, 5.3 µmol) and R(N$_3$)$_4$ **5** (1.4 mg, 1.20 µmol). The crude mixture was purified to afford the title compound as a white fluffy solid after lyophilization (7.7 mg, 0.82 µmol, 68%). HRMS (ESI$^+$-TOF) m/z: calculated for $C_{399}H_{630}N_{177}O_{178}$ $[M+5H]^{5+}$: 1887.5035, found 1887.5156; RP-HPLC: R_t = 8.37 min (C_{18}, λ = 214 nm, 0-30% B in 15 min).

N$_3$-RR(β-D-Gal)$_{16}$ **53**

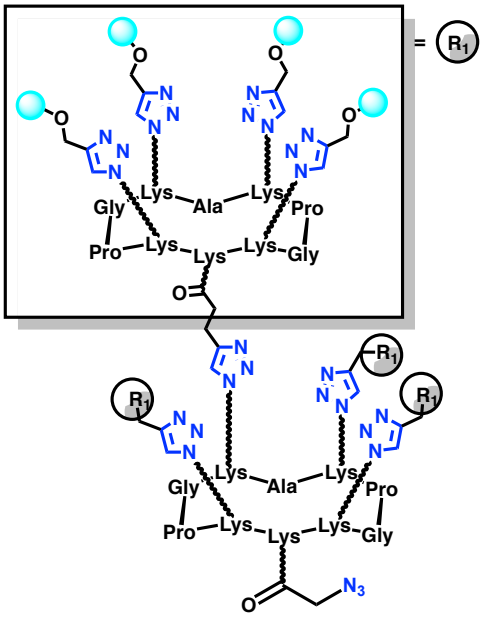

$C_{401}H_{631}N_{118}O_{151}$

Mw: 9510.53 g/mol

Prepared according general procedure **H** from **52** (7.0 mg, 0.74 µmol) and azidoacetic acid succinimide ester **27** (0.2 mg, 1.1 µmol). The crude mixture was purified to afford the title compound as a white fluffy solid after lyophilization (6.6 mg, 0.69 µmol, 93%). HRMS (ESI$^+$-TOF) m/z: calculated for $C_{401}H_{631}N_{118}O_{151}$ $[M+5H]^{5+}$: 1903.1059, found 1903.1151; RP-HPLC: R_t = 7.87 min (C_{18}, λ = 214 nm, 5-40% B in 15 min).

R(α-D-Gal)$_4$ **54**

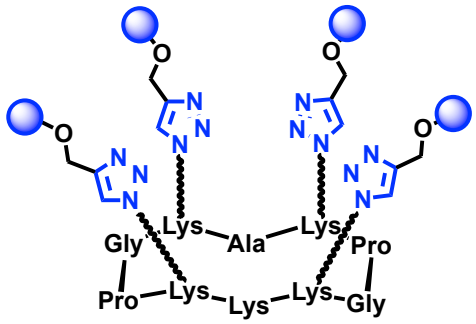

Prepared according general procedure **E** from propargyl α-D-galactopyranoside **30** (9.0 mg, 41.2 µmol) and R(N$_3$)$_4$ **5** (10.5 mg, 9.4 µmol). The crude mixture was purified to afford the title compound as a white fluffy solid after lyophilization (15.0 mg, 7.5 µmol, 80%). HRMS (ESI$^+$-TOF) m/z: calculated for $C_{83}H_{135}N_{23}O_{34}$ $[M+2H]^{2+}$: 998.9765, found 998.9770; RP-HPLC: R_t = 8.81 min (C_{18}, λ = 214 nm, 0-20% B in 15 min).

$C_{83}H_{133}N_{23}O_{34}$

Mw: 1995.95 g/mol

Alk-R(α-D-Gal)$_4$ **55**

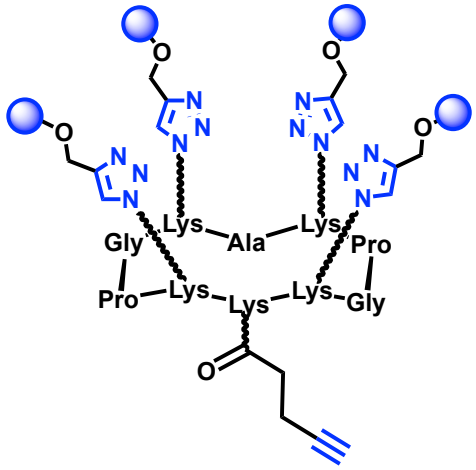

Prepared according general procedure **H** from **54** (15.0 mg, 7.51 µmol) and pentynoic acid succinimide ester **26** (2.2 mg, 11.30 µmol). The crude mixture was purified to afford the title compound as a white fluffy solid after lyophilization (15.0 mg, 7.22 µmol, 96%). HRMS (ESI$^+$-TOF) m/z: calculated for $C_{88}H_{139}N_{23}O_{35}$ $[M+2H]^{2+}$: 1038.9896, found 1038.9937; RP-HPLC: R_t = 9.18 min (C_{18}, λ = 214 nm, 0-30% B in 15 min).

$C_{88}H_{139}N_{23}O_{35}$

Mw: 2075.97 g/mol

RR(α-D-Gal)$_{16}$ **56**

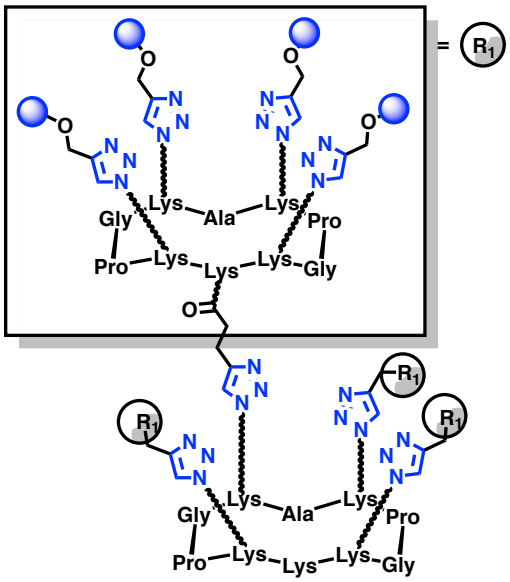

Prepared according general procedure **E** from **55** (15.0 mg, 7.22 µmol) and R(N$_3$)$_4$ **5** (1.8 mg, 1.64 µmol). The crude mixture was purified to afford the title compound as a white fluffy solid after lyophilization (9.1 mg, 0.96 µmol, 59%). HRMS (ESI$^+$-TOF) m/z: calculated for $C_{399}H_{630}N_{177}O_{178}$ $[M+5H]^{5+}$: 1887.5035, found 1887.5156; RP-HPLC: R_t = 8.63 min (C_{18}, λ = 214 nm, 0-40% B in 15 min).

$C_{399}H_{630}N_{177}O_{178}$

Mw: 9432.52 g/mol

N$_3$-RR(α-D-Gal)$_{16}$ **57**

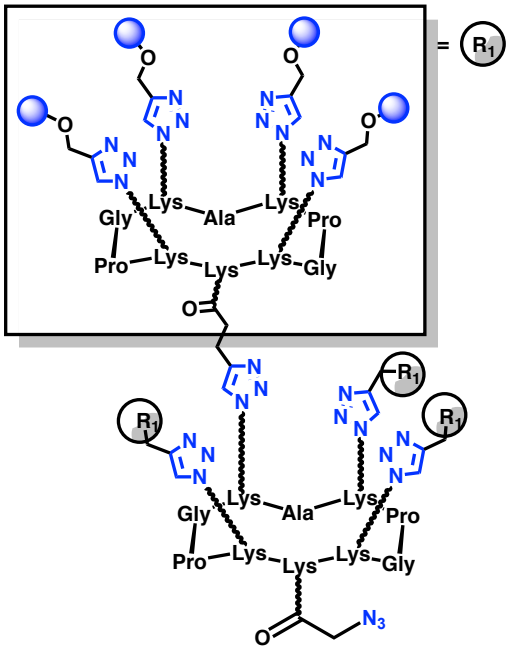

Prepared according general procedure **H** from **56** (9.0 mg, 0.95 µmol) and azidoacetic acid succinimide ester **27** (0.2 mg, 1.4 µmol). The crude mixture was purified to afford the title compound as a white fluffy solid after lyophilization (8.6 mg, 0.91 µmol, 96%). HRMS (ESI$^+$-TOF) m/z: calculated for $C_{401}H_{631}N_{118}O_{151}$ $[M+5H]^{5+}$: 1903.1059, found 1903.1151; RP-HPLC: R_t = 7.64 min (C_{18}, λ = 214 nm, 5-40% B in 15 min).

$C_{399}H_{630}N_{177}O_{178}$

Mw: 9432.52 g/mol

V.1.D.IV. Tumoral Binding Modules (TBMs)

R(cRGD)$_4$ **58**

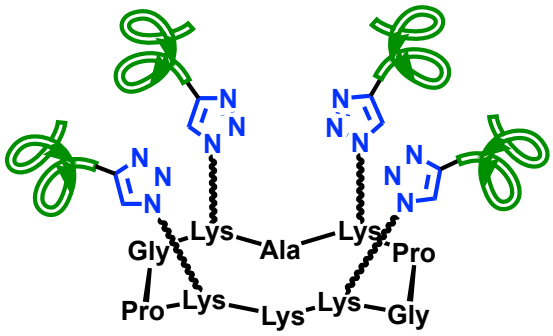

$C_{175}H_{257}N_{59}O_{42}$

Mw: 3857.01 g/mol

Prepared according general procedure **F** from Alk-cRGD **17** (41.9 mg, 61.0 µmol) and R$(N_3)_4$ **5** (14.8 mg, 13.0 µmol). The crude mixture was purified to afford the title compound as a white fluffy solid after lyophilization (32.1 mg, 8.3 µmol, 64%). HRMS (ESI$^+$-TOF) m/z: calculated for $C_{175}H_{261}N_{59}O_{42}$ $[M+4H]^{4+}$: 965.2525, found: 965.2523; RP-HPLC: R_t = 7.69 min (C_{18}, λ = 214 nm, 5-60% B in 15 min).

Alk-R(cRGD)$_4$ **59**

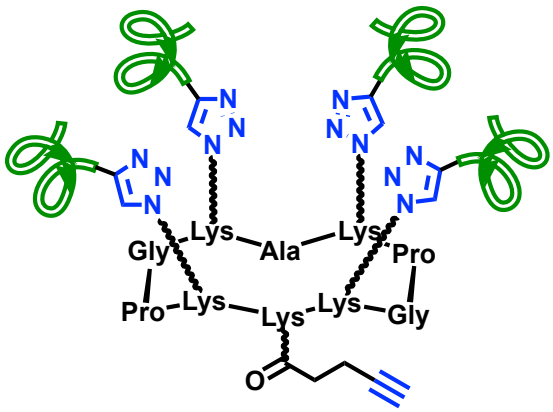

$C_{180}H_{261}N_{59}O_{43}$

Mw: 3937.01 g/mol

Prepared according general procedure **H** from **58** (50.78 mg, 13.0 µmol) and pentynoic acid succinimide ester **26** (5.1 mg, 26.0 µmol). The crude mixture was purified to afford the title compound as a white fluffy solid after lyophilization (48.4 mg, 12.3 µmol, 94%). HRMS (ESI$^+$-TOF) m/z: calculated for $C_{180}H_{265}N_{59}O_{43}$ $[M+4H]^{4+}$: 985.2585, found 985.2585; RP-HPLC: R_t = 8.53 min (C_{18}, λ = 214 nm, 5-60% B in 15 min).

D(cRGD)$_4$ **60**

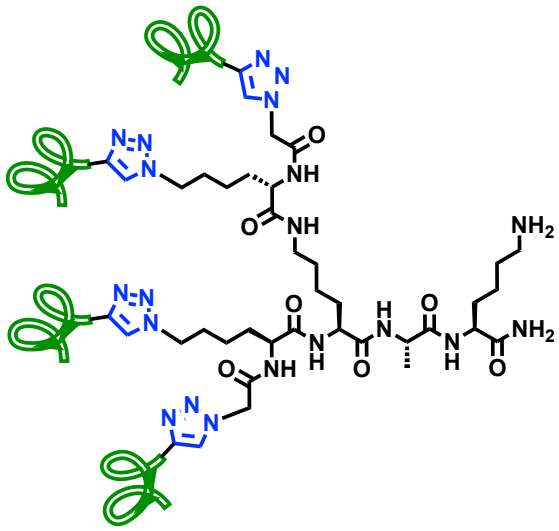

$C_{159}H_{234}N_{56}O_{39}$

Mw: 3551.80 g/mol

Prepared according general procedure **F** from Alk-cRGD **17** (3.8 mg, 5.6 µmol) and D(N_3)$_4$ **8** (1.0 mg, 1.2 µmol). The crude mixture was purified to afford the title compound as a white fluffy solid after lyophilization (3.2 mg, 0.9 µmol, 75%). MALDI-ToF m/z: calculated for $C_{159}H_{235}N_{56}O_{39}$ $[M+H]^+$: 3552.805, found 3552.720 ; RP-HPLC: R_t = 7.51 min (C_{18}, λ = 214 nm, 5-60% B in 15 min).

Alk-D(cRGD)$_4$ **61**

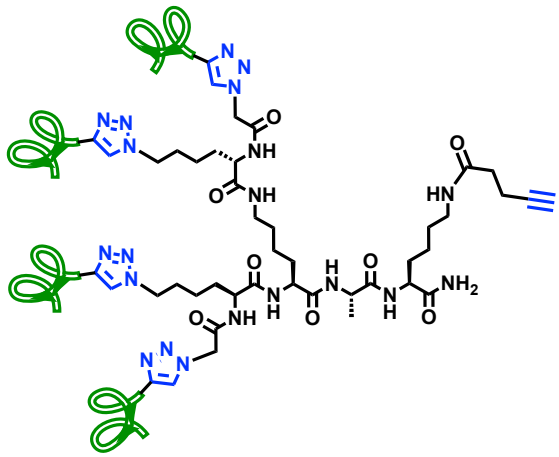

$C_{164}H_{238}N_{56}O_{40}$

Mw: 3631.85 g/mol

Prepared according general procedure **H** from **60** (6 mg, 1.7 µmol) and pentynoic acid succinimide ester **26** (0.5 mg, 2.5 µmol). The crude mixture was purified to afford the title compound as a white fluffy solid after lyophilization (6 mg, 1.6 µmol, 97%). HRMS (ESI$^+$-TOF) m/z: calculated for $C_{164}H_{241}N_{56}O_{40}$ $[M+3H]^{3+}$: 1211.6176, found 1211.6202; RP-HPLC: R_t = 8.46 min (C_{18}, λ = 214 nm, 5-60% B in 15 min).

$R(LT)_4$ **62**

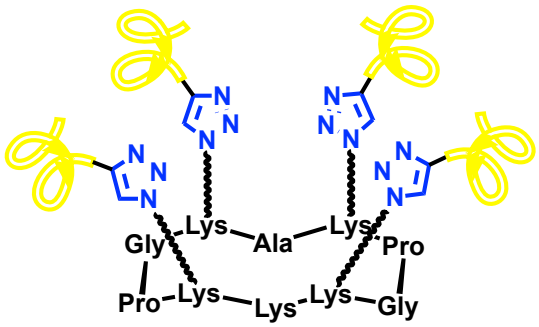

Prepared according general procedure **F** from Alk-LT **21** (35.0 mg, 46.0 µmol) and $R(N_3)_4$ **5** (11.7 mg, 10.0 µmol). The crude mixture was purified to afford the title compound as a white fluffy solid after lyophilization (15.8 mg, 3.8 µmol, 38%). HRMS (ESI$^+$-TOF) m/z: calculated for $C_{191}H_{333}N_{63}O_{42}$ $[M+4H]^{4+}$: 1046.4002, found: 1046.5100; RP-HPLC: R_t = 13.01 min (C_{18}, λ = 214 nm, 5-60% B in 15 min).

$C_{191}H_{333}N_{63}O_{42}$

Mw: 4181.61 g/mol

Alk-$R(LT)_4$ **63**

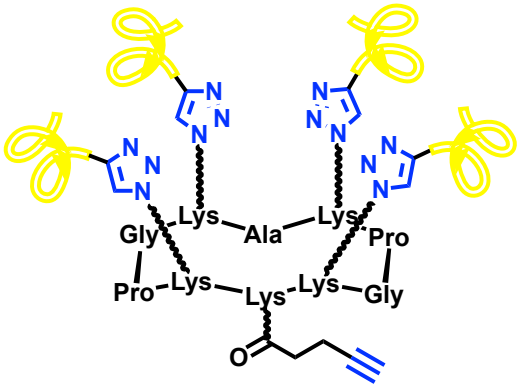

Prepared according general procedure **H** from **62** (15.8 mg, 3.8 µmol) and pentynoic acid succinimide ester **26** (1.1 mg, 5.6 µmol). The crude mixture was purified to afford the title compound as a white fluffy solid after lyophilization (8.4 mg, 1.9 µmol, 52%). HRMS (ESI$^+$-TOF) m/z: calculated for $C_{196}H_{341}N_{63}O_{43}$ $[M+4H]^{4+}$: 1066.4103, found 1066.4102; RP-HPLC: R_t = 13.61 min (C_{18}, λ = 214 nm, 5-60% B in 15 min).

$C_{196}H_{337}N_{63}O_{43}$

Mw: 4261.60 g/mol

R(β-D-Glc)$_4$ **65**

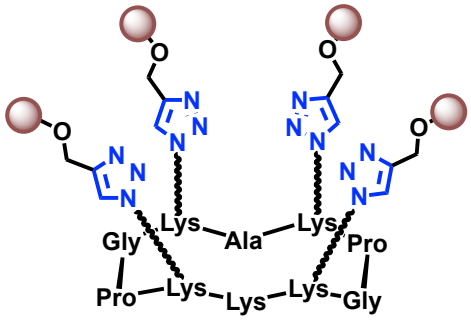

$C_{83}H_{133}N_{23}O_{30}$

Mw: 1995.95 g/mol

Prepared according general procedure **E** from propargyl β-D-Glucose **64** (91.95 mg, 421 µmol) and R$(N_3)_4$ **5** (107.6 mg, 95 µmol). The crude mixture was purified to afford the title compound as a white fluffy solid after lyophilization (160.0 mg, 80 µmol, 84%). HRMS (ESI$^+$-TOF) m/z: calculated for $C_{83}H_{135}N_{23}O_{30}$ $[M+2H]^{2+}$: 998.9765, found 998.9760; RP-HPLC: R_t = 5.52 min (C_{18}, λ = 214 nm, 5-30% B in 15 min).

Alk-R(β-D-Glc)$_4$ **66**

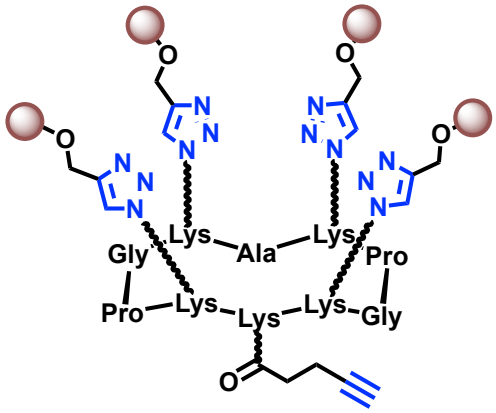

$C_{88}H_{137}N_{23}O_{35}$

Mw: 2075.98 g/mol

Prepared according general procedure **H** from **65** (31.3 mg, 15.7 µmol) and pentynoic acid succinimide ester **26** (6.1 mg, 31.4 µmol). The crude mixture was purified to afford the title compound as a white fluffy solid after lyophilization (30.9 mg, 14.8 µmol, 95%). HRMS (ESI$^+$-TOF) m/z: calculated for $C_{88}H_{139}N_{23}O_{35}$ $[M+2H]^{2+}$: 1038.9896, found 1038.9894; RP-HPLC: R_t = 7.65 min (C_{18}, λ = 214 nm, 5-30% B in 15 min).

R[Ac-HVH(Alloc)]$_4$ **67**

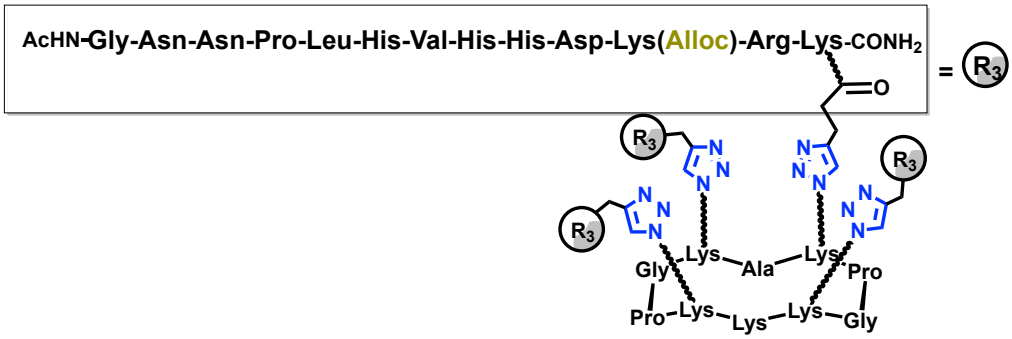

$C_{355}H_{545}N_{131}O_{94}$
Mw: 8147.20
g/mol

Prepared according general procedure **F** from Alk-[Ac-HVH(Alloc)] **25** (58.6 mg, 33.0 µmol) and R$(N_3)_4$ **5** (7.8 mg, 7.0 µmol). The reaction was stirred for 3 days. The crude mixture was purified to afford the title compound as a white fluffy solid after lyophilization (35.0 mg, 42.9 µmol, 61%). MALDI-ToF m/z: calculated for $C_{355}H_{550}N_{131}O_{94}$ $[M+5H]^{5+}$: 8152.200, found 8152.484; RP-HPLC: R_t = 7.20 min (C_{18}, λ = 214 nm, 5-60% B in 15 min).

Alk-R[Ac-HVH(Alloc)]$_4$ **68**

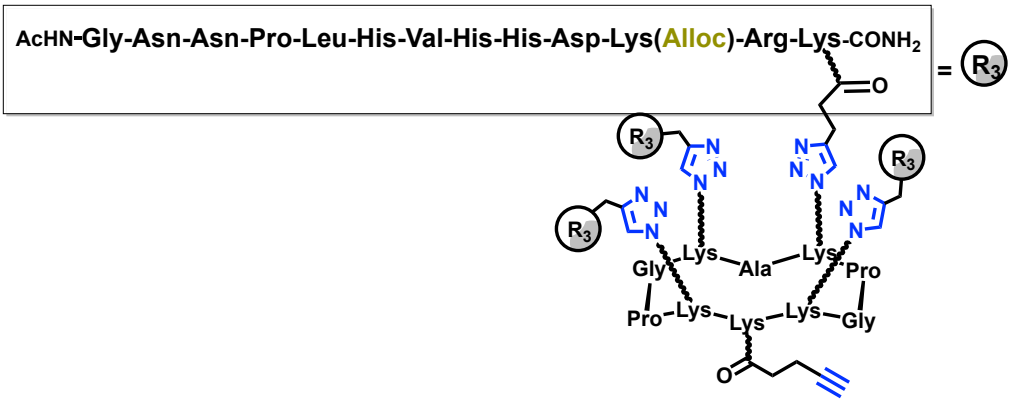

$C_{360}H_{549}N_{131}O_{95}$
Mw: 8227.20
g/mol

Prepared according general procedure **H** from **67** (20.3 mg, 2.5 µmol) and pentynoic acid succinimide ester **26** (1.0 mg, 5.0 µmol). The crude mixture was purified to afford the title compound as a white fluffy solid after lyophilization (16.1 mg, 2.0 µmol, 78%). MALDI-ToF m/z: calculated for $C_{360}H_{553}N_{131}O_{95}$ $[M+4H]^{4+}$: 8231.200, found 8231.718; RP-HPLC: R_t = 7.33 min (C_{18}, λ = 214 nm, 5-60% B in 15 min).

Alk-R[Ac-HVH]$_4$ **69**

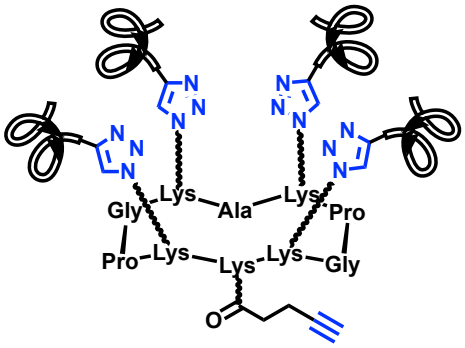

$C_{344}H_{533}N_{131}O_{87}$

Mw: 7891.10 g/mol

Prepared according general procedure **D2** from **68** (32.9 mg, 4.0 µmol) in 50 mL dry DMF, $PhSiH_3$ (50.0 µL, 400.0 µmol) and $Pd(PPh_3)_4$ (7.0 mg, 6 µmol), under Argon. After 6 hours, MeOH (5 mL) was added and the mixture stirred for 1 hour. The Alloc-deprotected product **69**, which was filtrated and dried under vacuum, was purified to afford the title compound as a white fluffy solid after lyophilization (10.2 mg, 1.3 µmol, 32%) MALDI-ToF m/z: calculated for $C_{344}H_{533}N_{131}O_{87}Na$ $[M+Na]^+$: 7914.120, found 7913.889; RP-HPLC: R_t = 5.90 min (C_{18}, λ = 214 nm, 5-60% B in 15 min).

V.1.D.V. Antibody Recruiting Molecules (ARMs)

ARM **70** (R-R)

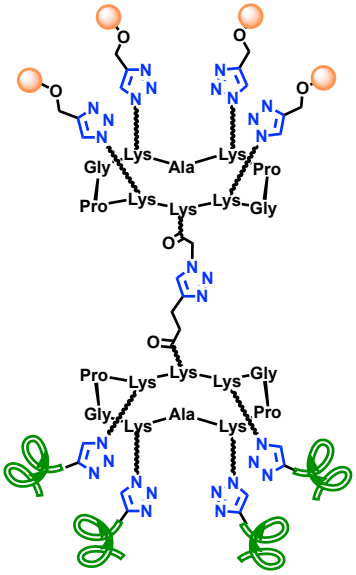

Prepared according general procedure **G** from **33** (5.1 mg, 2.5 µmol) and **59** (9.8 mg, 2.5 µmol). The crude mixture was purified to afford the title compound as a white fluffy solid after lyophilization (12.9 mg, 2.2 µmol, 86%). HRMS (ESI$^+$-TOF) m/z: calculated for $C_{265}H_{398}N_{85}O_{74}$ $[M+3H]^{3+}$: 1984.9992, found 1985.0065; RP-HPLC: R_t = 7.72 min (C_{18}, λ = 214 nm, 5-60% B in 15 min).

$C_{265}H_{395}N_{85}O_{74}$

Mw: 5951.99 g/mol

ARM **71** (RR-R)

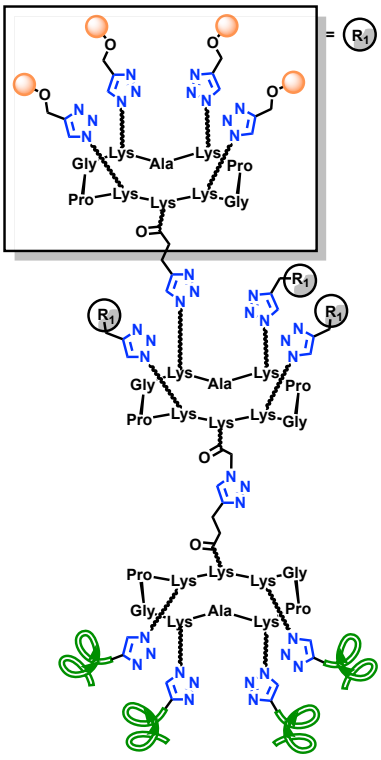

Prepared according general procedure **G** from **40** (7.2 mg, 0.78 µmol) and **59** (3.1 mg, 0.78 µmol). The crude mixture was purified to afford the title compound as a white fluffy solid after lyophilization (12.9 mg, 0.60 µmol, 78%). HRMS (ESI$^+$-TOF) m/z: calculated for $C_{581}H_{887}N_{177}O_{178}$ $[M+7H]^{7+}$: 1885.5187, found 1885.6754; RP-HPLC: R_t = 4.90 min (C_{18}, λ = 214 nm, 5-100% B in 15 min).

$C_{581}H_{880}N_{177}O_{178}$

Mw: 13191.63 g/mol

ARM **72** (RR-D)

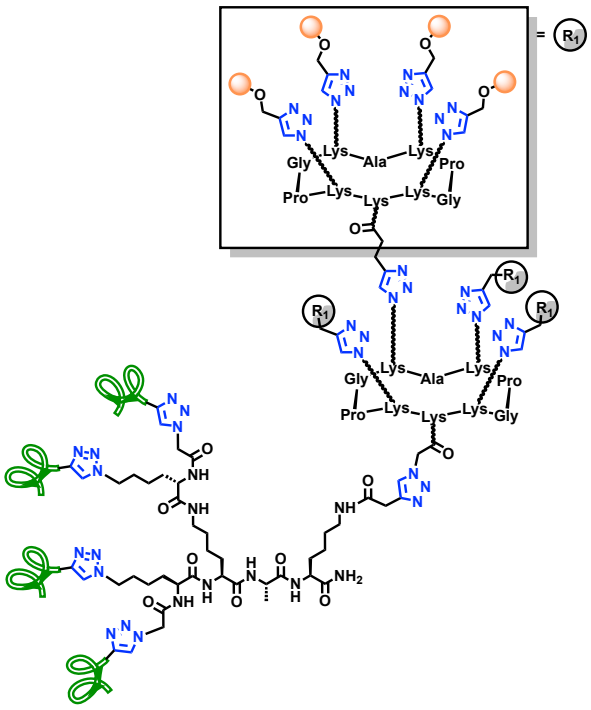

Prepared according general procedure **G** from **40** (9.7 mg, 1.0 µmol) and **61** ((3.8 mg, 1.0 µmol). The crude mixture was purified to afford the title compound as a white fluffy solid after lyophilization (7.0 mg, 0.54 µmol, 54%). MALDI-ToF m/z: calculated for $C_{565}H_{865}N_{174}O_{175}$ $[M+H]^+$: 12887.4057, found 12887.0090; RP-HPLC: R_t = 7.49 min (C_{18}, λ = 214 nm, 5-60% B in 15 min).

$C_{565}H_{864}N_{174}O_{175}$

Mw: 12886.41 g/mol

ARM **73** (DR-R)

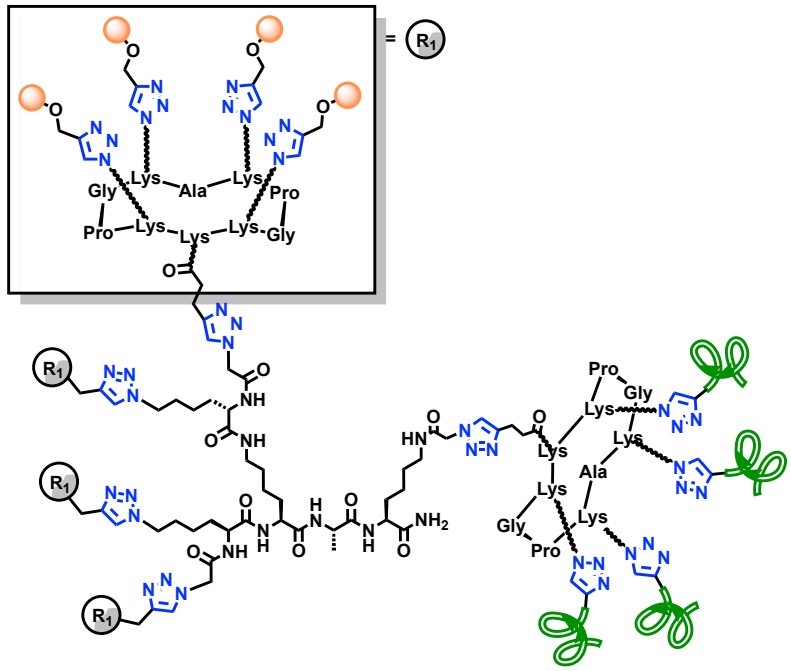

Prepared according general procedure **G** from **40** (9.7 mg, 1.0 µmol) and **61** ((3.8 mg, 1.0 µmol). The crude mixture was purified to afford the title compound as a white fluffy solid after lyophilization (7.0 mg, 0.54 µmol, 54%). MALDI-ToF m/z: calculated for $C_{565}H_{865}N_{174}O_{175}$ $[M+H]^+$: 12887.4057, found 12887.0090; RP-HPLC: R_t = 7.49 min (C_{18}, λ = 214 nm, 5-60% B in 15 min).

$C_{565}H_{864}N_{174}O_{175}$

Mw: 12886.41 g/mol

ARM **74** (RD-R)

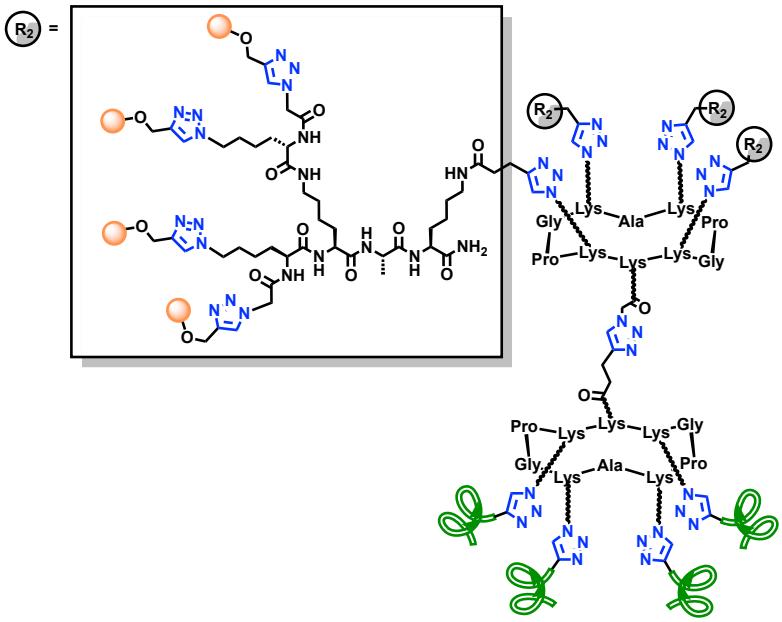

Prepared according general procedure **G** from **46** (2.4 mg, 0.3 µmol) and **59** (1.2 mg, 0.3 µmol). The crude mixture was purified to afford the title compound as a white fluffy solid after lyophilization (2.0 mg, 0.16 µmol, 56%). HRMS (ESI$^+$-TOF) m/z: calculated for $C_{517}H_{795}N_{165}O_{166}$ $[M+6H]^{6+}$: 1996.9902, found 1996.9913; RP-HPLC: R_t = 5.30 min (C_{18}, λ = 214 nm, 5-100% B in 15 min).

$C_{517}H_{789}N_{165}O_{166}$

Mw: 11975.94 g/mol

ARM **75** (DD-R)

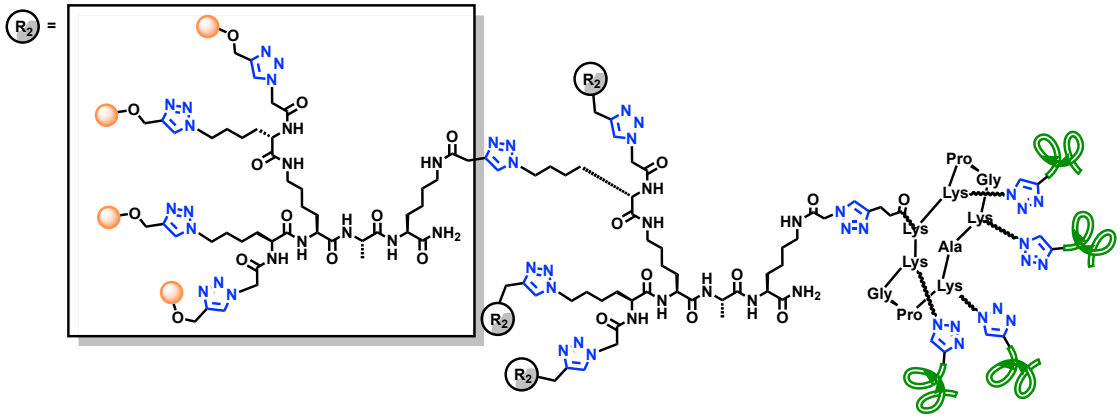

$C_{501}H_{766}N_{162}O_{163}$

Mw: 11670.77 g/mol

Prepared according general procedure **G** from **48** (3.5 mg, 0.45 µmol) and **59** (1.8 mg, 0.45 µmol). The crude mixture was purified to afford the title compound as a white fluffy solid after lyophilization (4.1 mg, 0.35 µmol, 78%). HRMS (ESI$^+$-TOF) m/z: calculated for $C_{501}H_{772}N_{162}O_{163}$ $[M+6H]^{6+}$: 1946.1279, found 1946.2959; RP-HPLC: R_t = 5.31 min (C_{18}, λ = 214 nm, 5-100% B in 15 min).

ARM **76** (R-R PEG)

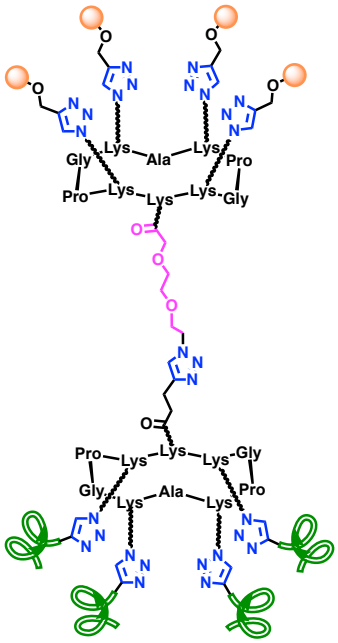

Prepared according general procedure **G** from **35** (4.1 mg, 1.9 µmol) and **59** (7.7 mg, 1.9 µmol). The crude mixture was purified to afford the title compound as a white fluffy solid after lyophilization (10 mg, 1.6 µmol, 87%). HRMS (ESI$^+$-TOF) m/z: calculated for $C_{269}H_{407}N_{85}O_{76}$ $[M+4H]^{4+}$: 1511.0143, found 1511.7819; RP-HPLC: R_t = 5.49 min (C_{18}, λ = 214 nm, 5-100% B in 15 min).

$C_{269}H_{403}N_{85}O_{76}$

Mw: 6040.01 g/mol

ARM **77** (RR-R PEG)

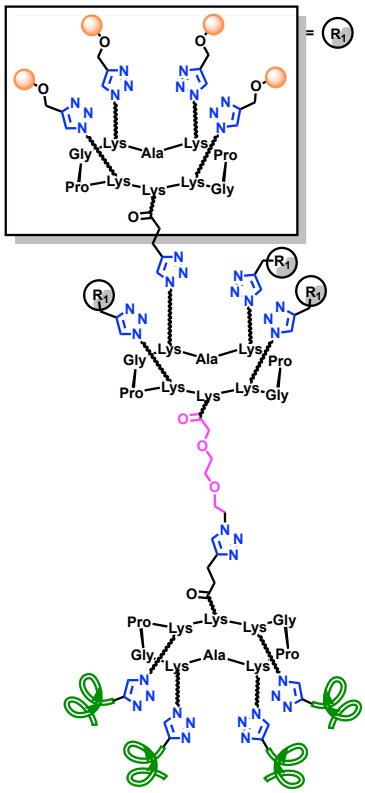

Prepared according general procedure **G** from **42** (5.2 mg, 0.5 µmol) and **59** (2.2 mg, 0.5µmol). The crude mixture was purified to afford the title compound as a white fluffy solid after lyophilization (5.1 mg, 0.38 µmol, 77%). HRMS (ESI$^+$-TOF) m/z: calculated for $C_{585}H_{895}N_{177}O_{180}$ $[M+7H]^{7+}$: 1898.9571, found 1899.1003; RP-HPLC: R_t = 5.30 min (C_{18}, λ = 214 nm, 5-100% B in 15 min).

$C_{585}H_{888}N_{177}O_{180}$

Mw: 13285.70 g/mol

ARM **78** (R-c)

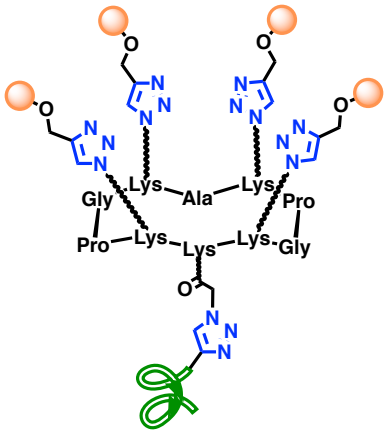

Prepared according general procedure **G** from **33** (7.6 mg, 3.7 µmol) and Alk-cRGD **17** (3.1 mg, 4.5 µmol). The crude mixture was purified to afford the title compound as a white fluffy solid after lyophilization (8.0 mg, 2.9 µmol, 80%). HRMS (ESI$^+$-TOF) m/z: calculated for $C_{117}H_{181}N_{39}O_{35}$ $[M+2H]^{2+}$: 1350.1622, found 1350.1652; RP-HPLC: R_t = 6.51 min (C_{18}, λ = 214 nm, 5-60% B in 15 min).

$C_{117}H_{179}N_{39}O_{35}$

Mw: 2698.32 g/mol

ARM **79** (RR-c)

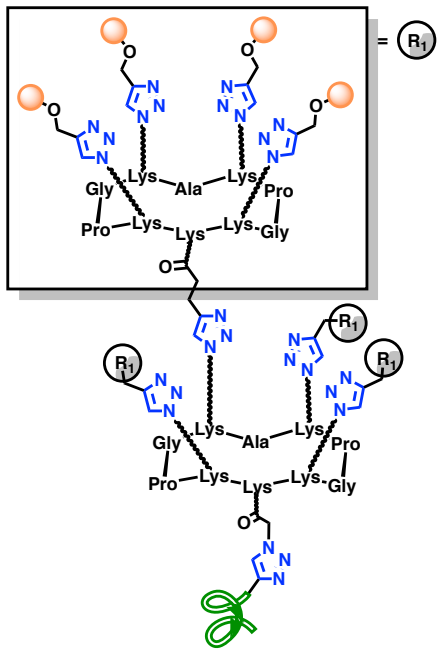

Prepared according general procedure **G** from **40** (3.0 mg, 0.3 µmol) and Alk-cRGD **17** (0.2 mg, 0.3 µmol). The crude mixture was purified to afford the title compound as a white fluffy solid after lyophilization (2.7 mg, 0.27 µmol, 85%). MALDI-ToF m/z: calculated for $C_{433}H_{677}N_{127}O_{143}$ $[M+H]^{1+}$: 9938.90, found 9944.18; RP-HPLC: R_t = 6.71 min (C_{18}, λ = 214 nm, 5-60% B in 15 min).

$C_{433}H_{671}N_{127}O_{143}$

Mw: 9937.90 g/mol

ARM **80** (D-R)

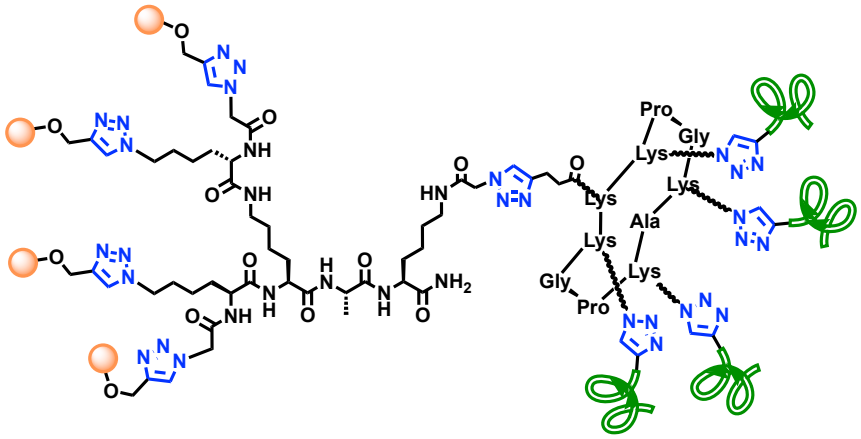

$C_{249}H_{372}N_{82}O_{71}$

Mw: 5646.80 g/mol

Prepared according general procedure **G** from **37** (1.1 mg, 0.6 µmol) and **59** (1.7 mg, 0.5 µmol). The crude mixture was purified to afford the title compound as a white fluffy solid after lyophilization (1.4 mg, 0.25 µmol, 50%). HRMS (ESI$^+$-TOF) m/z: calculated for $C_{249}H_{372}N_{82}O_{71}$ $[M+3H]^{3+}$: 1883.2666, found 1883.2670; RP-HPLC: R_t = 7.96 min (C_{18}, λ = 214 nm, 5-60% B in 15 min).

ARM **81** (R-R (ß-D-Gal))

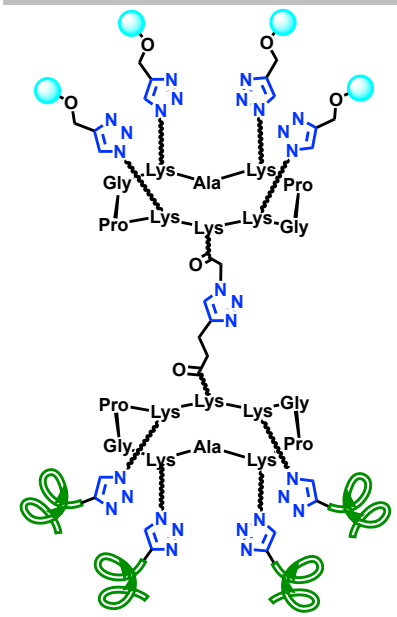

Prepared according general procedure **G** from **50** (0.7 mg, 0.3 µmol) and **59** (1.1 mg, 0.3 µmol). The crude mixture was purified to afford the title compound as a white fluffy solid after lyophilization (1.4 mg, 0.23 µmol, 78%). HRMS (ESI$^+$-TOF) m/z: calculated for $C_{265}H_{399}N_{85}O_{78}$ $[M+4H]^{4+}$: 1504.9962, found 1505.7482; RP-HPLC: R_t = 7.72 min (C_{18}, λ = 214 nm, 5-60% B in 15 min).

$C_{265}H_{395}N_{85}O_{78}$

Mw: 6015.98 g/mol

ARM **82** (RR-R (ß-D-Gal))

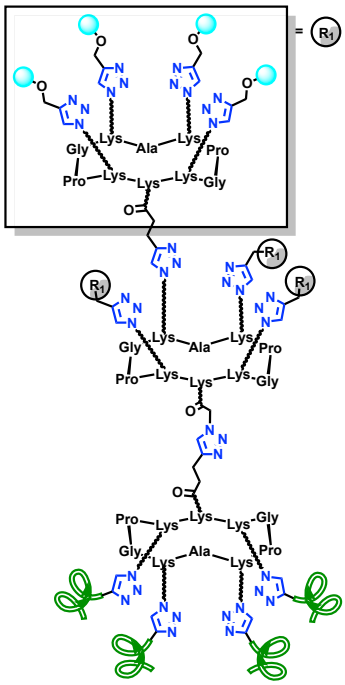

Prepared according general procedure **G** from **53** (6.2 mg, 0.65 µmol) and **59** (2.6 mg, 0.65 µmol). The crude mixture was purified to afford the title compound as a white fluffy solid after lyophilization (6.9 mg, 0.51 µmol, 78%). HRMS (ESI$^+$-TOF) m/z: calculated for $C_{581}H_{887}N_{177}O_{194}$ $[M+7H]^{7+}$: 1922.0785, found 1922.0818; RP-HPLC: R_t = 7.16 min (C_{18}, λ = 214 nm, 5-40% B in 15 min).

$C_{581}H_{880}N_{177}O_{194}$

Mw: 13447.55 g/mol

ARM **83** (RR-R (α-D-Gal))

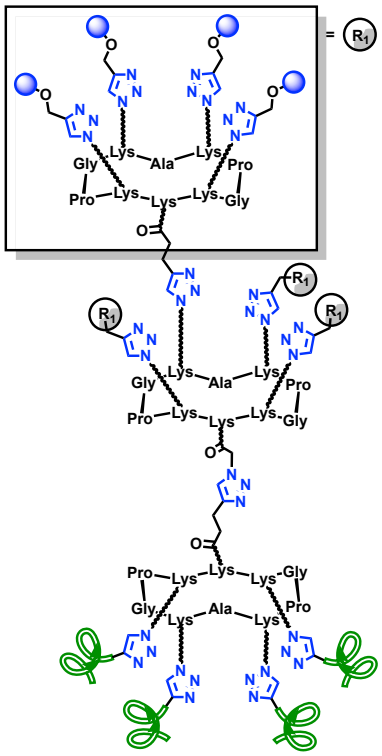

Prepared according general procedure **G** from **57** (8.6 mg, 0.91 µmol) and **59** (3.6 mg, 0.91 µmol). The crude mixture was purified to afford the title compound as a white fluffy solid after lyophilization (8.9 mg, 0.66 µmol, 73%). HRMS (ESI$^+$-TOF) m/z: calculated for $C_{581}H_{887}N_{177}O_{194}$ $[M+7H]^{7+}$: 1922.0785, found 1922.9500; RP-HPLC: R_t = 7.16 min (C_{18}, λ = 214 nm, 5-60 % B in 15 min).

$C_{581}H_{880}N_{177}O_{194}$

Mw: 13447.55 g/mol

ARM **85** (R-I (LT))

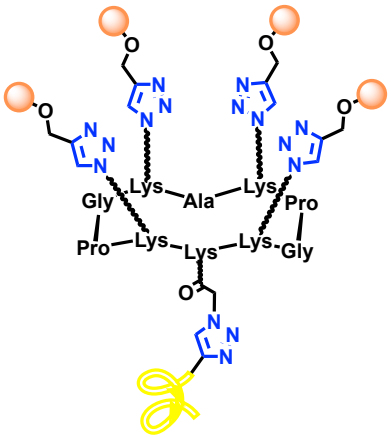

Prepared according general procedure **G** from **33** (9.4 mg, 4.6 µmol) and **21** (3.8 mg, 4.9 µmol). The crude mixture was purified to afford the title compound as a white fluffy solid after lyophilization (9.0 mg, 3.2 µmol, 70%). HRMS (ESI$^+$-TOF) m/z: calculated for $C_{121}H_{200}N_{39}O_{36}$ $[M+2H]^{2+}$: 1390.7381, found 1390.7389; RP-HPLC: R_t = 9.87 min (C_{18}, λ = 214 nm, 5-60% B in 15 min).

$C_{121}H_{198}N_{39}O_{36}$

Mw: 2779.47 g/mol

ARM **86** (RR-I (LT))

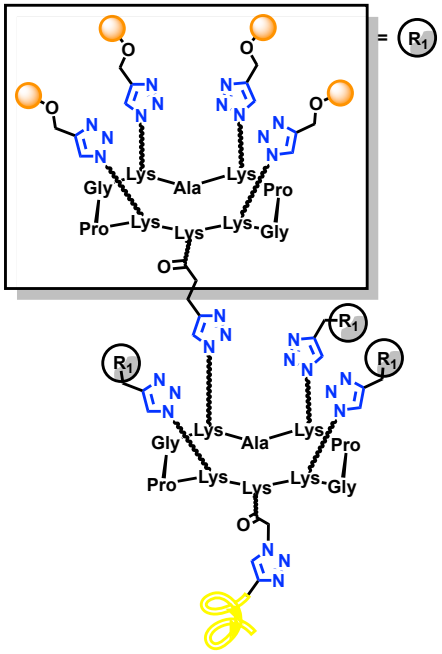

Prepared according general procedure **G** from **40** (4.5 mg, 0.5 µmol) and **21** (0.4 mg, 0.5 µmol). The crude mixture was purified to afford the title compound as a white fluffy solid after lyophilization (4.0 mg, 0.4 µmol, 83%). HRMS (ESI$^+$-TOF) m/z: calculated for $C_{437}H_{696}N_{128}O_{143}$ $[M+6H]^{6+}$: 1671.6872, found 1671.6887; RP-HPLC: R_t = 5.91 min (C_{18}, λ = 214 nm, 5-100% B in 15 min).

$C_{437}H_{690}N_{128}O_{143}$

Mw: 10019.06 g/mol

ARM **87** (RR-R (LT))

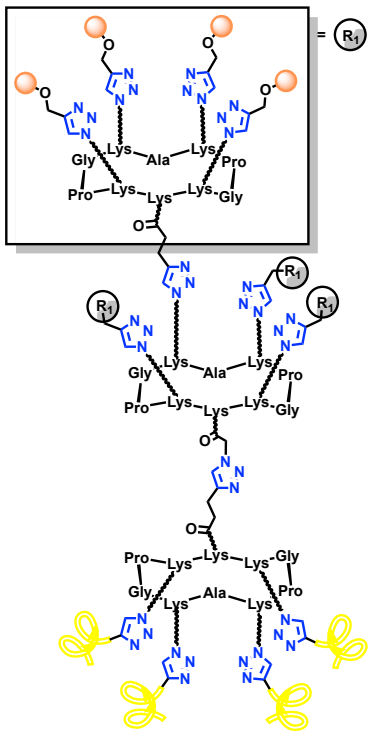

Prepared according general procedure **G** from **40** (6.6 mg, 0.71 µmol) and **63** (3.05 mg, 0.71 µmol). The crude mixture was purified to afford the title compound as a white fluffy solid after lyophilization (3.0 mg, 0.22 µmol, 31%). MALDI-ToF m/z: calculated for $C_{597}H_{964}N_{181}O_{178}$ $[M+H]^+$: 13517.190, found 13516.606; RP-HPLC: R_t = 12.20 min (C_{18}, λ = 214 nm, 5-60% B in 15 min).

$C_{597}H_{963}N_{181}O_{178}$

Mw: 13516.190 g/mol

ARM **88** (R-g (ß-D-Glc))

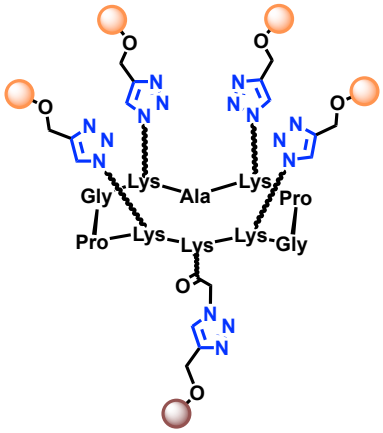

Prepared according general procedure **G** from **33** (6.0 mg, 3.0 µmol) and propargyl β-D-Glucose **64** (0.7 mg, 3.0 µmol). The crude mixture was purified to afford the title compound as a white fluffy solid after lyophilization (5.0 mg, 2.2 µmol, 75%). HRMS (ESI^+-TOF) m/z: calculated for $C_{194}H_{150}N_{26}O_{37}$ $[M+2H]^{2+}$: 1117.5322, found 1117.5320; RP-HPLC: R_t = 5.13 min (C_{18}, λ = 214 nm, 5-60% B in 15 min).

$C_{194}H_{148}N_{26}O_{37}$

Mw: 2233.06 g/mol

ARM **89** (R-R (ß-D-Glc))

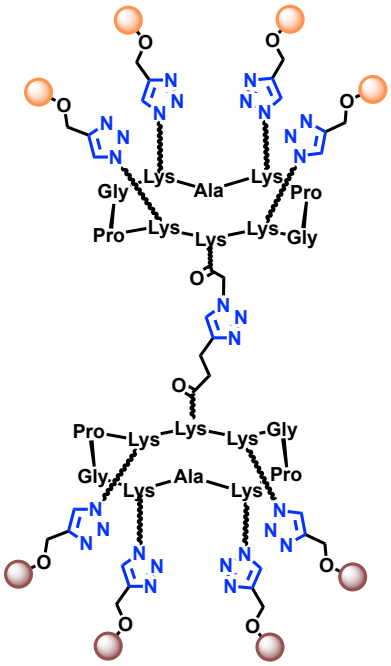

Prepared according general procedure **G** from **33** (7.4 mg, 3.6 µmol) and **66** (7.6 mg, 3.6 µmol). The crude mixture was purified to afford the title compound as a white fluffy solid after lyophilization (13.6 mg, 3.3 µmol, 88%). HRMS (ESI$^+$-TOF) m/z: calculated for $C_{173}H_{271}N_{49}O_{66}$ $[M+3H]^{3+}$: 1364.6525, found 1365.3210; RP-HPLC: R_t = 4.04 min (C_{18}, λ = 214 nm, 5-100% B in 15 min).

$C_{173}H_{271}N_{49}O_{66}$

Mw: 4090.96 g/mol

ARM **90** (RR-R (ß-D-Glc))

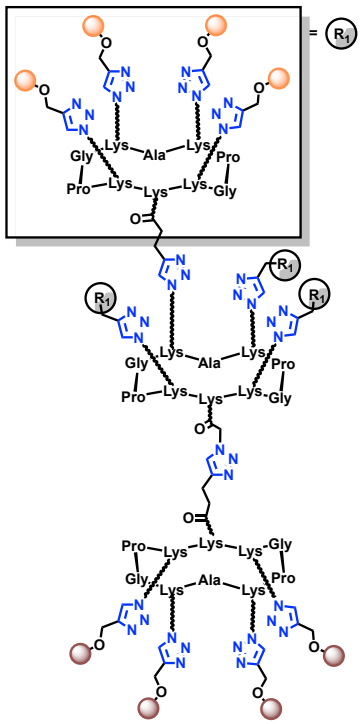

Prepared according general procedure **G** from **40** (7.7 mg, 0.8 µmol) and **66** (1.7 mg, 0.8 µmol). The crude mixture was purified to afford the title compound as a white fluffy solid after lyophilization (7.9 mg, 0.7 µmol, 87%). HRMS (ESI$^+$-TOF) m/z: calculated for $C_{489}H_{769}N_{141}O_{170}$ $[M+6H]^{6+}$: 1890.2662, found 1890.4332; RP-HPLC: R_t = 4.63 min (C_{18}, λ = 214 nm, 5-100% B in 15 min).

$C_{489}H_{763}N_{141}O_{170}$

Mw: 11330.54 g/mol

ARM **91** (R-h (HVH))

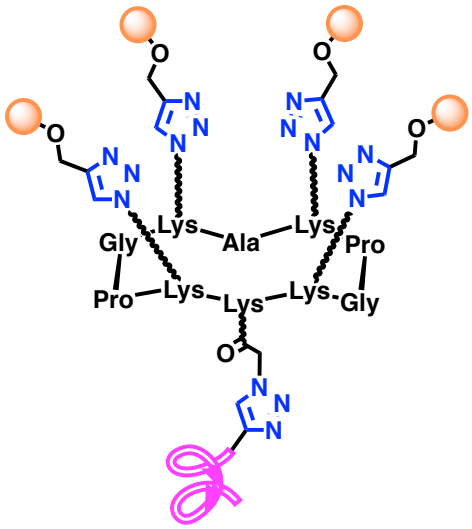

Prepared according general procedure **G** from **33** (7.1 mg, 3.5 µmol) and Alk-HVH **23** (5.7 mg, 3.5 µmol). The crude mixture was purified to afford the title compound as a white fluffy solid after lyophilization (6.5 mg, 1.8 µmol, 51%). MALDI-ToF m/z: calculated for $C_{156}H_{246}N_{53}O_{49}$ $[M+H]^+$: 3645.804, found 3646.434; RP-HPLC: R_t = 4.19 min (C_{18}, λ = 214 nm, 5-100% B in 15 min).

$C_{156}H_{245}N_{53}O_{49}$

Mw: 3644.80 g/mol

ARM **92** (RR-h (HVH))

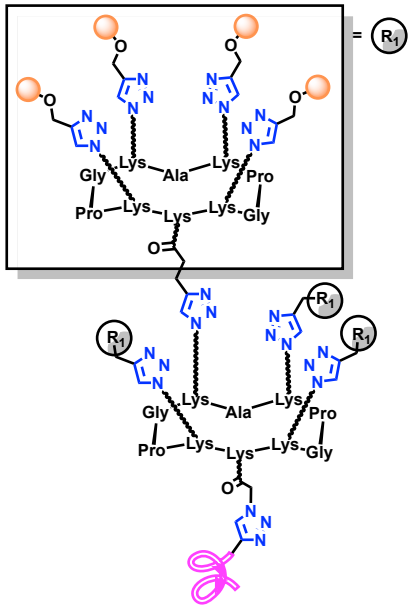

Prepared according general procedure **G** from **40** (5.7 mg, 0.6 µmol) and Alk-HVH **23** (1.0 mg, 0.6 µmol). The crude mixture was purified to afford the title compound as a white fluffy solid after lyophilization (2.5 mg, 0.23 µmol, 38%). HRMS (ESI$^+$-TOF) m/z: calculated for $C_{472}H_{737}N_{145}O_{153}$ $[M+6H]^{6+}$: 1816.0825, found 1816.0816; RP-HPLC: R_t = 6.47 min (C_{18}, λ = 214 nm, 5-60% B in 15 min).

$C_{472}H_{737}N_{145}O_{153}$

Mw: 10886.44 g/mol

ARM **93** (RR-R (Ac-HVH))

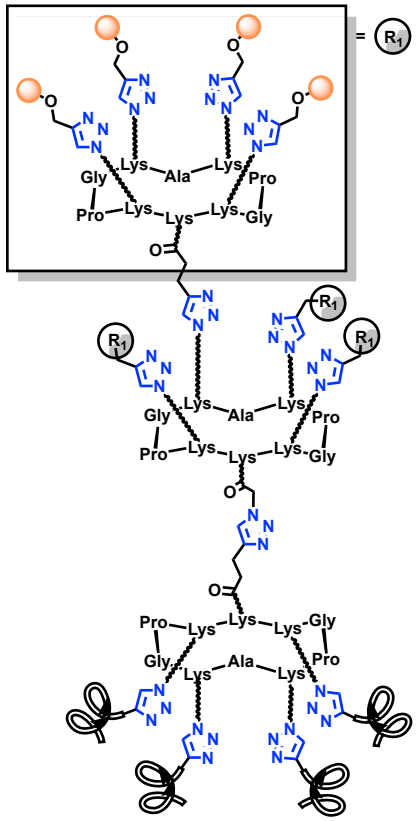

Prepared according general procedure **G** from **40** (2.6 mg, 0.27 µmol) and **69** (2.2 mg, 0.27 µmol). The crude mixture was purified to afford the title compound as a white fluffy solid after lyophilization (1.4 mg, 0.08 µmol, 30%). MALDI-ToF m/z: calculated for $C_{745}H_{1159}N_{249}O_{222}NaK$ $[M+Na+K]^+$: 17207.780, found 17208.687; RP-HPLC: R_t = 6.834 min (C_{18}, λ = 214 nm, 5-60% B in 15 min).

$C_{745}H_{1159}N_{249}O_{222}$

Mw: 17145.71 g/mol

V.2. Biological evaluations

V.2.A. Products and reagents

Culture media, human sera, enzymes, antibiotics and equipment for eukaryotic cell culture were purchased from either Sigma-Aldrich® (Saint-Quentin Fallavier, France) or Fisher Scientific SAS (Illkirch, France). The cells were either ordered from LGC Standards S.à.r.l (Molsheim, France) or provided by Jean-Luc Coll (IAB laboratory, Grenoble, France). Human serum was obtained from a healthy human male donor (Sigma-Aldrich, H4522). The antibodies were ordered from Davids Biotechnologie Gmbh (Regensburg, Germany), Becton Dickinson S.A.S. (Grenoble, France) and Fisher Scientific SAS (Illkirch, France). Cytotoxicity plates were purchased from and Fisher Scientific SAS (Illkirch, France).

Cancer cell lines:

Name	**Disease**	**Species of origin**	**Sex of cell**
	Melanoma	Homo sapiens (Human) (NCBI Taxonomy: 9606)	Female
M_21	**Culture media**	**Source**	**Comment**
	DMEM + 10 % SVF + 3 % Pen/Strep	Dr. Jean-Luc Coll (IAB, Grenoble)	-

Name	**Disease**	**Species of origin**	**Sex of cell**
	Melanoma	Homo sapiens (Human) (NCBI Taxonomy: 9606)	Female
M_21L	**Culture media**	**Source**	**Comment**
	DMEM + 10 % SVF + 3 % Pen/Strep	Dr. Jean-Luc Coll (IAB, Grenoble)	Lack expression of integrin α_v

Name	Disease	Species of origin	Sex of cell
HeLa	Adenocarcinoma (from Henrietta Lacks)	Homo sapiens (Human) (NCBI Taxonomy: 9606)	Female
	Culture media	**Source**	**Comment**
	DMEM + 10 % SVF + 1 % Pen/Strep	Dr. Jean-Luc Coll (IAB, Grenoble)	Human papillomavirus-related endocervical adenocarcinoma.

Name	Disease	Species of origin	Sex of cell
MCF_7	Adenocarcinoma (acronym of Michigan Cancer Foundation-7)	Homo sapiens (Human) (NCBI Taxonomy: 9606)	Female
	Culture media	**Source**	**Comment**
	DMEM + 10 % SVF + 3 % Pen/Strep + Insulin 10 µg/mL	ATCC® HTB-22™	Derived from a female mammary gland metastasis

V.2.B. Equipment

The cells were spun at 500 rpm for 5 min in an Heraeus multifuge X3R centrifuge (Thermo Scientific).

The fluorescence of the cells is analysed on a flow cytometer BD LSR FORTESSA (BD Biosciences, Le Pont de Claix, France) equipped with a 488 nm laser at 100 mW and a 532 nm laser at 50 mW for excitation. The fluorescence emission of the FITC and Alexa Fluor 488™ fluorophores is collected through a BP 525/50 filter.

The cell fluorescence images were recorded thanks to the Leica TCS SP8 CSU confocal microscope equipped with an HC PL APO CS2 40x/1.30 OIL lens. The images are acquired using the Leica LAS X software. For the FITC and Alexa Fluor 488™ fluorophores the excitation is done by a 488 nm laser and the emission is recorded by a spectral detector to precisely adjust the emission band (from 495 to 545 nm).

For the cytotoxic assessment the Fluo COSTAR Assay plates were used and fluorescent signal was read on an POLARstar Omega plate reader (BMG labtech).

V.2.C. Protocols

V.2.C.I. Cell cultures

Cells were cultured in Dulbecco's Modified Eagle Medium (DMEM) supplemented with 10% (v/v) of fetal bovine serum, 100 U/mL penicillin and 100 µg/mL streptomycin. Cells were maintained at 37°C in a humidified atmosphere containing 5% CO_2. A solution of trypsin-EDTA at 0.05% in DMEM was used for subculture to maintain cells in the exponential growth phase.

V.2.C.II. Flow cytometry test

Near confluent cells were harvested, washed, counted and resuspended at a density of 1 x 10^6 cells/mL in HBSS* binding buffer for 60 min at 4°C. After a centrifugation step, to minimize any risk of internalization of ARM when it links its receptor, cells were treated with paraformaldehyde (PFA) 4% in PBS buffer, for 10 minutes at 37°C, followed by neutralization on ice for 1 min. After two washes steps, cells were incubated with 100 nM ARMs for 1 hour at room temperature. After one wash with HBSS* binding buffer, cells were incubated with 100 µL of HS (Human Serum, 50% in HBSS*) for 2 hours at room temperature. After one more washing, the anti-ABM motif antibody binding was finally revealed by adding AlexaFluor™ 488-coupled anti-human IgM secondary antibody (1:400). After 1 hour of incubation at room temperature and one washing step with HBSS* binding buffer, cells were analysed by FACS. The control was represented by cell incubated with HS and secondary anti-Rha conjugated AF-488 antibody. λ excitation: 488 nm.; λ emission: 525 nm.

V.2.C.III. Cytotoxic assessment

U-shaped 96-well microtiter plates were treated with 200 µL of "blocking buffer" (25 mM Na_2CO_3, pH 9.6, BSA (1.5% w/v), and Tween-20 (0.5% w/v)) at rt for 120 min. The blocking solution was removed. Confluent cultures of cells were detached with trypsin-EDTA solution, washed, counted, and suspended at 1.25x10^6 cells/mL in PBS. Cells were fluorescently labelled with BCECF_AM (2 µg/mL) for 30 min at 37 °C and then washed and diluted to 1x10^5 cells/mL for activation in HBSS* binding buffer. After 60 min on ice, ten thousand cells per well were added to the rinsed wells and, after centrifugation and removal of supernatant, different concentration of ARMs were added. Incubation occurred at rt for 60 min, followed by washing step. Therefore 50% HS was added to appropriates wells and incubation proceeded for 120 min at rt. For maximum cell lysis, the non-ionic detergent TRITON was added to the wells at a 1% (w/v) final concentration after 1h30. Following this period, cells were spun at 500 rpm for 5 min in an Heraeus multifuge X3R centrifuge and surnagiant was transferred to Fluo COSTAR Assay plate and was quantified as the fluorescent signal was read on an POLARstar Omega plate reader. Cytotoxicity is calculated by the following equation: [(sample-BG)/(max-BG)] x100 where BG is background, the

spontaneous release of fluorescence which is determined without addition of ARM, and max is the signal corresponding to the 100% death cells. λ excitation: 450 nm.; λ emission: 531 nm.

Chapter VI.

Annexes

VI.1. Publications:

- Benjamin Liet, Eugenie Laigre, David Goyard, Biagio Todaro, Claire Tiertant, Didier Boturyn, Nathalie Berthet, and Olivier Renaudet Multifunctional Glycoconjugates for Recruiting Natural Antibodies against Cancer Cells. *Chem. Eur. J.* **2019**, *25*, 1–9.
- Biagio Todaro, Silvia Achilli, Benjamin Liet, Eugénie Laigre, Claire Tiertant, David Goyard, Nathalie Berthet, and Olivier Renaudet. Structural influence of Antibody Recruiting Glycodendrimers (ARGs) on antitumoral cytotoxicity. *submitted*.

VI.2. Congress attendance and oral communications:

- RECOB 17 – Rencontres en Chimie Organique Biologique. March 18th-22th 2018. Aussois (France).

- XVI edition of CSCC (Conference-School Carbohydrate Chemistry). 17 – 20 June 17th-20th 2018. Certosa di Pontignano, Siena (ITALY).
  [Oral Communication]: "Engineering of Biomolecular Systems for Anti-Tumoral Immunotherapy", Biagio Todaro, David Goyard, Eugenie Laigre, Benjamin Liet and Olivier Renaudet.

- Global Challenges Science Week 2019. June 5th-6th 2019. Grenoble (France).

VI.3. Educational courses:

Scientific courses:

- La RMN pour les chimistes en pratique
- Chimie des Processus Biologiques : Mécanismes de réactions enzymatiques et chimie de l'Évolution et Coenzymes
- Heterocyclic Chemistry

Courses for job placement:

- Label Recherche, Entreprise et Innovation (REI)
- French course for non-French speaking Ph.D. student

Chapter VII.

Bibliographic data

1. Ferlay J, Colombet M, Soerjomataram I, Dyba T, Randi G, Bettio M, Gavin A, Visser O, Bray F. Cancer incidence and mortality patterns in Europe: Estimates for 40 countries and 25 major cancers in 2018. Eur J Cancer. 2018 Nov;103:356-387. doi: 10.1016/j.ejca.2018.07.005.

2. Liotta LA, Kleinerman J, Saidel GM. Quantitative relationships of intravascular tumor cells, tumor vessels, and pulmonary metastases following tumor implantation. Cancer Res. 1974;34(5):997-1004.

3. Chambers AF, Groom AC, MacDonald IC. Dissemination and growth of cancer cells in metastatic sites. Nat Rev Cancer. 2002;2(8):563-572. doi:10.1038/nrc865

4. Horowitz M, Neeman E, Sharon E, Ben-Eliyahu S. Exploiting the critical perioperative period to improve long-term cancer outcomes. Nat Rev Clin Oncol. 2015;12(4):213-226. doi:10.1038/nrclinonc.2014.224

5. Michelson S, Leith JT. Dormancy, regression, and recurrence: towards a unifying theory of tumor growth control. J Theor Biol. 1994;169(4):327-338. doi:10.1006/jtbi.1994.1155

6. Baskar R, Lee KA, Yeo R, Yeoh KW. Cancer and radiation therapy: current advances and future directions. Int J Med Sci. 2012;9(3):193-199. doi:10.7150/ijms.3635

7. Begg AC, Stewart FA, Vens C. Strategies to improve radiotherapy with targeted drugs. Nat Rev Cancer. 2011;11(4):239-253. doi:10.1038/nrc3007

8. Colvin M. Alkylating Agents. Holland-Frei Cancer Medicine. 2003, 6th edition.

9. Kaye SB. New antimetabolites in cancer chemotherapy and their clinical impact. Br J Cancer. 1998;78 Suppl 3(Suppl 3):1-7. doi:10.1038/bjc.1998.747

10. Wang F, Liu X, Liu C, Liu Z, Sun L. Effects of antibiotic antitumor drugs on nucleotide levels in cultured tumor cells: an exploratory method to distinguish the mechanisms of antitumor drug action based on targeted metabolomics. Acta Pharm Sin B. 2015;5(3):223-230. doi:10.1016/j.apsb.2015.03.010

11. Delgado JL, Hsieh CM, Chan NL, Hiasa H. Topoisomerases as anticancer targets. Biochem J. 2018;475(2):373-398. Published 2018 Jan 23. doi:10.1042/BCJ20160583

12. Henriques AC, Ribeiro D, Pedrosa J, Sarmento B, Silva PMA, Bousbaa H. Mitosis inhibitors in anticancer therapy: When blocking the exit becomes a solution. Cancer Lett. 2019;440-441:64-81. doi:10.1016/j.canlet.2018.10.005

13. Bhullar KS, Lagarón NO, McGowan EM, et al. Kinase-targeted cancer therapies: progress, challenges and future directions. Mol Cancer. 2018;17(1):48. doi:10.1186/s12943-018-0804-2

14. Fabian CJ. The what, why and how of aromatase inhibitors: hormonal agents for treatment and prevention of breast cancer. Int J Clin Pract. 2007;61(12):2051-2063. doi:10.1111/j.1742-1241.2007.01587.x

15. Lee JH, Choy ML, Ngo L, Foster SS, Marks PA. Histone deacetylase inhibitor induces DNA damage, which normal but not transformed cells can repair. Proc Natl Acad Sci U S A. 2010;107(33):14639-14644. doi:10.1073/pnas.1008522107

16. Morales J, Li L, Fattah FJ, Dong Y, Bey EA, Patel M, Gao J, Boothman DA. Review of poly (ADP-ribose) polymerase (PARP) mechanisms of action and rationale for targeting in cancer and other diseases. Crit Rev Eukaryot Gene Expr. 2014;24(1):15-28. doi: 10.1615/critreveukaryotgeneexpr.2013006875. PMID: 24579667; PMCID: PMC4806654.

17. Saxton RA, Sabatini DM. mTOR Signaling in Growth, Metabolism, and Disease [published correction appears in Cell. 2017 Apr 6;169(2):361-371]. Cell. 2017;168(6):960-976. doi:10.1016/j.cell.2017.02.004

18. Cai F, Luis MAF, Lin X, Wang M, Cai L, Cen C, Biskup E. Anthracycline-induced cardiotoxicity in the chemotherapy treatment of breast cancer: Preventive strategies and treatment. Mol Clin Oncol. 2019 Jul;11(1):15-23. doi: 10.3892/mco.2019.1854. Epub 2019 May 8. PMID: 31289672; PMCID: PMC6535635.

19. Bushue N, Wan YJ. Retinoid pathway and cancer therapeutics. Adv Drug Deliv Rev. 2010;62(13):1285-1298. doi:10.1016/j.addr.2010.07.003

20. Zhang D, Kanakkanthara A. Beyond the Paclitaxel and Vinca Alkaloids: Next Generation of Plant-Derived Microtubule-Targeting Agents with Potential Anticancer Activity. Cancers (Basel). 2020;12(7):1721. doi:10.3390/cancers12071721

21. Leppert W, Buss T. The role of corticosteroids in the treatment of pain in cancer patients. Curr Pain Headache Rep. 2012;16(4):307-313. doi:10.1007/s11916-012-0273-z

22. Yardley DA. Drug resistance and the role of combination chemotherapy in improving patient outcomes. Int J Breast Cancer. 2013;2013:137414. doi:10.1155/2013/137414

23. Hatzimichael E, Tuthill M. Hematopoietic stem cell transplantation. Stem Cells Cloning. 2010;3:105-117. Published 2010 Aug 26. doi:10.2147/SCCAA.S6815

24. Nelson AL. Antibody fragments: hope and hype. MAbs. 2010;2(1):77-83. doi:10.4161/mabs.2.1.10786

25. Schroeder HW Jr, Cavacini L. Structure and function of immunoglobulins. J Allergy Clin Immunol. 2010;125(2 Suppl 2):S41-S52. doi:10.1016/j.jaci.2009.09.046

26. Kellner C, Otte A, Cappuzzello E, Klausz K, Peipp M. Modulating Cytotoxic Effector Functions by Fc Engineering to Improve Cancer Therapy. Transfus Med Hemother. 2017;44(5):327-336. doi:10.1159/000479980

27. Zhang JY, Looi KS, Tan EM. Identification of tumor-associated antigens as diagnostic and predictive biomarkers in cancer. Methods Mol Biol. 2009;520:1-10. doi:10.1007/978-1-60327-811-9_1

28. Castle JC, Uduman M, Pabla S, Stein RB, Buell JS. Mutation-Derived Neoantigens for Cancer Immunotherapy. Front Immunol. 2019;10:1856. Published 2019 Aug 7. doi:10.3389/fimmu.2019.01856

29. Davis ID. An overview of cancer immunotherapy. Immunol Cell Biol. 2000;78(3):179-195. doi:10.1046/j.1440-1711.2000.00906.x

30. Rosenberg SA. IL-2: the first effective immunotherapy for human cancer. J Immunol. 2014;192(12):5451-5458. doi:10.4049/jimmunol.1490019

31. Pardoll DM. The blockade of immune checkpoints in cancer immunotherapy. Nat Rev Cancer. 2012;12(4):252-264. Published 2012 Mar 22. doi:10.1038/nrc3239

32. Rotte A, D'Orazi G, Bhandaru M. Nobel committee honors tumor immunologists. J Exp Clin Cancer Res. 2018;37(1):262. Published 2018 Oct 30. doi:10.1186/s13046-018-0937-6

33. Martins F, Sofiya L, Sykiotis GP, Lamine F, Maillard M, Fraga M, Shabafrouz K, Ribi C, Cairoli A, Guex-Crosier Y, Kuntzer T, Olivier Michielin O, Peters S, Coukos G, Spertini F, Thompson JA & Obeid M. Adverse effects of immune-checkpoint inhibitors: epidemiology, management and surveillance. Nat Rev Clin Oncol. 2019;16(9):563-580. doi:10.1038/s41571-019-0218-0

34. Yang F, Jin H, Wang J, Sun Q, Yan C, Wei F, Ren X. Adoptive Cellular Therapy (ACT) for Cancer Treatment. Adv Exp Med Biol. 2016;909:169-239. doi:10.1007/978-94-017-7555-7_4

35. Conlon KC, Miljkovic MD, Waldmann TA. Cytokines in the Treatment of Cancer. J Interferon Cytokine Res. 2019;39(1):6-21. doi:10.1089/jir.2018.0019

36. Klapper JA, Downey SG, Smith FO, Yang JC, Hughes MS, Kammula US, Sherry RM, Royal RE, Steinberg SM, Rosenberg S. High-dose interleukin-2 for the treatment of metastatic renal cell carcinoma : a retrospective analysis of response and survival in patients treated in the surgery branch at the National Cancer Institute between 1986 and 2006. Cancer. 2008 Jul 15;113(2):293-301. doi: 10.1002/cncr.23552. PMID: 18457330; PMCID: PMC3486432.

37. Creusot RJ, Moraga I. Superkines, des cytokines aux fonctions mieux ciblées [Superkines: cytokines displaying better targeted functions]. Med Sci (Paris). 2013;29(4):345-349. doi:10.1051/medsci/2013294004

38. Park K, Dhupal M, Kim CS, Park YS, Kim SK. Implication of immunokine profiling for cancer staging. Med Hypotheses. 2016;88:46-48. doi:10.1016/j.mehy.2016.01.005

39. Apostolopoulos V. Cancer Vaccines: Research and Applications. Cancers (Basel). 2019;11(8):1041. Published 2019 Jul 24. doi:10.3390/cancers11081041

40. Bolhassani A, Talebi S, Anvar A. Endogenous and Exogenous Natural Adjuvants for Vaccine Development. Mini Rev Med Chem. 2017;17(15):1442-1456. doi:10.2174/1389557517666170228115801

41. Anassi E, Ndefo UA. Sipuleucel-T (provenge) injection: the first immunotherapy agent (vaccine) for hormone-refractory prostate cancer. P T. 2011;36(4):197-202.

42. Weiner LM, Murray JC, Shuptrine CW. Antibody-based immunotherapy of cancer. Cell. 2012;148(6):1081-1084. doi:10.1016/j.cell.2012.02.034

43. Pasqualini R, Arap W. Hybridoma-free generation of monoclonal antibodies. Proc Natl Acad Sci U S A. 2004;101(1):257-259. doi:10.1073/pnas.0305834101

44. Trenevska I, Li D, Banham AH. Therapeutic Antibodies against Intracellular Tumor Antigens. Front Immunol. 2017;8:1001. Published 2017 Aug 18. doi:10.3389/fimmu.2017.01001

45. Sedykh SE, Prinz VV, Buneva VN, Nevinsky GA. Bispecific antibodies: design, therapy, perspectives. Drug Des Devel Ther. 2018;12:195-208. doi:10.2147/DDDT.S151282

46. Chiavenna SM, Jaworski JP, Vendrell A. State of the art in anti-cancer mAbs. J Biomed Sci. 2017;24(1):15. Published 2017 Feb 20. doi:10.1186/s12929-016-0311-y

47. Coulson A, Levy A, Gossell-Williams M. Monoclonal Antibodies in Cancer Therapy: Mechanisms, Successes and Limitations. West Indian Med J. 2014;63(6):650-654. doi:10.7727/wimj.2013.241

48. Hansel TT, Kropshofer H, Singer T, Mitchell JA, George AJ. The safety and side effects of monoclonal antibodies. Nat Rev Drug Discov. 2010;9(4):325-338. doi:10.1038/nrd3003

49. Nejadmoghaddam MR, Minai-Tehrani A, Ghahremanzadeh R, Mahmoudi M, Dinarvand R, Zarnani AH. Antibody-Drug Conjugates: Possibilities and Challenges. Avicenna J Med Biotechnol. 2019;11(1):3-23.

50. McEnaney PJ, Parker CG, Zhang AX, Spiegel DA. Antibody-recruiting molecules: an emerging paradigm for engaging immune function in treating human disease. ACS Chem Biol. 2012;7(7):1139-1151. doi:10.1021/cb300119g

51. McEnaney PJ, Parker CG, Zhang AX. Antibody-Recruiting Small Molecules: Synthetic Constructs as Immunotherapeutics. Annual Reports in Medicinal Chemistry, Vol. 50, Elsevier, 2017

52. O'Reilly MK, Collins BE, Han S, Liao L, Rillahan C, Kitov PI, Bundle DR, Paulson JC. Bifunctional CD22 ligands use multimeric immunoglobulins as protein scaffolds in assembly of immune complexes on B cells. J Am Chem Soc. 2008 Jun 18;130(24):7736-45. doi: 10.1021/ja802008q.

53. Farah FS. Natural antibodies specific to the 2,4-dinitrophenyl group. Immunology. 1973;25(2):217-226. Ju KS, Parales RE.

54. Ju KS, Parales RE. Nitroaromatic compounds, from synthesis to biodegradation. Microbiol Mol Biol Rev. 2010;74(2):250-272. doi:10.1128/MMBR.00006-10

55. Cui L, Kitov PI, Completo GC, Paulson JC, Bundle DR. Supramolecular complexing of membane Siglec CD22 mediated by a polyvalent heterobifunctional ligand that templates on IgM. Bioconjug Chem. 2011;22(4):546-550. doi:10.1021/bc100579d

56. Lu Y, Low PS. Folate targeting of haptens to cancer cell surfaces mediates immunotherapy of syngeneic murine tumors. Cancer Immunol Immunother. 2002;51(3):153-162. doi:10.1007/s00262-002-0266-6

57. Lu Y, Sega E, Leamon CP, Low PS. Folate receptor-targeted immunotherapy of cancer: mechanism and therapeutic potential. Adv Drug Deliv Rev. 2004;56(8):1161-1176. doi:10.1016/j.addr.2004.01.009

58. Lu Y, Sega E, Low PS. Folate receptor-targeted immunotherapy: induction of humoral and cellular immunity against hapten-decorated cancer cells. Int J Cancer. 2005;116(5):710-719. doi:10.1002/ijc.21126

59. Lu Y, You F, Vlahov I, Westrick E, Fan M, Low PS, Leamon CP. Folate-targeted dinitrophenyl hapten immunotherapy: effect of linker chemistry on antitumor activity and allergic potential. Mol Pharm. 2007 Sep-Oct;4(5):695-706. doi: 10.1021/mp070050b. Epub 2007 Sep 5. PMID: 17784727.

60. Cheung A, Bax HJ, Josephs DH, Ilieva KM, Pellizzari G, Opzoomer J, Bloomfield J, Fittall M, Grigoriadis A, Figini M, Canevari S, Spicer JF, Tutt AN, Karagiannis SN. Targeting folate

receptor alpha for cancer treatment. Oncotarget. 2016 Aug 9;7(32):52553-52574. doi: 10.18632/oncotarget.9651. PMID: 27248175; PMCID: PMC5239573.

61. Fernández M, Javaid F, Chudasama V. Advances in targeting the folate receptor in the treatment/imaging of cancers. Chem Sci. 2017;9(4):790-810. Published 2017 Dec 18. doi:10.1039/c7sc04004k

62. Yi YS. Folate Receptor-Targeted Diagnostics and Therapeutics for Inflammatory Diseases. Immune Netw. 2016;16(6):337-343. doi:10.4110/in.2016.16.6.337

63. Carlson CB, Mowery P, Owen RM, Dykhuizen EC, Kiessling LL. Selective tumor cell targeting using low-affinity, multivalent interactions. ACS Chem Biol. 2007;2(2):119-127. doi:10.1021/cb6003788

64. Owen, R. M., Carlson, C. B., Xu, J., Mowery, P., Fasella, E., and Kiessling, LL. Bifunctional ligands that target cells displaying the alpha vbeta 3 integrin. ChemBioChem 2007; 8, 68−82.

65. Galili U, Rachmilewitz EA, Peleg A, Flechner I. A unique natural human IgG antibody with anti-alpha-galactosyl specificity. J Exp Med. 1984;160(5):1519-1531. doi:10.1084/jem.160.5.1519

66. Galili U, Clark MR, Shohet SB, Buehler J, Macher BA. Evolutionary relationship between the natural anti-Gal antibody and the Gal alpha 1→3Gal epitope in primates. Proc Natl Acad Sci U S A. 1987;84(5):1369-1373. doi:10.1073/pnas.84.5.1369

67. Galili U, Shohet SB, Kobrin E, Stults CL, Macher BA. Man, apes, and Old World monkeys differ from other mammals in the expression of alpha-galactosyl epitopes on nucleated cells. J Biol Chem. 1988;263(33):17755-17762.

68. Galili, U., Mandrell, R. E., Hamadeh, R. M., Shohet, S. B., and Griffiss, J. M. Interaction between human natural anti-α- galactosyl IgG and bacteria of the human flora, Infect. Immun. 1988; 56, 1730–1737.

69. Galili U. The α-Gal epitope (Galα1-3Galβ1-4GlcNAc-R) in xenotransplantation. Biochimie. 2001;83(7):557-563. doi:10.1016/s0300-9084(01)01294-9

70. Wang, J.-Q., Chen, X., Zhang, W., Zacharek, S., Chen, Y., and Wang, P. G. Enhanced inhibition of human anti-Gal antibody binding to mammalian cells by synthetic α-Gal epitope polymers, J. Am. Chem. Soc. 1999; 121, 8174–8181.

71. Pierschbacher MD, Ruoslahti E. Cell attachment activity of fibronectin can be duplicated by small synthetic fragments of the molecule. Nature. 1984;309(5963):30-33. doi:10.1038/309030a0

72. Ruoslahti E. The RGD story: a personal account. Matrix Biol. 2003;22(6):459-465. doi:10.1016/s0945-053x(03)00083-0

73. Kapp TG, Rechenmacher F, Neubauer S, Maltsev OV, Cavalcanti-Adam EA, Zarka R, Reuning U, Notni J, Wester HJ, Mas-Moruno C, Spatz J, Geiger B, Kessler H. A Comprehensive Evaluation of the Activity and Selectivity Profile of Ligands for RGD-binding Integrins. Sci Rep. 2017 Jan 11;7:39805. doi: 10.1038/srep39805. PMID: 28074920; PMCID: PMC5225454.

74. Corbett, J. W., Graciani, N. R., Mousa, S. A., and DeGrado, W. F. Solid-phase synthesis of a selective $\alpha_v\beta_3$ integrin antagonist library, Bioorg. Med. Chem. Lett. 1997; 7, 1371–1376

75. Arap W, Pasqualini R, Ruoslahti E. Cancer treatment by targeted drug delivery to tumor vasculature in a mouse model. Science. 1998;279(5349):377-380.

76. de Groot, F. M. H., Broxterman, H. J., Adams, H., van Vliet, A., Tesser, G. I., Elderkamp, Y. W., Schraa, A. J., Kok, R. J., Molema, G., Pinedo, H. M., and Scheeren, H. W. (2002) Design, synthesis, and biological evaluation of a dual tumor-specific motive containing integrintargeted plasmin-cleavable doxorubicin prodrug, Mol. Cancer Ther. 1, 901–911

77. Morgan BP, Meri S. Membrane proteins that protect against complement lysis. Springer Semin Immunopathol. 1994;15(4):369-396. doi:10.1007/BF01837366

78. Dho SH, Lim JC, Kim LK. Beyond the Role of CD55 as a Complement Component. Immune Netw. 2018;18(1):e11. Published 2018 Feb 20. doi:10.4110/in.2018.18.e11

79. Murelli RP, Zhang AX, Michel J, Jorgensen WL, Spiegel DA. Chemical control over immune recognition: a class of antibody-recruiting small molecules that target prostate cancer. J Am Chem Soc. 2009;131(47):17090-17092. doi:10.1021/ja906844e

80. Zhang AX, Murelli RP, Barinka C, Michel J, Cocleaza A, Jorgensen WL, Lubkowski J, Spiegel DA. A remote arene-binding site on prostate specific membrane antigen revealed by antibody-recruiting small molecules. J Am Chem Soc. 2010 Sep 15;132(36):12711-6. doi: 10.1021/ja104591m. PMID: 20726553; PMCID: PMC2965167.

81. Holmes, E. H., Greene, T. G., Tino, W. T., Boynton, A. L., Aldape, H. C., Misrock, S. L., and Murphy, G. P. Analysis of glycosylation of prostate-specific membrane antigen derived from LNCaP cells, prostatic carcinoma tumors, and serum from prostate cancer patients. Prostate Suppl. 1996; 7, 25−29.

82. Wernicke, A. G., Edgar, M., Lavi, E., Liu, H., Salerno, P., Bander, N., and Gutin, P. Prostate-specific membrane antigen as a potential novel vascular target for treatment of glioblastoma multiforme. Archi. Pathol. Lab. Med. 2011; 135, 1486−1489.

83. Samplaski, M., Heston, W., Elson, P., Magi Galluzzi, C., and Hansel, D. Folate hydrolase (prostate-specific antigen) 1 expression in bladder cancer subtypes and associated tumor neo-vasculature. Mod. Pathol. 2011; 24, 1521−1529.

84. Haffner, M., Kronberger, I., Ross, J., Sheehan, C., Zitt, M., Mhlmann, G., Ofner, D., Zelger, B., Ensinger, C., Yang, X., Geley, S., Margreiter, R., and Bander, N. Prostate-specific membrane antigen expression in the neovasculature of gastric and colorectal cancers. Hum. Pathol. 2009; 40, 1754−1761.

85. Swaminathan A, Lucas RM, Dear K, McMichael AJ. Keyhole limpet haemocyanin - a model antigen for human immunotoxicological studies. Br J Clin Pharmacol. 2014;78(5):1135-1142. doi:10.1111/bcp.12422

86. Blasi, F., and Carmeliet, P. uPAR: a versatile signalling orchestrator. Nat. Rev. Mol. Cell Biol. 2002; 3, 932−943.

87. Romer, J., Nielsen, B., and Ploug, M. The urokinase receptor as a potential target in cancer therapy. Curr. Pharm. Des. 2004; 10, 2359−2376.

88. Jakobsche CE, McEnaney PJ, Zhang AX, Spiegel DA. Reprogramming urokinase into an antibody-recruiting anticancer agent. ACS Chem Biol. 2012;7(2):316-321. doi:10.1021/cb200374e

89. Rullo AF, Fitzgerald KJ, Muthusamy V, Liu, M, Yuan, C, Huang, M, Kim, M, Cho, AE, Spiegel, DA. Re-engineering the Immune Response to Metastatic Cancer: Antibody-Recruiting Small Molecules Targeting the Urokinase Receptor. Angew Chem Int Ed Engl. 2016;55(11):3642-3646. doi:10.1002/anie.201510866

90. Liu D, Zhou D, Wang B, Knabe WE, Meroueh SO. A new class of orthosteric uPAR·uPA small-molecule antagonists are allosteric inhibitors of the uPAR·vitronectin interaction. ACS Chem Biol. 2015;10(6):1521-1534. doi:10.1021/cb500832q

91. Khanna M, Wang F, Jo I, Knabe WE, Wilson SM, Li L, Bum-Erdene K, Li J, Sledge G, Khanna R, Meroueh SO Targeting multiple conformations leads to small molecule inhibitors of the uPAR·uPA protein-protein interaction that block cancer cell invasion. ACS Chem Biol. 2011;6(11):1232-1243. doi:10.1021/cb200180m

92. Douglass EF Jr, Miller CJ, Sparer G, Shapiro H, Spiegel DA. A comprehensive mathematical model for three-body binding equilibria. J Am Chem Soc. 2013;135(16):6092-6099. doi:10.1021/ja311795d

93. Oyelaran O, McShane LM, Dodd L, Gildersleeve JC. Profiling human serum antibodies with a carbohydrate antigen microarray. J. Proteome Res. 2009;8, 4301–4310.

94. Huflejt ME, Vuskovic M, Vasiliu D, Xu H, Obukhova P, Shilova N, Tuzikov A, Galanina O, Arun B, Lu K, Bovin N. Anti-carbohydrate antibodies of normal sera: findings, surprises and challenges. Mol. Immunol. 2009;46, 3037–3049.

95. Macher BA, Galili U. The Galalpha1,3- Galbeta1,4GlcNAc-R (alpha-Gal) epitope: a carbohydrate of unique evolution and clinical relevance. Biochim. Biophys. Acta. 2008; 1780, 75–88.

96. Chen W, Gu L, Zhang W, Motari E, Cai L, Styslinger TJ, Wang PG. L-rhamnose antigen: a promising alternative to α-gal for cancer immunotherapies. ACS Chem Biol. 2011 Feb 18;6(2):185-91. doi: 10.1021/cb100318z. Epub 2010 Nov 11. PMID: 21043478.

97. Sheridan RT, Hudon J, Hank JA, Sondel PM, Kiessling LL. Rhamnose glycoconjugates for the recruitment of endogenous anti-carbohydrate antibodies to tumor cells. ChemBioChem. 2014;15(10):1393-1398. doi:10.1002/cbic.201402019

98. Lin B, Wu X, Zhao H, Tian Y, Han J, Liu J, Han S. Redirecting immunity via covalently incorporated immunogenic sialic acid on the tumor cell surface. Chem Sci. 2016 Jun 1;7(6):3737-3741. doi: 10.1039/c5sc04133c. Epub 2016 Feb 24. PMID: 29997860; PMCID: PMC6008587.

99. Shanshan Li, Bingchen Yu, Jiajia Wang, Yueqin Zheng, Huajie Zhang, Margaret J. Walker, Zhengnan Yuan, He Zhu, Jun Zhang, Peng George Wang, and Binghe Wang. Biomarker-Based Metabolic Labeling for Redirected and Enhanced Immune Response. ACS Chem. Biol. 2018, 13, 1686−1694

100. Jewett JC, Bertozzi CR. Cu-free click cycloaddition reactions in chemical biology. Chem. Soc. Rev. 2010; 39, 1272−1279.

101. Kuzmin, A., Poloukhtine, A., Wolfert, M. A., and Popik, V. V. Surface Functionalization Using Catalyst-Free Azide−Alkyne Cycloaddition. Bioconjugate Chem. 2010; 21, 2076−2085.

102. Debets MF, van Berkel SS, Schoffelen S, Rutjes FPJT, van Hest JCM, van Delft FL. Aza-dibenzocyclooctynes for fast and efficient enzyme PEGylation via copper-free (3 + 2) cycloaddition. 2010; Chem. Commun. 46, 97−99.

103. Rader C, Sinha SC, Popkov M, Lerner RA, Barbas CF 3rd. Chemically programmed monoclonal antibodies for cancer therapy: adaptor immunotherapy based on a covalent

antibody catalyst. Proc Natl Acad Sci USA. 2003;100(9):5396-5400. doi:10.1073/pnas.0931308100

104. Rader C. Chemically programmed antibodies. Trends Biotechnol. 2014;32(4):186-197. doi:10.1016/j.tibtech.2014.02.003

105. Popkov M, Gonzalez B, Sinha SC, Barbas CF 3rd. Instant immunity through chemically programmable vaccination and covalent self-assembly. Proc Natl Acad Sci U S A. 2009;106(11):4378-4383. doi:10.1073/pnas.0900147106

106. Bagnato A, Loizidou M, Pflug BR, Curwen J, Growcott J. Role of the endothelin axis and its antagonists in the treatment of cancer. Br J Pharmacol. 2011;163(2):220-233. doi:10.1111/j.1476-5381.2011.01217.x

107. Doppalapudi, V., Tryder, N., Li, L., Aja, T., Griffith, D., Liao, F.- F., Roxas, G., Ramprasad, M., Bradshaw, C., and Barbas, C. Chemically programmed antibodies: endothelin receptor targeting CovX-Bodies. Bioorg. Med. Chem. Lett. 2007; 17, 501−506.

108. Gavrilyuk JI, Wuellner U, Barbas CF 3rd. Beta-lactam-based approach for the chemical programming of aldolase antibody 38C2. Bioorg Med Chem Lett. 2009;19(5):1421-1424. doi:10.1016/j.bmcl.2009.01.028

109. Zhang Y, Lai BS, Juhas M. Recent Advances in Aptamer Discovery and Applications. Molecules. 2019;24(5):941. doi:10.3390/molecules24050941

110. Goel HL, Mercurio AM. VEGF targets the tumour cell. Nat Rev Cancer. 2013;13(12):871-882. doi:10.1038/nrc3627

111. Wuellner U, Gavrilyuk JI, Barbas CF 3rd. Expanding the concept of chemically programmable antibodies to RNA aptamers: chemically programmed biotherapeutics. Angew Chem Int Ed Engl. 2010;49(34):5934–5937.

112. Gavrilyuk, J, Wuellner U, Salahuddin S, Goswami R, Sinha S, Barbas C. An efficient chemical approach to bispecific antibodies and antibodies of high valency. Bioorg. Med. Chem. Lett. 2009; 19, 3716−3720.

113. Li X, Taratula O, Taratula O, Schumann C, Minko T. LHRH-Targeted Drug Delivery Systems for Cancer Therapy. Mini Rev Med Chem. 2017;17(3):258–267.

114. Revets H, De Baetselier P, Muyldermans S. Nanobodies as novel agents for cancer therapy. Expert Opin Biol Ther. 2005;5(1):111-124. doi:10.1517/14712598.5.1.111

115. Allegra A, Innao V, Gerace D, Vaddinelli D, Allegra AG, Musolino C. Nanobodies and Cancer: Current Status and New Perspectives. Cancer Invest. 2018;36(4):221-237. doi:10.1080/07357907.2018.1458858

116. Gray MA, Tao RN, DePorter SM, Spiegel DA, McNaughton BR. A Nanobody Activation Immunotherapeutic that Selectively Destroys HER2-Positive Breast Cancer Cells. Chembiochem. 2016;17(2):155–158. doi:10.1002/cbic.201500591

117. Ménard S, Balsari A, Casalini P, Tagliabue E, Campiglio M, Bufalino R, Cascinelli N. HER-2-positive breast carcinomas as a particular subset with peculiar clinical behaviors. Clin Cancer Res. 2002 Feb;8(2):520-5. PMID: 11839672.

118. Gutierrez C, Schiff R. HER2: biology, detection, and clinical implications. Arch Pathol Lab Med. 2011;135(1):55-62. doi:10.1043/2010-0454-RAR.1

119. Belkaid Y, Harrison OJ. Homeostatic Immunity and the Microbiota. Immunity. 2017;46(4):562-576. doi:10.1016/j.immuni.2017.04.008

120. Ventola, C. L., The Antibiotic Resistance Crisis: Part 1: Causes and Threats. Pharmacy and Therapeutics 2015, 40 (4), 277-283.

121. Walsh, C., Molecular mechanisms that confer antibacterial drug resistance. Nature 2000, 406 (6797), 775-781.

122. Cox G, Wright GD. Intrinsic antibiotic resistance: mechanisms, origins, challenges and solutions. Int J Med Microbiol. 2013;303(6-7):287-292. doi:10.1016/j.ijmm.2013.02.009

123. Fair RJ, Tor Y. Antibiotics and bacterial resistance in the 21st century. Perspect Medicin Chem. 2014;6:25-64. doi:10.4137/PMC.S14459

124. Walsh, F. Superbugs to kill 'more than cancer' by 2050. www.bbc.com, 2014.

125. Boucher HW, Talbot GH, Bradley JS, Edwards JE, Gilbert D, Rice LB, Scheld M, Spellberg B, Bartlett J. Bad bugs, no drugs: no ESKAPE! An update from the Infectious Diseases Society of America. Clin Infect Dis. 2009 Jan 1;48(1):1-12. doi: 10.1086/595011. PMID: 19035777.

126. Lee Y, Lim WI, Bloom CI, Moore S, Chung E, Marzella N. Bezlotoxumab (Zinplava) for Clostridium Difficile Infection: The First Monoclonal Antibody Approved to Prevent the Recurrence of a Bacterial Infection. P T. 2017;42(12):735-738.

127. Bertozzi, CR, Bednardski MD. Antibody targeting to bacterial cells using receptor-specific ligands J. Am. Chem. Soc. 1992, 114, 2242–2245.

128. Sauer MM, Jakob RP, Eras J, Baday S, Eriş D, Navarra G, Bernèche S, Ernst B, Maier T, Glockshuber R. Catch-bond mechanism of the bacterial adhesin FimH. Nat Commun. 2016 Mar 7;7:10738. doi: 10.1038/ncomms10738. PMID: 26948702; PMCID: PMC4786642.

129. Bertozzi, CR, Bednarski MD. A Receptor-Mediated Immune Response Using Synthetic Glycoconjugates. J. Am. Chem. Soc. 1992, 114, 5543-5546.

130. Li J, Zacharek S, Chen X, Wang J, Zhang W, Janczuk A, Wang PG. Bacteria targeted by human natural antibodies using alpha-Gal conjugated receptor-specific glycopolymers. Bioorg Med Chem. 1999 Aug;7(8):1549-58. doi: 10.1016/s0968-0896(99)00099-1. PMID: 10482447.

131. Metallo SJ, Kane RS, Holmlin RE, Whitesides GM. Using Bifunctional Polymers Presenting Vancomycin and Fluorescein Groups To Direct Anti- Fluorescein Antibodies to Self-Assembled Monolayers Presenting d-Alanine-d- Alanine Groups. Journal of the American Chemical Society 2003, 125 (15), 4534- 4540.

132. Krishnamurthy VM, Quinton LJ, Estroff LA, Metallo SJ, Isaacs JM, Mizgerd JP, Whitesides GM. Promotion of opsonization by antibodies and phagocytosis of Gram-positive bacteria by a bifunctional polyacrylamide. Biomaterials 2006, 27 (19), 3663-3674.

133. Fura JM, Sabulski MJ, Pires MM. D-amino acid mediated recruitment of endogenous antibodies to bacterial surfaces. ACS Chem Biol. 2014;9(7):1480-1489. doi:10.1021/cb5002685

134. Fura JM, Pires MM. D-amino carboxamide-based recruitment of dinitrophenol antibodies to bacterial surfaces via peptidoglycan remodeling. Biopolymers 2015; 104, 351–359.

135. Fura JM, Pidgeon SE, Birabaharan M, Pires MM. Dipeptide- based metabolic labeling of bacterial cells for endogenous antibody recruit- ment. ACS Infect. Dis. 2016; 2, 302–309

136. Lupoli TJ, Tsukamoto H, Doud EH, Wang TS, Walker S, Kahne D. Transpeptidase-mediated incorporation of D-amino acids into bacterial peptidoglycan. J Am Chem Soc. 2011;133(28):10748-10751. doi:10.1021/ja2040656

137. Spirig T, Weiner EM, Clubb RT. Sortase enzymes in Gram-positive bacteria. Mol Microbiol. 2011;82(5):1044-1059. doi:10.1111/j.1365-2958.2011.07887.x

138. Koonin EV, Senkevich TG, Dolja VV. The ancient Virus World and evolution of cells. Biol Direct. 2006;1:29. doi:10.1186/1745-6150-1-29

139. Woolhouse M, Scott F, Hudson Z, Howey R, Chase-Topping M. Human viruses: discovery and emergence. Philos Trans R Soc Lond B Biol Sci 2012; 367:2864 –2871

140. Margeridon-Thermet, S, Shafer RW. Comparison of the mechanisms of drug resistance among HIV, Hepatitis B, and Hepatitis C. Viruses 2010;2, 2696−2739.

141. Griffiths PD. A perspective on antiviral resistance. J. Clin. Virol. 2009; 46, 3−8.

142. De Clercq E. Strategies in the design of antiviral drugs. Nat. Rev. Drug Discovery 2002; 1, 13−25.

143. Berzofsky JA, Ahlers JD, Janik J, Morris J, Oh S, Terabe M, Belyakov IM. Progress on new vaccine strategies against chronic viral infections. J. Clin. Invest. 2004; 114:450–462.

144. Resch B. Product review on the monoclonal antibody palivizumab for prevention of respiratory syncytial virus infection. Human vaccines & immunotherapeutics 2017, Vol. 13, n 9, 2138–2149

145. Wilen CB, Tilton JC, Doms RW. HIV: cell binding and entry. Cold Spring Harb Perspect Med. 2012;2(8):a006866. doi:10.1101/cshperspect.a006866

146. Alkhatib G. The biology of CCR5 and CXCR4. Curr Opin HIV AIDS. 2009;4(2):96-103. doi:10.1097/COH.0b013e328324bbec

147. Shokat KM, Schultz PG. "Redirecting the Immune Response: Ligand Mediated Immunogenicity." J. Am. Chem. Soc., 1991;113:1861-1862.

148. Naicker KP, Li H, Heredia A, Song H, Wang LX. Design and synthesis of alpha Gal-conjugated peptide T20 as novel antiviral agent for HIV-immunotargeting. Org. Biomol. Chem. 2004; 2, 660−664.

149. Perdomo MF, Levi M, Sällberg M, Vahlne A. Neutralization of HIV-1 by redirection of natural antibodies. Proc Natl Acad Sci USA. 2008;105(34):12515-12520. doi:10.1073/pnas.0805777105 ù

150. Parker CG, Domaoal RA, Anderson KS, Spiegel DA. An antibody-recruiting small molecule that targets HIV gp120. J Am Chem Soc. 2009;131(45):16392-16394. doi:10.1021/ja9057647

151. Parker CG, Dahlgren MK, Tao RN, Li DT, Douglass EF Jr, Shoda T, Jawanda N, Spasov KA, Lee S, Zhou N, Domaoal RA, Sutton RE, Anderson KS, Jorgensen WL, Krystal M, Spiegel DA. Illuminating HIV gp120-Ligand Recognition through Computationally-Driven Optimization of Antibody-Recruiting Molecules. Chem Sci. 2014 Jun 1;5(6):2311-2317. doi: 10.1039/C4SC00484A. PMID: 25379167; PMCID: PMC4217211.

152. Haigwood NL, Stamatatos L. Role of neutralizing antibodies in HIV infection. AIDS 17(Suppl 4):S67–S71, 2003.

153. Wyatt R, Sodroski J. The HIV-1 envelope glycoproteins: Fusogens, antigens, and immunogens. Science 1998; 280:1884–1888.

154. Pifferi C. Design and synthesis of multivalent glycoconjugates for anti-cancer immunotherapy, 2017.

155. Kolb HC, Finn MG, Sharpless KB. Click Chemistry: Diverse Chemical Function from a Few Good Reactions. Angew. Chem. Int. Ed. 2001; 40 (11), 2004–2021.

156. Tang W, Becker ML. “Click” Reactions: A Versatile Toolbox for the Synthesis of Peptide-Conjugates. Chem. Soc. Rev. 2014; 43 (20), 7013–7039.

157. Thomas B, Fiore M, Bossu I, Dumy P, Renaudet O. Synthesis of heteroglycoclusters by using orthogonal chemoselective ligations. Beilstein J Org Chem. 2012; 8:421-427. doi:10.3762/bjoc.8.47

158. Huisgen R, Szeimies G, Möbius L, Kinetics and Mechanism of 1,3-Dipolar Cycloadditions Chem. Ber., 1967; 100, 2494.

159. Rodionov VO, Fokin VV, Finn MG. Mechanism of the ligand-free CuI-catalyzed azide-alkyne cycloaddition reaction. Angew Chem Int Ed Engl. 2005 Apr 8;44(15):2210-5. doi: 10.1002/anie.200461496. PMID: 15693051.

160. Hein JE, Fokin VV. Copper-Catalyzed Azide–alkyne Cycloaddition (CuAAC) and beyond: New Reactivity of Copper(i) Acetylides. Chem. Soc. Rev. 2010, 39 (4), 1302–1315.

161. Worrell BT, Malik JA, Fokin VV. Direct evidence of a dinuclear copper intermediate in Cu(I)-catalyzed azide-alkyne cycloadditions. Science. 2013;340(6131):457-460. doi:10.1126/science.1229506

162. Tornøe CW, Christensen C, Meldal M. Peptidotriazoles on solid phase: [1,2,3]-triazoles by regiospecific copper(i)-catalyzed 1,3-dipolar cycloadditions of terminal alkynes to azides. J Org Chem. 2002;67(9):3057-3064. doi:10.1021/jo011148j

163. Rostovtsev VV, Green LG, Fokin VV, Sharpless KB. A stepwise huisgen cycloaddition process: copper(I)-catalyzed regioselective "ligation" of azides and terminal alkynes. Angew Chem Int Ed Engl. 2002;41(14):2596-2599. doi:10.1002/1521-3773(20020715)41:14<2596::AID-ANIE2596>3.0.CO;2-4

164. Besanceney-Webler C, Jiang H, Zheng T, Feng L, Soriano del Amo D, Wang W, Klivansky LM, Marlow FL, Liu Y, Wu P. Development and Applications of the Copper-Catalyzed Azide-Alkyne Cycloaddition (CuAAC) as a Bioorthogonal Reaction; Angew. Chem. Int. Ed., 2011, 50, 8051.

165. Gaetke LM, Chow CK. Copper toxicity, oxidative stress, and antioxidant nutrients. Toxicology. 2003;189(1-2):147-163. doi:10.1016/s0300-483x(03)00159-8

166. Yoon K, Goyal P, Weck M. Monofunctionalization of dendrimers with use of microwave-assisted 1,3-dipolar cycloadditions. Org Lett. 2007 May 24;9(11):2051-4. doi: 10.1021/ol062949h. Epub 2007 May 2. PMID: 17472392; PMCID: PMC2559814.

167. Merrifield RB. Solid Phase Peptide Synthesis. I. The Synthesis of a Tetrapeptide. J. Am. Chem. Soc. 1963, 85 (14), 2149–2154.

168. Shelton PT, Jensen KJ. Linkers, resins, and general procedures for solid-phase peptide synthesis. Methods Mol Biol. 2013;1047:23-41. doi:10.1007/978-1-62703-544-6_2

169. Laigre E. Conception, synthèse et étude de modules de reconnaissance multivalents pour des anticorps, 2018.

170. El-Faham A, Albericio F. Peptide coupling reagents, more than a letter soup. Chem Rev. 2011;111(11):6557-6602. doi:10.1021/cr100048w

171. Stawikowski M, Gregg B. Fields, Introduction to Peptide Synthesis. Curr Protoc Protein Sci. 2002 Feb; CHAPTER: Unit–18.1. doi: 10.1002/0471140864.ps1801s26

172. Carpino LA, Imazumi H, El-Faham A, et al. The uronium/guanidinium Peptide coupling reagents: finally the true uronium salts. Angew Chem Int Ed Engl. 2002;41(3):441-445. doi:10.1002/1521-3773(20020201)41:3<441::aid-anie441>3.0.co;2-n

173. El-Faham A, Subirós Funosas R, Prohens R, Albericio F. COMU: a safer and more effective replacement for benzotriazole-based uronium coupling reagents. Chemistry. 2009;15(37):9404-9416. doi:10.1002/chem.200900615

174. Jad YE, Khattab SN, de la Torre BG, et al. TOMBU and COMBU as Novel Uronium-type peptide coupling reagents derived from Oxyma-B. Molecules. 2014;19(11):18953-18965. Published 2014 Nov 18. doi:10.3390/molecules191118953

175. Lee YC, Lee RT. Carbohydrate-protein interactions: Basis of glycobiology, Acc. Chem. Res. 1995, 28, 321-327.

176. Kiessling LL, Gestwicki JE, Strong LE. Synthetic multivalent ligands in the exploration of cell-surface interactions. Curr Opin Chem Biol. 2000;4(6):696-703. doi:10.1016/s1367-5931(00)00153-8

177. Roy R, Shiao TC. Glyconanosynthons as powerful scaffolds and building blocks for the rapid construction of multifaceted, dense and chiral dendrimers. Chem. Soc. Rev., 2015,44, 3924-3941

178. Dumy P, Eggleston IM, Cervigni S, Sila U, Sun X, Mutter M. A convenient synthesis of cyclic peptides as regioselectively addressable functionalized templates (RAFT). 1995; Tetra Lett, 36, 1255-1258

179. Galan MC, Dumy P, Renaudet O. Multivalent glyco(cyclo)peptides. 2013 ; Chem Soc Rev, 42(11):4599-612

180. Tuchscherer G, Dömer B, Sila U, Kamber B, Mutter M. The TASP concept : Mimetics of peptide ligands, protein surfaces and folding units. 1993; Tetrahedron, 49, 3559-3575.

181. Tuschscherer, G.; Mutter, M. Template Assisted Protein de Novo Design. Pure Appl. Chem. 1996, 68 (11), 2153–2162.

182. Peluso, S.; Rückle, T.; Lehmann, C.; Mutter, M.; Peggion, C.; Crisma, M. Crystal Structure of a Synthetic Cyclodecapeptide for Template-Assembled Synthetic Protein Design. ChemBioChem 2001, 2 (6), 432–437.

183. Renaudet, O, Dumy, P. Chemoselectively Template-Assembled Glycoconjugates as Mimics for Multivalent Presentation of Carbohydrates. Org. Lett. 2003, 5 (3), 243–246.

184. Tomalia, D. A., et al., In Preprints of the 1st SPSJ International Polymer Conference, Society of Polymer Science, Kyoto, Japan, 1984, 65

185. Tomalia, D. A. The dendritic state. Mater. Today. Elsevier, 2005.

186. Oyelaran O, McShane LM, Dodd L, Gildersleeve JC. Profiling human serum antibodies with a carbohydrate antigen microarray. J Proteome Res. 2009;8(9):4301-4310. doi:10.1021/pr900515y

187. Macher BA, Galili U. The Galalpha1,3Galbeta1,4GlcNAc-R (alpha-Gal) epitope: a carbohydrate of unique evolution and clinical relevance. Biochim Biophys Acta. 2008;1780(2):75-88. doi:10.1016/j.bbagen.2007.11.003

188. Samraj AN, Läubli H, Varki N, Varki A. Involvement of a non-human sialic Acid in human cancer. Front Oncol. 2014;4:33. Published 2014 Feb 19. doi:10.3389/fonc.2014.00033

189. Ribeiro JP, Pau W, Pifferi C, Renaudet O, Varrot A, Mahal LK, Imberty A. Characterization of a high-affinity sialic acid-specific CBM40 from Clostridium perfringens and engineering of a

divalent form. Biochem J. 2016 Jul 15;473(14):2109-18. doi: 10.1042/BCJ20160340. Epub 2016 May 17. PMID: 27208171.

190. Roy B, Mukhopadhyay B. Sulfuric Acid Immobilized on Silica: An Excellent Catalyst for Fischer Type Glycosylation. Tetrahedron Lett. 2007, 48 (22), 3783–3787.

191. Herczeg M, Mező E, Molnár N, Ng SK, Lee YC, Dah-Tsyr Chang M, Borbás A. Inhibitory Effect of Multivalent Rhamnobiosides on Recombinant Horseshoe Crab Plasma Lectin Interactions with Pseudomonas aeruginosa PAO1. Chem Asian J. 2016 Dec 6;11(23):3398-3413. doi: 10.1002/asia.201601162. Epub 2016 Nov 3. PMID: 27685372.

192. Liet B, Laigre E, Goyard D, Todaro B, Tiertant C, Boturyn D, Berthet N, Renaudet O. Multifunctional Glycoconjugates for Recruiting Natural Antibodies against Cancer Cells. Chem.–Eur. J. 2019 Dec 5;25(68):15508-15515. doi: 10.1002/chem.201903327. Epub 2019 Oct 15. PMID: 31613028; PMCID: PMC6916168.

193. Pfaff M, Tangemann K, Müller B, et al. Selective recognition of cyclic RGD peptides of NMR defined conformation by alpha IIb beta 3, alpha V beta 3, and alpha 5 beta 1 integrins. J Biol Chem. 1994;269(32):20233-20238.

194. Turaga RC, Yin L, Yang JJ, Lee H, Ivanov I, Yan C, Yang H, Grossniklaus HE, Wang S, Ma C, Sun L, Liu ZR. Rational design of a protein that binds integrin αvβ3 outside the ligand binding site. Nat Commun. 2016 May 31;7:11675. doi: 10.1038/ncomms11675. PMID: 27241473; PMCID: PMC4895024.

195. Ma H, Hao P, Zhang L, Ma C, Yan P, Wang RF, Zhang CL. A new cyclic RGD peptide dimer for integrin αvβ3 imaging. Eur Rev Med Pharmacol Sci. 2016;20(4):613-9. PMID: 26957261.

196. Thoreau F, Vanwonterghem L, Henry M, Coll JL, Boturyn D. Design of RGD-ATWLPPR peptide conjugates for the dual targeting of αVβ3 integrin and neuropilin-1. Org Biomol Chem. 2018;16(22):4101-4107. doi:10.1039/c8ob00669e

197. Han CY, Yue LL, Tai LY, Zhou L, Li XY, Xing GH, Yang XG, Sun MS, Pan WS. A novel small peptide as an epidermal growth factor receptor targeting ligand for nanodelivery in vitro. Int J Nanomedicine. 2013;8:1541-9. doi: 10.2147/IJN.S43627. Epub 2013 Apr 19. PMID: 23626467; PMCID: PMC3632632.

198. Zhao N, Williams TM, Zhou Z, Fronczek FR, Sibrian-Vazquez M, Jois SD, Vicente MGH. Synthesis of BODIPY-Peptide Conjugates for Fluorescence Labeling of EGFR Overexpressing Cells. Bioconjug Chem. 2017 May 17;28(5):1566-1579. doi: 10.1021/acs.bioconjchem.7b00211. Epub 2017 Apr 28. PMID: 28414435; PMCID: PMC5507552.

199. Yu D, Du Z, Li W, Chen H, Ye S, Hoffman AR, Cui J, Hu JF.Targeting Jurkat T Lymphocyte Leukemia Cells by an Engineered Interferon-Alpha Hybrid Molecule. Cell Physiol Biochem. 2017;42(2):519-529. doi:10.1159/000477601

200. Galibert M, Dumy P, Boturyn D. One-pot approach to well-defined biomolecular assemblies by orthogonal chemoselective ligations. Angew Chem Int Ed Engl. 2009;48(14):2576-2579. doi:10.1002/anie.200806223

201. Yan Q, Lu Y, Zhou L, Chen J, Xu H, Cai M, Shi Y, Jiang J, Xiong W, Gao J, Wang H. Mechanistic insights into GLUT1 activation and clustering revealed by super-resolution imaging. Proc Natl Acad Sci U S A. 2018 Jul 3;115(27):7033-7038. doi: 10.1073/pnas.1803859115.

202. Lanza P, Felding-Habermann B, Ruggeri ZM, Zanetti M, Billetta R. Selective interaction of a conformationally-constrained Arg-Gly-Asp (RGD) motif with the integrin receptor alphavbeta3 expressed on human tumor cells. Blood Cells Mol Dis. 1997 Aug;23(2):230-41. doi: 10.1006/bcmd.1997.0140. PMID: 9268674.

203. Felding-Habermann B, Mueller BM, Romerdahl CA, Cheresh DA. Involvement of integrin alpha V gene expression in human melanoma tumorigenicity. J Clin Invest. 1992 Jun;89(6):2018-22. doi: 10.1172/JCI115811. PMID: 1376331; PMCID: PMC295910.

204. Soule HD, Vazquez J, Long A, Albert S, Brennan M. "A human cell line from a pleural effusion derived from a breast carcinoma". Journal of the National Cancer Institute. 1973;51 (5): 1409–1416.

205. Miller DL, el-Ashry D, Cheville AL, Liu Y, McLeskey SW, Kern FG. Emergence of MCF-7 Cells Overexpressing a Transfected Epidermal Growth Factor Receptor (EGFR) Under Estrogen-Depleted Conditions: Evidence for a Role of EGFR in Breast Cancer Growth and Progression. Cell Growth Differ, 1994 Dec;5(12):1263-74.

206. Scherer WF, Syverton JT, Gey GO. Studies on the propagation in vitro of poliomyelitis viruses. IV. Viral multiplication in a stable strain of human malignant epithelial cells (strain HeLa) derived from an epidermoid carcinoma of the cervix. Journal of Experimental Medicine. 1953;97 (5): 695–710.

207. Rodríguez-Enríquez S, Marín-Hernández A, Gallardo-Pérez JC, Moreno-Sánchez R. Kinetics of transport and phosphorylation of glucose in cancer cells. J Cell Physiol. 2009 Dec;221(3):552-9. doi: 10.1002/jcp.21885.

208. Hynes RO. Integrins: bidirectional,allosteric signaling machines. Cell. 2002 Sep 20;110(6):673-87. doi: 10.1016/s0092-8674(02)00971-6. PMID: 12297042.

209. Liet B, Conception, synthèse et étude de conjugués peptidiques multimériques pour la reconnaissance sélective des cellules cancéreuses, 2019

210. Yoshida T, Kakizuka A, Imamura H. BTeam, a Novel BRET-based Biosensor for accurate quantification of ATP Concentration within Living Cells. Sci Rep. 2016; 6:39618.

211. Van Meerloo J, Kaspers GJ, Cloos J. Cell sensitivity assays: the MTT assay. Methods Mol Biol. 2011;731:237-45. doi: 10.1007/978-1-61779-080-5_20. PMID: 21516412.

212. Sellers JR, Cook S, Goldmacher VS. A cytotoxicity assay utilizing a fluorescent dye that determines accurate surviving fractions of cells. J Immunol Methods. 1994 Jun 24;172(2):255-64. doi: 10.1016/0022-1759(94)90112-0.

213. Koley D, Bard AJ. Triton X-100 concentration effects on membrane permeability of a single HeLa cell by scanning electrochemical microscopy (SECM). Proc Natl Acad Sci U S A. 2010 Sep 28;107(39):16783-7. doi: 10.1073/pnas.1011614107. Epub 2010 Sep 13. PMID: 20837548; PMCID: PMC2947864.

214. Miskiewicz EI, MacPhee DJ. Lysis Buffer Choices Are Key Considerations to Ensure Effective Sample Solubilization for Protein Electrophoresis. Methods Mol Biol. 2019;1855:61-72. doi: 10.1007/978-1-4939-8793-1_5. PMID: 30426406.

215. Einwallner E, Subasic A, Strasser A, Augustin D, Thalhammer R, Steiner I, Schwarzinger I. Lysis matters: red cell lysis with FACS Lyse affects the flow cytometric enumeration of circulating leukemic blasts. J Immunol Methods. 2013 Apr 30;390(1-2):127-32. doi: 10.1016/j.jim.2013.01.013. Epub 2013 Feb 4. PMID: 23388694.

216. Liu Y, Zhao F, Gu W, Yang H, Meng Q, Zhang Y, Yang H, Duan Q. The roles of platelet GPIIb/IIIa and alphavbeta3 integrins during HeLa cells adhesion, migration, and invasion to monolayer endothelium under static and dynamic shear flow. J Biomed Biotechnol. 2009;2009:829243. doi: 10.1155/2009/829243.

217. Orgovan N, Peter B, Bősze S, Ramsden JJ, Szabó B, Horvath R. Dependence of cancer cell adhesion kinetics on integrin ligand surface density measured by a high-throughput label-free resonant waveguide grating biosensor. Sci Rep. 2014 Feb 7;4:4034. doi: 10.1038/srep04034.

218. Gao J, Wang Y, Cai M, Pan Y, Xu H, Jiang J, Ji H, Wang H. Mechanistic insights into EGFR membrane clustering revealed by super-resolution imaging. Nanoscale. 2015 Feb 14;7(6):2511-9. doi: 10.1039/c4nr04962d.

219. Barnett JE, Holman GD, Chalkley RA, Munday KA. Evidence for two asymmetric conformational states in the human erythrocyte sugar-transport system. Biochem J. 1975 Mar; 145(3): 417–429. doi: 10.1042/bj1450417a

220. Carruthers A, DeZutter J, Ganguly A, Devaskar SU. Will the original glucose transporter isoform please stand up! Am J Physiol Endocrinol Metab. 2009 Oct;297(4):E836-48. doi: 10.1152/ajpendo.00496.2009.

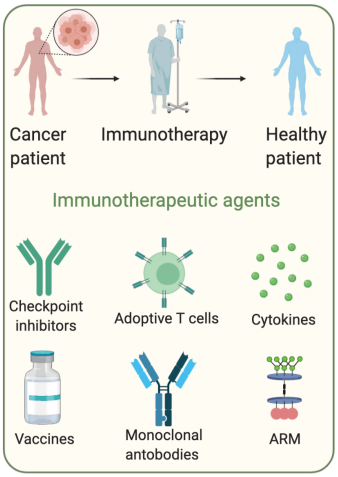
Cancer patient
Immunotherapy
Healthy patient
Immunotherapeutic agents
Checkpoint inhibitors
Adoptive T cells
Cytokines
Vaccines
Monoclonal antobodies
ARM

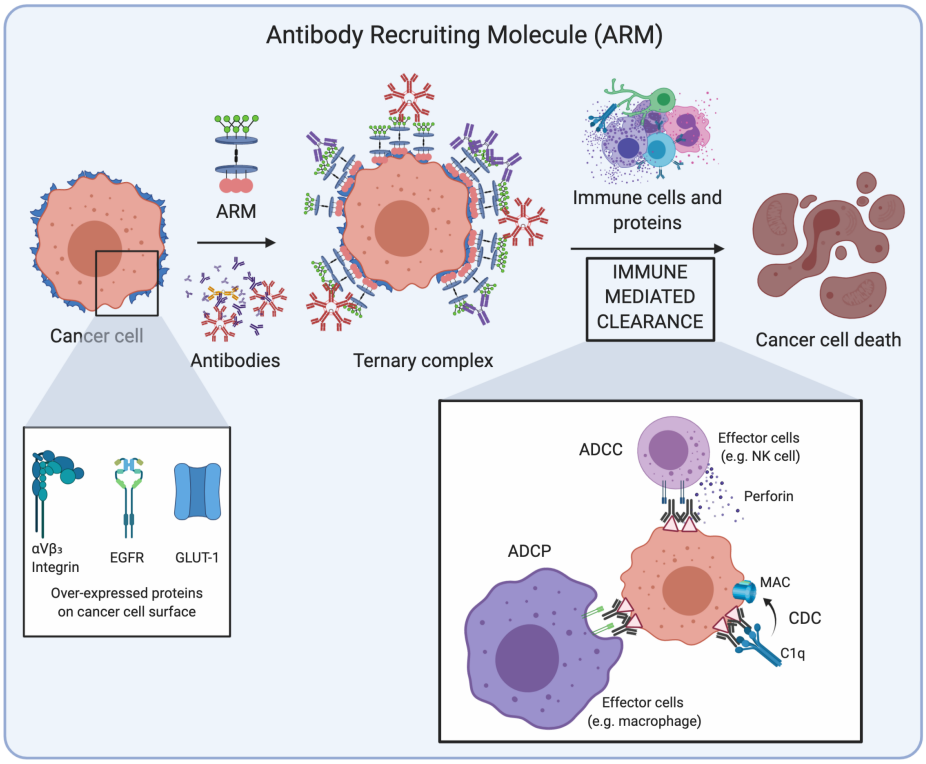
Antibody Recruiting Molecule (ARM)
ARM
Cancer cell
Antibodies
Ternary complex
Immune cells and proteins
IMMUNE MEDIATED CLEARANCE
Cancer cell death
αVβ3 Integrin
EGFR
GLUT-1
Over-expressed proteins on cancer cell surface
ADCC
Effector cells (e.g. NK cell)
Perforin
ADCP
MAC
CDC
C1q
Effector cells (e.g. macrophage)

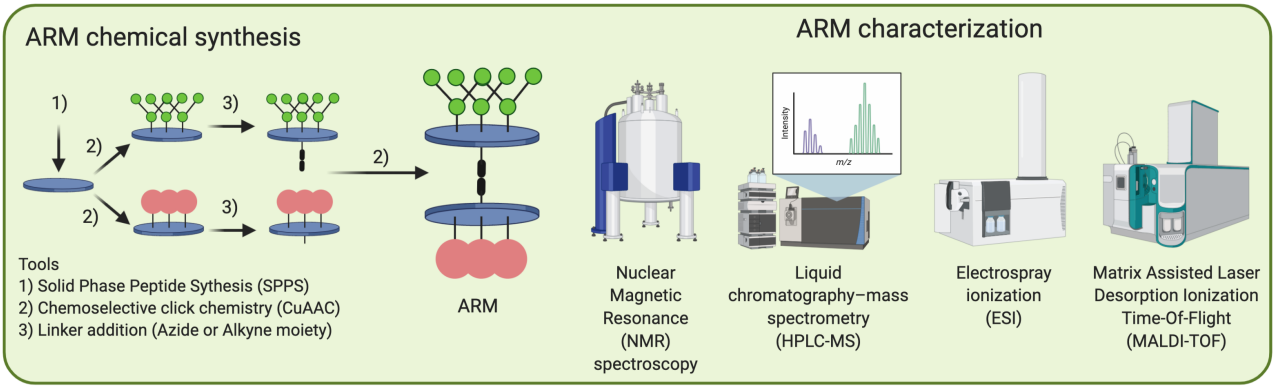
ARM chemical synthesis
ARM characterization
1)
2)
3)
ARM
Tools
1) Solid Phase Peptide Sythesis (SPPS)
2) Chemoselective click chemistry (CuAAC)
3) Linker addition (Azide or Alkyne moiety)
Nuclear Magnetic Resonance (NMR) spectroscopy
Liquid chromatography–mass spectrometry (HPLC-MS)
Electrospray ionization (ESI)
Matrix Assisted Laser Desorption Ionization Time-Of-Flight (MALDI-TOF)

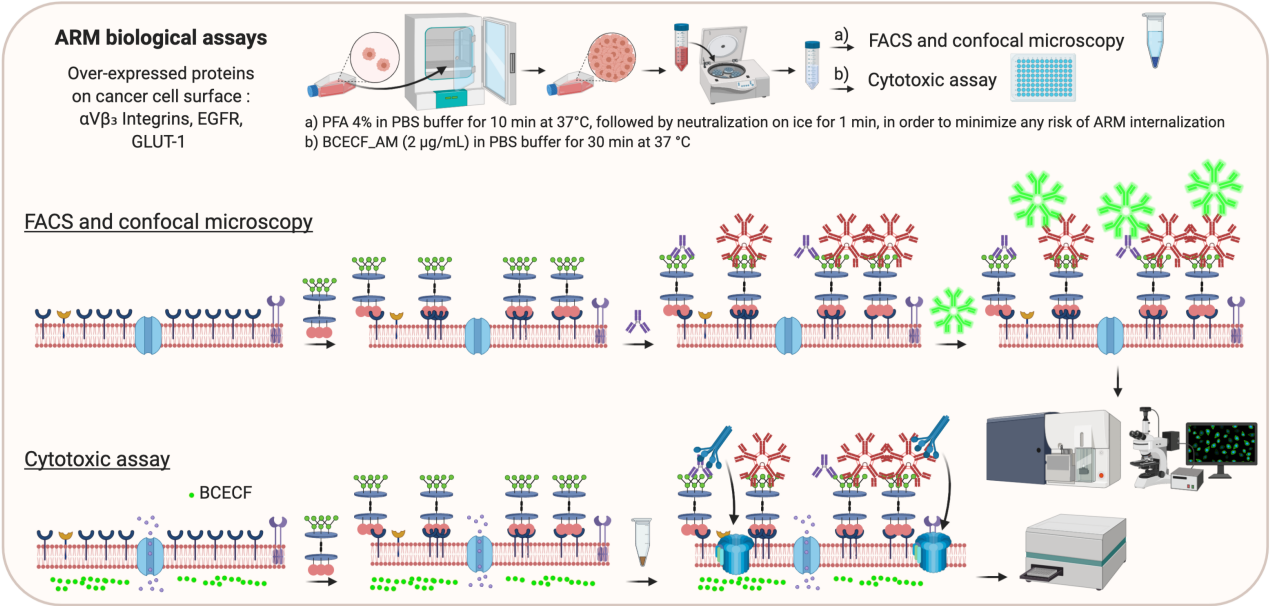
ARM biological assays
Over-expressed proteins on cancer cell surface : αVβ3 Integrins, EGFR, GLUT-1
a) FACS and confocal microscopy
b) Cytotoxic assay
a) PFA 4% in PBS buffer for 10 min at 37°C, followed by neutralization on ice for 1 min, in order to minimize any risk of ARM internalization
b) BCECF_AM (2 µg/mL) in PBS buffer for 30 min at 37 °C
FACS and confocal microscopy
Cytotoxic assay
BCECF

Abstract: Engineering of biomolecular systems for anti-tumoral immunotherapy

The Antibody Recruiting Molecules (ARMs) are belongs to the promising alternative in immunotherapy against cancer and pathogens. In the tumoral contest, an ARM has the singular ability to interface between the target cell and components of the immune system present on the environment leading to an immune response. In this Ph.D. work, we reported the design and the synthesis by click chemistry of several ARMs able to target over-expressed proteins on cancer cell surface through peptides-based tumoral binding modules (TBMs) and to engage natural endogenous antibodies through carbohydrate-based antibody binding modules (ABMs). Next, we demonstrated the formation of a ternary complex between cell-ARM-antibodies and the specific killing of cancer cells by our agents only in the presence of human serum as unique source of immune effectors, without pre-immunization. In addition, we established that the molecule flexibility, the length of the linker between ABM and TBM, the nature of the haptens (carbohydrates and peptides) and their valency play a significant role. Due to the efficiency of the synthetic process, a large diversity of ARMs could be easily created, opening new outlooks in diverse therapeutic fields.

Key words: Antibody Recruiting Molecules (ARMs), cancer immunotherapy, click chemistry, multivalency, flow cytometry, cell-based cytotoxicity assay.

Résumé: Ingénierie de systèmes biomoléculaires pour l'immunothérapie anti-tumorale

Les "Antibody Recruiting Molecules" (ARMs) font partie des pistes prometteuses en immunothérapie contre le cancer et les pathogènes. Dans le contexte tumoral, un ARM a la capacité de relier la cellule cible et des composants du système immunitaire pour conduire à une réponse cytotoxique. Dans ce travail de thèse, nous avons décrit la conception et la synthèse par chimie click de plusieurs ARMs capables de cibler des protéines surexprimées à la surface des cellules cancéreuses par de "tumoral binding modules" (TBMs) basés sur des peptides et d'engager des anticorps endogènes naturels par l'intermédiaire de "antibody binding modules" basés sur des glucides. Nous avons ensuite démontré la formation d'un complexe ternaire cellule-ARM-anticorps et la destruction spécifique des cellules cancéreuses par nos agents uniquement en présence de sérum humain, comme seule source de d'effecteurs immunitaires, sans pré-immunisation. Nous avons également établi que la flexibilité de la molécule, la longueur de la liaison entre ABM et TBM, la nature des haptens (glucides et peptides) et leur valence jouent un rôle important. Compte tenu de la grande efficacité du processus de synthèse, une large gamme de ARM pourrait être facilement créée, ouvrant de nouvelles perspectives dans différents domaines thérapeutiques.

Mots-clés: Antibody Recruiting Molecules (ARMs), Immunothérapie anticancéreuse, chimie click, multivalence, cytométrie en flux, analyse de cytotoxicité sur cellules.